

**The Study of *ortho*-Boronoimine
Formation Using a FRET-Based
Reporter Assay**

Nicholas Curt Rose

PhD

University of York

Chemistry

January 2023

Abstract

The overarching aim of this PhD was to develop chemistries that allow us to form strong covalent bonds under physiological conditions, but which are reversible upon application of a stimuli. We propose to form such bonds using *ortho*-boronoaldehydes (oBAs) in combination with amine-based nucleophiles, which react at dramatically increased rates when compared to standard benzaldehydes, to form stabilised *ortho*-boronoimines, and related derivatives (collectively oBIDs). These oBIDs have emerged as powerful tools for bioconjugation and materials chemistry over the past decade, due to a combination of rapid reaction rates and tuneable product stability. Initially, our aim was to monitor the rapid rates of oBID formation and calculate dissociation constants for their formation in order to gain a detailed understanding of this chemistry. We therefore developed a sensitive and versatile platform to monitor oBID formation, through a Förster resonance energy transfer (FRET)-based assay. In this FRET assay, oBIDs were found to have increased stability compared to standard imine linkages, with a staggering 13-order magnitude difference in dissociation constants depending on the nature of the nucleophile ($K_d = 10^{-11}$ - 10^3 M). This assay is highly tolerant of environmental conditions, allowing us to provide critical new insights into the effects of pH, additives, media and oBA structure on oBID formation. In addition, we applied many different analytical techniques such as UV-Vis, fluorescence and NMR spectroscopy to probe the reversibility of the oBID linkages. We also synthesised different oBA isomers, to test the effects of oBA electronics on rates of formation and oBID stability. Different electronic configurations around the aromatic ring had a significant effect on the boronoimine linkages, and subsequently the kinetics of the system. These results therefore highlight the critical importance of studying derivatised oBIDs which more accurately reflect the substrates used in real-world applications. Our studies better position oBIDs to be used more widely in reversible bioconjugation reactions providing design criteria for further innovations and applications in the field.

List of Contents

i)	Abstract	
ii)	List of Contents	
iii)	Declaration	
iv)	Acknowledgements	
v)	Chapter I	
1.	Introduction	11
1.1.	Potential Application Using oBIDs	11
1.2.	Iminoboronates	14
1.2.1.	Amines	17
1.2.2.	1,2-Diamine	21
1.2.3.	1,2-Aminothiols	24
1.2.4.	Hydroxylamine	31
1.2.5.	Hydrazine	35
1.3.	Conclusion	40
2.	References	41
	Chapter II	
1.	FRET Spectroscopy	47
1.1	Background	47
1.2.	Dye selection	51
1.3.	Cyanine Dye Synthesis	52
1.4.	Reactive Handle Selection	54
2.	Results and Discussion	56
2.1.	Retrosynthetic Analysis of Dyes	56
2.2.	Dye Synthesis	57
2.2.	Boronoaldehyde Synthesis	60

2.2.1. Amide coupling	60
2.2.2. Final Step Borylation	63
2.2.3. Acetal Protection	64
2.2.4. Acyl Chloride	66
2.3. Cy3 Negative Control Synthesis.....	69
2.3.1. Aldehyde.....	69
2.3.2. Boronic Acid	69
2.4. Positive Control Synthesis	71
2.4.1. Carboxylic Acid.....	71
2.5. Cy5 Dye Synthesis	72
2.5.1. Amine Synthesis.....	72
2.5.2. Hydroxylamine Synthesis	73
2.5.3. Synthesis of Cy5 Hydrazine	74
2.6. Acetate Cap Synthesis	75
2.7. Elucidation of NMR assignment	76
3. Conclusion	78
4. Experimental	79
4.1 General considerations.....	79
4.2. Core dye synthesis	80
4.3. Synthesis of reactive handles	85
4.4. Reactive dye synthesis	92
4.5. Synthesis of control substrates for FRET studies.....	103
4.6. Synthesis of Cy3 negative controls	108
5. References.....	114

ii) **Chapter III**

1. FRET Binding Assay of oBIDS	119
1.1. Calculation of Cyanine Dye Concentration	119
1.2. Plate Reader Studies.....	122
1.2.1. Initial Screening of Photobleaching.....	122
1.2.2. Preliminary Fluorescence Measurements	123
1.2.3. Disulphide Reduction with TCEP	129

1.3. Fluorimeter FRET Measurements	133
1.3.1. Preliminary FRET Measurements.....	133
1.3.2. Second-Order Fluorimeter Measurements.....	137
1.4. Lack of Cy5 Emission at 641 nm	142
1.5. Extrapolation of Conversions	144
1.6. pH Dependency of oBID Formation	147
1.6.1 pH 6.....	147
1.6.2. pH 8.....	149
1.6.3. pH 4.....	150
1.7. Reaction Additives	151
2. Conclusion	155
3. Experimental	156
3.1. Determination of Substrate Concentration via UV/Vis Analysis	156
3.2. Initial Screening of Cy3 Quenching	156
3.3. FRET Studies	157
4. References	159

iii) **Chapter IV**

1. Reversibility Studies	164
1.1. Synthesis of non-labelled Nucleophile Derivatives	166
1.1.1. Propyl-Amine Synthesis	166
1.1.2. Propyl-Hydroxylamine Synthesis.....	166
1.1.3. Propyl-Hydrazine Synthesis	167
1.2 Plate Reader Studies	167
1.3. Mechanism of oBID Formation	173
1.4. Fluorimeter Studies	174
1.5. LC-MS Reversibility Studies	175
1.5.1 Synthesis of Methyl–Amine Competitors.....	176
1.5.2. LC-MS Assay.....	177
2. Alternative <i>ortho</i>-Boronoaldehyde Structures	179
2.1. Synthesis of Cy3-oBA Isomers	180
2.1.1. Synthesis of <i>para</i> -BA.....	182
2.1.2. Synthesis of <i>para</i> -carboxy oBA	183

2.1.3. Synthesis of <i>meta</i> -phenoxy <i>o</i> BA	184
2.1.4. Synthesis of <i>ortho</i> -boronoketone	185
2.2. Plate Reader Isomer Studies	186
2.3. Fluorimeter Isomer Studies	189
2.4. NMR Competition Studies.....	190
2.5. NMR Kinetic Isomer Studies.....	197
3 Additional Studies.....	200
3.1 DAB-Hydrazone pH Study.....	200
3.2. Glucose and Fructose Binding Study.....	202
4. Conclusion	207
5. Future Works	208
6. Experimental	209
6.1. Synthesis of Nucleophiles for NMR, LC-MS studies and FRET Controls...	209
6.2. Synthesis of <i>o</i> BA Substrates for NMR and LC-MS Studies.....	217
6.3. Initial Screening of Cy3 Quenching	224
6.4. LC-MS Reversibility Studies	225
6.5. NMR Studies of pH Dependent DAB-Hydrazone Exchange	226
6.6. NMR Studies of Sugar Binding.....	226
7. References.....	228

Declaration

I declare that this thesis is a presentation of original work, and I am the sole author. This work has not previously been presented for an award at this, or any other, University. All sources are acknowledged as References.

I acknowledge the publication 'Insight into *ortho*-boronoaldehyde conjugation *via* a FRET-based reporter assay', which arose from this thesis.

Acknowledgments

First and foremost, I would like to thank Dr. Christopher Spicer, my supervisor, mentor and friend. Chris has shown me patience and support for the past 4 years, which has helped me grow and develop as a research chemist. Chris has created a welcoming, healthy, and social environment for all of his students to thrive, which translates to a happy and successful group. I would like to thank my IPM, Dr. William Unsworth for his continuous feedback and guidance on both project and FPL throughout my duration at York. I am grateful to my second supervisor, Prof. David Smith for his time and advice at each of my TAP meetings. I would like to thank the entire chemistry department at the University of York, the graduate office and the EPSRC for funding.

Very importantly, I would like to thank my partner in crime Fraser 'Fresh' Arnold. I will cherish our countless memories together, from the singing and dancing to Spotify playlists in the lab, to the endless sporting events outside of the office. We helped each other through very tough times throughout both of our projects but were always the beacon of light to take away the pressures of the lab environment. Here's to many more memories together Fresh.

I would like to thank the entire Spicer group, past and present, for making my time at York so enjoyable. I am grateful to Natalia Swiatek, for being the third musketeer with Fresh and I, spending a year with lots of socials, laughs and new experiences. I appreciate the countless hours spent listening to presentations, giving feedback on pieces of work, and always staying positive and helping to get me through hard times on the project. I am grateful to Lydia Barber, for always being a social fiend, never saying no to another drink and helping plan fun events outside of the lab. I thank Reuben 'R9' Breetveld, for his Irish charm, kind heart and social prowess. I am thankful for him to opening up my world to darts and being a pure decent friend during my final year. I am also grateful to the rest of the Spicer group: Laetitia, Charis, Tom, Nico, Neil, Alicia, Miles and Angela for the laughter, support, and friendship.

I am grateful to my family and friends outside of York, for offering me a change in social environment which helped take my mind away from the stresses of the lab completely. I am grateful to the Organics football team, Fresh, R9, young Dan, Tobey Roney, James (x3), Stephen, Ivan, Mohammed, Jake and Will (x3). I am grateful to Zoe, Alison, and Jim for providing unwavering care and support during my time in York. I am also thankful for Iman Khazal, Alex Hyam and Karl Heaton for providing technical and analytical support throughout my project.

Chapter One

Introduction

Contents

1. Introduction	11
1.1. Potential Application Using oBIDs	11
1.2. Iminoboronates	14
1.2.1 Amines.....	17
1.2.2. 1,2-Diamine	21
1.2.3. 1,2-Aminothiols.....	24
1.2.4. Hydroxylamine.....	31
1.2.5. Hydrazine	35
1.3. Conclusion	40
2. References	41

1. Introduction

1.1. Potential Application Using oBIDs

Tissue engineering is an emerging and promising regenerative approach that uses materials to repair or replace damaged tissues for the treatment of disease or injury. Damage to healthy tissues has been the cause of countless deaths worldwide and has an enormous burden on healthcare systems.²⁻⁴ Thus, treatments to suppress the vast array of diseases and injuries implicated by tissue damage could revolutionise medicine.⁵ Many different cell types have been exploited in cell therapy approaches to tissue engineering based on their specific therapeutic effects. Mesenchymal stem cells are most frequently used due to their low cytotoxicity and unique regenerative capacities.⁶ Mesenchymal stem cells have the ability to self-renew and also exhibit significant differentiation into many types of cells. With the correct signalling cues, as well as optimal mechanical and physical environments, stem cells have the ability to differentiate into a plethora of tissue types (Fig. 1), towards replacement-needed tissues or organs.^{7,8}

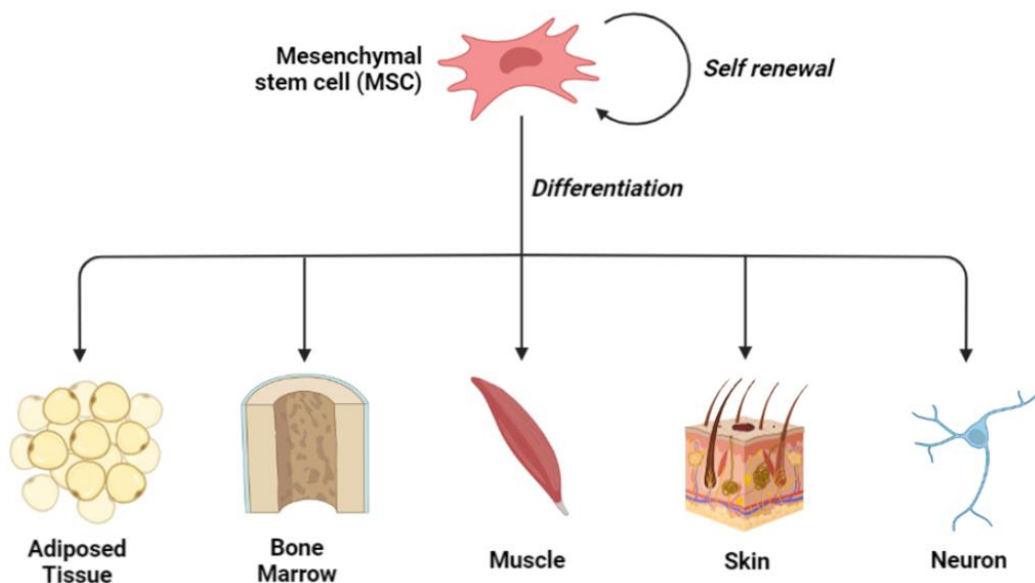


Figure 1: Mesenchymal stem cell which can differentiate into several different cells to form a range of tissues.

To grow these stem cells into highly specialised cells *in vitro*, a biocompatible material scaffold is needed. Hydrogels have emerged as the most promising biomaterial which can provide a 3-dimensional scaffold to stem cells to direct tissue development.^{9,10} Hydrogels can be designed to facilitate the functions of cell proliferation, differentiation, and migration, as well as providing cells with a water-rich environment that mimics native soft tissues.¹¹ Particularly attractive aspects of hydrogels, are their tuneable physicochemical properties, which are dictated by the chemistry of the underlying polymer they are composed from.¹⁰

Many different hydrophilic polymers which are capable of holding large volumes of water in an osmotically swollen scaffold (typically 0.1-10% polymer by weight), have been interwoven to create biocompatible aqueous conditions inside hydrogels.¹² These polymeric materials display either elastic or viscoelastic behaviour that mimics the extracellular matrix (ECM), governed by the polymer structure and architecture. Nutrients, oxygen and biomolecules are able to diffuse through the highly porous structure of the gel, whilst enabling the exchange of metabolites and toxins away from cells providing a suitable growth medium of cells. The porosity of hydrogels are often high enough to enable cell permeation and interconnectivity, providing an excellent cell reservoir for growing tissues.¹³ In addition, hydrogels offer the possibility to be functionalised with different chemical groups, nanocomposites, polymers, or bio components providing opportunities for specific photochemical, thermal, pH, or biomolecular stimuli responsive properties towards regenerative tissue engineering.¹⁴ Furthermore, hydrogels are easily handled and processed and possess tuneable hierarchical morphologies and structures, thus confirming their broad and highly biocompatible applications in biologically relevant conditions which are used in many clinical settings to date.¹⁵ *In vivo*, stem cells are provided with signalling proteins during normal development, which deliver biochemical signals to induce stem cell growth, maturation, differentiation and communication, amongst other processes. Despite their huge promise, much optimisation is needed for hydrogels, to provide a 3-dimensional scaffold upon which stem cells could grow on, while mimicking the activity of these correct signalling proteins which are essential for effective tissue development. The reversible attachment and detachment of these key signalling proteins essential for the growth and development of this stem cell is so far irreproducible within a synthetic material. Current protein-material conjugation chemistry employs static linkages formed via chemistries such as click, or photo chemistry.^{8,9} These linkages lead to static signalling which fails to recreate signalling *in vivo*, often resulting in the growth of immature tissues that are unfit for clinical applications for treating disease and injury.^{10,11} If the dynamic signalling of native tissues could be mimicked using dynamic linkages which are able to dissociate under applied stimuli in a 'tag' and 'release' mechanism then a major advance would be delivered (Fig. 2).

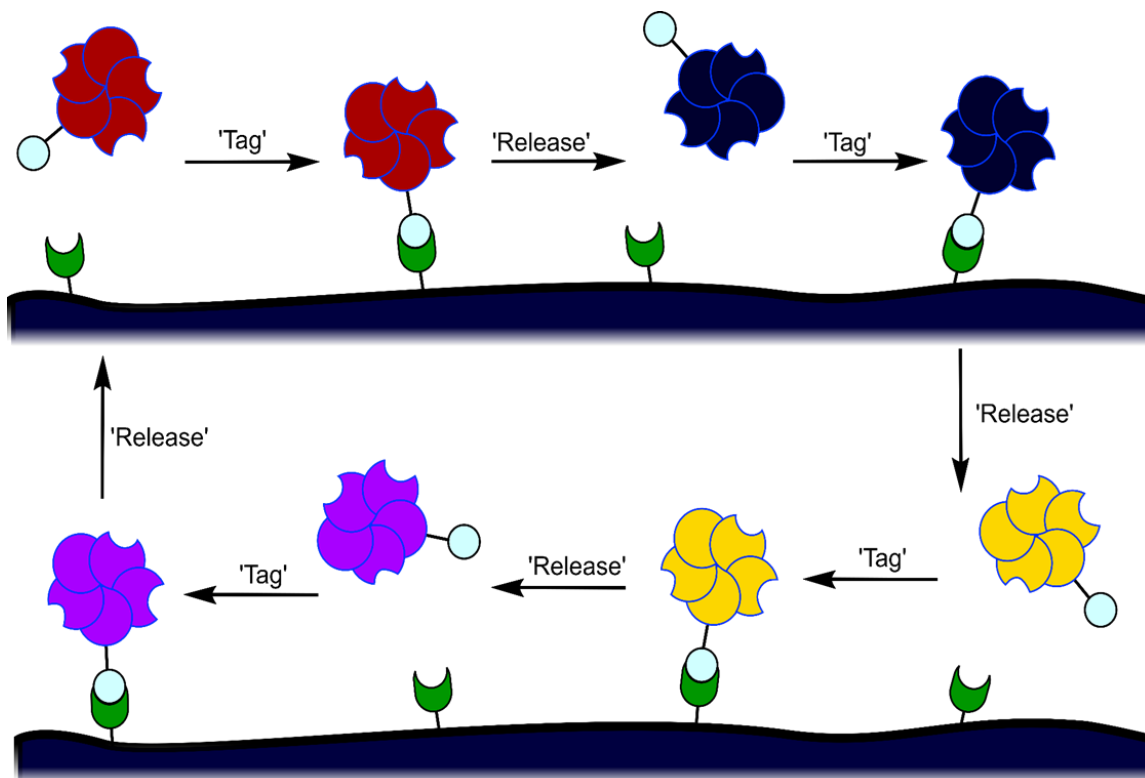
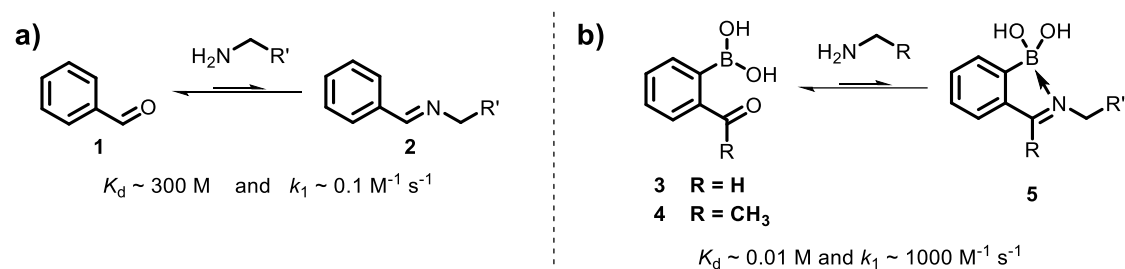


Figure 2: Proposed 'tag and release' mechanism for the attachment and detachment of a sequence of proteins (coloured) to a biomaterial, which could mimic signalling protein cascades used by nature to control tissue development.

We propose to develop such dynamic linkages using oBIDs, unlocking the potential to grow mature tissues *in vitro*, within a hydrogel, for subsequent implantation in regenerative medicine. By combining dynamic chemistry for the attachment of proteins to a hydrogel, this chemistry could be harnessed to develop technologies that can be used to help combat chronic diseases such as osteoarthritis, heart disease, chronic wounds, and organ failure, by repairing, regenerating, or improving the function of the damaged tissue.⁵

1.2. Iminoboronates

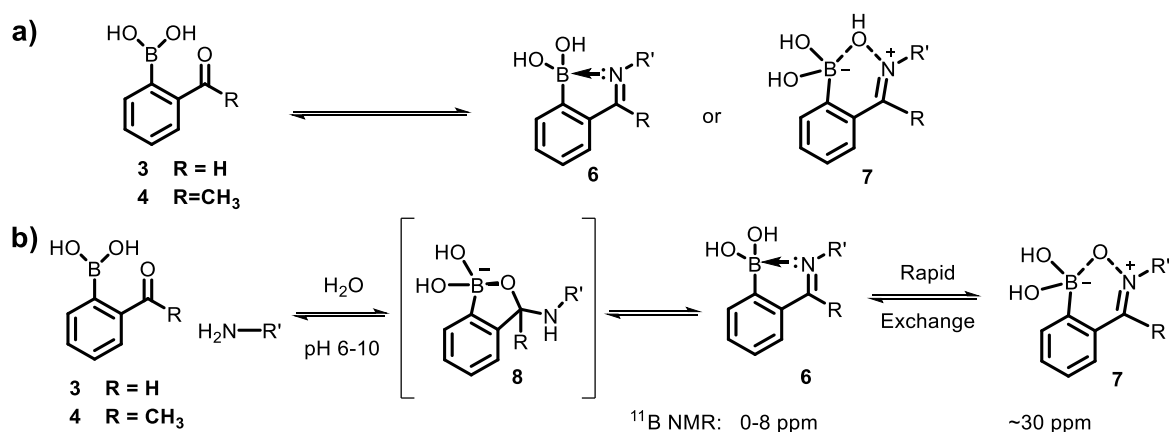
Aldehydes (**1**) can react with amines in organic solvents to form imines (**2**) with loss of water. Classical imines suffer from thermodynamic instability in aqueous conditions. As a result of the excess water in the system, the equilibrium lies over to the left-hand side of the reaction, favouring the aldehyde and amine counterparts (Scheme 1a). However, when a boronic acid moiety is *ortho*- to the aldehyde group, such as in 2-formylphenylboronic acid (2-FPBA, **3**), the subsequent rate of formation of the *ortho*-boronoimine (**5**), and conjugate stability is dramatically increased between biologically relevant pH ranges of 6-10.¹⁶ Analogous results are observed for ketones, such as 2-acetylphenyl boronic acid (2-APBA, **4**). The lone pair of electrons on the adjacent nitrogen can offer stabilising interactions by donation of electron density, into the empty p-orbital of the boronic acid (Scheme 1b).¹⁷



Scheme 1: Comparison of benzaldehyde and *ortho*-boronooaldehyde reactivity, with the *ortho*-borono group accelerating (k_1) and stabilising (K_d) imine formation.¹⁷

The *ortho*-boronic acid in **3** accelerates the rate of oBID formation (k_1), relative to the unfunctionalized benzaldehyde (**1**), by both activating the aldehyde to nucleophilic attack through a Lewis conjugate (N→B dative bond) and accelerating the rate-determining dehydration step. Though the rate of imine hydrolysis (k_{-1}) is also accelerated, stabilising B–N interactions lead to an overall significant shift in equilibrium towards product formation (decrease in dissociation constant, K_d). For example, while benzaldehyde reacts with alkyl amines with $k_1 \sim 0.1 \text{ M}^{-1} \text{ s}^{-1}$ and $K_d \sim 300 \text{ M}$,^{18,19} the *ortho*-borono analogue *ortho*-formylphenylboronic acid (FBPA) forms analogous iminoboronates with a $k_1 \sim 1000 \text{ M}^{-1} \text{ s}^{-1}$ and $K_d \sim 10 \text{ mM}$ (Scheme 1b).²⁰ This 5-order of magnitude increase in reaction rate, and 4-order of magnitude decrease in dissociation constant using a simple amine, typifies the unique reactivity of oBAs. By using 2-FPBA in combination with a range of different amine-based nucleophiles, K_d s have been found between the range 10^{-2} - 10^{-9} M , which shows a staggering range of conjugate stabilities.²⁰ Due to the diversity of these dissociation constants, *ortho*-boronoimines and their derivatives (oBIDs) have proven popular in bioconjugation techniques in chemical biology.¹

Although the exact mechanism of stabilisation of B–N interaction is disputed, the Ansyl group have undertaken mechanistic studies using ^{11}B NMR spectroscopy, the results of which contradict the dative covalent structure of *o*BIDs, widely accepted by the community.^{21,22} Studies done by Ansyl and James were in agreement that the solvent effects of the system play a significant role in iminoboronate structure. In a protic media, covalent insertion of the boronate can dominate, held by electrostatic ionic interactions which afford a hydrogen-bonded zwitterionic species (**7**) with little or no N–B dative bonding (Scheme 2a). Ansyl also states that in aprotic solvent where the solvent insertion pathway is absent, an N–B dative bond (**6**) is the most thermodynamically stable structure. This study of the structure of *o*BIDs was supported by the James group, via ^{11}B NMR, who reported substantial differences in stabilities in protic and aprotic solvent environments. In protic solvents, ionic interactions are stabilised favouring *o*BID **7**. However, Chapin *et al.* used ^{11}B NMR to suggest that this solvent insertion species **7** between the B and N bond would be protonated at neutral pH, and much more dynamic between interconverting structures **6** and **7**, rendering a kinetically labile imine bond in physiological conditions.^{22,23} Therefore, a rapid exchange between the dative **6** and charged species **7**, via intermediate **8**, was reported (Scheme 2b) which highlights the highly dynamic nature of boronoimine linkages.²¹



Scheme 2: a) Two widely accepted structures of *ortho*-boronoimines b) Mechanism of iminoboronate formation across pH 6-10 derived via ^{11}B NMR studies.

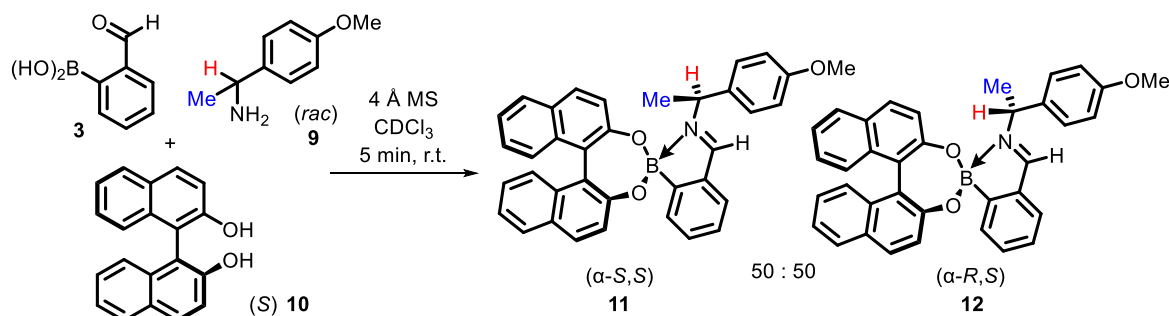
More complex iminoboronate structures have been reported with an array of amine-based nucleophiles to form complex *o*BIDs, which can cyclise to form five- and six-membered highly stabilised structures in aqueous environments, which will be covered in subsequent sections. These iminoboronate complexes are well-accepted to be dominated by solvent-insertion in protic media, including numerous aqueous buffers. Herein, the structures *o*BID structures will be denoted with a dative covalent linkage for simplicity, but protic solvent

effects should not be overlooked and it is likely that structures discussed are highly dynamic, with both the dative and solvent inserted versions being relevant and interchanging.

Many recent reviews have reported the versatility oBIDs in drug delivery,²⁴ *in vivo* labelling,²⁵ and responsive materials.²⁶ oBIDs offer a distinct advantage over alternative bioconjugation techniques, as they can offer reversibility under applied stimuli, imperative to mimicking the highly dynamic environment of living cells. Other bioconjugation strategies, such as click chemistry can be orthogonal, fast and highly selective, having been awarded the Nobel Prize in 2022, but form irreversible linkages. The unique reactions between *ortho*-boronoaldehydes and amine-based nucleophiles have emerged amongst the fastest bioconjugation reactions in literature ($k_1 > 1 \times 10^4 \text{ M}^{-1} \text{ s}^{-1}$), with the fastest being the inverse electron demand Diels-Alder reactions of strained alkenes with tetrazines ($k_1 \sim 10^5\text{--}10^6 \text{ M}^{-1} \text{ s}^{-1}$). As previously mentioned, much of our understanding is based on unsubstituted model compounds such as 2-FPBA and 2-APBA, which poorly reflect the stereo-electronic characteristics of the functionalised oBAs necessary for translational applications in chemical biology. Early research on the most simplistic *ortho*-boronoaldehydes and *ortho*-boronoketones, which could undergo reactions with amine nucleophiles were important,²⁷ but in using 2-FPBA and 2-APBA no additional electronic or steric effects were accounted for, which may influence the formation and stability of the subsequent oBIDs. Such studies have been performed with many amine-based nucleophiles, including simple amines,^{28–31} diamines,³² aminothiols,^{26,33–35} hydroxylamines¹⁶ as well as hydrazine analogues³⁶. Furthermore, there has not been a uniform study to test these oBIDs, in a coherent analytical study. So far, much of the understanding of oBID chemistry has been pieced together from a large number of independent studies, performed and analysed under varying conditions, making comparisons challenging. This is particularly important given the highly dynamic nature of oBID linkages, leading to a high sensitivity to environmental conditions and choice of analytical technique. Ultimately, this leads to significant discrepancies in reported rates of formation and stabilities of oBIDs, due to subtle differences in substrate choice, reaction conditions, or analysis method.^{29,34}

The first *ortho*-boronoimine reported was from the Dunn group in 1968,³⁷ who found a stabilisation effect between 2-FPBA and a reactive amine nucleophile relative to benzaldehyde in a range of organic solvents.³⁷ Since then, there has been a surge in publications over the last 30 years around *ortho*-boronoimines in organic solvents. James and Bull recently published a comprehensive review covering this work, which includes

work performed by numerous groups to explore how amines (**9**), diols (**10**) and boronic acids (**3**) can be reacted to form large complex structures with a chiral molecules (**12**).³⁸



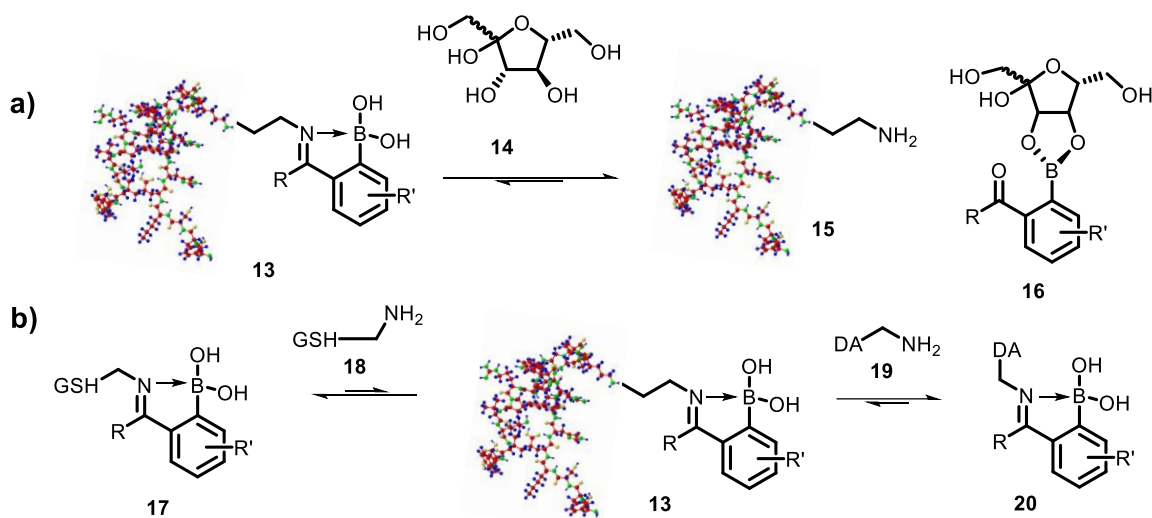
Scheme 3: Three-component assembly of 2-FPBA, (S)-BINOL and chiral amine to give diastereoisomers.³⁸

These iminoboronate linkages have found uses in smart polymers, as chiral auxiliaries for catalysis and in electrochemistry applications. These *ortho*-boronoimine reactions in organic solvents have been around for over 70 years, with a plethora of research on them in.³⁸ However, in order for iminoboronates to be useful in bioconjugation reactions and to find use in chemical biology, methods must be employed to stabilise these iminoboronates in biomedically relevant conditions. Therefore, there has been an interest in moving this research from organic solvent into aqueous media.

1.2.1 Amines

Over the past decade, many research groups have studied *o*BID formation and stability under aqueous conditions and have recognised the potential of using *ortho*-boronoimine's in bioconjugation chemistry. Much of the research was performed using the unfunctionalised models 2-formylphenyl boronic acid (2-FPBA) or 2-aminophenyl boronic acid (2-APBA) with lysine, which contains a primary amine which can act as a nucleophile for *o*BID formation under physiological conditions. The Gois group was the first to show that boronoimines could be formed between 2-FPBA and a primary amine located on a lysine side chain within a peptide between pH 6-9.²⁸ In a key early study, the formation of the iminoboronate linkage from *n*-butylamine with a functionalised boronoketone was observed between pH 6.01 and 9.17, and the stability was monitored over 7 days (Scheme 4a). ¹H NMR revealed that the iminoboronate remained stable over the 7-day period in an aqueous environment. This result was ground-breaking, as it was the first imine linkage of its kind which was stabilised over extended periods of time in water. Studies went on to test the reaction of protected lysine with both 2-FPBA and 2-APBA, which gave levels of

>60% conversion by ^1H NMR. This linkage opened the potential for protein modifications containing a lysine side chain and provided the basis for a spate of papers published on *ortho*-boronoimines.^{30,39} The reversibility of the iminoboronate linkage was also demonstrated, using lysosome as the model protein. The stability of the constructs **13** between lysosome and 2-FPBA were first evaluated in buffer solution at pH 7.0, which saw the constructs maintain integrity for 5 h. After this time, dopamine (DA), fructose or glutathione (GSH) were added, with the additives rapidly inducing hydrolysis of the boronoimine (Scheme 4b, **17/20**). Fructose (**14**) is well known in the literature to form complexes with boronic acids, to form stable boronic esters.^{40–44} When fructose (**14**) was added to the oBID, it could be reasoned that these competing interactions with the boronic acid formed, which means that the stabilisation of B–N interactions could have been lost, resulting in the reversibility observed for the iminoboronate **13** (Scheme 4a). Both dopamine (DA, **18**) and glutathione (GSH, **19**) have free amine reactive handles in their structures, which meant that they could behave as a competitor to the iminoboronate linkage on the lysosome. The addition of both dopamine and glutathione showed that the reversibility was not only fast but went to completion via mass spectrometry studies.



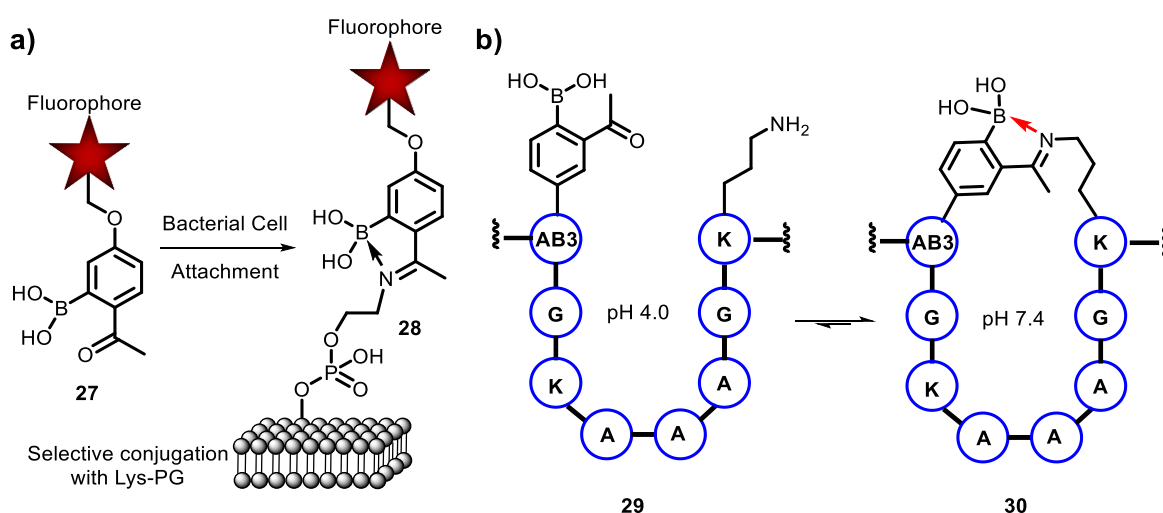
Scheme 4: a) Reaction of iminoboronate **13** with a fructose molecule **14**, which binds selectively at the boronic acid moiety to destabilise the iminoboronate to liberate the amine **15** and aldehyde **16** ; b) Reversibility of iminoboronate **15** with dopamine (DA, **18**) or glutathione (GSH, **19**).²⁸

Building upon this work, Bandyopadhyay *et al.* reported the selective targeting of bacterial *S. aureus* cells over mammalian cells with a fluorophore via iminoboronate formation at an overexpressed lysine-modified phosphatidylglycerol (Lys-PG) at the bacterial surface, with functionalised boronoketone (**27**).³¹ Nature primarily employs non-covalent mechanisms, such as hydrogen bonding to achieve specific molecular recognition. Covalent chemistry is therefore not well suited to targeting biomolecules of interest as the irreversibility can result in modification of unintended targets and consequently toxicity.^{45,46} Reversible

iminoboronate chemistry could solve this problem by creating a dynamic system under applied stimuli. An unnatural amino acid with a boronoketone handle **27** was synthesised to selectively target gram-positive bacteria which contained lipids with lysine functionalised head groups (Scheme 5a). *S. aureus* and *E. Coli* were selected as the initial bacterial targets, as they are known to have Lys-PG as the major lipids of their plasma membranes. In contrast, Lys-PG is absent from mammalian cell surfaces, allowing **28** to form selectively.^{47,48} The Gao group continued to use the dynamic linkage between Lys-PG and a boronoketone to screen diverse peptide libraries for the discovery of potent and selective targeting motifs against strain resistant bacteria.⁴⁹ The boronoketone can dynamically covalently bind with an overexpressed Lys-PG. The identified peptide probes of interest were then converted to bactericidal agents that deliver generic toxins to kill the targeted colistin-resistant *S. aureus* strain with high specificity. This work highlights the advantage of conducting large phage display libraries using iminoboronates compared to earlier phage display efforts where screening natural libraries were only able to yield sub-to-low millimolar binders of bacteria,^{50,51}

Further studies by Bandyopadhyay *et al.* described 'smart' peptides, in which the activity of the peptide can be switched on or off, mediated through macrocyclisation, enhancing their biological potency in response to biological stimuli.²⁹ Peptides have the capacity to engage in potent and selective interactions with protein surfaces, and hence their ability to modulate protein-protein interactions which are otherwise considered 'undruggable'. Cyclic peptides are a powerful tool in drug discovery, as they reduce the conformational entropy by pre-organising key functional groups, which increase target binding at the active site. By forming a cyclic peptide, the structures are rigidified in peptide conformations, they have prolonged biological activity by increases stability to proteolysis, and the binding efficiency for a target drug compound is improved. A boronoketone was installed at the termini of a peptide acid (Scheme 5b, **29**), whereby AB3 is an unnatural amino acid, which could undergo intramolecular cyclisation with a lysine side chain at the other end of the chain ($K_d \sim 10$ mM). This cyclic peptide could then reversibly become linear under applied stimuli, to bind to the target protein in response to pH changes or oxidation but was stable with respect to small molecule competitors. ¹H NMR showed that only the linear precursor **29** was observed at pH 4.0. Upon raising the pH to 7.4, the peptide sequence was then cyclised (**30**). The cyclised system **30** seemed to be very sensitive to the addition of hydrogen peroxide, and peroxytriate, which converted the boronic acid moiety into a phenol in less than 10 min. Due to loss of the dative bond from B–N interactions upon oxidation, rapid linearization of the cyclic peptide took place as confirmed by LC–MS analysis. In addition to pH and oxidation, the iminoboronate cyclised

peptides **30** show rapid response to α -effect nucleophiles, which were found to react with the boronoketone at neutral pH to form oximes and hydrazones as discussed in section 1.3.4 and 1.3.5.³¹ Although iminoboronate cyclised peptides **30**, were stable to endogenous nucleophiles like amines and thiols, they could be readily linearised by the addition of α -nucleophiles. To assess the potential of the iminoboronate cyclised peptides **30** for biological applications, the authors investigated the stability of the cyclic peptides in the presence of various biomolecules. Interestingly, it was found that the peptide cyclisation was not affected by small molecules like lysine, glucose, and glutathione, nor was it affected by model proteins or blood serum. This iminoboronate cyclised peptide offers a promising prospect which could serve as a powerful tool in biomedical therapeutics.



Scheme 5: **a)** Iminoboronate chemistry used to target and lysine-modified phosphoglycerol (Lys-PG) on bacterial cell surfaces;³¹ **b)** Iminoboronate-mediated peptide macrocyclisation with induced linearisation upon acidic pH or oxidation.²⁹

Akçay *et al.* reported the use of an *ortho*-boronoaldehyde and *ortho*-boronoketone to covalently target a noncatalytic lysine side chain **31** to give the first reversible covalent inhibitor of Myeloid cell leukemia 1 (Mcl-1), which is a protein-protein interaction target in cancer cell therapy (Fig. 4a).³⁰ Integrating a boronoketone or boronoaldehyde into the inhibitor **32** enhanced the binding affinity by 50 times compared to the non-covalent congeners, but also exhibited reversible binding at the Mcl-1 binding pocket. The reversible formation of the subsequent iminoboronate can therefore form much stronger interactions with the binding pocket compared to non-covalent interactions such as hydrogen bonding. This increase in potency revealed critical structure activity relationships and that *N*-alkylation of the indole was key to increasing the potency for Mcl-1. The increase in potency from the covalent interaction of the iminoboronate also demonstrated that the warheads did not appear to affect the compounds' ability to traverse the cell

membrane, which means that many different variations of warheads could be explored to find better protein-protein interaction of Mcl-1, without substantially affecting permeability. This binding serves as a useful starting point for the development of Mcl-1 therapeutics and probes to interrogate, which shows a potential long-term solution. However, much work is needed to functionalise the pharmacophore to form an effective drug as a competitive inhibitor of Mcl-1.

The Cockcroft group further explored the versatility of the lysine interactions with a functionalised boronoketone in forming reversible *ortho*-boronoimines (**33** and **34**) in nanopore systems.⁵² These approaches have proved to be a powerful technique for examining processes at the single-molecule level,^{46,53} providing information on molecular structure, binding and reactivity of a nanopore system.⁵⁴ The authors demonstrated the *in situ* synthetic modification of a wild-type α -hemolysin nanopore embedded in a membrane. The results show that reversible dynamic covalent iminoboronate formation and the resulting changes in the ion current flowing through an individual nanopore can be used to map the reactive behaviour of lysine residues within the nanopore channel (**33** and **34**). Crucially, the modification of lysine residues located outside the nanopore channel was found not to affect the stability or utility of the nanopore. Knowledge of the reactivity patterns enabled the irreversible functionalisation of a single, assignable lysine residue within the nanopore channel (Fig, 4b). Molecular information can therefore be deduced by monitoring the ion current flowing through a membrane, by use of iminoboronates as well as irreversible covalent interactions using click chemistry.⁵⁵

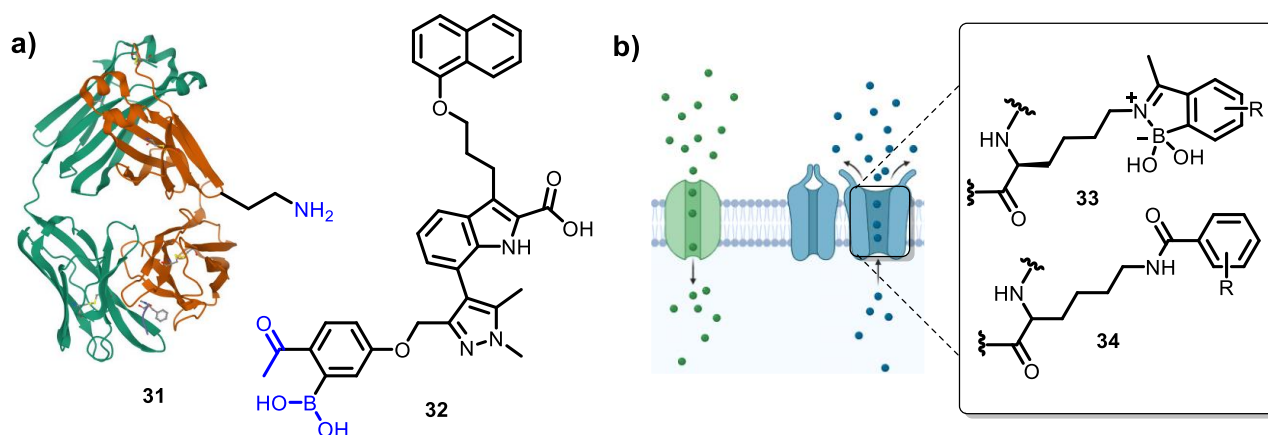
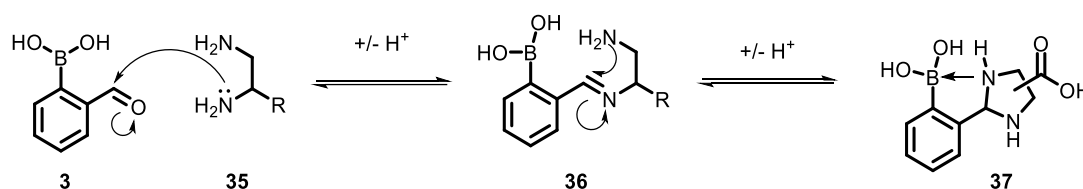


Figure 3: a) Mcl inhibitors with a boronoketone handle as new dynamic covalent Mcl-1 inhibitors targeting Lys-234.³⁰ b) Ion transport channel through an α -hemolysin trans-membrane protein using a lysine residue combined with a boronoketone.⁵²

1.2.2. 1,2-Diamines

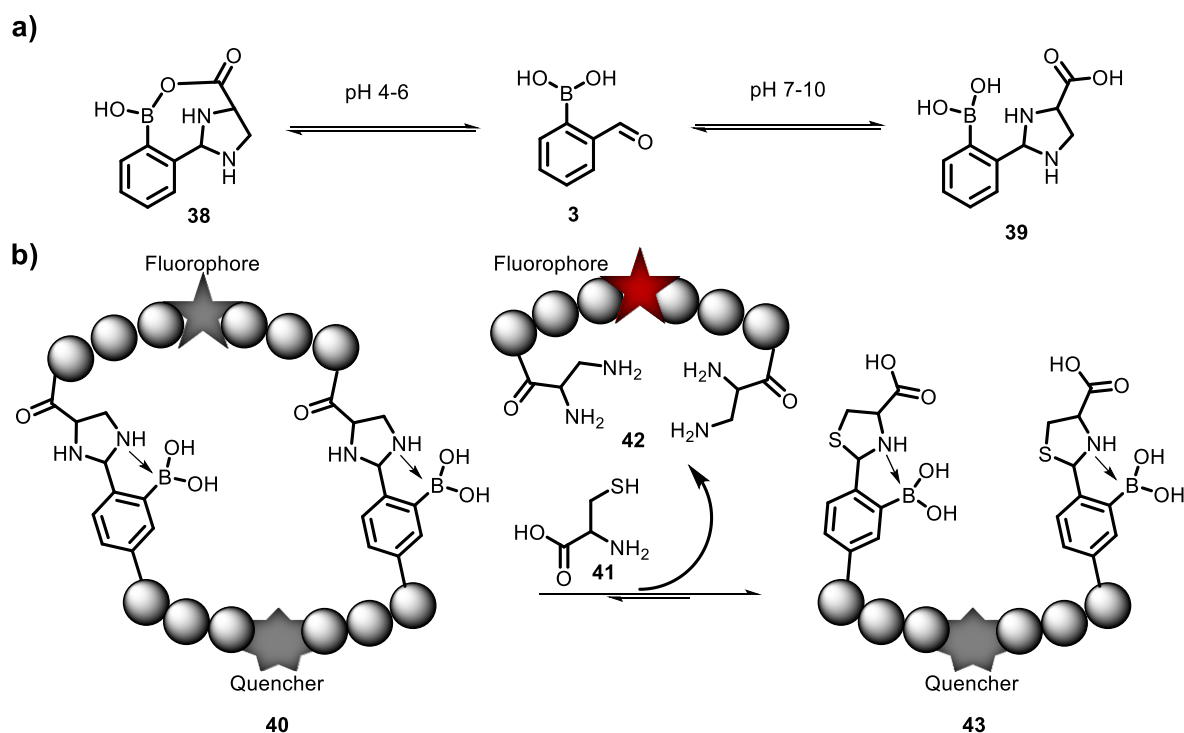
Simple amine building blocks were initially studied, but as a result of their diverse applications, more complicated amines have been explored. 1,2-Diamines such as **35** have emerged as a promising nucleophile for oBIDs, as they have two nucleophilic amines which can both react with the electrophilic carbonyl group of an aldehyde. Mechanistic and DFT studies have been performed which show that 1,2-diamine can react with 2-FPBA **3** to form an imidazolidino boronate **37**, as a stabilised 5 membered ring.²⁰ Mechanistically the first amine nucleophile generates imine **36**, followed by the attack of the second amine nucleophile to form a stabilised IzB derivative **37** (Scheme 6). The stability of the IzB group is increased by an order of magnitude with respect to a simple amine ($K_d \sim 10$ mM vs. 0.1 mM for diamine vs. amine respectively). The linkages also remain reversible, making them suitable for dynamic bio conjugation reactions, with two possible isomers.



*Scheme 6: Mechanism of imidazolidino boronate **37** formation with 2-FPBA **3** and diamine **35**.²⁰*

A study performed by the Gao group exploited the dynamicity of the reaction between 2-FPBA and a diaminopropanoic acid group to yield an imidazolidino boronate (IzB) complex.⁵⁶ A study of pH stability showed IzB formation **39** at higher pH between 7-10, but at lower pH saw a mixed anhydride formation between the -COOH of the propanoic acid group with the boronic acid to afford a cyclic structure **38** (Scheme 7a) Whilst this result is interesting in the context of this paper, it shows little significance in real-world applications as the 1,2-diamine group would rarely be functionalised with a carboxylic acid group. The authors reported the formation of the IzB complex with a $k_1 = 820 \text{ M}^{-1} \text{ s}^{-1}$, which is rapidly reversible under physiological conditions with a $k_{-1} = 0.082 \text{ s}^{-1}$ correlating to an apparent K_d of 100 μM . Despite the high dynamic reversibility of the IzB, surprisingly, the IzB linkage was found to be stable to addition of 10 equiv. of glucose, serine, lysine or glutathione via ¹H NMR. This result is even more surprising given the studies which report oBID cleavage to proceed via a dissociative mechanism, which with such a high dissociation constant, would be expected to lead to a significant amount of electrophilic aldehyde species to react with these additives.^{20,24,56,57}

However, addition of cysteine (Cys) did cause the dissociation of the IzB complex **40** via competitive thiazolidino boronate (TzB) formation. The reactivity of these groups will be discussed in detail in the next section. Specifically, the addition of 1 equiv. of Cys **41** converted 82% of the IzB complex **40** to the TzB complex **43**. Using the IzB kinetic data as a reference, a K_d of TzB could be calculated as 4.6 μM . The apparent bioconjugation of TzB **43** formation over IzB **40** formation was tested to form Cys-responsive peptides. The authors developed fluorogenic reporters of Cys **41** using the IzB/TzB exchange (Scheme 7b). This mechanism worked by quenching the fluorescence from a fluorophore connected to the IzB **42** bound complex, which was then able to fluoresce upon dissociation of the 1,2-diamino group, and subsequent formation of the TzB complex **43**. The fluorescence titration experiment appeared to be highly specific to Cys, with no fluorescence increase observed with the addition of glutathione, glucose, serine, or lysine. Given the apparent stability of the TzB complex in the presence of 10 equiv. of small molecule competitors, this work creates the potential to introduce ‘smart’ peptides, which specifically react with NCys in a number of dynamic applications providing an exciting prospect in bioconjugation.

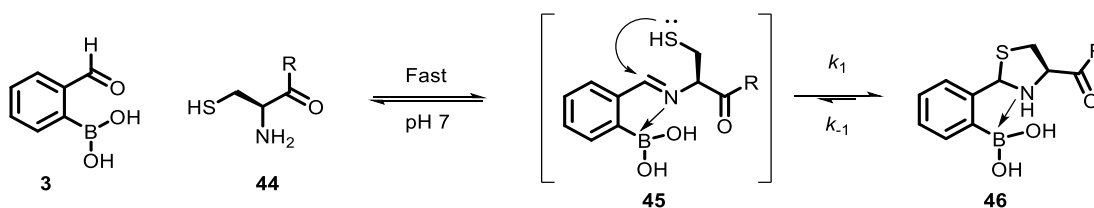


Scheme 7: a) imidazolidino boronate conjugation at varied pH, to show standard IzB formation between pH 8-10 and further cyclisation between pH 4-6.⁵⁶ b) Conversion from IzB iminoboronate quenched fluorophore to the thermodynamic TzB product with reaction of Cys, liberating the fluorophore causing an increase in fluorescence.⁵⁶

1.2.3. 1,2-Aminothiols

The low abundance of cysteine (Cys) and the high reactivity of the thiol side chain have made the Cys residue a popular handle for site-selective modification of peptides and proteins.⁵⁸ Placing this Cys at the *N*-terminus has an added benefit for selectivity, providing a 1,2-aminothiol for site-specific proteins modification. Therefore, efforts to target *N*-terminal cysteines (*NCys*) in bioconjugation reactions are advantageous over alternative binding sites for protein modifications and have been explored with reactions with *o*BA. Although *NCys* is well known to conjugate with aldehydes to give thiazolidines, the reaction requires acidic conditions and suffers from slow kinetics typically being formed with high concentrations of reactants and long incubation time (~2 days), even at pH 5.^{59,60} In contrast, when a *NCys* moiety reacts with an *o*BA, the reaction readily proceeds under neutral conditions with fast kinetics. Studies have shown that the sulphur group is able to form a 5-membered stabilised thiazolidino boronate (TzB) structure **46** (Scheme 8), similar to the IzB structure discussed previously. For a full and comprehensive broader understanding on the reactivity cysteines for protein modification, the reader is directed to an excellent review was recently published by the Gao group in 2022.⁵⁸

TzB formation was first established by the Gao group in 2016, with forward rate of reaction ($k_f = 5.5 \times 10^3 \text{ M}^{-1} \text{ s}^{-1}$) amongst the fastest bioconjugation reaction known at that time.^{61–63} The free *NCys* **44** of the peptide chain was able to react with FPBA **3** to form an imine intermediate **45**, before forming a thiazolidino boronate (TzB) structure **46**, which exhibits impressive stability due to the 5-membered ring formation. The authors were able to confirm the TzB structure through ¹H and ¹¹B NMR studies.³¹ To further demonstrate the utility of the TzB conjugation chemistry for protein labelling, the authors synthesised a fluorophore labelled *o*BA, as well as a small model protein bearing a Cys at its *N*-terminus, which when mixed together, at 10 mM concentration in a pH 7 buffer, complete conversion to the TzB occurred after 30 min. To explore the application of TzB chemistry in biological systems, the TzB structures were exposed to a number of competitive inhibitors. Remarkably, ¹H NMR studies found that TzB stability was not affected by fructose serine, lysine, glutathione or cystine. These results showcase the high specificity of the TzB conjugation chemistry towards 1,2-aminothiols. Further studies saw slight dissociation at pH 5 (10%) and 4 (26%) via ¹H NMR. Adding free Cys at equimolar concentration resulted in ~50% conversion of the functionalised TzB conjugate to the 2-FPBA–Cys conjugate. These data suggest boronoaldehyde labelled proteins may slowly exchange with free Cys. However, it should be noted that free Cys only exists at low mM concentrations in blood.

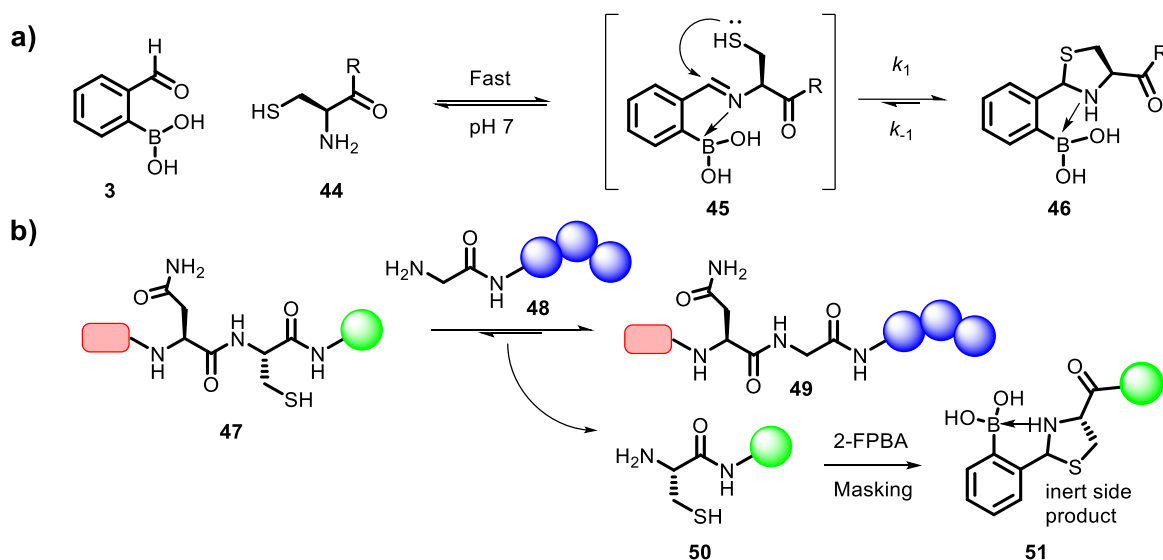


Scheme 8: Thiazolidino boronate **46** formation from cyclisation;⁶¹

Around the same time, the Gois group independently reported TzB formation. The structure of TzB 5-membered ring was confirmed by crystal structures and supported by the density functional theory (DFT) calculations, with boron activating the imine, promoting the formation of the S-C bond, as well as the stabilisation of the N→B interaction. However, the authors reported a rate of formation of TzB of $2.38 \times 10^2 \text{ M}^{-1} \text{ s}^{-1}$ in physiological conditions.³⁴ This reported rate of formation is almost an order magnitude discrepancy from the constants reported by Bandyopadhyay *et al.* This discrepancy highlights the need to conduct a uniform study of iminoboronates under exactly the same conditions as the highly dynamic nature of TzB formation and oBIDs in general are highly sensitive to environmental conditions and alternative analytical techniques used. The difference in these rates of formation is assumed to be due to subtle differences in the reaction conditions, backbone structure of the Cys moiety or analysis methods. For example, the studies performed by Gao were done in pH 7.0 buffer at room temperature, whereas Gois reported rates at pH 7.4 at 23 °C. Gao also measured the rate of formation using a titration experiment, whereas Gois elucidated rates using UV-Vis and mass spectrometry. These varying conditions and analytical techniques therefore lead to significant discrepancies in kinetic data, highlighting the need for a uniform study, which is recognised as a significant gap in the literature.

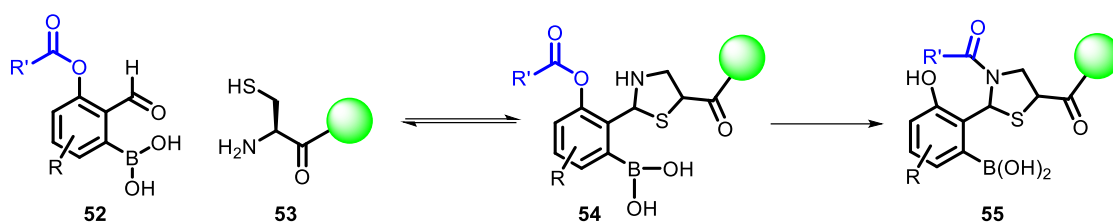
More recently, Tang *et al.* explored chemo-enzymatic protein labelling, using an asparaginyl endopeptidase (AEP).⁶⁴ AEPs can be used for protein labelling, but suffer from high reaction reversibility which therefore requires a large excess of modified substrate. Though this is possible for low value reagents it limits the biological potential of AEPs. Therefore, using iminoboronates to form these linkages was explored by reaction with a functionalised NCys with 2-FPBA. This reaction used an Asn-Cys-Leu sequence (**47**) recognised by AEP, to produce a Cys-Leu by-product (**50**). Commercially available 2-FPBA **3** then served as a scavenger to convert **50** into an inert TzB group (**51**) by formation of a stable oBI, preventing **50** taking part in the reverse reaction (Scheme 9). This consequently drove the AEP labelling reaction forward to product formation **49** with a lower ratio of label to protein substrate. This approach therefore allowed successful labelling of

green fluorescent proteins (eGFP), beta-lactamase and ubiquitin proteins using the endopeptidase in a highly selective reaction.



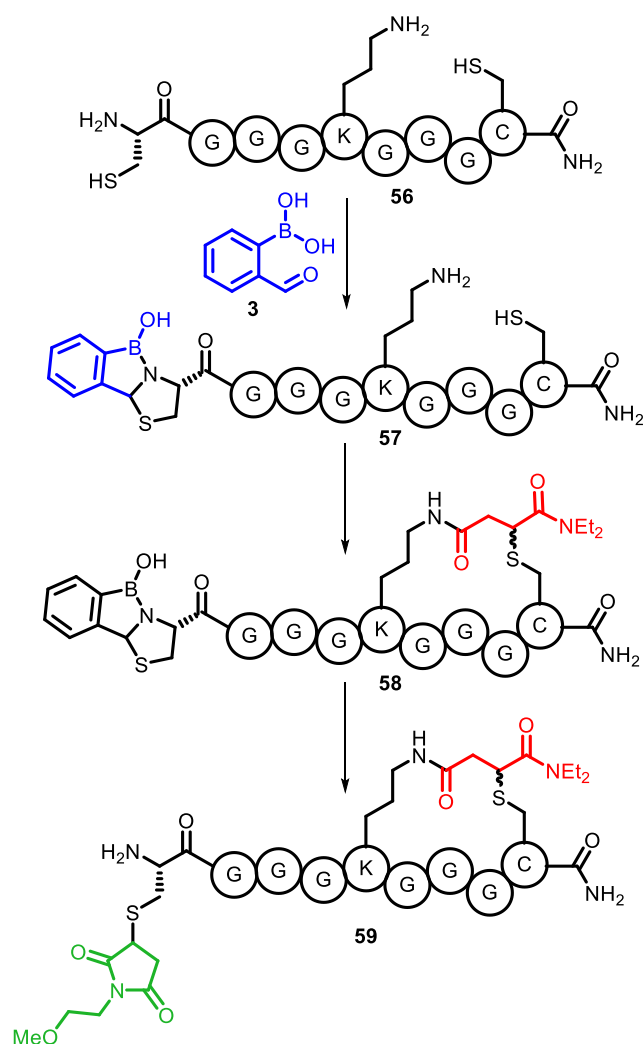
Scheme 9: a) Thiazolidino boronate **46** formation from cyclisation;⁶¹ b) Scavenging NCys in asparaginyl endopeptidase labelling **49** by tapping with 2-FPBA to give an inert side product **51**.⁶⁴

In the rapidly expanding literature in TzB formation, Li *et al.* recently published a rapid and selective NCys modification through acyl transfer (Scheme 10).³⁵ This NCys conjugation proceeded via a TzB intermediate with a functionalised boronoaldehyde group consistent with a previously reported rate of formation of $k_1 = 5.5 \times 10^3 \text{ M}^{-1} \text{ s}^{-1}$. Rather than exploiting the reversible nature of the TzB formation, Li *et al.* prevented the reversibility of this dynamic linkage, via a subsequent TzB-mediated acylation reaction of NCys that gave a stable amide bond (Scheme 10). In this system, **52** underwent reaction with the 1,2-aminothiol of NCys protein **53**, to form a TzB group **54**. The secondary amine of the TzB group then reacted with the *ortho*-acyl group to form a new TzB group **55**. This study was shown to selectively label proteins with NCys. The authors went on to test this chemistry on the surface of phage, treating with acyl functionalised boronoaldehyde and the extent of phage biotinylation was assessed. They found that NCys sites could be effectively biotinylated. This chemistry could therefore find applications in bacteriophage displays, to allow facile chemical modifications of phage libraries, which would greatly expand the chemical space amenable to phage display.



Scheme 10: Acyl transfer via thiazolidino boronate cyclisation to form kinetically stable acyl product.³⁵

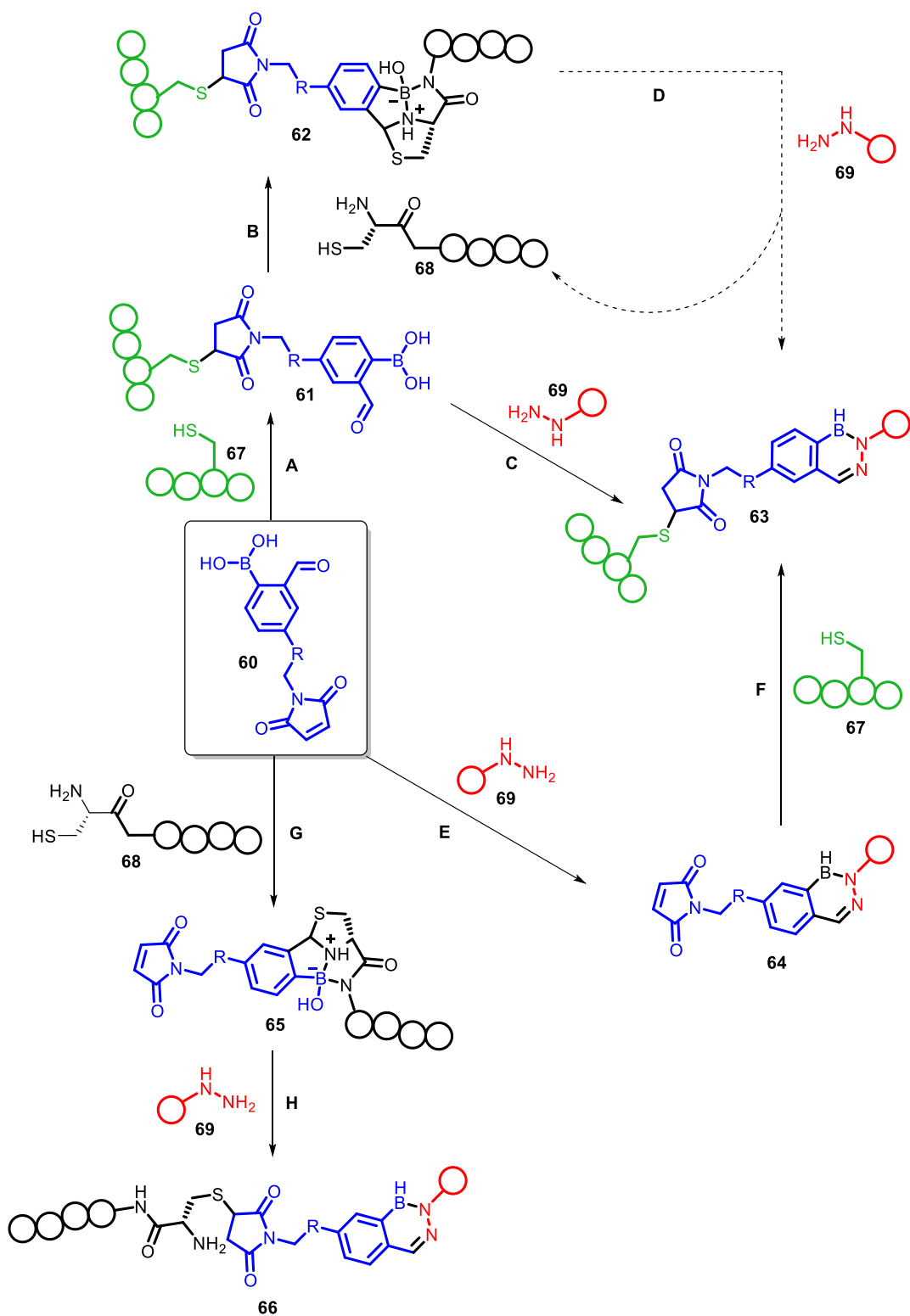
In two very recent studies, the Gois group have exploited the reversibility of the TzB linkage to form highly chemoselective reactions on peptides via initial TzB protection, peptide modifications at a different site, followed by cleavage of the TzB linkage. Firstly, an efficient peptide stapling method using amino-sulhydryl functional groups was reported.⁶⁵ The authors combined both a Michael acceptor as well as an *N*-hydroxysuccinimide (NHS)-activated ester to generate a bifunctional reagent in a chemoselective amino-sulhydryl reaction to further expand the utility of *N*-terminal Cys bioorthogonal modification of peptide structures (Scheme 11). In the selective modification of the *NCys*, the 1,2-aminothiol (**56**) is first protected using boronoaldehyde (**3**), to form a TzB group (**57**), which masks the reactivity of the Cys functionality. This therefore allows the selective formation of the macrocycle by addition of NHS-activated acrylamide to a lysine and internal cysteines to form intermediate **58**. The dynamic reversibility of the TzB can therefore allow for its cleavage, followed by the selective modification of the *NCys* with a maleimide to afford **59**. This therefore opens up the possibility for iminoboronates to serve as reversible protecting groups, to mask reactive amine-based nucleophiles to allow selective reactions. Iminoboronates can then be easily cleaved as a result of the dynamic reversible bond, which highlights their real-world applications.



Scheme 11: Orthogonal modification of model peptides using 2-FPBA protection group chemistry (**57**) to allow selective reaction of lysine reactive handle (**58**), followed by deprotection to allow further selective reaction at the Cys residue (**59**).⁶⁵

In the second study, a heterobifunctional 2-FPBA-maleimide crosslinker was developed to explore its versatility in the preparation of various bioconjugates.⁶⁶ Given the reversible nature of TzBs, the authors could add a more reactive hydrazine moiety to the steps C, D, E and H, which would displace the TzB and produce a hydrazone, which could later cyclise to form a diazoboronate (DAB) species (details are covered in Section 1.3.5.). The authors describe an easily modified peptide/proteins chain, by the reversible addition of an NCys for TzB formation, followed by hydrazine addition for DAB formation (Scheme 12). This allows the authors to form a wide variety of products from the same starting point, by the competition of oBID formed. Firstly, the *ortho*-boronic acid **60** reacted with an NCys residue **67** (step A) to form **61**, which then react with either another NCys **68** (step B) or a hydrazine **69** (step C) to form a TzB (**62**) or DAB (**63**) linkage respectively. Given the reversible nature of TzB ($K_d \sim 5 \mu\text{M}$), the addition of a more reactive hydrazine **69** (step D) to this mixture would displace the TzB (**62**) to form DAB (**63**). A complementary alternative

relies first on the addition of a hydrazine **69** that would react specifically at the 2-FPBA (step E, **64**) and, in a second step, the addition of a Cys-biomolecule **67** (step F) to produce the biofunctionalized DAB **63**, as in the previous path but through an alternative route. Using a different approach, in the presence of a protein/peptide bearing an *NCys* **68** (step G), the cross-linker could be reacted to form the TzB **65**. After the initial bioconjugation, hydrazine **69** could be added (step H) displacing the TzB, resulting in the formation of a DAB **66**. The cross-linker's maleimide would then be available to react with a terminal cysteine to afford the thio-succinimide bioconjugate (Scheme 12). The possibility of generating a broad range of products relying solely on the reagents used and their order of addition highlights oBIDs versatility and broad range of possible applications in chemical biology.

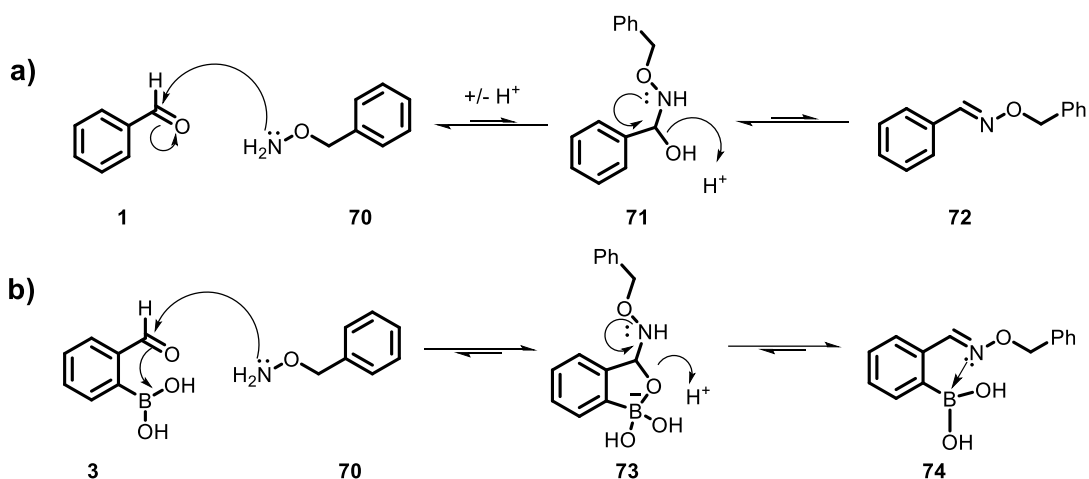


Scheme 12: Versatility of 2-FPBA-maleimide **60** crosslinker to form a range of products (**61-66**) using NHS-esters and oBID formation.⁶⁶

1.2.4. Hydroxylamines

A review on oxime formation by the Kool group highlights the significant potential of using hydroxylamines in bioconjugation reactions.⁶⁷ One of the oldest biorthogonal reactions is that of heteroatom bonded amines, which are referred to as α -nucleophile effect amines (hydroxylamine, hydrazine, and other amine-nitrogen compounds), with carbonyl groups (aldehydes or ketones).⁶⁸ Hydroxylamines can react with carbonyl groups in an aldehyde or ketone to form an oxime linkage (Scheme 13a) and have found uses in polymer chemistry, biomaterials, hydrogels, dynamic combinational therapy, chemistry and chemical biology.^{36,69,70} These diverse applications are owed to the comparatively fast rates of reaction compared to standard imine formation as well as the reversibility of these linkages via hydrolysis. These oximes are highly stabilised relative to a standard imine as a result of the oxygen species, which increases the electron density at the amine nucleophile. However, there are significant drawbacks to this chemistry, requiring large concentrations of aniline catalyst and low pHs for efficient oxime formation.⁷¹⁻⁷⁵ Without aniline and at neutral pH, these linkages are comparatively much slower to form. The low pH and high concentration of catalysts required therefore limit the applications of chemistry using hydroxylamine, impose significant impracticalities for biological studies. Boronoaldehydes and boronoketones can form much more rapid and stabilised linkages with the addition of an *ortho*-boronic acid group to drive borono-oxime formation to via introduction of stabilising B–N interactions. The accelerated rate of formation is driven by the thermodynamics of the stabilising B–N formation which is able to donate electron density into the empty p-orbital of the boron, significantly accelerating and stabilising the rate of borono-oxime formation (Scheme 13b). Specifically, the imine formation is typically rapid and hence dehydration is the rate determining step in oxime formation. Boronic acids are in an equilibrium with the boronate form in water, with the hemiaminal equilibrium shown in the bottom of Scheme 13b.⁷⁶ For oxime condensations, upon addition of a hydroxylamine **70** with 2-FPBA **3**, the resulting tetrahedral intermediate can substitute for a water on the boron to give a cyclic boronate **73**. In a normal oxime condensation (Scheme 13a), the O-alkylhydroxylamine **70** is more basic than the alcohol lone pair in the hemiaminal intermediate **71**; hence intermediate **71** is preferred, and the forward reaction is correspondingly slower. When boron is present the competition is now the boronate **73** versus the protonated O-alkylhydroxylamine **70** as the leaving group. The preference for boronate elimination favours productive oxime formation **73** leading to faster rates than in the parent oxime formation. The direct involvement of the vacant boron p-orbital is further supported by experiments where tripodal ligands or fluoride substituents on the boron

abolished the rate acceleration.³⁶ A disadvantage of the boron-assisted oxime formations is their reversibility. The formation of **74** that has been reported to give the most stable adducts but even these have a reverse rate constant of $k_{-1} 4.2 \pm 0.4 \times 10^{-5} \text{ s}^{-1}$, meaning adducts can be hydrolysed completely under the right conditions. Oxime condensations with 2-FPBA do, however, have large equilibrium constant of $>10^8 \text{ M}^{-1}$, and this mitigates the reversibility problem since even at nanomolar concentrations of starting materials the oxime will predominate at equilibrium.



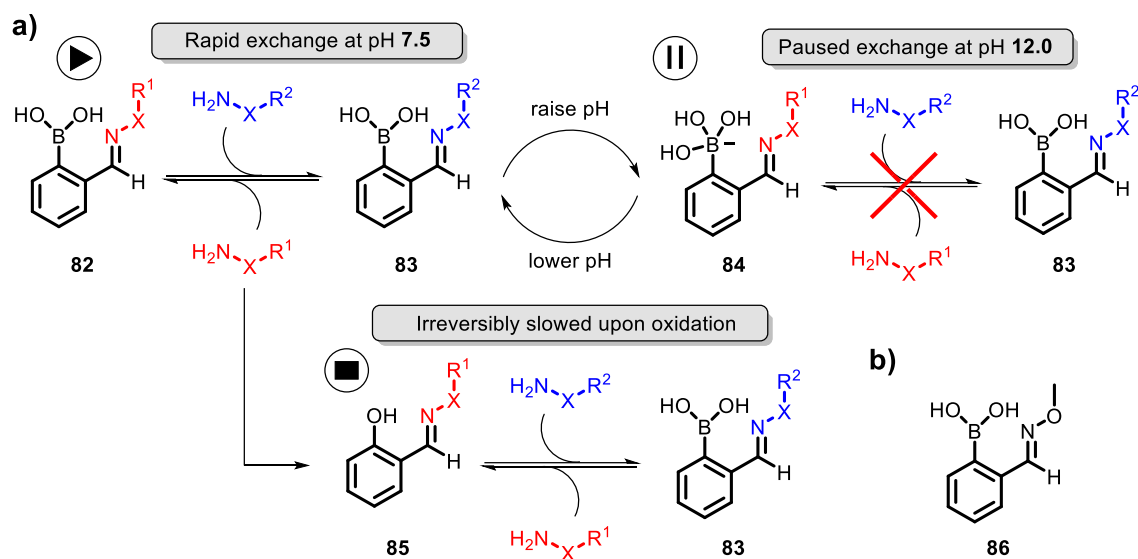
Scheme 13: a) Oxime formation between benzaldehyde and hydroxylamine to give slow formation of oxime linkage in the absence of aniline in physiological conditions. b) Rapid formation of borono-oxime linkage as a result of a stabilised boronate intermediate which drives the thermodynamics of the reaction to accelerate borono-oxime formation.

The first report of such borono-oxime was reported by the Gillingham group, with boron-assisted oxime formation proceeding with rate constants $> 1 \times 10^4 \text{ M}^{-1} \text{ s}^{-1}$, under physiological conditions.¹⁶ This rate of formation is faster than oxime formation, even in the presence of large concentrations of aniline catalyst, which have $k_1 \sim 1\text{-}100 \text{ M}^{-1} \text{ s}^{-1}$, and far faster than oxime formation in the absence of aniline catalyst ($k_1 \sim 1 \text{ M}^{-1} \text{ s}^{-1}$).^{71,77} Therefore subsequent borono-oxime formation is accelerated relative to a standard aldehyde by several orders, and can be performed in physiological conditions in the absence of catalysts, increasing the biological potential for these linkages. The dissociation of oxime conjugation with 2-FPBA, which was determined by an oxime-oxyamine exchange experiment was determined to be $k_{-1} = 4.2 \times 10^{-5} \text{ M}^{-1} \text{ s}^{-1}$, which is just slightly higher than that of oximes without a boronyl substituent.⁷⁸ Bandyopadhyay *et al.* reported another early study on oxime formation by an analogous reaction of a hydroxylamine combined with 2-APBA to form an borono-oxime linkage.⁷⁹ The boronic acid moiety greatly accelerates the conjugation of 2-APBA to various hydroxylamine nucleophiles at neutral pH. This study was also the first to recognise that the oBID conjugates also display faster rates of hydrolysis (k_{-1}) and dynamic exchange. In stark contrast to the previous study by Gillingham and co-workers, Bandyopadhyay *et al.* found

the conjugation of 2-APBA with an alkoxyamine to be instantaneously reversible upon dilution.⁷⁹ They estimated K_d to be 1.4×10^{-5} M, which is 3 orders of magnitude larger than that of 2-FPBA (K_d : $\sim 10^{-8}$ M). ^{11}B NMR analysis of the 2-APBA oxime conjugate revealed a broad and slightly upfield shift of the boron peak, indicating partial formation of the N–B dative bond, which accelerates the hydrolysis of the conjugate. The distinct difference in stability is remarkable given that 2-FPBA and 2-APBA only differ by a methyl group. At a first glance, these differences in stability could be attributed to different analytical techniques which were used to determine the reaction kinetics between these studies. The reaction kinetics were measured via a fluorescence-quenching assay with fluorophore/quencher-labelled reactants by Gillingham, and ^{11}B NMR and titration experiments via UV-Vis absorbance by Bandyopadhyay. However, these studies in fact highlight the difference in reactivity and stability between the aldehyde precursor of 2-FPBA, versus the ketone precursor in 2-APBA. Results from the Gao lab suggest that 2-FPBA adducts are generally more stable and better suited to bioconjugation, while 2-APBA adducts are more labile and better suited to applications like dynamic combinatorial chemistry. These results show that in 2-FPBA, boronic acids form stabilised B–N interactions through hydrogen bonding and the coulombic interactions which operate harmoniously to form oBIDs.¹⁸ Calculations on 2-APBA suggest that Lewis acid/base interactions are the key in stabilising oBIDs.²⁸

More recently, Han and Domaille attempted to tune the exchange dynamics of borono-oximes with pH and redox control.⁶⁹ The study used 2-FPBA to show that oxime substrates can undergo exchange with α -effect nucleophiles such as hydrazine, in a pH dependent manner (Scheme 15a). The reaction between 2-FPBA and *O*-methylhydroxylamine (MHA) forms **86** quickly and hydrolyses at a relatively fast rate ($k_1 = 460 \pm 14 \text{ M}^{-1} \text{ s}^{-1}$ and $k_{-1} = 3.2 \pm 0.2 \times 10^{-4} \text{ s}^{-1}$, respectively) at pH 7.5 (Scheme 15b). Next, a pH switch was established for the borono-oxime and DAB formations and stabilities. Hydrazone and oxime stabilities are well-established to be dependent on pH conditions.^{80,81} To explore how sensitive the dynamics of this particular class of 2-FPBA-derived hydrazones/diazaborines and oximes are to pH, the authors measured the kinetics of formation and hydrolysis of **86** at 15 °C at pH 6.5, 7.4, 8.5, 9.5, and 12.0. Kinetic analysis enabled the extraction of both k_1 and k_{-1} , which could delineate the influence of pH on each process independently. Within the explored range of pH, k_1 and k_{-1} decrease as a function of pH, which resulted in three orders of magnitude difference in the rates between pH 6.5 and 12.0. The K_d for oxime **86** also decreased as the pH increases, indicating a more stable linkage. From pH 6.5–12, borono-oxime **86** show K_d values on the order of 10^{-5} – 10^{-6} despite large changes in their k_1 and k_{-1} values. This data allowed the exchange of the borono-oxime moiety **82** for a

hydrazone/DAB formation **83** using this pH switch (Scheme 15a). At higher pH of 12.0, the switch from **84** to **83** was halted.

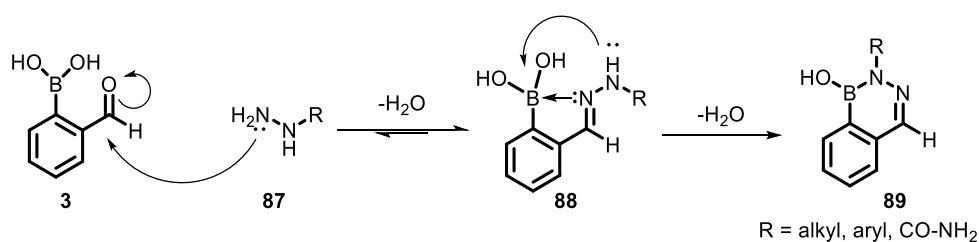


Scheme 14: **a)** 2-FPBA-derived oximes and hydrazones are activated by the proximal boronic acid catalyst. Reversibility is paused and activated with pH control and irreversibly slowed by oxidising the boronic acid with H_2O_2 . **b)** Borono-oxime conjugate **86** used for kinetic studies.⁶⁹

These reversible and stable linkages are useful in the context of bioconjugation, but critically, the reliance on pH switching limits the potential, as these pH changes are not biocompatible. The authors also showed that oxidation of the arylboronic acid **82** using hydrogen peroxide generated phenol **85** effectively which abolished the rapid dynamics of the borono-oxime,^{82,83} slowing the rate of oxime formation by more than 30 000 times and increasing the hydrolytic half-life from 50 minutes to 6 months at physiological pH (Scheme 15a). This was due to the loss of B–N interactions which means the borono-oxime derivative reverts back to a standard oxime, with very slow reaction kinetics ($k_1 \sim 0.1 \text{ M}^{-1} \text{ s}^{-1}$)^{71,77} However, upon oxidation of the *ortho*-boronic acid, the boron moiety is cleaved, making this process irreversible, unlike the pH switch described above. Additionally, considering the biocompatible nature of oBID linkages, the use of hydrogen peroxide reduces the scope of bioconjugation in chemical biology due to the high reactivity of peroxides. Nonetheless, these results consolidate knowledge on borono-oxime formation and stability and offer an effective way to cleave the stabilised linkages in dynamic combinational libraries, reverse bioconjugation and in self-healing materials.

1.2.5. Hydrazines

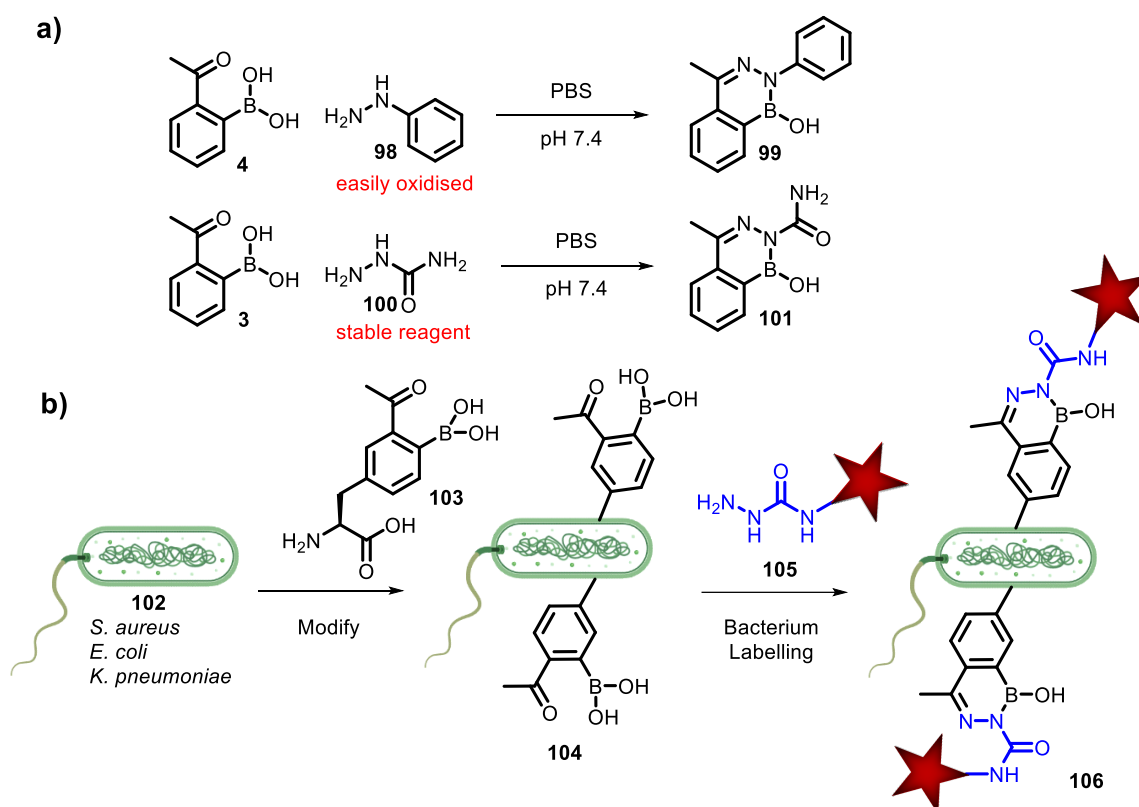
Another class of α -nucleophiles established to react with aldehyde and ketones in the literature are hydrazines, which react to form hydrazones. Although these linkages are used widely, these reactions suffer from the same drawbacks as oxime formation, with low pH needed and high concentrations of aniline catalysts required to achieve $k_1 \sim 1 \text{ M}^{-1} \text{ s}^{-1}$, limiting the scope of their potential in chemical biology.^{73,74} Following the same justification from the borono-oxime, by introduction of a boronic acid group *ortho*- to the carbonyl group, the formation of the resultant hydrazone linkage is both accelerated and stabilised by B–N interactions. The first report of 2-FPBA reacting with a hydrazine to form an oBID was from the Bane group,^{80,84} who found that an *ortho*-boronic acid on an aromatic aldehyde accelerates the speed of reaction by at least three orders of magnitude. The resulting product, however, was found not to be the expected hydrazone **88**. Instead, a second dehydration reaction occurs, forming a substituted 1,2-dihydro-1-hydroxy-2,3,1-benzodiazaborine (DAB, **89**) as the final product (Scheme 16a). The changes in the absorption spectrum as a function of time provide qualitative support that the DAB cycle forms rapidly after hydrazone formation. The authors characterised this by the immediate appearance of a lower energy band in the difference UV spectra which was characteristic of hydrazone formation.⁸⁵ Loss of this low energy band over time was accompanied by an increase in a higher energy region of the spectrum which is consistent with a conjugated system becoming an aromatic molecule.⁸⁶ X-ray crystallography and ^1H and ^{11}B NMR spectroscopy confirmed this structure to be a 6-membered DAB ring.



Scheme 15: Mechanism of DAB **89** formation through hydrazone intermediate **88** with hydrazine.^{80,84}

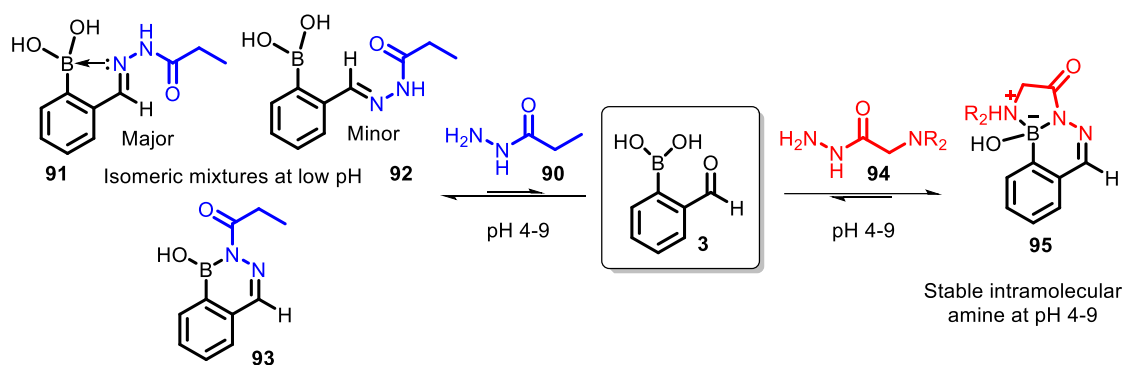
Building on this work, the Gao group reported DAB formation as a bio-conjugation strategy by reaction of 2-APBA and a hydrazide moiety.⁵⁷ Hydrazides have a subtle difference in their structures to hydrazines, by addition of a carbonyl group at the α -position. Hydrazone moieties are less ideal for bioconjugation reactions than hydrazides, due to the poor stability in physiological conditions and cytotoxicity of some derivatives such as phenylhydrazine **98** (Scheme 16a).⁵⁷ Rapid formation of the DAB ($>10^3 \text{ M}^{-1} \text{ s}^{-1}$) was used to selectively label bacterial pathogens (Scheme 16b). A synthetic amino acid D-AB3 **103**,

which presented a 2-APBA moiety on its side chain was found to incorporate into the cell wall of several bacterial species **104** by means of a fluorophore-labelled semicarbazide **106**. This therefore allowed the robust detection of bacterial pathogens in blood serum. This was the first report of a hydrazide being used to conjugate to 2-APBA, which reacts analogously to hydrazine, with a slightly different electronic effects due to the carbonyl functional group. The DAB linkages formed between the semicarbazide **100** and 2-APBA ($k_2 = \sim 3 \times 10^3 \text{ M}^{-1} \text{ s}^{-1}$) and 2-APBA ($k_2 = \sim 1 \times 10^3 \text{ M}^{-1} \text{ s}^{-1}$) have a backwards rate of reaction which were reported as irreversible linkages, and stable indefinitely in physiological conditions, buffers and serum. The formation of DAB **101** is 2-3 orders of magnitudes faster than widely used azide-alkyne click reactions.⁸⁷ Interestingly, this bioconjugation allows for the preferential labelling *E. coli* over several other bacterial species such as *S. aureus*, a gram-positive bacterium (Scheme 17b). The favourable incorporation of D-AB3 into *E. coli* is particularly interesting given that previously reported amino acids that modify peptidoglycans largely favour Gram-positive bacteria over Gram-negative ones.^{88–90} The Gram-positive selectivity of these amino acids was believed to originate from their poor outer membrane permeability, which meant the *S. aureus* was 50 times more selective than *E. coli*. according to flow cytometry analysis.



Scheme 16: a) Diazaborine formation of semicarbazide in comparison to that of phenylhydrazine. b) Two-step protocol for bacterial cell labelling with 2-APBA functionalised bacteria **103** with fluorescently labelled hydrazide **104** to form semicarbazide **105**.⁵⁷

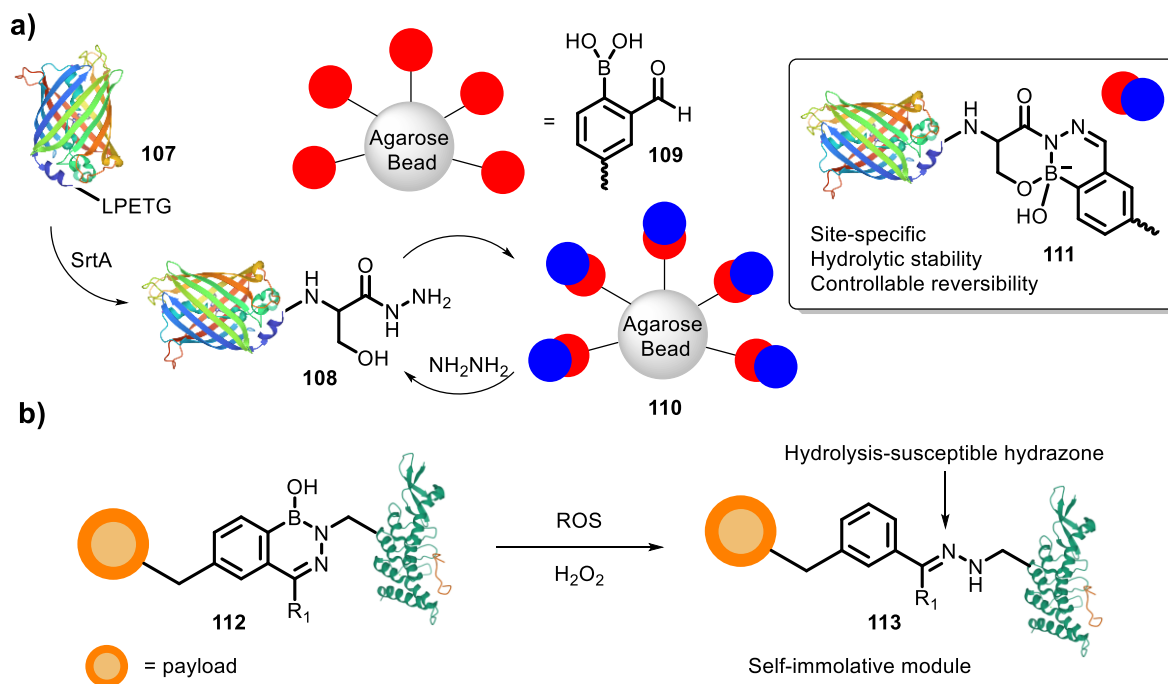
The Bane group found analogous reactivity with hydrazides and reported that at a high pH (pH 9), the DAB **93** exists as the only species, whilst at lower pH (pH 6), an equilibrium existed between **93** and two isomeric forms of the hydrazone **91** and **92**. This suggests that the Lewis acidity towards the boronic acid of the amide-like nitrogen triggers a ring closure at higher pH, with a pK_a of ~ 6.3 . The authors also noted a niche functionalised DAB stable across pH 4-9 in which a secondary amine conveniently placed to cyclise further with the boron moiety led to the formation of **95** (Scheme 17) In monitoring these interactions at mM concentrations using absorption spectra, the authors recognised that the reactions were too rapid to record meaningful rate constants for hydrazone/DAB formation though they estimate $k_1 \sim 1500\text{-}2500 \text{ M}^{-1} \text{ s}^{-1}$ (compared to $k_1 \sim 1 \text{ M}^{-1} \text{ s}^{-1}$ in absence of *ortho*-boronic acid), with a large error associated. This approximation highlights the necessity to find a more accurate method of analysing these rapid linkages.



Scheme 17: 2-FPBA reacting with hydrazine derivatives to form stable thermodynamic molecules, with a significant pH dependency.

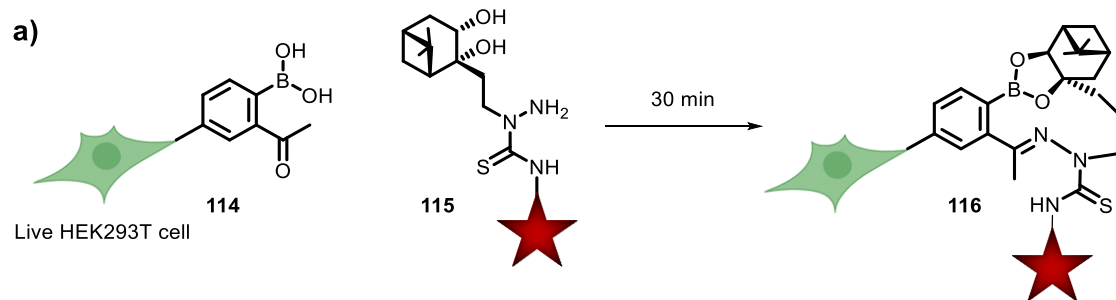
Further research recently explored by the Bane group exploited β -hydroxyl-functionalised hydrazides for C-terminal protein modification (Scheme 18a).⁷⁰ DAB structures can form quickly in physiological conditions, averting interference from endogenous biomolecules in selective reactions. C-terminal threonine and serine hydrazides were appended to a model enhanced green fluorescent protein **108** (eGFP), using sortase-mediated ligation (SML). Labelling with a functionalised boronoaldehyde **109**, through a hydrazone linkage **111**, with fluorescent probes could be performed rapidly at micromolar concentrations to modify the C-terminus of an over-expressed agarose bead **110**. Very recently, DABs linkages were used to form antibody drug conjugates (ADC) by the Gois group, which have emerged as a promising therapeutic class for cancer treatment due to their enhanced toxicological profile and selectivity.⁹¹ Boronoaldehydes and boronoketones reacted with a hydrazine species to form a hydrazone/DAB **112**, which was used to functionalise a laminin peptide by attachment of a payload (Scheme 18b). These DAB linkages (**112**) were stable for extended periods in buffer and plasma. However, a reactive oxygen species,

such as H_2O_2 in this case could be added, which selectively cleaved the boronic acid moiety in the DAB **113** linkage. The hydrazone/DAB linkage therefore became more sensitive to hydrolysis ($k_1 \sim 1 \text{ M}^{-1} \text{ s}^{-1}$), leading to the hydrolysis of the hydrazone (Scheme 18b). These linkages could therefore be used to form responsive linkages for forming ADCs for cancer therapy.



Scheme 18: **a)** Fluorescent labelling and immobilization of enhanced green fluorescent protein **110** through 2-FPBA- β -hydroxy hydrazide linkage **111**;⁷⁰ **b)** Oxidised DAB **113** using reactive oxygen species (H_2O_2) as responsive linkers for targeting drug conjugates.⁹¹

As well as these standard DAB linkages, analogous reaction of functionalised boronoketone **114** with thiosemicarbazide **115** were proposed be useful for cancer therapy. The Hall group harnessed this chemistry to biologically target and tag proteins in an effective 'on' and 'off' switch using a thiosemicarbazide derivative **115**. Successful methods to biologically label HEK293T cells with a fluorophore were achieved through a thiosemicarbazone intermediate **116**.⁹² These linkages also incorporated a distal diol which could form an boronic ester group to further stabilise the conjugate. Although slightly different chemistry to a standard hydrazine, with a resultant hydrazone/DAB linkage, these thiosemicarbazone linkages were stable in aqueous buffer, fast, irreversible, and allowed the attachment of a fluorophore to biologically label HEK293T cells (Scheme 19). Unlike reactions with hydrazines, thiosemicarbazones are unable to form a DAB-like stabilised structure, and therefore the rates of formation and subsequent stability are much lower relative to DAB.



Scheme 19: Synergistic design based on the optimal placement of a hydrazine or thiosemicarbazide on the nopol diol reagent, along with a carbonyl handle on the arylboronic acid.⁹²

1.3. Conclusion

Reactions between *ortho*-boronoaldehydes and *ortho*-boronoketones with a range amine-based nucleophile coupling partners have K_d s spanning 10^{-2} - 10^{-9} M.²⁰ When coupled with high biocompatibility and potential for stimuli responsive behaviour, this tunability greatly enhances the potential for biomedical applications of oBIDs. Despite this significant potential, much of our understanding of oBID chemistry comes from simple, unsubstituted model compounds such as 2-FPBA, which poorly reflect the stereo-electronic characteristics of the functionalised *ortho*-boronoaldehydes necessary for translational applications. Furthermore, much of this understanding is pieced together from many independent studies, performed and analysed under varying conditions, making comparison challenging. This is particularly important given the highly dynamic nature of oBID linkages, leading to a high sensitivity to environmental conditions and choice of analytical technique. Ultimately, this leads to significant discrepancies in reported rates of formation and stabilities of oBIDs, due to subtle differences in substrate choice, reaction conditions, or analysis method. In this thesis, we therefore propose to synthesise a panel of carbonyl-bearing electrophiles combined with a selection of amine-based nucleophiles derived from the literature, to study the reaction kinetics of these subsequent oBID linkages, in a uniform and standardised study, using a Förster resonance energy transfer (FRET) reporter assay. This assay will allow us to probe the rapid kinetics of oBID formation in detail, under complex and biomedically relevant conditions. We can monitor oBID formation, stability and cleavage, using a FRET platform which is highly tolerant of environmental conditions, providing critical new insights into the effects of pH, additives, media, and oBA structure on conjugation. We therefore anticipate that this assay will find future use for the high-throughput screening of novel oBIDs and their stimuli responsive behaviour.

2. References

1. S. Chatterjee, E. V. Anslyn and A. Bandyopadhyay, *Chem. Sci.*, 2021, **12**, 1585–1599.
2. S. Safiri *et al.* *Ann Rheum Dis*, 2020, **79**, 819–828.
3. C. O. Johnson *et al.*, *The Lancet Neurol.*, 2019, **18**, 439–458.
4. S. L. James *et al.*, *The Lancet Neurol.*, 2018, **392**, 1789–1858.
5. R. Langer and J. P. Vacanti, *Science*, 1993, **260**, 920–926.
6. W. Jung, T. Tschaplinski, L. Wang, J. Blazebrook, and J. Greenberg, *Science*, 2009, **324**, 89–91.
7. D. A. Robinton and G. Q. Daley, *Nature*, 2012, **481**, 295–305.
8. P. W. Burridge, G. Keller, J. D. Gold and J. C. Wu, *Cell Stem Cell*, 2012, **10**, 16–28.
9. J. A. Hunt, R. Chen, T. Van Veen and N. Bryan, *J. Mater. Chem. B*, 2014, **2**, 5319–5338.
10. C. D. Spicer, *Polym. Chem.*, 2020, **11**, 184–219.
11. A. M. Khakar, P. M. Kiick, K. L. Kloxin, *Chem. Soc. Rev.*, 2013, **42**, 7335–7372.
12. I. M. El-Sherbiny and M. H. Yacoub, *Glob. Cardiol. Sci.*, 2013, **3**, 316–342.
13. F. Khan, M. Tanaka and S. R. Ahmad, *J. Mater. Chem. B*, 2015, **3**, 8224–8249.
14. M. C. Koetting, J. T. Peters, S. D. Steichen and N. A. Peppas, *Mater. Sci. and Eng. R Rep.*, 2015, **93**, 1–49.
15. B. V. Slaughter, S. S. Khurshid, O. Z. Fisher, A. Khademhosseini and N. A. Peppas, *Adv. Mater.*, 2009, **21**, 3307–3328.
16. P. Schmidt, C. Stress and D. Gillingham, *Chem. Sci.*, 2015, **6**, 3329–3333.
17. N. C. Rose, E. Tipple, A. Sanchez, J. Lynam, C. D. Spicer, *Chem. Sci.*, 2022, **13**, 12791–12798.
18. J. Crueiras, A. Rios, E. Riveiros and J. P. Richard, *J. Am. Chem. Soc.*, 2009, **131**, 15815–15824.
19. T. C. French and T. C. Bruice, *Biochemistry*, 1965, **4**, 1, 77–84.
20. S. Cambray and J. Gao, *Acc. Chem. Res.*, 2018, **51**, 2198–2206.
21. B. M. Chapin, P. Metola, V. M. Lynch, J. F. Stanton, T. D. James and E. V. Anslyn, *Org. Chem.*, 2016, **81**, 8319–8330.
22. L. Zhu, S. H. Shabbir, M. Gray, V. M. Lynch, S. Sorey and E. V. Anslyn, *J. Am. Chem. Soc.*, 2006, **128**, 1222–1232.
23. K. L. Diehl, J. L. Bachman, B. M. Chapin, R. Edupuganti, P. Rogelio, Escamilla, A. M. Gade, E. T. Hernandez, H. H. Jo, A. M. Johnson, I. V. Kolesnichenko, J. Lim, C.-Y. Lin, M. K. Meadows, H. M. Seifert, D. Zamora-Olivares and E. V. Anslyn, *New J. Chem.*, 2018, **42**, 8577–8589.
24. J. P. M. António, R. Russo, C. P. Carvalho, P. M. S. D. Cal and P. M. P. Gois, *Chem. Soc. Rev.*, 2019, **48**, 3513–3536.
25. S. Palvai, J. Bhangu, B. Akgun, C. T. Moody, D. G. Hall and Y. Brudno, *Bioconjugate Chem.*, 2020, **31**, 2289–2292.
26. X. Ding, G. Li, P. Zhang, E. Jin, C. Xiao and X. Chen, *Adv. Funct. Mater.*, 2021, **31**, 2011–2024.
27. N. J. Gutiérrez-Moreno, F. Medrano and A. K. Yatsimirsky, *Org. Biomol. Chem.*, 2012, **10**, 6960–6972.
28. P. M. S. D. Cal, J. B. Vicente, E. Pires, A. V. Coelho, L. F. Veiros, C. Cordeiro and P. M. P. Gois, *J. Am. Chem. Soc.*, 2012, **134**, 10299–10305.
29. A. Bandyopadhyay and J. Gao, *J. Am. Chem. Soc.*, 2016, **138**, 2098–2101.
30. Akçay, M. A. Belmonte, B. Aquila, C. Chuaqui, A. W. Hird, M. L. Lamb, P. B. Rawlins, N. Su, S. Tentarelli, N. P. Grimster and Q. Su, *Nat. Chem. Biol.*, 2016, **12**, 931–936.

31. A. Bandyopadhyay, K. A. McCarthy, M. A. Kelly and J. Gao, *Nat. Commun.*, 2015, **6**, 6561–6570.
32. K. Li, C. Weidman and J. Gao, *Org. Lett.*, 2018, **20**, 20–23.
33. D. Bermejo-Velasco, G. N. Nawale, O. P. Oommen, J. Hilborn and O. P. Varghese, *Chem. Commun.*, 2018, **54**, 12507–12510.
34. H. Faustino, M. J. S. A. Silva, L. F. Veiros, G. J. L. Bernardes and P. M. P. Gois, *Chem. Sci.*, 2016, **7**, 5052–5058.
35. K. Li, W. Wang and J. Gao, *Angew. Chem. Int. Ed.*, 2020, **59**, 14246–14250.
36. C. J. Stress, P. J. Schmidt and D. G. Gillingham, *Org. Biomol. Chem.*, 2016, **14**, 5529–5538.
37. H. E. Dunn, J. C. Catlin and H. R. Snyder, *J. Org. Chem.*, 1968, **33**, 4483–4486.
38. R. R. Groleau, T. D. James and S. D. Bull, *Coord. Chem. Rev.*, 2021, **428**, 213–256.
39. P. M. S. D. Cal, R. F. M. Frade, C. Cordeiro and P. M. P. Gois, *Chem. Eur. J.*, 2015, **21**, 8182–8187.
40. K. Sugita, Y. Suzuki, Y. Tsuchido, S. Fujiwara, T. Hashimoto and T. Hayashita, *RSC Adv.*, 2022, **12**, 20259–20263.
41. E. H. Cordes and W. P. Jencks, *J. Am. Chem. Soc.*, 1962, **84**, 826–831.
42. K. Unger and A. M. Coclite, *Biomacromolecules*, 2022, **23**, 4289–4295.
43. J. Ren, H. Hu, S. Wang, Y. He, Y. Ji, Y. Chen, K. Wang, H. Zhang, Y. Zhao and F. Dai, *ACS Appl. Mater. Interfaces*, 2022, **14**, 23182–23193.
44. H. Fang, G. Kaur and B. Wang, *J. Fluoresc.*, 2004, **14**, 481–489.
45. J. Singh, R. C. Petter, T. A. Baillie and A. Whitty, *Nat. Rev. Drug Discov.*, 2011, **10**, 307–317.
46. D. S. Johnson, E. Weerapana and B. F. Cravatt, *Future Med. Chem.*, 2010, **2**, 949–964.
47. R. F. Epand, M. A. Schmitt, S. H. Gellman and R. M. Epand, *Biochim. Biophys.*, 2006, **1758**, 1343–1350.
48. R. F. Epand, P. B. Savage and R. M. Epand, *Biochim. Biophys.*, 2007, **1768**, 2500–2509.
49. K. A. McCarthy, M. A. Kelly, K. Li, S. Cambray, A. S. Hosseini, T. van Opijnen and J. Gao, *J. Am. Chem. Soc.*, 2018, **140**, 6137–6145.
50. J. X. Huang, S. L. Bishop-Hurley and M. A. Cooper, *Antimicrob. Agents Chemother.*, 2012, **56**, 4569–4582.
51. U. Gasanov, C. Koina, K. W. Beagley, R. J. Aitken and P. M. Hansbro, *Infect Immun*, 2006, **74**, 566–577.
52. S. Borsley and S. L. Cockroft, *ACS Nano*, 2018, **12**, 786–794.
53. J. Schmidt, *J. Mater. Chem.*, 2005, **15**, 831–840.
54. J. A. Cooper, S. Borsley, P. J. Lusby and S. L. Cockroft, *Chem. Sci.*, 2017, **8**, 5005–5009.
55. D. F. Cairns-Gibson and S. L. Cockroft, *Chem. Sci.*, 2022, **13**, 1869–1882.
56. K. Li, C. Weidman and J. Gao, *Org. Lett.*, 2018, **20**, 20–23.
57. A. Bandyopadhyay, S. Cambray and J. Gao, *J. Am. Chem. Soc.*, 2017, **139**, 871–878.
58. F. Chen and J. Gao, *Chemistry A European J*, 2022, **28**, 34–49.
59. G. J. L. Bernardes, M. Steiner, I. Hartmann, D. Neri and G. Casi, *Nat. Protoc.*, 2013, **8**, 2079–2089.
60. G. Casi, N. Huguenin-Dezot, K. Zuberbühler, J. Scheuermann and D. Neri, *J. Am. Chem. Soc.*, 2012, **134**, 5887–5892.
61. A. Bandyopadhyay, S. Cambray and J. Gao, *Chem. Sci.*, 2016, **7**, 4589–4593.
62. D. Wang, W. Chen, Y. Zheng, C. Dai, K. Wang, B. Ke and B. Wang, *Org. Biomol. Chem.*, 2014, **12**, 3950–3959.
63. A. Darko, S. Wallace, O. Dmitrenko, M. M. Machovina, R. A. Mehl, J. W. Chin and J. M. Fox, *Chem. Sci.*, 2014, **5**, 3770–3776.

64. T. M. S. Tang, D. Cardella, A. J. Lander, X. Li, J. S. Escudero, Y.-H. Tsai and L. Y. P. Luk, *Chem. Sci.*, 2020, **11**, 5881–5888.
65. M. J. S. A. Silva, H. Faustino, J. A. S. Coelho, M. V. Pinto, A. Fernandes, I. Compañón, F. Corzana, G. Gasser and P. M. P. Gois, *Angew. Chem. Int. Ed.*, 2021, **60**, 10850–10857.
66. J. P. M. António, H. Faustino and P. M. P. Gois, *Org. Biomol. Chem.*, 2021, **19**, 6221–6226.
67. D. K. Kölmel and E. T. Kool, *Chem. Rev.*, 2017, **117**, 10358–10376.
68. R. K. V. Lim and Q. Lin, *Chem. Commun.*, 2010, **46**, 1589–1596.
69. G. S. Han and D. W. Domaille, *Org. Biomol. Chem.*, 2021, **19**, 4986–4991.
70. Gu, S. Ghosh, R. J. Staples and S. L. Bane, *Bioconjugate Chem.*, 2019, **30**, 10, 2604–2613.
71. A. Dirksen and P. E. Dawson, *Bioconjugate Chem.*, 2008, **19**, 2543–2548.
72. A. Dirksen, S. Dirksen, T. M. Hackeng and P. E. Dawson, *J. Am. Chem. Soc.*, 2006, **128**, 15602–15603.
73. A. Dirksen, T. M. Hackeng and P. E. Dawson, *Angew. Chem. Int. Ed.*, 2006, **45**, 7581–7584.
74. D. Larsen, M. Pittelkow, S. Karmakar and E. T. Kool, *Org. Lett.*, 2015, **17**, 274–277.
75. P. Crisalli and E. T. Kool, *J. Org. Chem.*, 2013, **78**, 1184–1189.
76. A. Adamczyk-Woźniak, K. M. Borys, I. D. Madura, A. Pawełko, E. Tomecka and K. Żukowski, *New J. Chem.*, 2013, **37**, 188–194.
77. T. P. Reilly, F. H. Bellevue, P. M. Woster and C. K. Svensson, *Biochem. Pharmacol.*, 1998, **55**, 803–810.
78. J. Kalia and R. T. Raines, *Angew. Chem. Int. Ed.*, 2008, **47**, 7523–7526.
79. A. Bandyopadhyay and J. Gao, *Chem. Eur. J.*, 2015, **21**, 14748–14752.
80. H. Gu, T. I. Chio, Z. Lei, R. J. Staples, J. S. Hirschi and S. Bane, *Org. Biomol. Chem.*, 2017, **15**, 7543–7548.
81. Q. Wang and K. J. Franz, *Bioorganic Med. Chem. Lett.*, 2017, **27**, 4165–4170.
82. H. G. Kuivila, *J. Am. Chem. Soc.*, 1954, **76**, 3, 870–874
83. G. S. Han and D. W. Domaille, *J. Mater. Chem. B*, 2022, **10**, 6263–6278.
84. O. Dilek, Z. Lei, K. Mukherjee and S. Bane, *Chem. Commun.*, 2015, **51**, 16992–16995.
85. R. L. Hinman, *J. Org. Chem.*, 1960, **25**, 1775–1778.
86. M. J. S. Dewar and R. C. Dougherty, *J. Am. Chem. Soc.*, 1964, **86**, 433–436.
87. C. S. McKay and M. G. Finn, *Chem. Biol.*, 2014, **21**, 1075–1101.
88. G. W. Liechti, E. Kuru, E. Hall, A. Kalinda, Y. V. Brun, M. VanNieuwenhze and A. T. Maurelli, *Nature*, 2014, **506**, 507–510.
89. A. R. Sherratt, M. Chigrinova, D. A. MacKenzie, N. K. Rastogi, M. T. M. Ouattara, A. T. Pezacki and J. P. Pezacki, *Bioconjugate Chem.*, 2016, **27**, 1222–1226.
90. S. E. Pidgeon and M. M. Pires, *Chem. Commun.*, 2015, **51**, 10330–10333.
91. C. M. Mckertish and V. Kayser, *Biomedicines*, 2021, **9**, 872–880.
92. B. Akgun, C. Li, Y. Hao, G. Lambkin, R. Derda and D. G. Hall, *J. Am. Chem. Soc.*, 2017, **139**, 40, 14285–14291.

Chapter Two

Cyanine Dye Synthesis

Contents

1. FRET Spectroscopy	47
1.1 Background	47
1.2. Dye selection	51
1.3. Cyanine Dye Synthesis	52
1.4. Reactive Handle Selection	54
2. Results and Discussion	56
2.1. Retrosynthetic Analysis of Dyes	56
2.2. Dye Synthesis	57
2.2. Boronoaldehyde Synthesis	60
2.2.1. Amide coupling	60
2.2.2. Final Step Borylation	63
2.2.3. Acetal Protection	64
2.2.4. Acyl Chloride	66
2.3. Cy3 Negative Control Synthesis	69
2.3.1. Aldehyde	69
2.3.2. Boronic Acid	69
2.4. Positive Control Synthesis	71
2.4.1. Carboxylic Acid	71
2.5. Cy5 Dye Synthesis	72
2.5.1. Amine Synthesis	72
2.5.2. Hydroxylamine Synthesis	73
2.5.3. Synthesis of Cy5 Hydrazine	74
2.6. Acetate Cap Synthesis	75
2.7. Elucidation of NMR assignment	76
3. Conclusion	78
4. Experimental	79
4.1 General considerations	79
4.2. Core dye synthesis	80
4.3. Synthesis of reactive handles	85
4.4. Reactive dye synthesis	92

4.5. Synthesis of control substrates for FRET studies.....	103
4.6. Synthesis of Cy3 negative controls	108
5. References.....	114

1. FRET Spectroscopy

In this chapter, we outline the key steps in synthesising cyanine dyes for a Förster resonance energy transfer (FRET)-based platform. A selection of Cy3 and Cy5 dye targets are synthesised here which are combined and analysed using FRET for monitoring oBID reaction kinetics in aqueous conditions.

1.1 Background

Förster resonance energy transfer (FRET) is a comparatively simple and accessible analytical technique which gives both qualitative and quantitative data through a direct readout of conjugation, with high precision and low background noise. FRET measurements between two reactive species provide information on intra- and intermolecular distances on a nanometer scale (1-10 nm). FRET reporter assays have been developed which can probe the rapid kinetics of bond formation in physiological conditions *in situ* at sub-micromolar concentrations.^{1,2} Furthermore, FRET has been employed for applications in detecting or imaging metals, biomacromolecules, intracellular environments and analyte systems as well as in fluorescent labelling.³⁻⁵ Using analogous FRET technology, in this thesis we develop a novel FRET-based assay as a powerful tool for monitoring dynamic linkages through conjugation, with unprecedented sensitivity and accuracy under standardised conditions monitored at low concentrations, giving a direct readout of conjugation. This FRET assay would provide a key new insight into the reactivity of *ortho*-boronoaldehydes (oBA) with amine-based nucleophiles and to track these rapid reactions. Although alternative techniques such as X-ray crystallography and NMR spectroscopy give higher spatial or structural resolution respectively, these technologies are either more technically complex, use restrictive sample preparation or require much higher analyte concentrations to measure reaction kinetics. With increasing analyte concentrations, the analysis techniques were unable to monitor the rapid oBID formation and therefore the reaction kinetics of some amine nucleophiles, particularly hydrazine ($k_1 > 10^4 \text{ M}^{-1} \text{ s}^{-1}$), could not be determined. Studies performed previously using UV-Vis also fail to capture the rapid dynamics of *ortho*-boronoimines, and related derivatives (collectively oBIDs). The independent studies reported up to date have been performed with subtle differences in substrate choice, reaction conditions and analysis methods, leading to significant discrepancies in reported rates of formation and stabilities of oBID formation.^{6,7}

FRET is a non-radiative energy transfer that occurs through dipole-dipole coupling from an excited donor fluorophore to a ground state acceptor. This phenomena was first described by Theodor Förster in 1946, whom reported that in order for energy transfer to occur, certain spectral overlap and proximity requirements must be satisfied.⁸ In order for FRET to occur, a FRET pair is required, whereby the donor and acceptor are complimentary to one another. Much research has been done in the past decade to establish a library of suitable FRET pairs. Many comprehensive reviews have been published which summarise the diverse potential of FRET applications.^{1,9,10} FRET pairs are only compatible if certain spectral and spatial principles are satisfied, where one of the emission bands of the donor must overlap with an absorption band of the acceptor. FRET has an inherent inverse-sixth-power distance dependency (Equation 1, R^6) which requires the pair to be brought in close spatial proximity (<20 nm) in order for the energy transfer to occur. These nanoscopic distances make FRET spectroscopy suitable for monitoring dynamic linkages at nanoscale proximity (1-10 nm).¹¹ This high spatial sensitivity of FRET has been coined as the 'spectroscopic ruler', by Stryer and Haugland, used to probe molecular structures at the nanoscale.¹² Förster proposed a FRET efficiency equation, to quantify the electronic excitation transfer efficiency from a given energy donor and acceptor (Equation 2).

$$E = \frac{R_0^6}{R_0^6 + R^6} \quad (1)$$

$$R_0^6 = 0.021J\kappa^2\Phi_D n^{-4} \quad (2)$$

Where E is the FRET efficiency, R_0 is the Förster distance, representing the donor and acceptor molecular separation at which energy transfer is 50% efficient, and R is the variable separation distance from the donor and acceptor with distances reported in angstroms. J is the overlap integral, which depends on donor emissions and acceptor absorption, and κ^2 is the orientation factor, dependent on the orientation of the respective dipole moments. Φ_D is the donor quantum yield and n , the refractive index of the medium. R_0 can be calculated from Equation 2, in nm⁶.

$$J = \int I_D \varepsilon_A \lambda^4 d\lambda \quad (3)$$

The spectral overlap J has the common spectroscopic units M⁻¹ cm⁻¹ nm⁴ and can be calculated using Equation 3. In order to exhibit FRET, a good spectral overlap is required between the emission of the donor (Fig. 1b, pink line), with the absorbance of the acceptor

(Fig. 1b, red line), corresponding to a large extinction coefficient for the acceptor. Small changes in the donor/acceptor, distances can give significant changes in FRET efficiency values. Spectral overlap is determined by the integral of the normalised donor emission intensity (I_D), multiplied by the molar extinction coefficient of the acceptor (ϵ_A) multiplied by the wavelength of light to the fourth power, as shown in Equation 3.

The Jablonski diagram of FRET illustrates the various electronic states of a molecule and shows the possible transitions between them (Fig. 1a). In the context of a FRET pair, this shows how the donor moiety can be promoted to the excited state through absorbance of light, which can then drop back down to the ground state, via either radiative or non-radiative decay. When the FRET pair is brought into close spatial proximity, the excited state can also undergo non-radiative donor energy transfer to promote the complementary acceptor partner to the excited state. This excited state then releases energy at a different wavelength to drop back down to the ground state. The Jablonski diagram therefore helps rationalise the R^{-6} distance dependency which promotes this non-radiative energy transfer to occur (Equation 2). The orbital energy overlap diagram highlights the importance of the relative distance in wavelength between the donor emission maxima, and acceptor excitation maxima, and the resulting overlap between the donor emission and acceptor excitation (Fig. 1b). The larger the spectral overlap of a given FRET pair the higher the FRET efficiency (Equation 1). A schematic of a FRET assay is illustrated in Fig. 1c. When a donor moiety absorbs light of a particular wavelength (λ_1), it becomes excited, and subsequently releases radiative energy at a corresponding wavelength (λ_2). However, when the FRET pair is brought into close spatial proximity, through bond formation, a non-radiative donor energy transfer occurs which excites the acceptor, indicated by a new emission wavelength (λ_3) corresponding to the acceptor moiety. Monitoring the ratio of λ^2 to λ^3 can therefore be used to indirectly monitor conjugation.

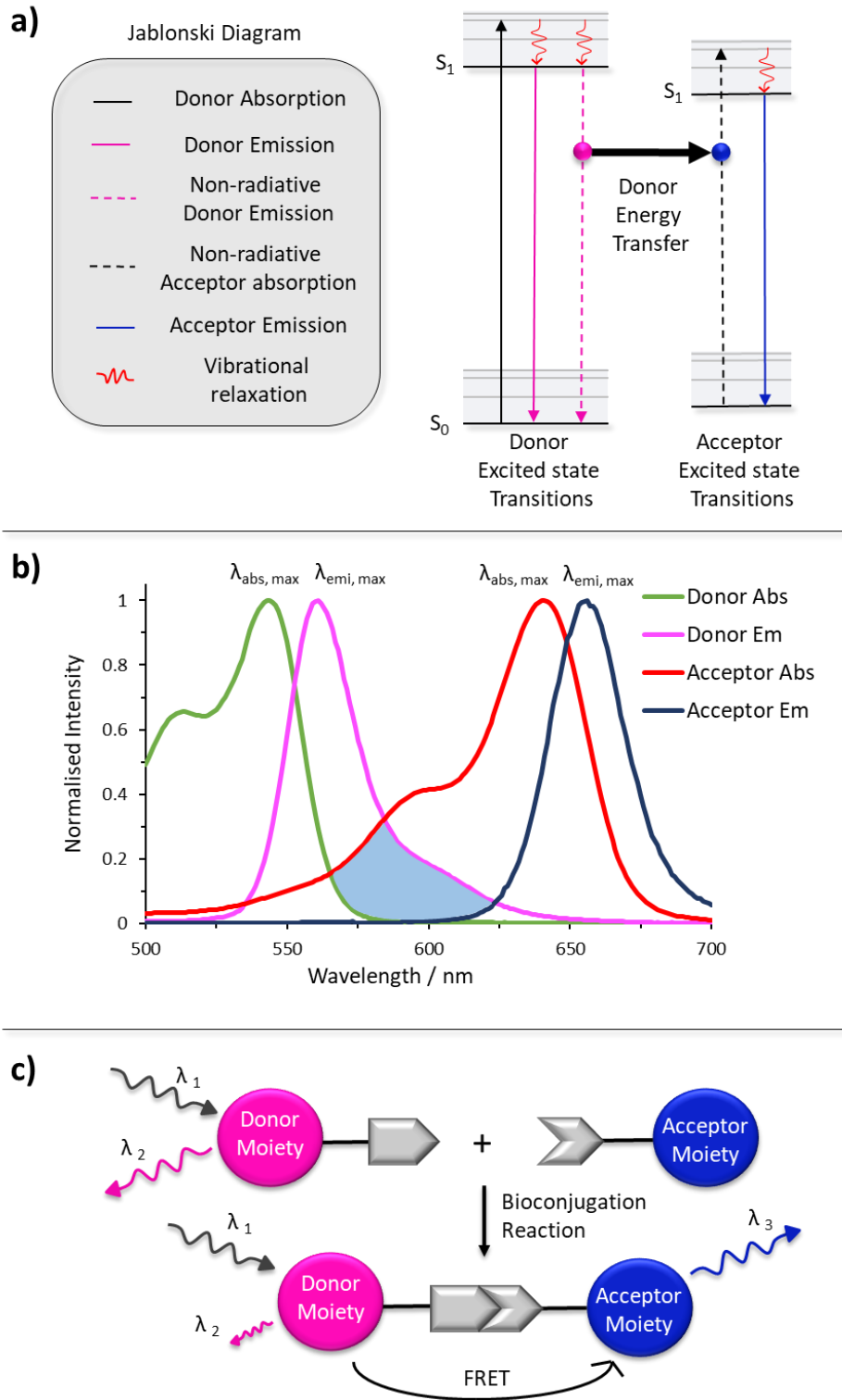


Figure 1: a) FRET Jablonski diagram of orbital energy levels to show non-radiative energy transfer of the process of FRET. b) Orbital overlap diagram of a FRET pair showing the absorption and emission wavelengths. c) Mechanism of how FRET works with a donor and acceptor with a proximity dependency.

1.2. Dye Selection

In our studies, there are several design criteria which must be satisfied to make a suitable FRET based dye pair. Firstly, the two dyes must have an appropriate spectral overlap to obey the standard FRET principle mentioned previously. A turn-on FRET system is employed here, whereby as the oBID linkage is formed, the two dyes come into close spatial proximity to switch FRET on, allowing energy transfer to occur. The fluorescent dye must be at least partially soluble in aqueous conditions, in order to probe these studies in biologically relevant conditions. The chosen fluorescent dye must also be fluorescent at nanomolar concentration, as the oBID interactions are rapid under these concentrations. Finally, the dye must also be easily modified with an appropriate reactive handle which can be tethered a short distance from the dye, as to enhance the FRET efficiency. There are several fluorescent dyes which suit our requirements, and have found many applications in chemical biology, such as BODIPY, coumarin, rhodamine, fluorescein, and quinoline or benzothiazole derived dyes.¹ Whilst these dyes could be used in combination with one another, they are often better suited for the detection or imaging of metals, small neutral molecules or multi-analyte responsive systems. Cyanine dyes, particularly cyanine-3 (Cy3) and cyanine-5 (Cy5), are easily functionalised dyes routinely used for the fluorescent labelling of biological macromolecules, DNA detection and bioconjugation chemistry. Their excellent biocompatibility, low toxicity, good photophysical properties and excitation in the visible region allows expansion into biological systems.^{2,13-16} Cy3 and Cy5, have high photosensitivity, good fluorescence properties and can be easily modified to make water-soluble. Cy3 and Cy5 are well documented in literature and are strongly fluorescent even at nanomolar concentrations across a wide pH range, as well as being chemically very stable with respect to temperature and pH.^{2,13,17} The cyanine backbone chain, is largely independent from the pendant reactive handles (R) which allows functionalisation at these sites. Previous studies incorporate a pendant sulphonate chain to aid with water solubility.¹⁵ The length and functionality of the modified reactive 'R' group can be chemically altered with ease. We therefore set out to synthesise analogous cyanine dyes exploiting the easily modified reactive 'R' group (Fig. 2).

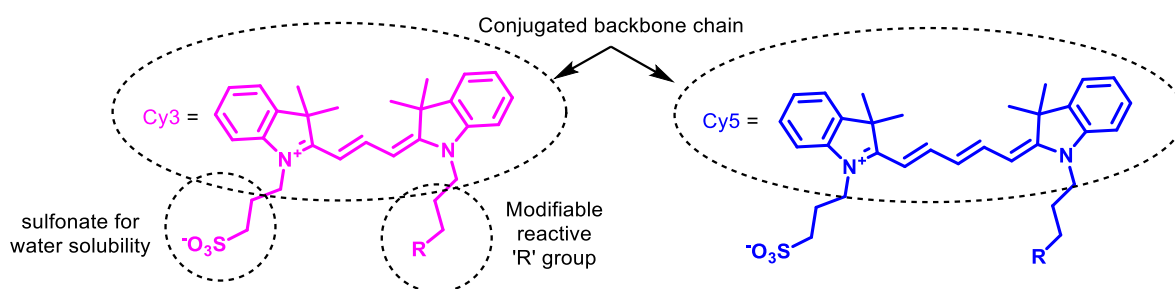


Figure 2: Generic structure of Cy3 and Cy5 dyes with a long and conjugated backbone chain, with two functional indolenine handles, a sulfonate to improve water solubility on one side, and a modifiable reactive R group handle on the other side.

1.3. Cyanine Dye Synthesis

The cyanine dyes that we use in our work, are based on the core structure from a paper published in 2016 by Herbst and Shabat, who demonstrated native chemical ligation and oxime ligations between Cy3 (**3**) and Cy5 (**4**) dyes (Fig. 3).¹⁵ These reactions selectively connected the two dyes under physiological conditions, where the fluorescence output was monitored as a result of energy transfer from FRET occurring.



Figure 3: Cyanine dyes **3** and **4** used by Herbst and Shabat to probe native chemical ligation reactions.¹⁵

The native chemical ligation was first set up by connecting a cysteine to a Cy3 dye, which was able to displace an SPh group on a Cy5 dye in the presence of tris(2-carboxyethyl)phosphine hydrochloride (TCEP), to bring the two dyes in close spatial proximity. The fluorescence emission intensity of Cy3 at 560 nm decreased, with a simultaneous increase in Cy5 emission at 650 nm, which demonstrated that FRET was occurring (Fig. 4). Following this success, oxime ligation was performed in an analogous set up with a Cy3-hydroxylamine, combining with a Cy5-aldehyde in the presence of an aniline catalyst. This oxime ligation was again successfully monitored using FRET, evidenced by a gradual quenching of Cy3 emission, and gradual increase in Cy5 emission as a result of energy transfer.

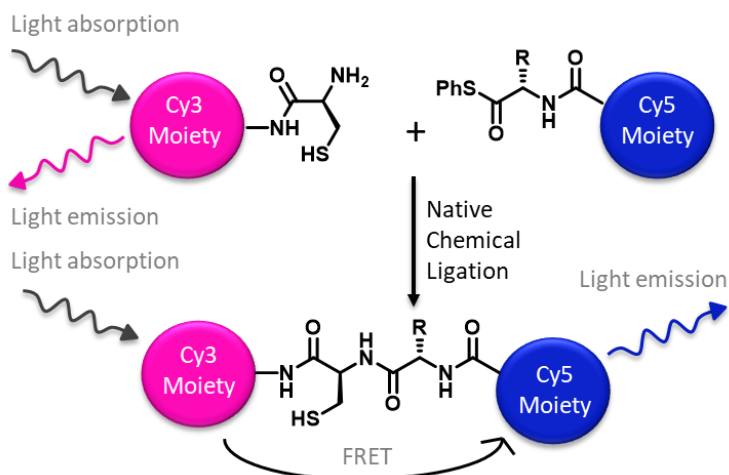


Figure 4: A schematic illustration of a native chemical ligation between a Cy3 probe with cysteine and Cy5 probe with SPh leaving group to allow FRET to occur.

This ground-breaking paper has provided the inspiration for the platform design in this thesis. The cyanine dyes used in this work were synthesised based on these core structures and employed a pendant sulphonate chain to aid water-solubility, as well as a long flexible carboxylic acid reactive handle. These were then functionalised through amide coupling reactions to form the active hydroxylamine and 1,2-aminothiol groups. We designed our functional cyanine dyes following the precedent of this work from Herbst and Shabat, where we substituted the carboxylic acid reactive handle, with a short-chained amine (Fig. 5). We did this due to the inverse-sixth-power distance dependency of FRET, which aimed to minimise the linker length of the functional handles that we would use for oBID formation. Analogous to the previous study, we chose to incorporate a pendant sulphonate chain that would provide water solubility whilst not affecting fluorescence on one side,² with the amine on the other side derivatised via a simple amide coupling. As such, an *ortho*-boronoaldehyde could be attached to the Cy3 dye, and amine-based nucleophiles could be attached to the Cy5 dye in a bioconjugation reaction in biologically relevant media.



Figure 5: Cy3 1 and cy5 2 dyes used in this work, with pendant sulphonate chain for water solubility, and a functional nucleophilic amine handle.

1.4. Reactive Handle Selection

A selection of oBA and nucleophile reactive handles were selected for covalent attachment via amide linkages to cyanine (Cy3 or Cy5) dyes, compounds **1** and **2** respectively (Fig. 6). Compounds **1a-e** were selected to analyse the effect of the boronic acid group on the oBID stability. Compound **1b** was expected to form a stabilised oBID, due to the empty p-orbital located on boron which can accept electron density from the resultant electron dense imine derivative. The lone pair of electrons on the adjacent nitrogen atom can offer stabilising interactions by donation of electron density, into the empty p-orbital of the boronic acid. Compounds **1a** and **1c** were synthesised as controls to analyse the effects of the complete system, and to ensure that the expected increase in stability and associated reaction rates were due to the ability of the boronic acid to stabilise imine formation. Compound **1d** was explored to compare the difference between an *ortho*-boronic acid versus a boronic pinacol ester. The ability to form oBID linkages through stabilising B–N interactions using the pinacol ester was therefore explored through compound **1d**. Compound **1e** was synthesised to allow the production of a covalently linked Cy3-Cy5 pair via an irreversible amide bond, bringing the two dyes in stable close spatial proximity, to serve as a positive control for later FRET studies.

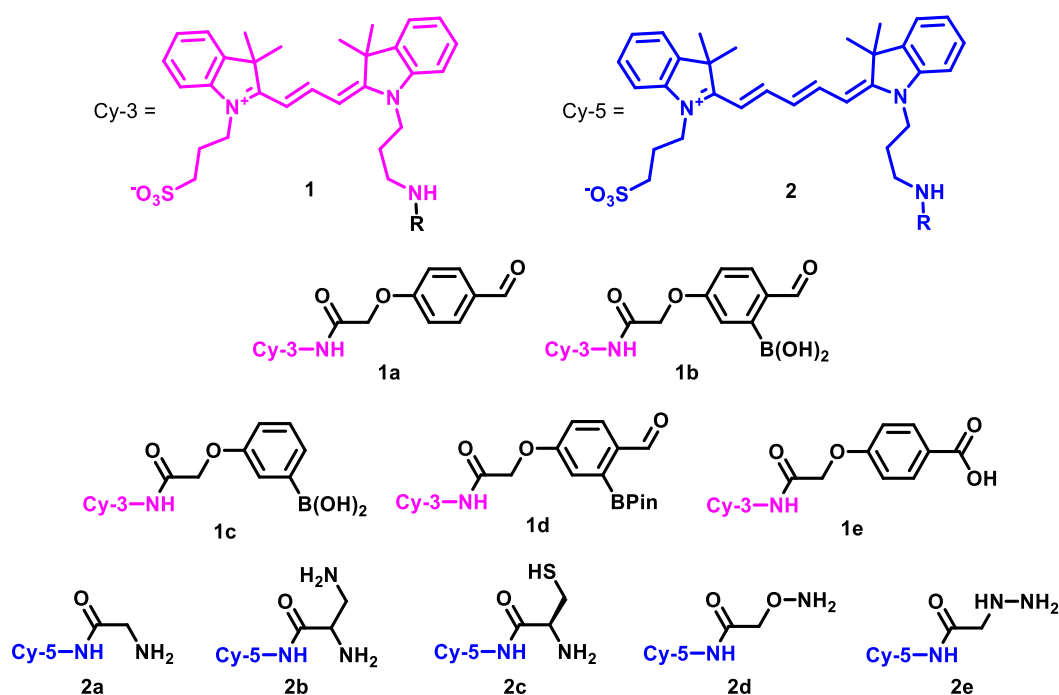


Figure 6: Target Cy3 (**1a-e**) and Cy5 (**2a-e**) molecules that were synthesised during this study.

Molecules **2a-e** were selected for synthesis as these nucleophiles were expected to lead to conjugation products with a broad range of reaction rates and stabilities, which enable us to probe a variety of dynamically linked conjugates.¹⁸⁻²². These analogues encompass the

archetypal amine nucleophile (**2a**), associated with iminoboronate formation. 1,2-diamine (**2b**) and 1,2-aminothiol (**2c**) have two effective nucleophiles each, which can react at the aldehyde centre to cyclise, to form cyclic imidazolino- (IzB) and thazolidino- (TzB) boronates respectively. Hydroxylamine (**2d**) has been reported in literature to form highly stabilised structures, due to the large amount of electron density at the amine nucleophile resulting in strong oxime bond formation.¹⁹ Hydrazine (**2e**) is also known to form highly stabilised hydrazone and diazaborine (DAB) structures, however, the rates of formation of these species have been too rapid that the rate constants have been unable to be accurately reported using alternative analytical techniques and are therefore of particular interest here.

2. Results and Discussion

2.1. Retrosynthetic Analysis of Dyes

The cyanine dye analogues prepared in this thesis were based on the optimisation of literature compounds with a longer amine chain, **3** and **4**, as detailed above. However, the synthesis of these dyes had to be re-engineered to install a free amine (**6**) on one side of the dye, rather than a carboxylic acid group (**5**), to shorten the reactive handle chain (Fig. 7), and to increase FRET efficiency. As a consequence of the reactivity of the primary amine reactive handle, the amine group required protection during the synthesis of the dye. Protection via a Boc group was unsuitable as these groups are susceptible to deprotection in acidic or high temperature environments. In the coupling step of the dye, acetic anhydride and temperatures of 120 °C are required which would result in Boc deprotection. Protection via an Fmoc group was also unsuitable as they are unstable with respect to basic conditions, with pyridine being a strong enough base for deprotection.^{23–25} We hypothesised that a phthalimide protecting group would be stable to high temperatures and acidic and basic reaction conditions and would therefore be a suitable protecting group to shield the reactivity of the free amine. The phthalimide protecting group could then be deprotected using robust literature conditions following the synthesis of the cyanine dyes.

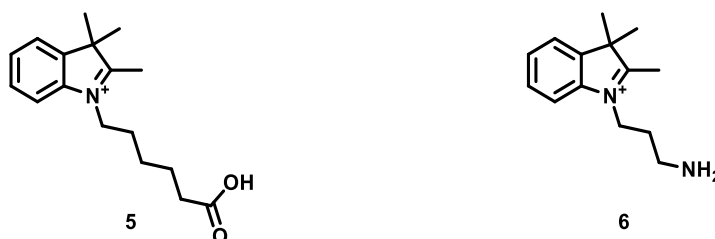
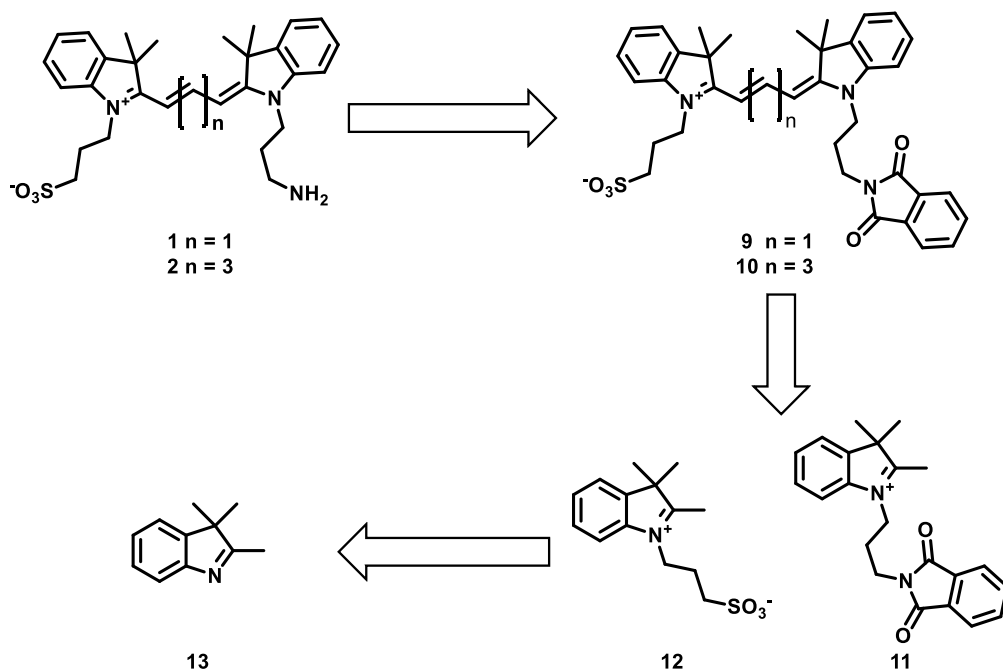


Figure 7: Literature analogue (5) synthesised previously and free amine alternative (6) that we targeted in this study to increase FRET efficiency.

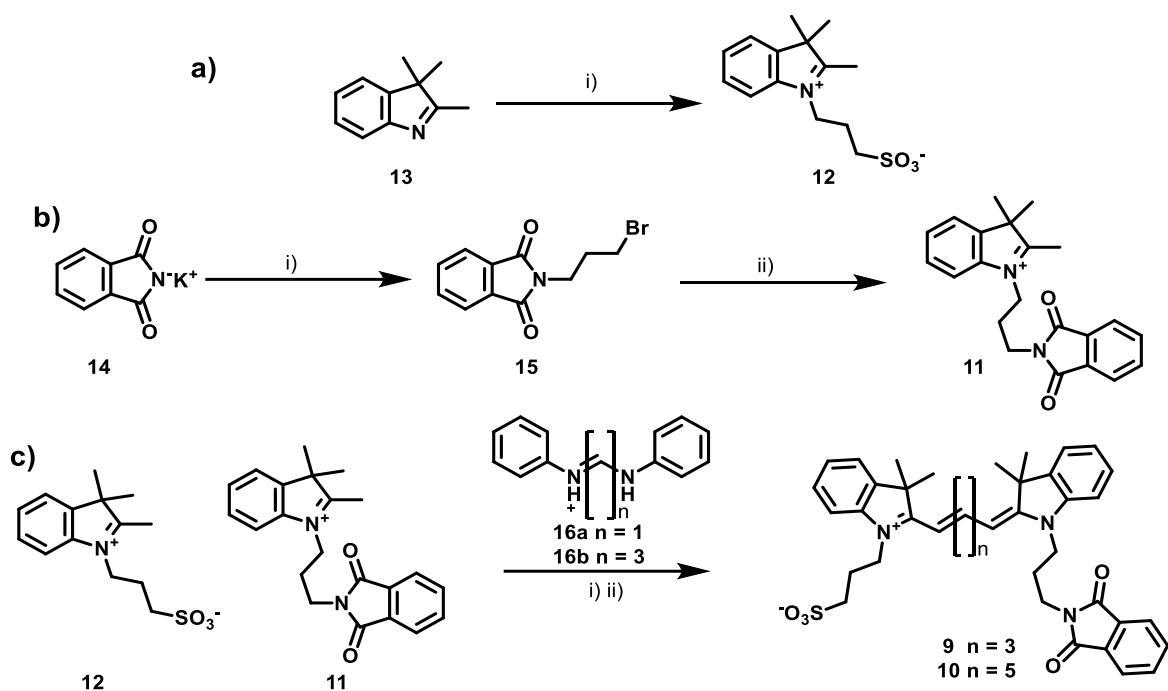
Synthesis of the short-chained cyanine dye (Scheme 1, **1** and **2**) would begin with commercially available indolenine **13**. The indolenine could then undergo a reaction with a cyclic sultone group, to form the sulphate salt **12**. In a similar reaction, the indolenine could undergo an alkylation with a bromo-substituted phthalimide group to generate **11**. Having formed each half of the dye, they would then be coupled using a 1- or 3- carbon linker to synthesise Cy3 and Cy5 respectively (**9/10**). The dyes could then undergo phthalimide deprotecting step to form the free amine cyanine dyes (**1/2**).



Scheme 1: Retrosynthetic analysis of cyanine dyes **1** and **2** from indolenine precursor **13**.

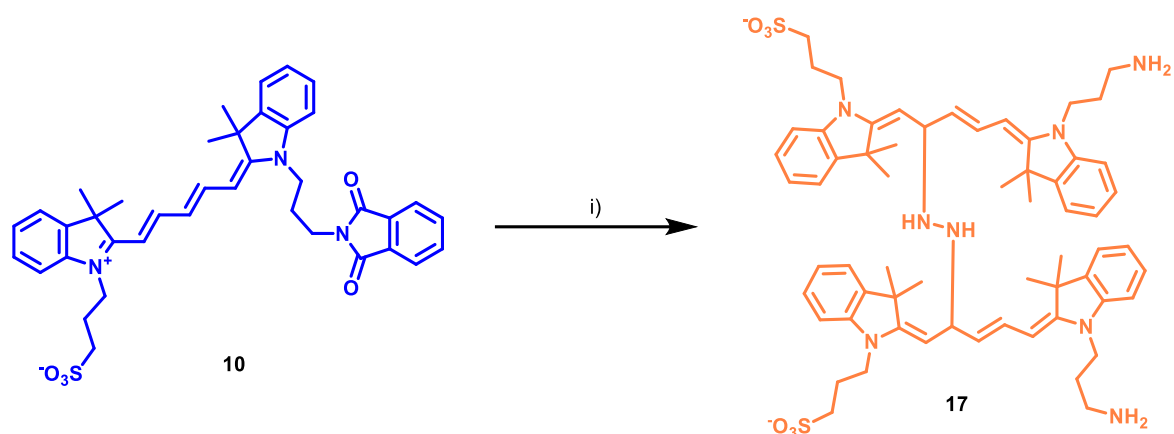
2.2. Dye Synthesis

To build the sulphonated dye building block (Scheme 2a), indolenine **13** was heated at reflux with 1,3-propanesultone to afford the sulphonate salt **12**. In a separate reaction to build the amine side (Scheme 2b), potassium phthalimide **14** was alkylated with dibromopropane to form **15**, and then reacted with **13** to form the Phth-protected indolenine **11**. Upon forming the left and right-hand sides of the dye, these were then coupled (Scheme 2c) with a 1- (**16a**) or 3- (**16b**) carbon donor in order to form the protected Cy3 **9** or Cy5 **10** dyes respectively.



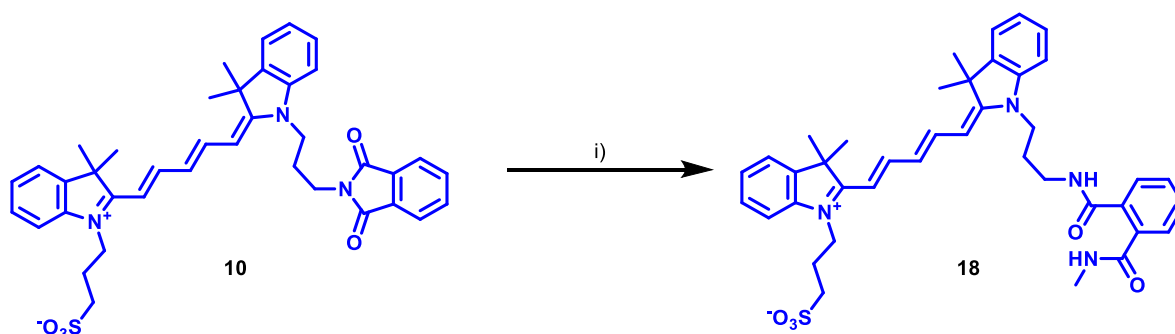
Scheme 2: **a)** Alkylation of indolenine **13**. Reagents and conditions: i) 1,3-propanesultone, toluene, reflux, 20 h, 85%. **b)** Synthesis of the phthalimide protected indolenine **11**, Reagents and conditions: i) dibromopropane, acetone, reflux, 16 h, 44% ii) **13**, acetonitrile, reflux, 20 h, 68%; **c)** Synthesis of **9** and **10**. Reagents and conditions: i) Ac_2O , 120 °C, 1.5 h, then ii) pyridine, r.t. 20 h. **16a**, where $n = 1$ for **9**: 27%; **16b**, where $n = 3$ for **10**: 29%.

We initially envisaged removal of the phthalimide protection group using hydrazine, as this method of phthalimide cleavage is very well documented in the literature.^{26–30} However, this process led to a major side reaction, indicated by an intense colour change from deep blue to orange. One hypothesis for this loss of conjugation and subsequent colour change was through the attack of hydrazine on the Cy5 dye following deprotection. The excess hydrazine could have attacked the conjugated chain of the dye, disrupting conjugation and leading to the intense colour change, which could have subsequently dimerised to form compound **17** (Scheme 3). This may be due to the lower energy of the backbone chain relative to standard alkenes, as a result of extended conjugation throughout the unsaturated system. This makes the electrophilic backbone alkene chain more susceptible to nucleophilic attack of the hydrazine. Attempts were made to limit side product formation by lowering the temperature to 55 °C rather than at reflux, but the side product formation persisted. However, it should be noted that similar conditions did not affect the Cy3 dye, which could mean that the loss of conjugation is a result of the more electrophilic extended conjugated chain. Nevertheless, deprotection of Cy3 **9** using hydrazine was avoided, as hydrazine was difficult to remove from the reaction, and reacted with further reactants in sequential steps, which will be discussed later.



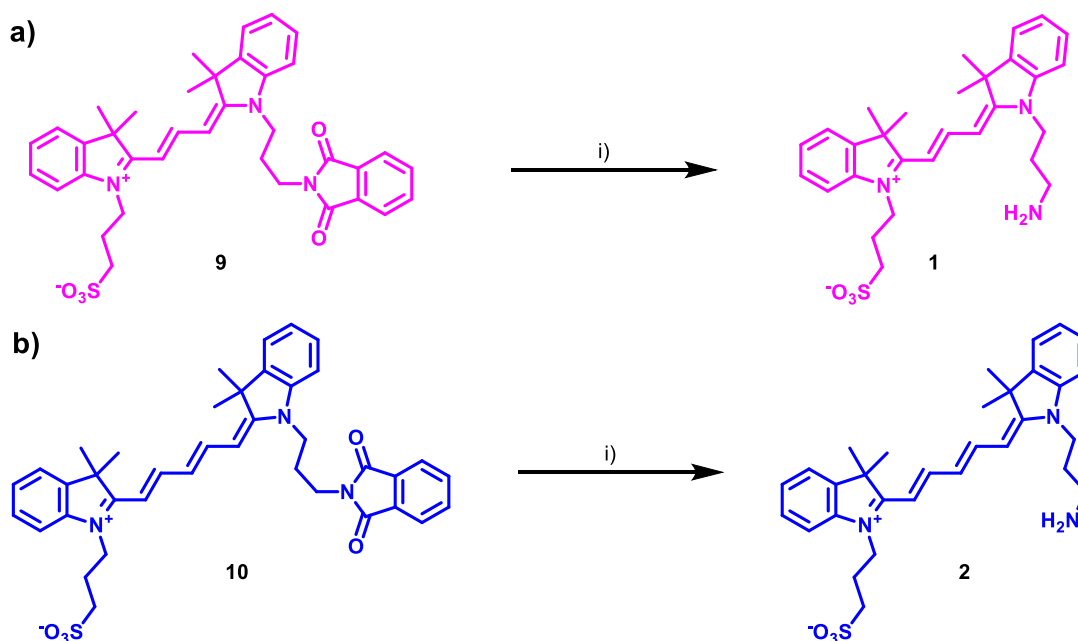
Scheme 3: Proposed dimerization of the Cy5 dye **10** as well as deprotection of the phthalimide group to form side product **17** using hydrazine. Reagents and conditions: i) Hydrazine, ethanol, 55 °C, 3 h.

Hence, an alternative method for phthalimide deprotection was found in the literature,^{31,32} which utilises methylamine as the deprotection reagent. The subsequent removal of the phthalimide group under these conditions required some optimisation, with much higher concentrations of methylamine needed than those reported in the literature, to drive the reaction to completion.³¹ Mass spectrometry and NMR analysis indicated that the phthalimide group was undergoing low conversion to the fully deprotected Cy5 dye **2**, with intermediate **18** forming at the initial concentration of methylamine used (w/w 1.3%), with higher concentrations (w/w 6.7%) required to drive the reaction to completion. This partial deprotection (Scheme 4) could have been due to the necessity of a second equivalent of methylamine to intermolecularly attack the secondary amide of **18**, rather than the intramolecular attack of hydrazine that mediates traditional hydrazinolysis. Additionally, the amide reactivity of **18**, in which the nitrogen lone pair is partially delocalised into the carbonyl could cause a slower reaction. Therefore, a comparatively higher concentration of methylamine was necessary for full deprotection of the phthalimide group.



Scheme 4: Conversion of **10** to partially cleaved intermediate **18**. Reagents and conditions: MeNH₂ (w/w 1.3%), EtOH, r.t, 4 h.

The concentration of methylamine was therefore increased from 1.3% to 6.7% in ethanol which subsequently yielded the fully deprotected product (Scheme 5). With this increased concentration of methylamine, both of the free-amino cyanine dyes (**1** and **2**) could now be achieved with >90% conversion, and free from contamination with hydrazine.

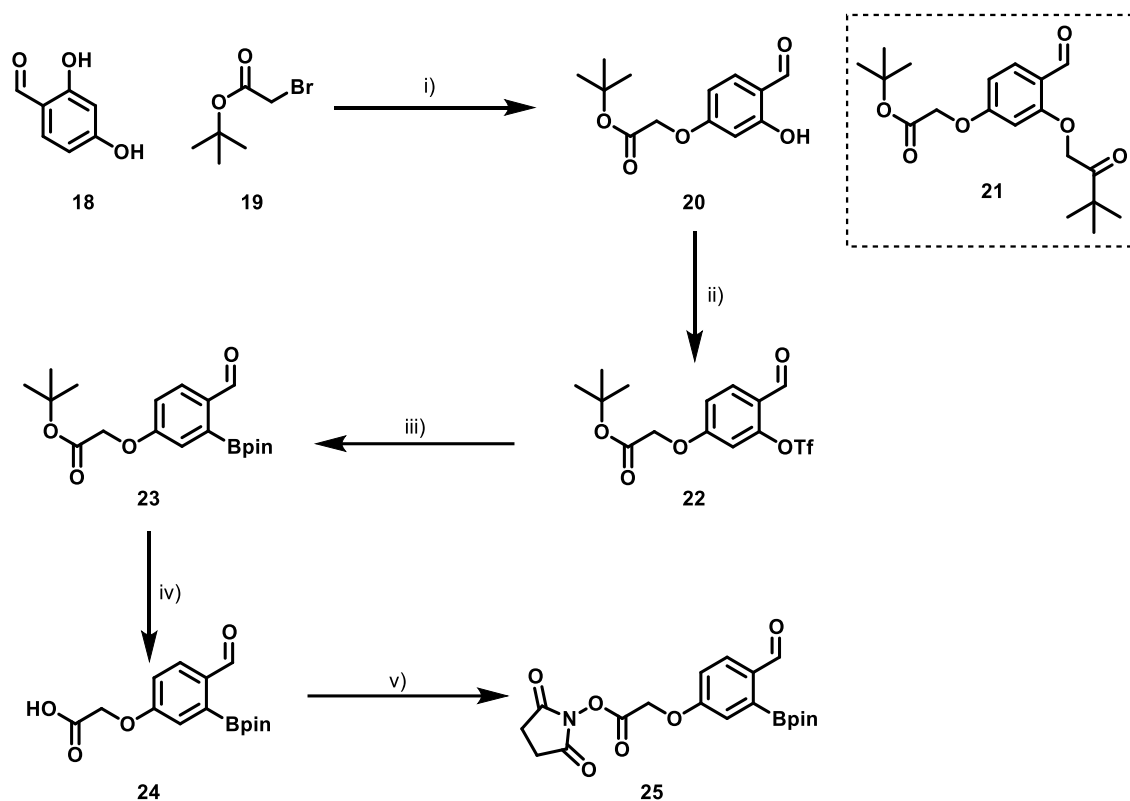


Scheme 5: a) Deprotection of the Cy3 dye **9** using methylamine to form **1**. Reagents and conditions: i) methylamine (w/w 6.7%), ethanol, r.t., 16 h 92%; b) Deprotection of the Cy5 dye **10** using methylamine to form **2**. Reagents and conditions: i) methylamine (w/w 6.7%), ethanol, r.t., 16 h 94%

2.2. Boronoaldehyde Synthesis

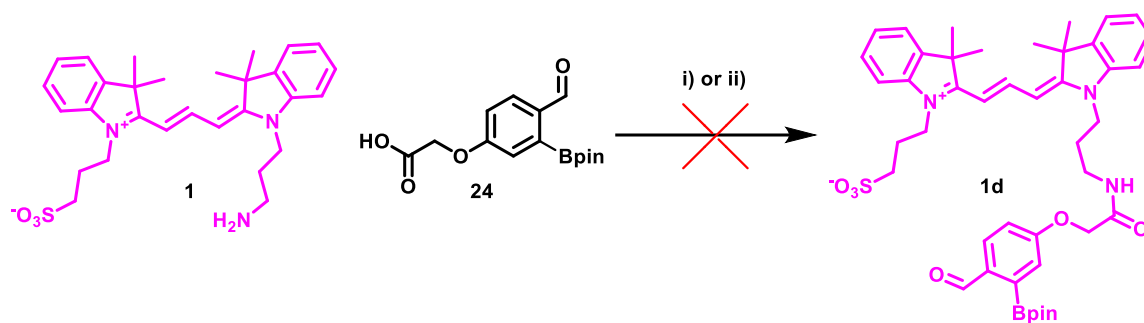
2.2.1. Amide Coupling

Synthesis of the boronoaldehyde precursor began with a commercially available 2,4-dihydroxybenzaldehyde **18** which was transformed into the *N*-hydroxysuccinimide (NHS) ester **25** in a five-step synthesis (Scheme 6). Phenol **18** was first reacted with bromoacetate **19** to form a mixture of mono-substituted phenol **20** and di-substituted species **21** in a 4:1 ratio respectively. The *ortho*-phenol group of **20** was then activated to form triflate **22** and borylated via a Miyaura borylation to form the boronic pinacol ester **23**. Synthesis continued with the *tert*-butyl ester group of **23** being deprotected (**24**) using TFA and then converted into the succinimide ester **25**.



Scheme 6: Synthesis of succinimide ester **25**. Reagents and conditions: i) K_2CO_3 , acetone, $65^\circ C$, 16 h, 33%; ii) $(CF_3SO_2)_2O$, Et_3N , CH_2Cl_2 , $-78^\circ C$, 30 min, 83%; iii) $Pd(dppf)Cl_2$, B_2Pin_2 , AcOK, dioxane, $80^\circ C$, 1 h, 57%; iv) TFA, CH_2Cl_2 , r.t. 1 h, quantitative yield; v) EDC, NHS, CH_2Cl_2 , r.t., 20 h, 94%

It was originally thought that compound **25** could subsequently be coupled to the free amine Cy3 dye (**1**) and the boronic acid deprotected to yield final Cy3-boronoaldehyde **1b** (Scheme 7). However, this synthesis was unsuccessful as confirmed by mass spectrometry and NMR analysis. Many spots were present via TLC, which made chromatography and separating these fractions challenging. We reasoned that methanol, which was used as the eluent due to its high polarity, had reacted with the boronic acid to form various adducts, but there was no indication that the product was present. The reaction was repeated, and the product was stirred in methanol for 1 h, to drive the formation of a single product, but the reaction was still unsuccessful, with no major product isolated. As a result, propylphosphonic anhydride (T3P) was used as an alternate coupling agent with carboxylic acid **24**, rather than forming the NHS intermediate ester **25**, which showed promising preliminary results. Using T3P coupling conditions, a signal consistent with the mass of **1d** was found by MS analysis. However, purification could not be achieved, as there was coelution of the product along with excess acid (**24**) starting material. The reaction was repeated with excess cyanine dye, but the reaction was still unsuccessful as the starting material was recovered, and product **1d** could not be isolated (Scheme 7).



Scheme 7: Amide coupling of Cy3 dye **1** with a carboxylic acid **24** with T3P to form the boronoaldehyde **1d**. Reagents and conditions: i) EDC, NHS, CH₂Cl₂, r.t, 20 h, 94% then Et₃N, CH₂Cl₂, r.t, 3 h, 0%; ii) T3P (50% w/w/ EtOAc), Et₃N, CH₂Cl₂, r.t, 3 h, 0%.

We hypothesised that rather than the free amine of cyanine dye **1** coupling to the activated carboxylic acid, it instead reacted at the aldehyde group of **24**, to form imine **26** (Fig. 8). In the case of a standard benzaldehyde, this would be a reversible reaction, with sufficient free amine to allow for amide coupling. However, the resultant *ortho*-boronoimine bond is stabilised significantly in organic solvent, by donation of electrons from the lone pair on the nitrogen, into the empty p-orbital of the boron (Fig. 9). This increased stabilisation prevented the *ortho*-boronoimine from reverting to the aldehyde and amine, and in turn prevented the formation of the desired amide bond. Therefore, the product peak identified by MS was presumably a result of only a small quantity of amide **1d**, which made its isolation difficult. Functionalisation of Cy3 side-product **26** was also not able to be isolated, as this too would be formed in low quantities, and may have dissociated on the column during purification. Whilst this result is promising for the goals of the project, as it shows the imine can be stabilised by use of an *ortho*-boronic acid pinacol ester (**26**), compound **1d** first had to be synthesised. Therefore, we moved towards a synthesis, which required borylation in the final step of the synthesis, thus allowing the amide coupling to take place prior to the formation of the reactive boronoaldehyde.

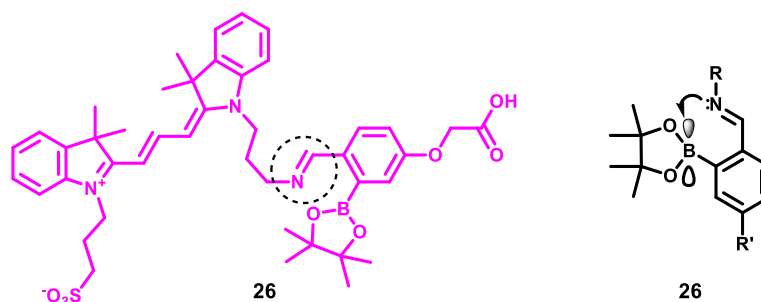
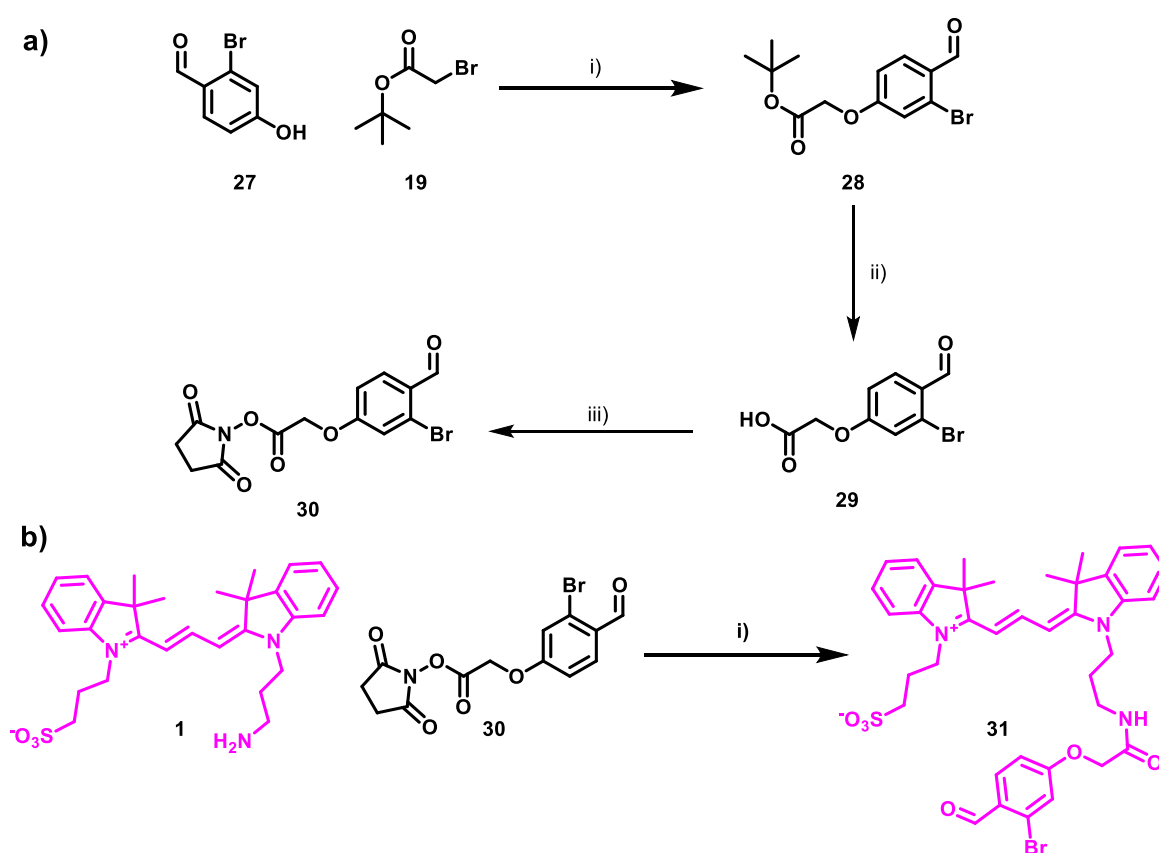


Figure 8: Hypothesised structure **26** with imine formation due to stabilising B-N interaction.

2.2.2. Final Step Borylation

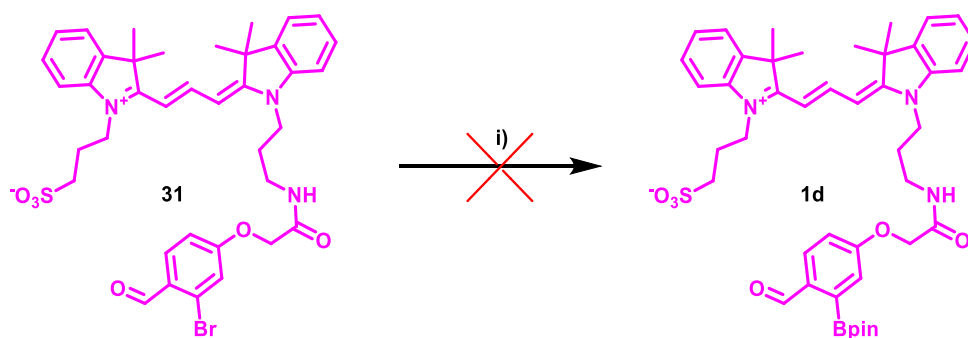
Compound **30** was synthesised in analogous reactions to those reported in section 2.2.1 (Scheme 6), but a solvent change was needed during the alkylation of **27** (Scheme 8a). Acetone was used originally during the alkylation reaction, but in this case underwent a competing aldol reaction with the aldehyde functionality. Acetone was therefore replaced with acetonitrile, and 2-bromo,4-hydroxybenzaldehyde **27** was first reacted with bromoacetate **19** to afford ester **28**. Ester **28** was then deprotected using TFA/CH₂Cl₂ to give the carboxylic acid **29** and activated by conversion to NHS ester to form **30**. Compound **31** was isolated in a 37% yield and in high purity (Scheme 8b).



Scheme 8: a) Synthesis of NHS ester **30**. Reagents and conditions: i) K₂CO₃, MeCN, 65 °C, 16 h, 96%; ii) TFA, CH₂Cl₂, r.t. 3 h, 97%; iii) EDC, NHS, CH₂Cl₂, r.t., 3 h, 80%. b) Amide coupling reaction to form compound **31**. Reagents and conditions: Et₃N, CH₂Cl₂, r.t., 3 h, 37%.

It was then hypothesised that **31** could be borylated to give the Cy3 boronoaldehyde pinacol ester **1d** through a Miyaura borylation. However, this reaction was unsuccessful and the pinacol ester was unable to be synthesised via this route. Mass spectrometry and NMR analysis followed purification, which showed that starting material was recovered from the reaction. This Miyaura borylation reaction was therefore unsuccessful. We hypothesise that

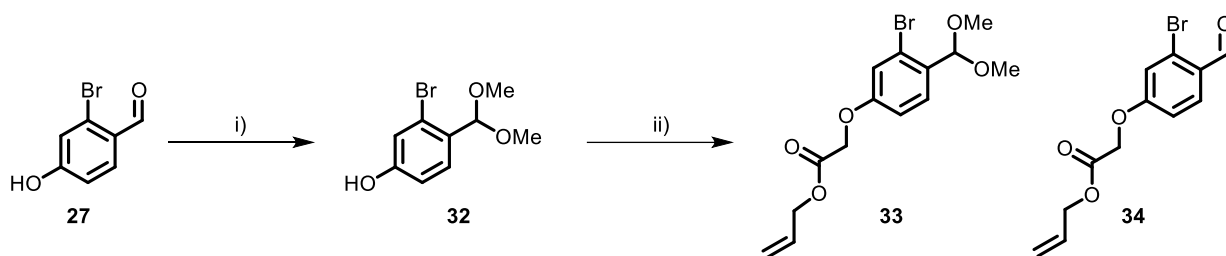
this was a result of the catalytic quantity of palladium which complexed to the conjugated alkene chain of the cyanine chromophore. Palladium could form a complex with the propyl alkene, whereby the palladium inserts itself into the conjugated chain. Whilst this does not alter the reactivity of the bromine for the borylation step, it means that the palladium is not available to catalyse the subsequent borylation reaction, leaving only starting material behind (Scheme 9).³³ Consequently, alternative methods were explored to yield the desired Cy3 *ortho*-boronoaldehyde.



Scheme 9: Attempted synthesis of *ortho*-boronoaldehyde **1d**. Reagents and conditions: i) Pd(dppf)Cl₂, B₂Pin₂, AcOK, dioxane, 80 °C, 1 h.

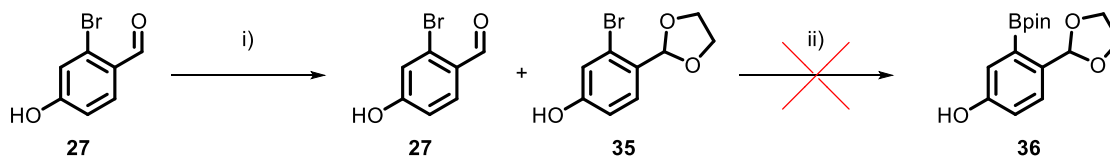
2.2.3. Acetal Protection

Considering previous unsuccessful reactions, the Cy3 *ortho*-boronoaldehyde synthesis was revised, this time with the idea to protect the aldehyde to prevent an imine group from forming during the amide coupling reaction. It was initially envisaged that aldehyde **27** could be protected to form dimethyl acetal **32** using trimethylorthoformate, which was achieved in a 93% yield (Scheme 10). Following the acetal protection to form **32**, the OH group then underwent alkylation with bromoacetate, bearing an allyl protecting group rather than the *tert*-butyl ester used in previous syntheses (Scheme 10). The alteration to the ester was made to prevent the need for acidic conditions to deprotect the *tert*-butyl group, which would likely lead to acetal cleavage. Instead, we envisaged employing palladium-catalysed ester cleavage. However, following the alkylation of **32**, it was identified that a mixture of the aldehyde (**34**) and the acetal (**33**) in a 1:2 ratio was formed.



Scheme 10: Acetal protection followed by alkylation reaction, leading to two different products **33** and **34** in a 1:2 ratio respectively. Reagents and conditions: i) $\text{HC}(\text{OCH}_3)_2$, $p\text{TsOH}\cdot\text{H}_2\text{O}$, MeOH , 70°C , 1 h, 93%; ii) Allyl bromoacetate, K_2CO_3 , MeCN , 75°C , 16 h.

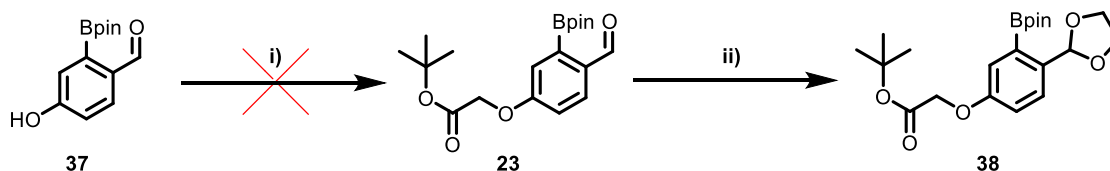
Therefore, the dimethyl acetal was too unstable with respect to the reagents and conditions required for the complete synthesis of the boronoaldehyde. A cyclic acetal was expected to be significantly more stable, so we therefore set out to synthesise **35** (Scheme 11). A trial reaction was set up with a literature compound 2-bromo-5-hydroxybenzaldehyde whereby the phenolic OH group was *meta*- to the aldehyde, which yielded the cyclic acetal in a 90% yield. However, the synthesis using 2-bromo-4-hydroxybenzaldehyde to yield acetal **35** was challenging and required extended periods of heating at reflux to achieve a 2:1 ratio of acetal **35** to aldehyde **27** respectively. The lack of reactivity could have been due to the increased electron density located at the aldehyde group of phenol **27** as a result of the electronic mesmeric effects from the *para*-OH group on the phenol vs the *meta*-OH group used previously, rendering the aldehyde less susceptible to nucleophilic attack. Additionally, this reaction showed only one spot by TLC which suggested that the acetal and aldehyde have very similar R_f values, which made purification challenging. The mixture was therefore carried through to the next step of the synthesis, which was envisaged to be more readily separated after addition of a bulky pinacol ester group. However, upon reaction, it was evident that the cyclic acetal was not able to withstand the Miyaura borylation reaction conditions, with only the borylated aldehyde recovered from the reaction mixture.



Scheme 11: Cyclic acetal protection using Dean-Stark conditions. Reagents and conditions: i) Ethylene glycol, $p\text{TsOH}$, Toluene, Dean-Stark conditions, 16 h; ii) $\text{Pd}(\text{dppf})\text{Cl}_2$, B_2Pin_2 , AcOK , dioxane, 80°C , 1 h, 0%.

In a final attempt at employing acetal protection to synthesise the target molecule, aldehyde **37** was first alkylated to form aldehyde **23** prior to the addition of the acetal to give ester **38** (Scheme 12). We anticipated that after the addition of the alkyl group to form ester **23** the lone pair of the electrons on the oxygen located *para*- to the aldehyde will be less available for

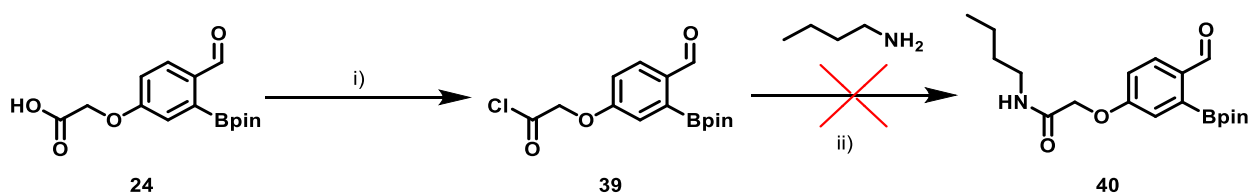
delocalisation into the aromatic ring, and therefore will make the aldehyde more electrophilic than in the synthesis attempted previously, promoting acetal formation. However, acetal **38** could not be isolated in pure form, potentially due to analogous electronic mesmeric effects in the ring. Due to the overall instability of the acetal derivative, the retrosynthetic analysis had to be revised to synthesise the Cy3 *ortho*-boronoaldehyde using an alternative approach.



Scheme 12: Unsuccessful synthesis of cyclic acetal protection (**38**). Reagents and conditions: i) K_2CO_3 , acetonitrile, 70 °C, 16 h, 48%; ii) ethylene glycol, $pTsOH.H_2O$, MeOH, Dean-Stark conditions, 16 h.

2.2.4. Acyl Chloride

It was envisaged that if the carboxylic acid group of **24** could be activated to be more reactive than the NHS ester in **25**, then imine formation at the aldehyde would be less likely to outcompete amide formation. As such, synthesis of **1d** was attempted through an acyl chloride reaction intermediate **39**. Compound **24** was resynthesised using the same reaction conditions shown previously (Scheme 6). We initially tested this hypothesis by attempting the formation of butyl amide **40** looking at imine formation. The carboxylic acid was converted into the acyl chloride **39** using thionyl chloride, which was immediately coupled with *n*-butylamine without purification to prevent hydrolysis of the acyl chloride (Scheme 13).



Scheme 13: Synthesis of amide **40** from carboxylic acid **24** using an activated acyl chloride (**39**). Reagents and conditions: i) $SOCl_2$, DMF, 2 h, reflux, quantitative yield; ii) Et_3N , anhydrous THF, r.t., 3 h, 0%.

Upon analysis, it was found that **40** had not formed. We hypothesised that thionyl chloride had reacted with the aldehyde of **24**, resulting in a dichlorinated species **41** as well as forming the desired acyl chloride (Fig. 10).³⁴ The attachment of the butyl amine group was successful, with the corresponding aromatic and aliphatic protons being present with the correct integrals and splitting patterns. However, the 1H NMR however showed the aldehyde peak had shifted

from around 11.0 ppm to 7.8 ppm, indicative of the dichlorinated species (**41**). However, analysis by mass spectrometry was not able to confirm the dichlorinated species.

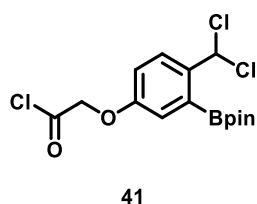
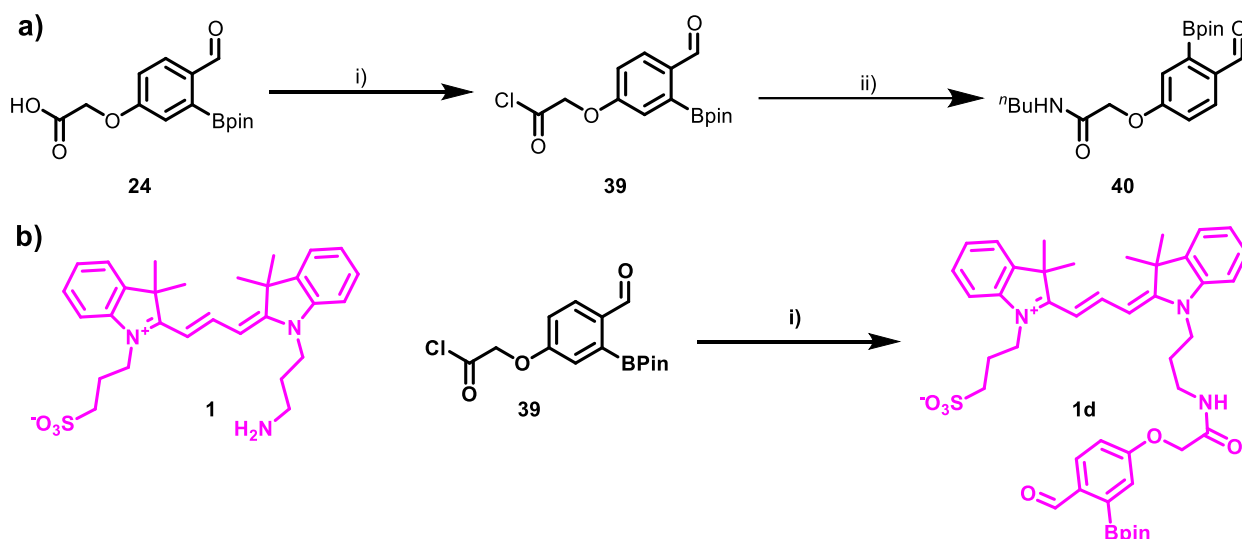


Figure 9: Suspected product **41** formed by reaction with thionyl chloride.

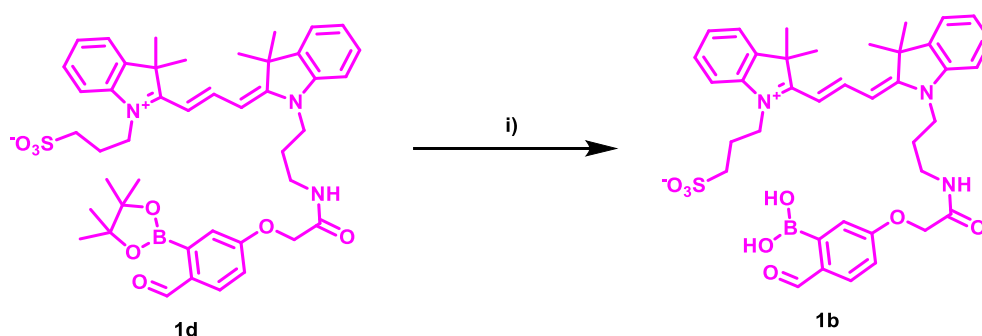
Synthesis of **39** was therefore performed using oxalyl chloride as the chlorinating reagent, which employed much more mild conditions, with the reaction being carried out at room temperature (Scheme 14a). Following subsequent reaction with butyl amine and the successful isolation of butyl amide **40** (Scheme 14a), this provided precedent to carry forward the reaction conditions to synthesis boronoaldehyde **1d**, in an analogous synthesis (Scheme 14b). Therefore, activated acyl chloride **39** was synthesised and coupled to the Cy3 dye (**1**) to form the boronoaldehyde pinacol ester **1d**.



Scheme 14: a) Synthesis of *n*-butylamide product **40**. Reagents and conditions: i) $(\text{COCl})_2$, DMF, r.t., 2 h, quantitative yield; ii) Et_3N , *N*-butylamine, anhydrous THF, r.t., 3 h, 54%. b) Coupling of Cy3 dye with acyl chloride **39** to form pinacol ester protected boronoaldehyde **1d**. Reagents and conditions: DMAP, K_2CO_3 , anhydrous DMF, r.t., 3 h, 43%.

The initial results of this experiment appeared to be promising as the structure was identified by MS and NMR analysis. However, upon further analysis there was a large contamination of triethylamine (23 equivalents) in the final product. Instead, three equivalents of 4-dimethylaminopyridine (DMAP) were added as a base, to avoid excess contamination. Once again, the product structure was identified by both MS and NMR analysis. However, upon isolation, there seemed to be DMAP present in the product in a 1:1 ratio with the product (Fig. 10a). This ratio may have been due to the lone pair of electrons on DMAP which can complex

to the empty p-orbital of the boronic ester stoichiometrically. The product was therefore mixed with hydrochloric acid (0.1 M) to break up the predicted DMAP-pinacol complex, which yielded the pinacol ester **1d** in high purity, but low yield. Due to the poor solubility of cyanine dyes, NMR data was collected in *d*-methanol, which yielded the acetal product (Fig. 10b), but correlated to the desired product. Pinacol ester **1d** was then deprotected via transesterification with methyl boronic acid to yield the final boronoaldehyde compound **1b**.³⁵ Following isolation, a portion of **1b** underwent a test reaction with *n*-butylamine, to confirm the presence of the *ortho*-boronoaldehyde (Scheme 15). Formation of a borono-stabilised imine caused the acetal peak in deuterated methanol to shift from 5.65 ppm to a peak at 8.62 ppm, indicating boronoimine formation (Fig. 10c).³⁶



Scheme 15: Deprotection of the pinacol ester to give the final oBA **1b**. Reagents and conditions: MeB(OH)₂, TFA CH₂Cl₂, 3 h, r.t. quantitative yield.

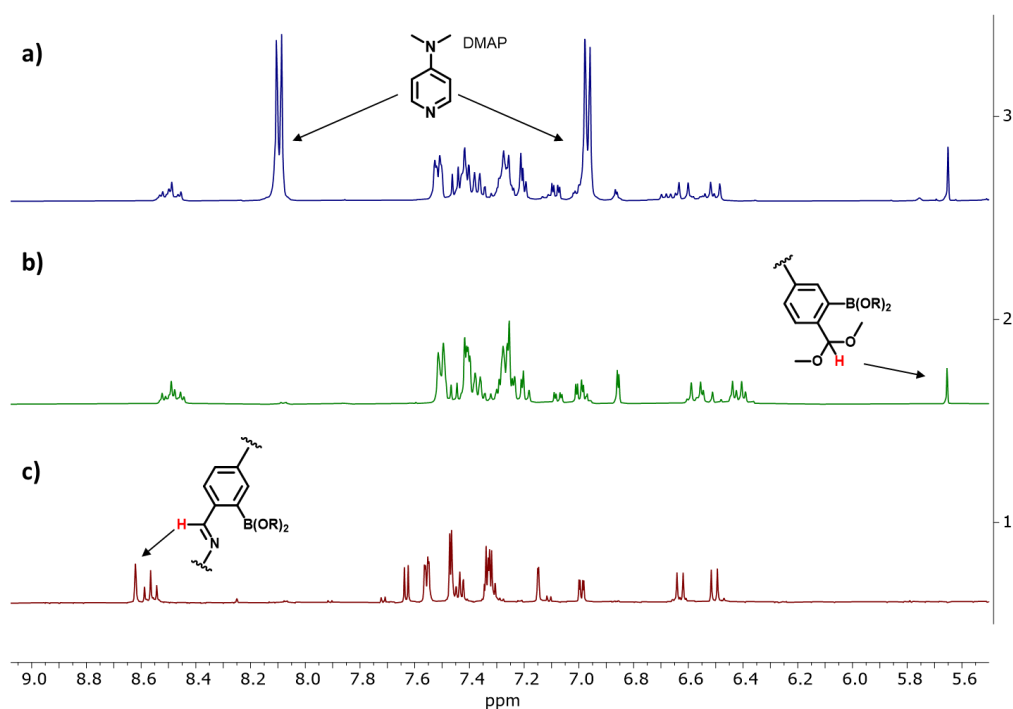
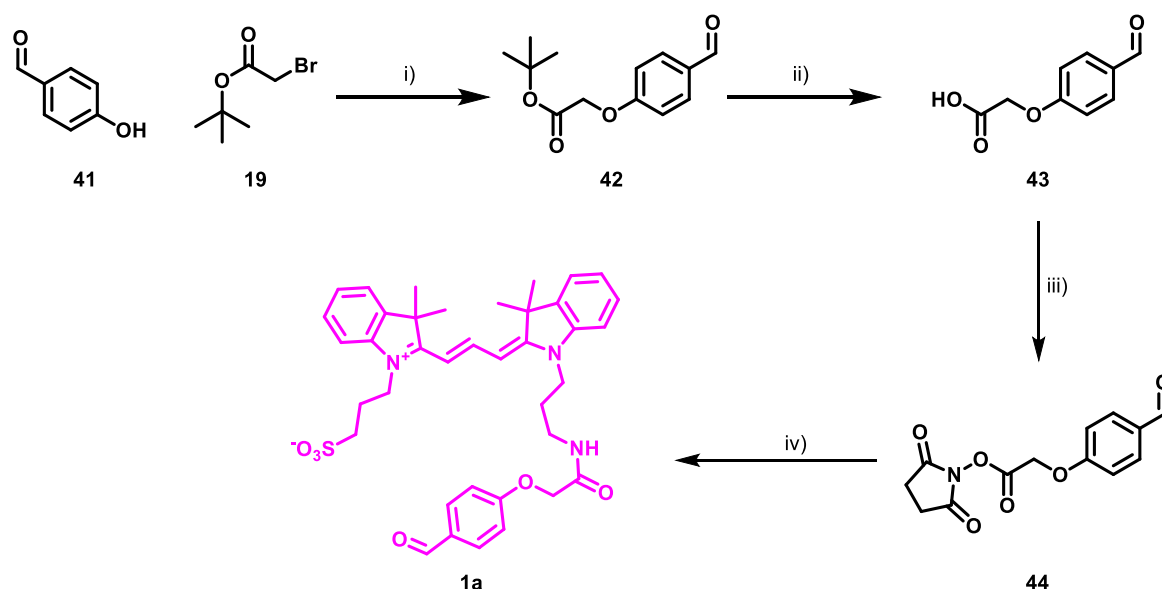


Figure 10: NMR structures of isolated intermediates in CD₃OD of **1b** showing different stages of purification; a) Pinacol ester **1d** with DMAP (7.00 and 8.10 ppm) impurity; b) *ortho*-boronoaldehyde in *d*-methanol existing as the acetal (5.65 ppm); c) imine (8.61 ppm) product formation with reaction of *n*-butylamine showing acetal absence (5.65 ppm).

2.3. Cy3 Negative Control Synthesis

2.3.1. Aldehyde

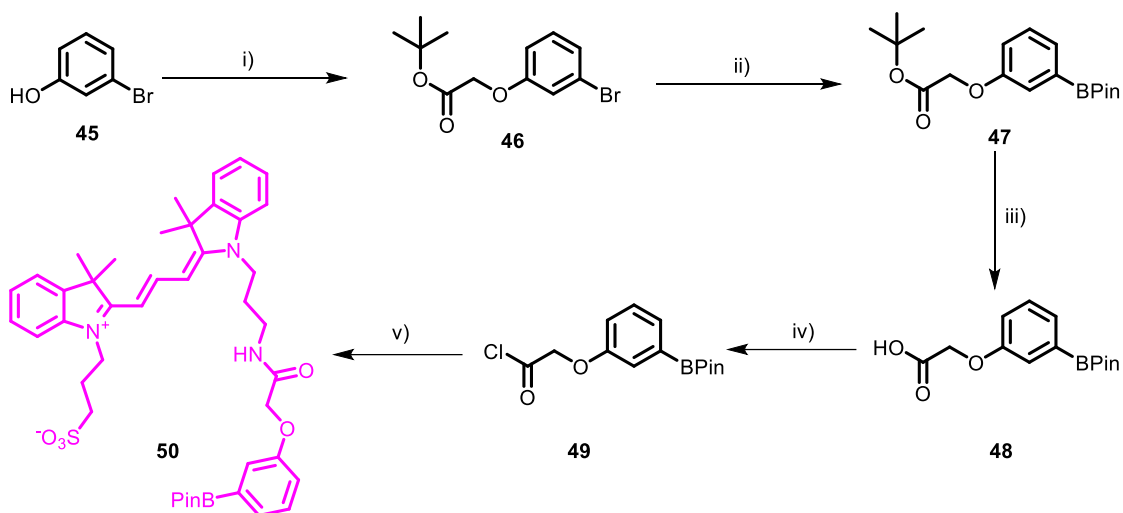
The Cy3 negative controls were necessary to analyse the stabilisation effect of the boronic acid moiety of the *ortho*-boronoaldehyde **1b** and gave a baseline that results could be compared against. The synthesis of the aldehyde control began with commercially available 4-hydroxybenzaldehyde **41** which was transformed into the Cy3 aldehyde **1a** in a four-step synthesis (Scheme 16) with an overall 34% yield. In the first step, **41** was reacted with a bromoacetate **19** to afford ether **42**. This was then deprotected (**43**) using trifluoroacetic acid and reacted with *N*-hydroxysuccinimide to form the NHS ester **44**. NHS ester **44** was used again in a coupling reaction with the free amine Cy3 dye **1**, to yield Cy3 aldehyde **1a** in a 45% yield (Scheme 16). This negative control was later used to produce baseline FRET data to compare the *ortho*-boronoaldehyde against as described in Chapter 3.



Scheme 16: Synthesis of aldehyde **1a**. Reagents and conditions: i) K_2CO_3 , acetone, 65 °C, 16 h, 74%, ii) TFA, CH_2Cl_2 , r.t. 1 h, 99%, iii) EDC, NHS, CH_2Cl_2 , r.t, 20 h, 46%, iv) Et_3N , CH_2Cl_2 r.t, 3 h, 45%

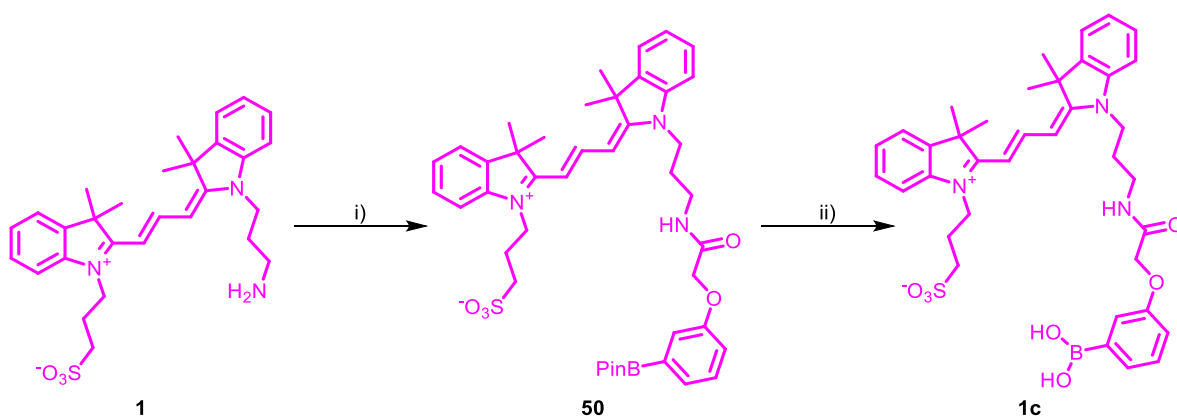
2.3.2. Boronic Acid

The synthesis began with commercially available 3-bromophenol **45** which was transformed into pinacol ester **51** in a five-step synthesis with an overall 73% yield (Scheme 17). Phenol **45** was first alkylated with bromoacetate **19** to afford ether **46**, which then underwent Miyaura borylation to give **47**, before deprotection with TFA to give carboxylic acid **48**.



Scheme 17: Synthesis of protected boronic pinacol ester (**50**). Reagents and conditions: i) *tert*-Butyl bromoacetate, K_2CO_3 , acetone, 65 °C, 16 h, quantitative yield; ii) B_2Pin_2 , $Pd(dppf)Cl_2$, AcOK, anhydrous dioxane, 80 °C, 1 h, 88%; iii) TFA, CH_2Cl_2 , 3 h, r.t., 83%; iv) $(COCl)_2$, DMF, r.t., 2 h, quantitative yield.

Carboxylic acid **48** was finally activated to form acyl chloride **49** by reaction with oxalyl chloride, to increase the electrophilicity of the carbonyl, which could then be reacted with the Cy3 dye **1** to provide borylated dye **50** (Scheme 18). Cy3 dye **50** was subsequently deprotected via transesterification with methyl boronic acid to yield the final boronic acid **1c** (Scheme 18),³⁵ which could then be used as a negative control for subsequent FRET assays as it has no clear binding site for oBID formation.

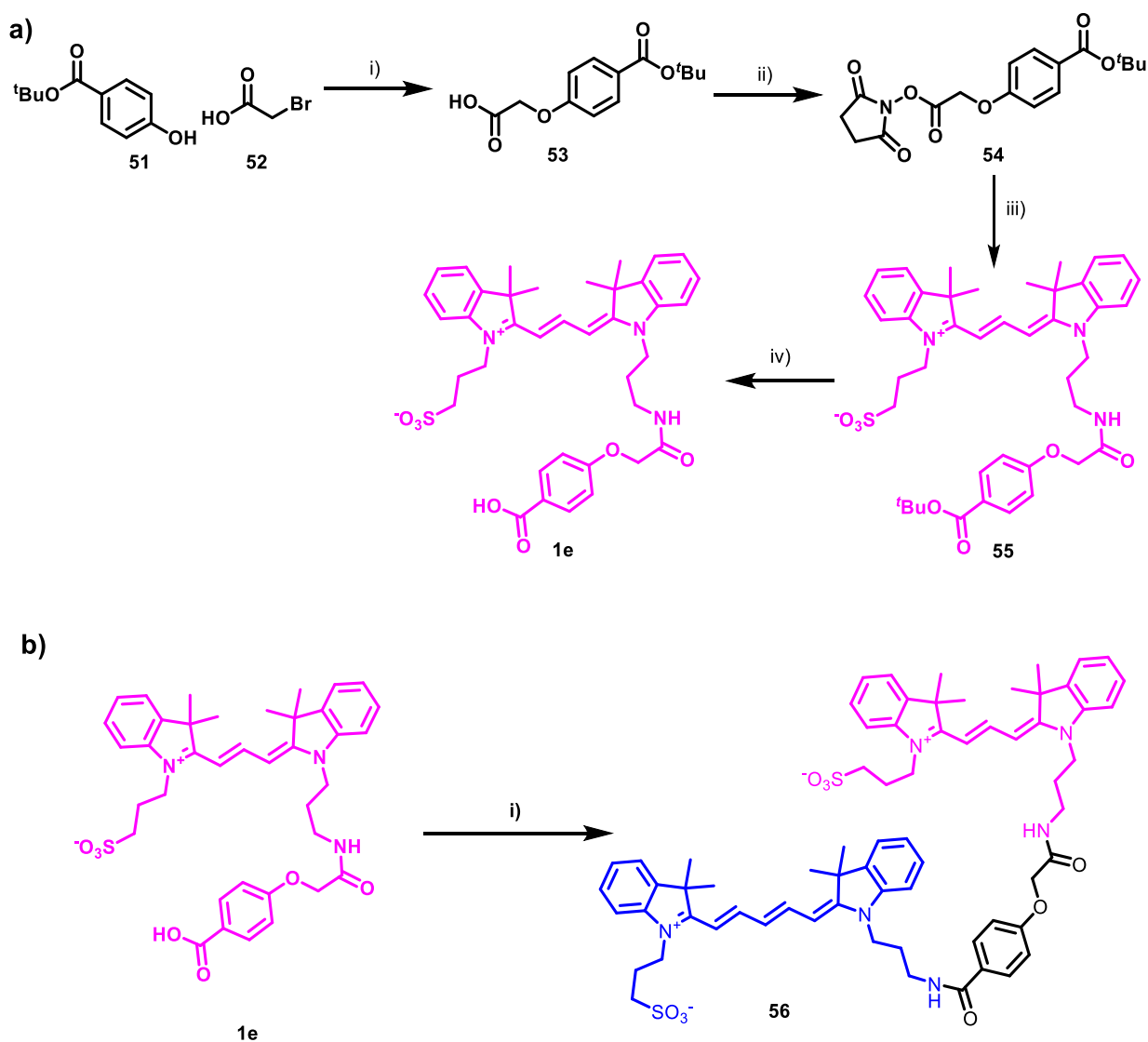


Scheme 18: Synthesis of boronic acid (**1c**). Reagents and conditions: i) **30**, DMAP, K_2CO_3 , DMF, 3 h, r.t., 14%; ii) $MeB(OH)_2$, CH_2Cl_2 , r.t., 16 h, quantitative yield.

2.4. Positive Control Synthesis

2.4.1. Carboxylic Acid

The synthesis of Cy3-carboxylic acid **1e** was analogous to the previously discussed aldehyde synthesis (section 2.4) to give a precursor for the synthesis of a positive control for FRET studies. Synthesis began with phenol **51** undergoing alkylation with 2-bromo acetic acid **52** to give acid **53**. This was then activated to give reactive succinimide ester **54** which then underwent an amide coupling reaction to give the protected acid Cy3 **55**. Compound **55** was finally deprotected with TFA/CH₂Cl₂ to give the unprotected acid **1e** (Scheme 19a). **1e** was then coupled to the free amine Cy5 dye **2** using T3P, to synthesise the positive control **56** (Scheme 19b).

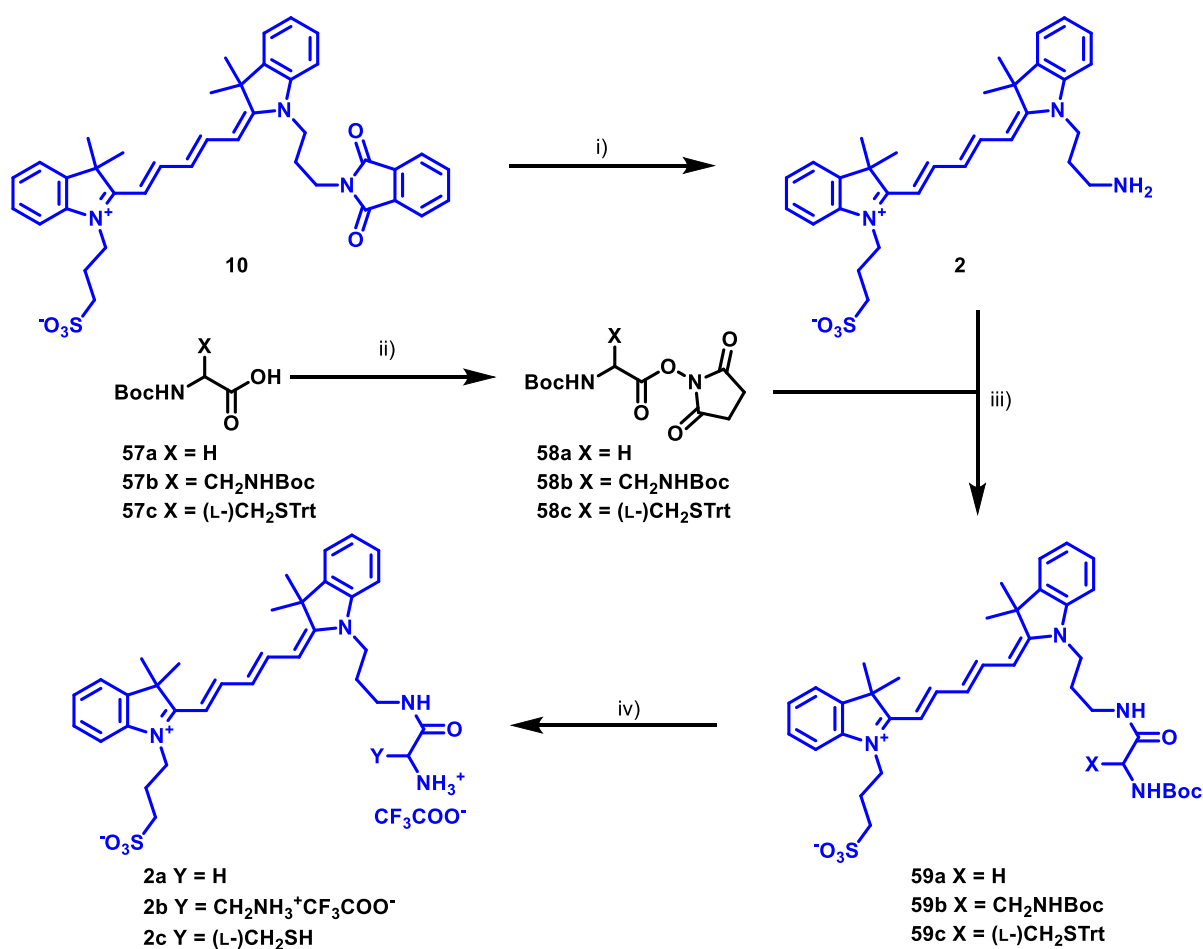


Scheme 19: a) Synthesis of carboxylic acid **1e**. Reagents and conditions: i) K₂CO₃, DMF, 80 °C, 16 h, 6%, ii) EDC, NHS, CH₂Cl₂, r.t., 3 h, 56%; iii) **1**, Et₃N, CH₂Cl₂, r.t., 3 h, 45%; iv) TFA, CH₂Cl₂, r.t., 2 h, 37%. **b)** Synthesis of covalently linked positive control **56**. Reagents and conditions: **2**, T3P (50% w/w/ EtOAc), Et₃N, CH₂Cl₂, r.t., 16 h, 33%

2.5. Cy5 Dye Synthesis

2.5.1. Amine Synthesis

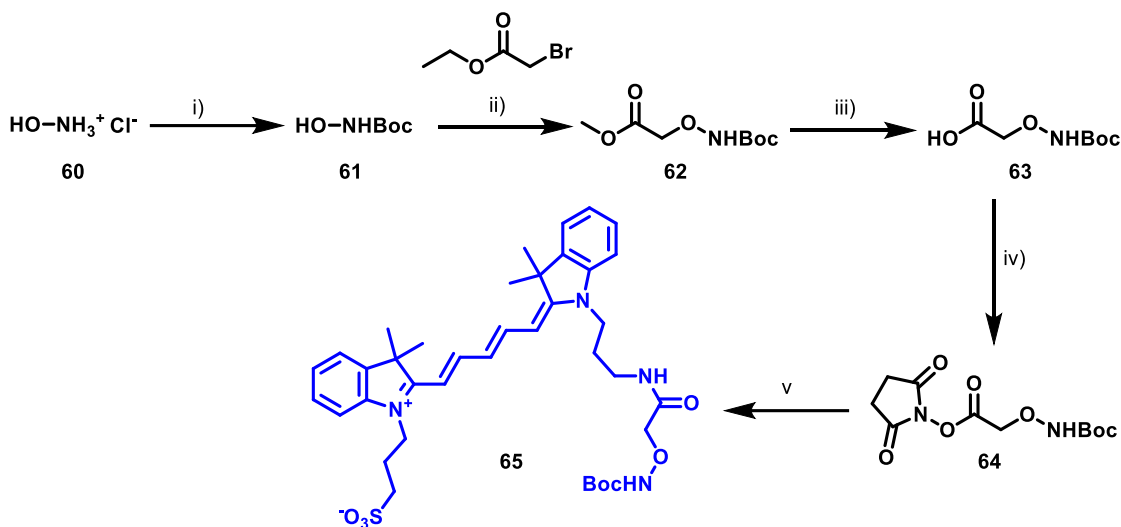
Synthesis of the amine series began with a protected amino acid derivative, whereby the acid group (**57a/b/c**) was functionalised into the succinimide esters (**58a/b/c**). These were then coupled with the deprotected Cy5 dye (**2**) to form **59a/b/c**, which were further deprotected via an acid workup to afford the final amine trifluoroacetate salts (**2a/b/c**). The syntheses of compounds **2a-c** were relatively straightforward due to optimised procedures carried out by previous group members,³⁷ which allowed good yields to be obtained. With a good understanding of the optimised route, many compounds can be synthesised using this generic route to generate a library of compounds (Scheme 20).



Scheme 20: Complete synthesis of compounds **2a**, **2b** and **2c** with coupling of the Cy5 dye. Reagents and conditions: i) methylamine (w/w 40%), ethanol, r.t. 67%, ii) EDC, NHS, CH₂Cl₂, r.t. 20 h, **58a** 100%, **58b** 74%, **58c** 89%; iii) Et₃N, CH₂Cl₂, r.t. 3 h, **59a** 84%, **59b** 76%, **59c** 74%, iv) TFA, CH₂Cl₂, r.t. 1 h, **2a** quantitative yield, **2b** 86%, **2c** 91%

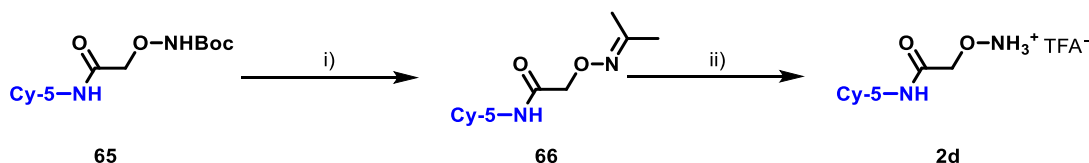
2.5.2. Hydroxylamine Synthesis

Hydroxylamine synthesis (Scheme 21) began with a commercially available solution of hydroxylamine hydrochloride **60**, which was protected with Boc anhydride **61** and alkylated to afford ester **62**. The ester group was then hydrolysed with lithium hydroxide to yield acid **63** and activated as the NHS ester **64**, which was ready to be coupled to the Cy5 dye. The newly formed hydroxylamine succinimide ester **64** underwent an amide coupling with the Cy5 dye yielding the Boc protected hydroxylamine dye **65**.



Scheme 21: Synthesis of hydroxylamine dye **65**. Reagents and conditions: i) Boc_2O , NaHCO_3 , $\text{THF}:\text{H}_2\text{O}$ (1:1), r.t., 20 h, 89% ii) KOH , MeOH , 60°C , 16 h, 53%, iii) LiOH , $\text{THF}:\text{H}_2\text{O}$ (1:1), r.t., 16 h, 77% iv) EDC , NHS , CH_2Cl_2 , r.t., 2 h, 81%; v) Et_3N , CH_2Cl_2 , r.t., 2 h, 38%,

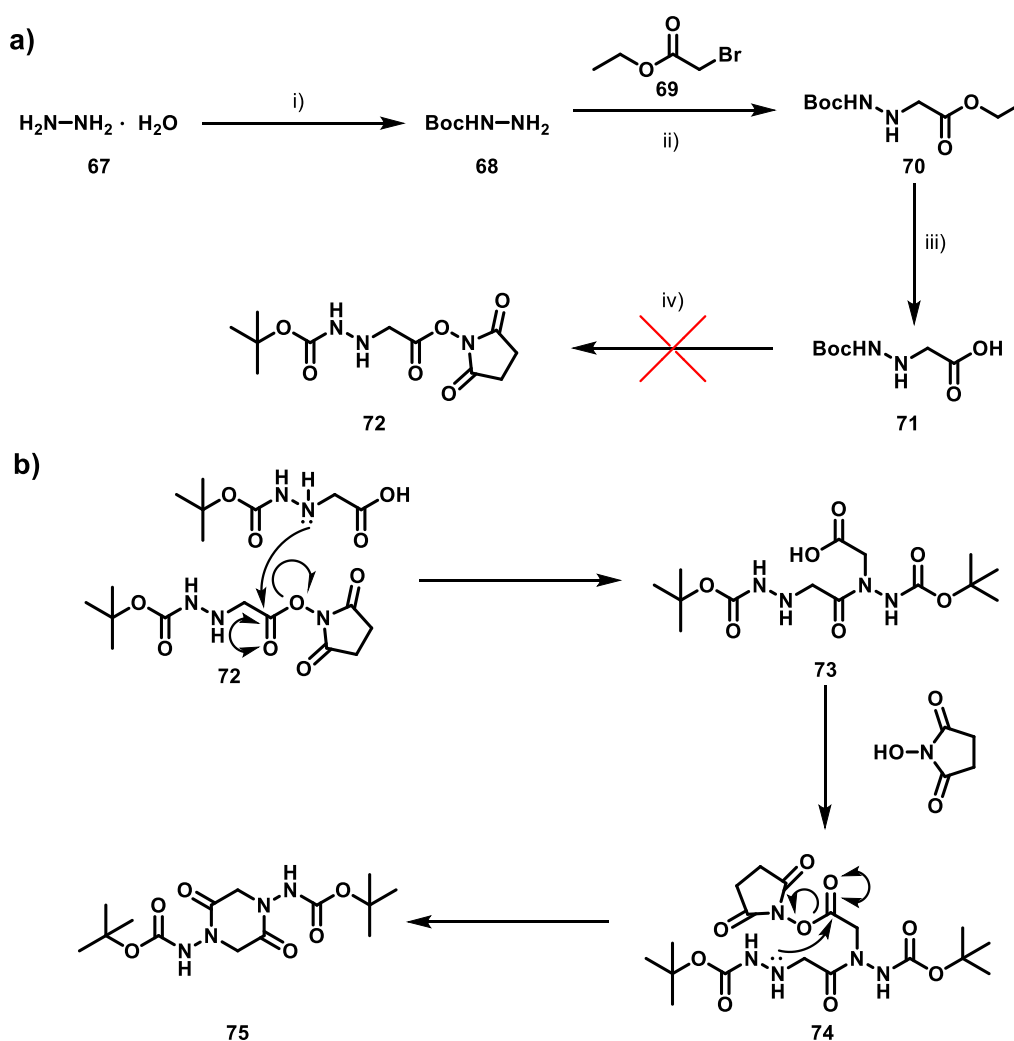
The reactivity of the hydroxylamine group meant that the subsequent Boc deprotection of **65** should be undertaken in anhydrous conditions and free of acetone. Despite efforts to suppress the reactivity of the hydroxylamine group, the hydroxylamine functionality reacted with trace acetone, resulting in complete conversion of the hydroxylamine to the oxime **66**. As a result of this further reaction, we found literature precedent that heating an oxime in aqueous acidic conditions at reflux could reinstate the hydroxylamine functionality (Scheme 22).^{38–40} However, considering the risk of decomposing the dye, the reaction vessel was heated to 80°C rather than 100°C , in more moderate conditions for 2 h, which reinstated the hydroxylamine functional group. Hydroxylamine **2d** could then be used in subsequent FRET studies.



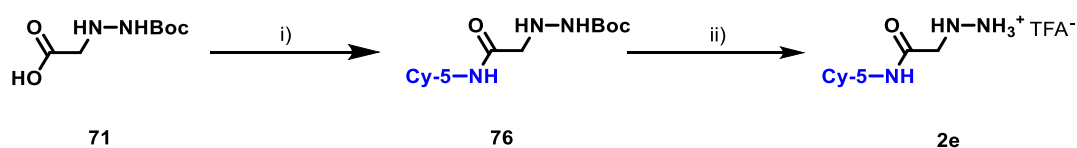
Scheme 22: Removal of the Boc group (**65**) and subsequent reaction with acetone to form imine **66** followed by deprotection (**2d**). Reagents and conditions: i) TFA , CH_2Cl_2 , r.t., 2 h, 74%; ii) HCl (2 M), 80°C , 3 h, quantitative yield.

2.5.3. Synthesis of Cy5 Hydrazine

Synthesis of the Cy5 hydrazine began with commercially available hydrazine monohydrate **67** which was transformed into the activated NHS ester **72** in a four-step synthesis (Scheme 23a). Hydrazine monohydrate **67** was first reacted with Boc anhydride to afford carbamate **68**. Carbamate **68** then underwent an alkylation reaction with ethyl bromoacetate **69** to form amide **70** before deprotection using lithium hydroxide to give carboxylic acid **71**, which was then activated to form the NHS ester **72**. However, NHS ester **72** was not observed by NMR and mass spectrometry, which suggested that possible side reactions potentially involving intramolecular cyclisation of the activated NHS ester **72** may have occurred, which were supported by NMR and mass spectrometry.



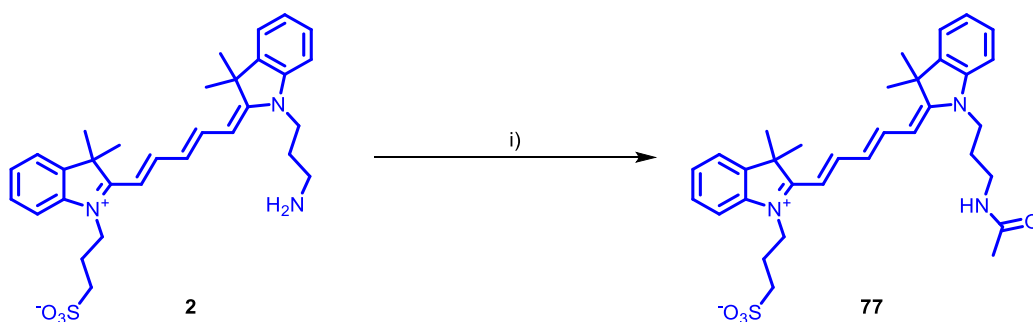
We propose that upon forming NHS ester **72**, the secondary amine of an additional equivalent of carboxylic acid **71** was able to attack to form tertiary amine **73**. The amine could then form a further NHS ester **74**, which could now undergo intramolecular cyclisation with the remaining secondary amine to form diketopiperazine **75** (Scheme 23b). This hypothesis is supported by mass spectrometry, and ^1H NMR analysis showing a symmetric product **75** isolated. This hypothesis was also in line with recent literature.^{41,42} Therefore, an alternative coupling agent was explored to couple carboxylic acid **71** with Cy5 dye **2** (Scheme 24). This amide coupling was successful with the use of T3P and was subsequently deprotected with TFA to give the final product (**2e**), which could then be used in FRET assays.



Scheme 24: Synthesis of **2e** using T3P coupling reagent. Reagents and conditions: i) T3P (w/w 50% EtOAc), CH_2Cl_2 , Et_3N , r.t. 3 h, 43%; ii) TFA, CH_2Cl_2 , r.t. 3 h, quantitative yield.

2.6. Acetate Cap Synthesis

To provide a negative control for FRET studies where conjugation is not possible, we synthesised a Cy5 dye capped with an acetate group. This compound provides a reference for 0% conjugation in subsequent FRET studies when reacted with a range of Cy3 dye analogues. Amino Cy5 dye (**2**) was reacted with acetyl chloride, to form the acetate cap reference dye **77** (Scheme 25).



Scheme 25: Synthesis of the Cy5 acetate cap **77** to form an unbound reference sample. Reagents and conditions: i) AcCl , CH_2Cl_2 , r.t., 2 h, 64%.

2.7. Elucidation of NMR assignment

The exact assignment of the ^1H and ^{13}C NMR signals of the cyanine dyes was challenging due to its complex and conjugated structure. The cyanine dyes are almost symmetric, which means that the proton environments come at almost exactly the same chemical shifts but with subtle differences in some parts. This made protons H5–8 in Fig. 12 difficult to assign accurately, as shown in Fig. 11a between 7.20–7.60 ppm. As H-5 and H-8 neighbour quaternary carbon atoms, it is difficult to conclusively choose a starting point, to assign all of the protons in close proximity.

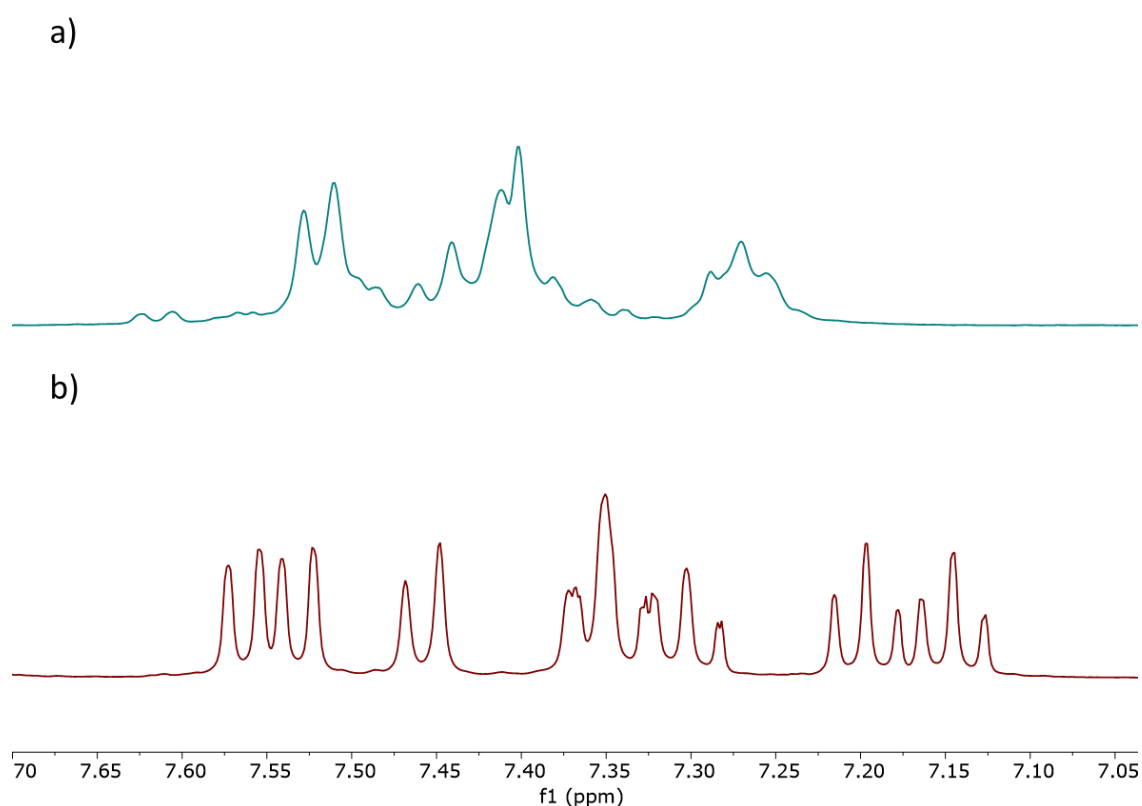


Figure 11: ^1H NMR of aromatic protons in cyanine dyes in a) CD_3OD and b) $\text{DMSO}-d_6$; showing difference in splitting pattern.

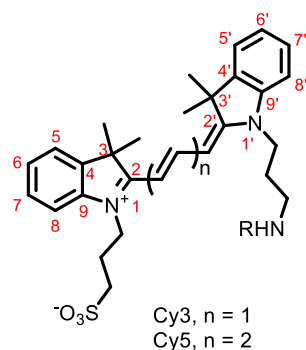


Figure 12: Generic scheme for Cy3 and Cy5 dyes for assigning NMR data.

Nuclear Overhauser Effect Spectroscopy (NOESY) NMR was therefore employed to correlate the two dimethyl groups at C3 of the indole rings, with H-5 and CH, as shown on in Fig. 12. This provided a definitive starting point to assign the remaining protons in the spectrum. NMR analysis was also carried out in a more concentrated solution in DMSO- d_6 (Fig. 11b) to aid assignment. The NMR spectra ran in DMSO- d_6 showed much more defined individual splitting patterns. As shown in Fig. 12, H-5, H-6 and H-7 all have almost perfect symmetry, and therefore show integrals of 2.0 for each peak, corresponding to each side of the almost symmetric molecule. However, H-8, which neighbours a positively charged nitrogen atom, conjugated across the whole unsaturated backbone, was split into two separate peaks, corresponding to H-8 and H-8', which offsets their intensity. This has allowed the elucidation of the complete ^1H NMR spectrum, and subsequently ^{13}C spectrum of a challenging set of molecules.

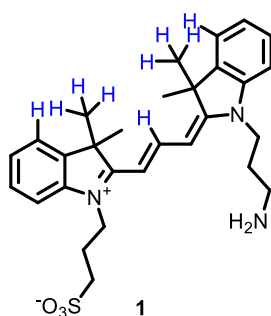


Figure 13: The use of NOESY NMR to determine the assignment of H-5, which allowed the subsequent assignment of H-6, H-7 and H-8.

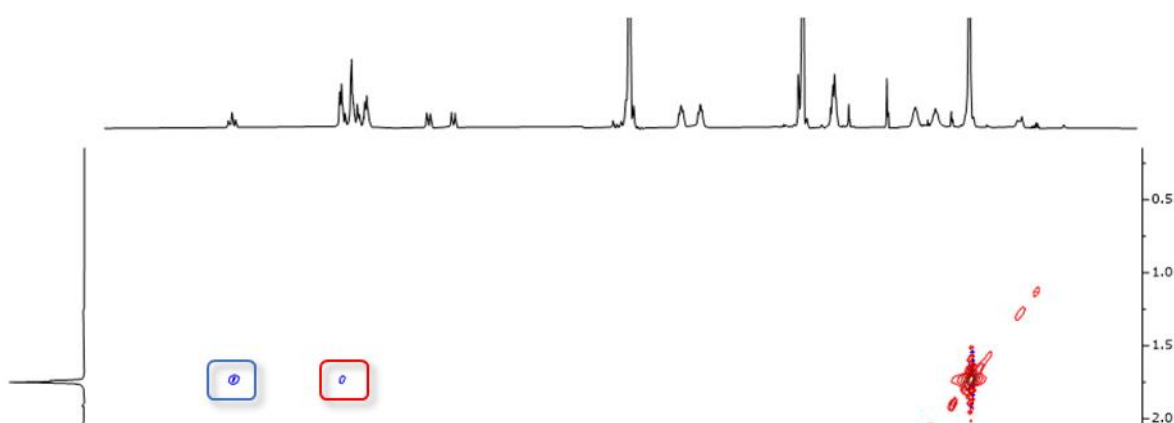


Figure 14: NOESY spectra of **1** to show coupling proximity of dimethyl groups at C3 with H-5 (red box) and CH group (blue box).

3. Conclusion

In this chapter, we have outlined the benefits of using a FRET-based platform over alternative analytical techniques to monitor oBID formation. We have established an optimised five-step synthesis for Cy3 and Cy5 dyes, which can be made on a gram-scale over 5 days in an overall yield of ~30% to generate cyanine dyes which are otherwise highly expensive. Methylamine was used over longer reaction times rather than a hydrazine functionality for the deprotection of the phthalimide group. These cyanine dyes were used in this work to monitor oBID formation from respective Cy3 oBAs and Cy5 amine-based nucleophiles (Fig. 15). The cyanine dyes synthesised in this work have led to many collaborations in the field of chemical biology, such as bioconjugation, fluorescent labelling and indeed other FRET assays. A Cy3 oBA (**1b**) was generated following an array of different reaction conditions including amide coupling, a final step borylation, acetal protecting chemistry before finally using an activated acyl chloride group to outcompete interfering B–N interactions, to form the Cy3 oBA. Cy3 negative control dyes were synthesised bearing either an aldehyde (**1a**) or boronic acid (**1c**) moiety, as well as a positive control with a Cy3 carboxylic acid group (**1e**), which could be irreversibly bound to a Cy5 dye, which will be used in subsequent FRET studies. Finally, a panel of Cy5 amine-based nucleophiles (**2a-e**) were synthesised, which were used to form several oBIDs.

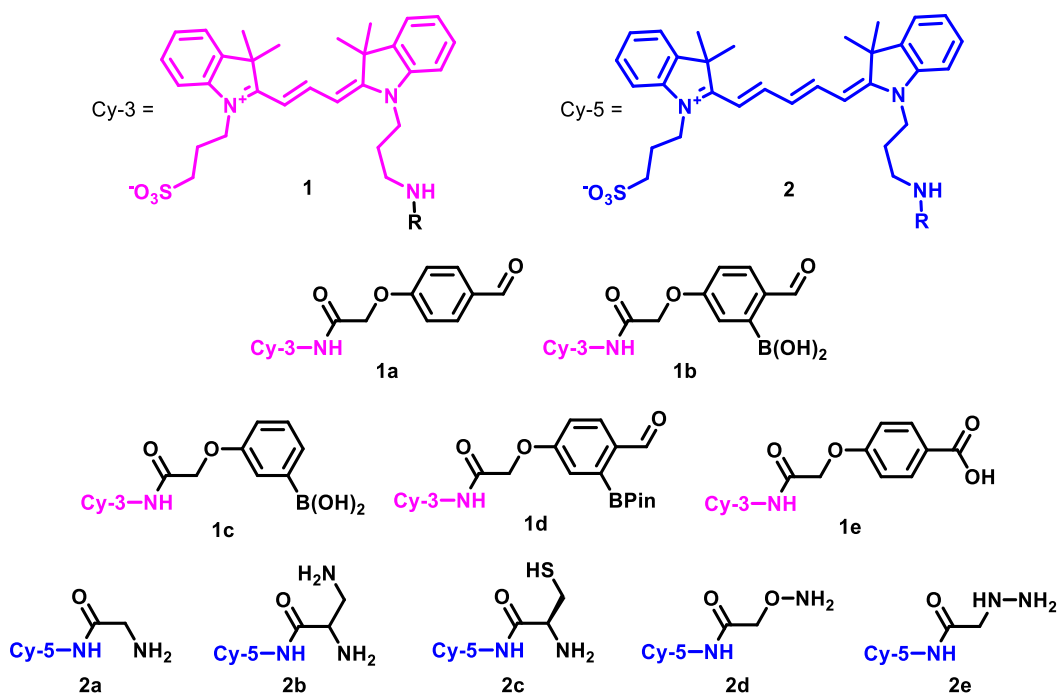


Figure 15: Cy3 (**1a-e**) and Cy5 (**2a-e**) molecules that were synthesised during this study.

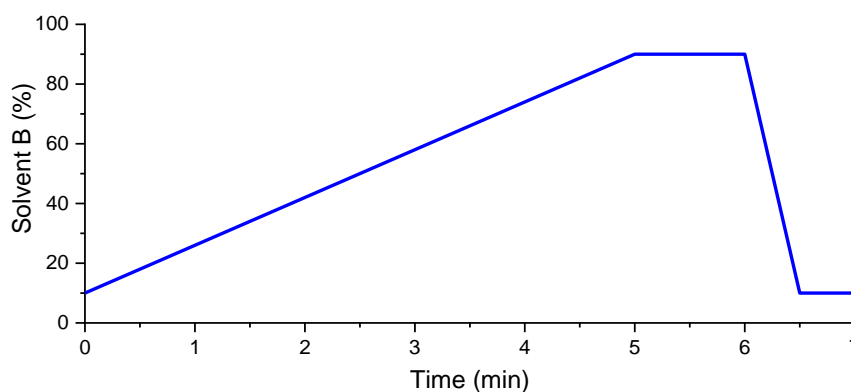
4. Experimental

4.1 General Considerations

Proton and carbon nuclear magnetic resonance (^1H and ^{13}C NMR respectively) spectra were recorded on a Jeol ECX-400 (400 MHz) or Bruker AVIIIHD (500 MHz) spectrometer. NMR shifts were assigned using COSY, HSQC and HMBC spectra. All chemical shifts are quoted on the δ scale in ppm using residual solvent as the internal standard (^1H NMR: $\text{CDCl}_3 = 7.26$; $\text{MeOD} = 3.31$; $\text{D}_2\text{O} = 4.69$; $\text{DMSO-}d_6 = 2.50$ and ^{13}C NMR: $\text{CDCl}_3 = 77.16$, $\text{MeOD} = 49.00$, $\text{DMSO-}d_6 = 39.52$). Coupling constants (J) are reported in Hz with the following splitting abbreviations: s = singlet, d = doublet, t = triplet, q = quartet, , m = multiplet, app = apparent, br = broad. Melting points (m.p.) were recorded on a Gallenkamp melting point apparatus. Infrared (IR) spectra were recorded on a Perkin Elmer UATR Two FT-IR spectrometer. Absorption maxima (ν_{max}) are reported in wavenumbers (cm^{-1}). UV-Vis spectra were recorded on a Shimadzu UV-1800 UV spectrophotometer in a glass cuvette, using a 480/30 nm excitation filter and a 580/10 nm emission filter, a pathlength of 1 cm, and a sampling interval of 1 nm. 96-well plate fluorescence measurements were recorded on a PerkinElmer VICTOR Nivo Multimode Plate Reader. Fluorescence spectra were recorded on a Shimadzu RF-5301PC spectrofluorophotometer in a glass fluorescence cuvette with a pathlength of 1 cm, a sampling interval of 1 nm, and excitation and emission slit widths of 5 nm. High resolution electrospray ionisation (ESI) mass spectra (HRMS) were recorded on a Bruker Compact TOF-MS or a Jeol AccuTOF GCx-plus spectrometer. Nominal and exact m/z values are reported in Daltons.

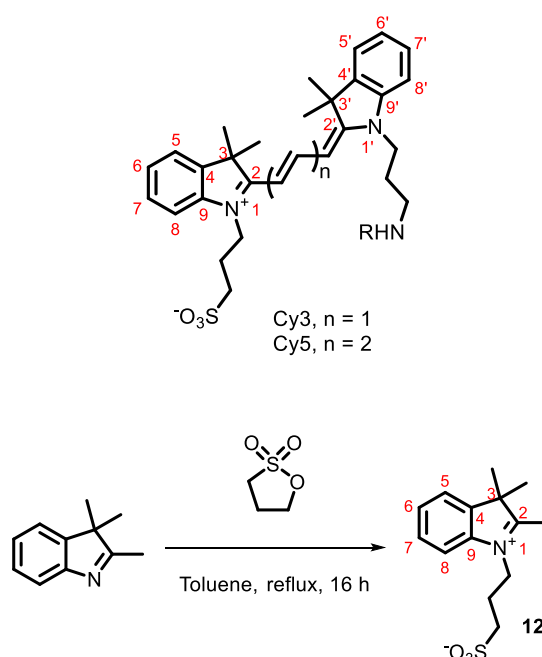
Thin layer chromatography (TLC) was carried out using aluminium backed sheets coated with 60 F₂₅₄ silica gel (Merck). Visualization of the silica plates was achieved using a UV lamp ($\lambda_{\text{max}} = 254, 302, \text{ or } 366 \text{ nm}$), and/or ammonium molybdate (5% in 2M H_2SO_4), and/or potassium permanganate (5% KMnO_4 in 1M NaOH with 5% potassium carbonate), and/or ninhydrin (1.5% ninhydrin, 3% AcOH in *n*-butanol), and/or bromocresol green (0.4% bromocresol green in ethanol, basified till blue with 0.1 M NaOH). Flash column chromatography was carried out using Geduran Si 60 (40-63 μm) (Merck). Mobile phases are reported as ratios of more polar solvent to less polar solvent. Anhydrous solvents were dried over a PureSolv MD 7 Solvent Purification System. Deionized water was used for chemical reactions. All other solvents were used as supplied (Analytical or HPLC grade), without prior purification. Reagents were purchased from Sigma-Aldrich and used as supplied, unless otherwise indicated. Brine refers to a saturated solution of sodium chloride. Petrol refers to the fraction of petroleum ether boiling in the range 40-60 $^\circ\text{C}$. Anhydrous magnesium sulphate (MgSO_4) was used as the drying agent after reaction workup unless otherwise stated.

Liquid chromatography-mass spectrometry (LC-MS) was performed on a HCTultra ETD II ion trap spectrometer, coupled to an Ultimate300 HPLC using an Accucore C18 column (150 × 2.1 mm, 2.6 μm particle size). Water (solvent A) and acetonitrile (solvent B), both containing 0.1% formic acid, were used as the mobile phase at a flow rate of 0.3 mL min⁻¹. LC traces were measured via UV absorption at 220, 270, and 280. The gradient was programmed as shown below:



4.2. Core Dye Synthesis

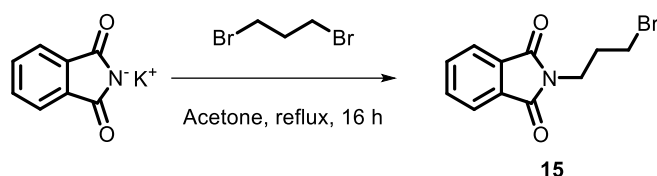
Numbering system for Cy3/5 NMR assignments



A mixture of 2,3,3-trimethylindolenine (2.00 mL, 12.7 mmol) and 1,3-propanesultone (1.55 g, 12.7 mmol) in toluene (50 mL) was refluxed for 20 h, during which time a dark red precipitate formed. After cooling to r.t., the reaction mixture was concentrated under reduced pressure. The residue was redissolved in dichloromethane (5 mL) and the solution added dropwise to diethyl ether (200 mL). The resultant precipitate was collected by filtration, washed with diethyl

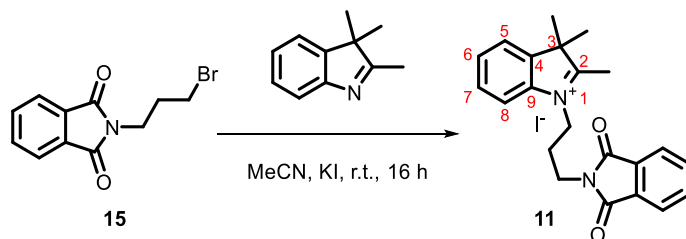
ether (50 mL), and dried in air to yield a red oil (3.10 g, 11.0 mmol, 87%). Data were consistent with those previously reported.⁴³

¹H NMR (400 MHz, CD₃OD) δ = 8.01-7.93 (m, 1H, H5), 7.78-7.70 (m, 1H, H7), 7.68-7.59 (m, 2H, H6, H8), 4.78-4.67 (m, 2H, NCH₂), 3.03-2.93 (m, 2H, CH₂SO₃⁻), 2.43-2.26 (m, 2H, CH₂CH₂SO₃⁻), 1.58 (s, 6H, 2 × CH₃), Me at 2-position exchanges with CD₃OD; **HRMS**: m/z (ESI⁺) calc. for C₁₄H₁₉NO₃S [M+H]⁺: 282.1158; Obs.: 282.1162; **v**_{max}: (FT-ATR)/cm⁻¹: 3426, 2989, 1641, 1460, 1212, 1160, 1035, 758, 522.



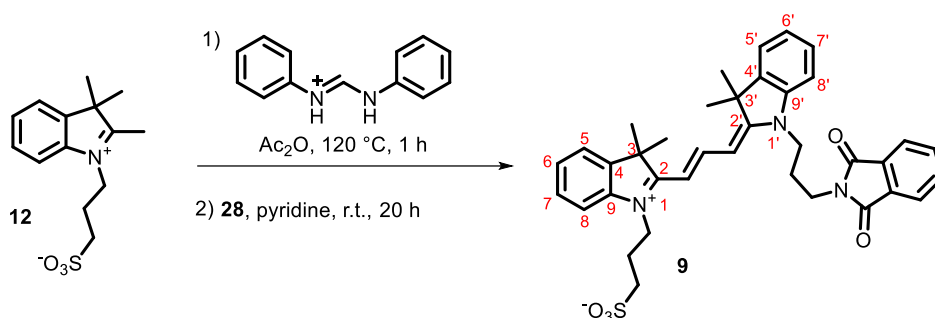
Potassium phthalimide (1.85 g, 10.0 mmol) was added in portions over 5 min to a stirred solution of 1,3-dibromopropane (1.00 mL, 10.0 mmol) in acetone (50 mL). The solution was then refluxed for 18 h. After cooling to r.t., the reaction mixture was filtered under vacuum, and the filtrate concentrated under reduced pressure. The residue was purified via flash column chromatography on silica gel, eluting with EtOAc:petrol (3:8). Fractions containing the product were concentrated under reduced pressure to provide a white solid (1.17 g, 4.38 mmol, 44%). Data were consistent with those previously reported.⁴⁴

R_f: 0.21 (2:8, EtOAc:petrol, UV active); **¹H NMR** (400 MHz, CD₃OD) δ = 7.91-7.79 (m, 2H, PhthH2), 7.78-7.66 (m, 2H, PhthH3), 3.83 (t, *J* = 6.8 Hz, 2H, CH₂N), 3.41 (t, *J* = 6.8 Hz, 2H, CH₂Br), 2.25 (tt, *J*₁ = *J*₂ = 6.8 Hz, 2H, CH₂CH₂Br); **HRMS**: m/z (ESI⁺) calc. for C₁₁H₁₀⁷⁹BrNO₂ [⁷⁹M+Na]⁺: 289.9787; Obs.: 289.9774; **v**_{max}: (FT-ATR)/cm⁻¹: 3454, 2985, 1765, 1705, 1442, 1406, 1375, 1230, 1055, 966, 870, 723; **m.p.**: 71-74 °C.



Potassium iodide (744 mg, 4.48 mmol) was added to a stirred solution of 2,3,3-trimethylindolenine (710 μ L, 4.48 mmol), and **31** (1.00 g, 3.73 mmol) in anhydrous acetonitrile (20 mL) under an argon atmosphere. The resulting mixture was refluxed for 5 h. After cooling to r.t., the reaction was filtered under vacuum and the filtrate concentrated under reduced pressure. The residue was then redissolved in acetone (10 mL) and the solution added dropwise to diethyl ether (200 mL). The resultant brown precipitate was collected by filtration, washed with diethyl ether (30 mL) and dried in air. The solid was then redissolved in acetone (10 mL) and concentrated under reduced pressure to afford the product as a brown solid (878 mg, 2.53 mmol, 68%).

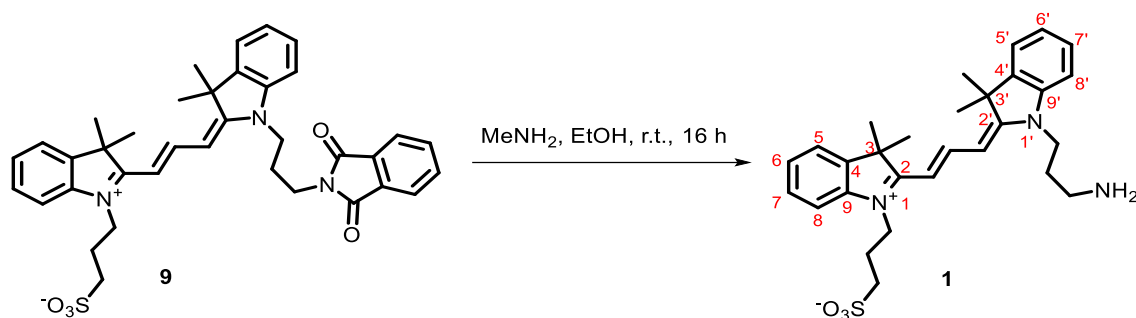
R_f: 0.29 (1:9, MeOH:CH₂Cl₂, UV active); **¹H NMR** (400 MHz, CD₃OD) δ = 7.89-7.85 (m, 1H, H₅), 7.84-7.80 (m, 2H, PhthH₂), 7.79-7.73 (m, 3H, PhthH₃, H₇), 7.64-7.55 (m, 2H, H₈, H₆), 4.64 (t, *J* = 7.0 Hz, 2H, CH₂N⁺), 3.88 (t, *J* = 7.0 Hz, 2H, CH₂NPhth), 2.37 (tt, *J*₁ = *J*₂ = 7.0 Hz, 2H, CH₂CH₂N), 1.61 (s, 6H, 2 × CH₃); **¹³C NMR** (400 MHz, CD₃OD) δ = 168.5 (PhthC_{ON}), 142.0 (C₉), 141.2 (C₄), 134.2 (PhthC₂), 132.0 (PhthC₁), 129.9 (C₇), 129.2 (C₆), 123.4 (PhthC₃), 123.0 (C₅), 115.1 (C₈), 46.1 (CH₂NPhth), 34.8 (CH₂CH₂CH₂NPhth), 26.5 (CH₂CH₂NPhth), 21.5 (CyCH₃); **HRMS**: *m/z* (ESI⁺) calc. for C₂₂H₂₂N₂O₂ [M]⁺: 347.1754; Obs.: 347.1761; **v_{max}**: (FT-ATR)/cm⁻¹: 3441, 2976, 1769, 1707, 1608, 1463, 1398, 765, 721, 530; **m.p.**: 176-179 °C.



A mixture of **27** (3.10 g, 11.0 mmol) and *N,N'*-diphenylformamidine (2.17 g, 11.0 mmol) in acetic anhydride (10 mL) was heated to 120 °C for 1 h. After the reaction mixture was cooled to r.t., a solution of **28** (3.44 g, 9.91 mmol) in pyridine (10 mL) was added and the mixture stirred at r.t. for a further 20 h. After this time, the mixture was added dropwise to diethyl ether (500 mL). The resultant precipitate was collected by filtration, washed with diethyl ether (30 mL), and dried in air. The solid was then redissolved in methanol (20 mL) and concentrated under reduced pressure. The residue was purified via flash column chromatography on silica gel, eluting with MeOH:CH₂Cl₂ (5:95). Fractions containing the product were concentrated under reduced pressure to provide a pink powder (2.65 g, 4.16 mmol, 42%).

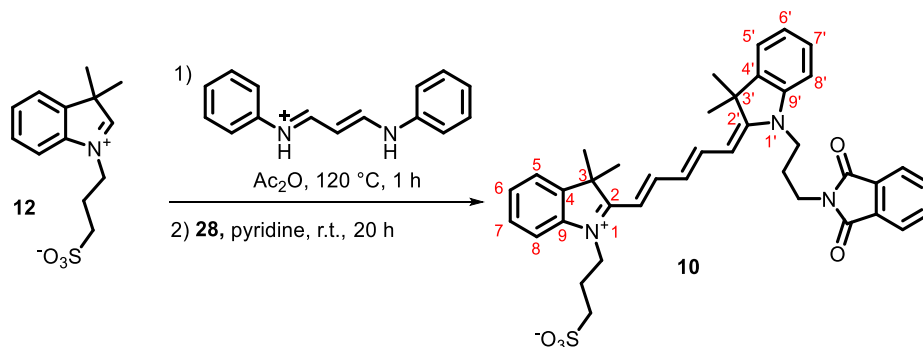
R_f: 0.16 (1:9, MeOH:CH₂Cl₂, visible light active); **¹H NMR** (400 MHz, DMSO-*d*₆) δ = 8.32 (dd, *J*₁ = *J*₂ = 13.4 Hz, 1H, CHCHCN), 7.84-7.75 (m, 4H, PhthH₂, PhthH₃), 7.62-7.54 (m, 3H, H₅, H_{5'}, H₈/H_{8'}), 7.45-7.35 (m, 3H, H₇, H_{7'}, H₈/H_{8'}), 7.25 (ddd, *J*₁ = *J*₂ = 7.5 Hz, *J*₃ = 2.8 Hz, 2H, H₆, H_{6'}), 6.50 (d, *J* = 13.4 Hz, 2H, CHCN), 4.26-4.18 (m, 4H, CH₂CH₂CH₂SO₃⁻, CH₂CH₂CH₂NPhth), 3.69 (t, *J* = 7.1 Hz, 2H, CH₂NPhth), 2.52 (t, *J* = 7.4 Hz, 2H, CH₂SO₃⁻), 2.08 (tt, *J*₁ = *J*₂ = 7.1 Hz, 2H, CH₂CH₂NPhth), 2.00 (tt, *J*₁ = *J*₂ = 7.4 Hz, 2H, CH₂CH₂SO₃⁻), 1.67 (s, 12H, CyCH₃); **¹³C NMR** (101 MHz, DMSO-*d*₆) δ = 174.9 (CHCHCN), 174.6 (C₂, C_{2'}), 168.4 (PhthC_{ON}), 151.1 (C₃, C_{3'}), 141.9 (C₉, C_{9'}), 140.9 (C₄, C_{4'}), 134.1 (PhthC₂), 132.1 (PhthC₁), 128.7 (C₇, C_{7'}), 125.6 (C₆, C_{6'}), 123.9 (PhthC₃), 122.2 (C₅, C_{5'}), 111.3 (C₈/C_{8'}), 111.0 (C₈/C_{8'}), 103.8 (CHCN), 103.7 (CHCN), 49.4 (CH₂SO₃⁻), 42.7 (CH₂CH₂CH₂SO₃⁻), 41.6 (CH₂NPhth), 35.1 (CH₂CH₂CH₂NPhth), 27.6 (CH₂CH₂NPhth), 26.1 (CyCH₃), 22.8 (CH₂CH₂SO₃⁻); **HRMS**: *m/z* (ESI⁺) calc. for C₃₇H₃₉N₃O₅S [M+H]⁺: 638.2683; Obs.: 638.2695;

ν_{\max} : (FT-ATR)/ cm^{-1} : 3443, 2975, 2930, 1709, 1555, 1428, 1373, 1152, 1037, 929, 759, 723;
m.p.: 272-276 °C.



A mixture of methylamine (40% in methanol, 30 mL) and **3** (500 mg, 0.78 mmol) in methanol (5 mL) was stirred at r.t. for 16 h. The reaction mixture was then concentrated under reduced pressure to ~5 mL, and the solution added dropwise to diethyl ether (400 mL). The resultant precipitate was collected by filtration, washed with diethyl ether (30 mL) and dried in air. The solid was then redissolved in methanol (20 mL) and concentrated under reduced pressure to give a pink solid (498 mg, 0.78 mmol, quantitative yield).

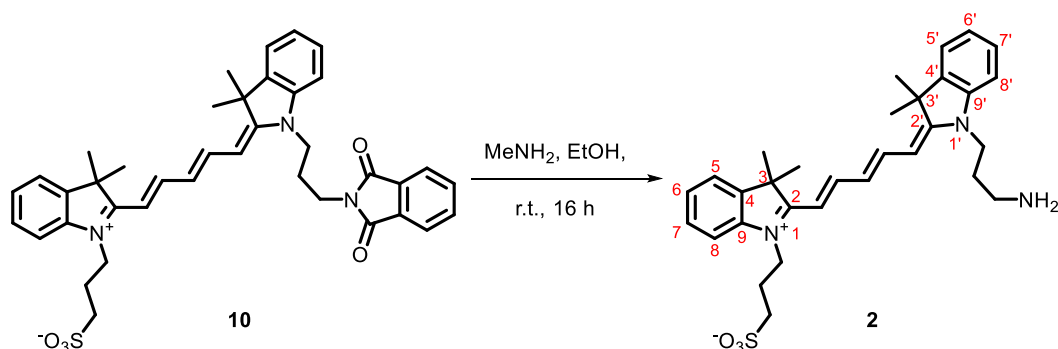
R_f: 0.18 (1:9, MeOH:CH₂Cl₂, visible light active); **¹H NMR** (400 MHz, CD₃OD) δ = 8.52 (dd, $J_1 = J_2 = 13.5$ Hz, 1H, CHCHCN), 7.53 (d, $J = 7.5$ Hz, 2H, H₅, H_{5'}), 7.45-7.30 (m, 4H, H₇, H_{7'}, H₈, H_{8'}), 7.34-7.22 (m, 2H, H₆, H_{6'}), 6.82 (d, $J = 13.5$ Hz, 1H, CHCN), 6.60 (d, $J = 13.5$ Hz, 1H, CHCN), 4.41 (t, $J = 7.7$ Hz, 2H, CH₂CH₂CH₂SO₃⁻), 4.27 (t, $J = 7.7$ Hz, 2H, CH₂CH₂CH₂NH₂), 3.21 (t, $J = 7.7$ Hz, 2H, CH₂NH₂), 3.02 (t, $J = 7.7$ Hz, 2H, CH₂SO₃⁻), 2.29-2.23 (m, 2H, CH₂CH₂NH₂), 2.20-2.16 (m, 2H, CH₂CH₂SO₃⁻), 1.73 (s, 12H, CyCH₃); **¹³C NMR** (101 MHz, CD₃OD) δ = 174.8 (CHCHCN), 174.5 (C₂, C_{2'}), 151.0 (C₃, C_{3'}), 141.9 (C₉, C_{9'}), 140.9 (C₄, C_{4'}), 128.8 (C₇, C_{7'}), 125.5 (C₆, C_{6'}), 122.3 (C₅, C_{5'}), 111.3 (C₈/C_{8'}), 111.1, (C₈/C_{8'}), 103.1 (CHCN⁺), 102.8 (CHCN), 49.3 (CH₂SO₃⁻), 42.6 (CH₂CH₂CH₂SO₃⁻), 41.5 (CH₂NH₂), 37.9 (CH₂CH₂CH₂NH₂), 28.1 (CH₂CH₂NH₂), 27.0 (CyCH₃), 23.0 (CH₂CH₂SO₃⁻); **HRMS**: m/z (ESI⁺) calc. for C₂₉H₃₆N₃O₃S [M+H]⁺: 508.2636; Obs.: 508.2636; ν_{\max} : (FT-ATR)/ cm^{-1} : 3437, 2975, 1711, 1556, 1429, 1207, 1147, 1037, 971, 930, 758; **m.p.**: >325 °C.



A mixture of **27** (2.00 g, 7.12 mmol) and malonaldehyde bis(phenylimine) monohydrochloride (1.75 g, 7.83 mmol) in acetic anhydride (10 mL) was heated to 120 °C for 1.5 h. After cooling to r.t., a solution of **28** (2.25 g, 6.48 mmol) in pyridine (10 mL) was added and stirring was

continued at r.t. for a further 16 h. The reaction mixture was then concentrated under reduced pressure to ~5 mL, and the remaining solution added dropwise to diethyl ether (200 mL). The resultant precipitate was collected by filtration, washed with diethyl ether (30 mL), and dried in air. The solid was then redissolved in methanol (10 mL) and concentrated under reduced pressure. The residue was purified via flash column chromatography on silica gel eluting with MeOH:CH₂Cl₂ (5:95). Fractions containing the product were concentrated under reduced pressure to provide a blue solid (1.35 g, 2.04 mmol, 29%).

R_f: 0.29 (5:95, MeOH:CH₂Cl₂, visible light active); **¹H NMR** (400 MHz, DMSO-*d*₆) δ = 8.28 (dd, *J* = 13.2, 10.1 Hz, 2H, 2 × CHCHCN), 7.85-7.75 (m, 4H, PhthH₂, PhthH₃), 7.56 (d, *J* = 7.4 Hz, 1H, H₅/H_{5'}), 7.53 (d, *J* = 7.4 Hz, 1H, H₅/H_{5'}), 7.46 (d, *J* = 7.9 Hz, 1H, H₈/H_{8'}), 7.38-7.32 (m, 2H, H₇, H_{7'}), 7.29 (d, *J* = 7.9 Hz, 1H, H₈/H_{8'}), 7.20 (dd, *J* = 7.4 Hz, 1H, H₆/H_{6'}), 7.15 (dd, *J* = 7.4 Hz, 1H, H₆/H_{6'}), 6.45-6.33 (m, 2H, CHCHCHCN, CHCN), 6.20 (d, *J* = 13.2 Hz, 1H, CHCN), 4.34-4.22 (m, 2H, CH₂CH₂CH₂SO₃⁻), 4.17 (t, *J* = 7.2 Hz, 2H, CH₂CH₂CH₂NPhth), 3.67 (t, *J* = 7.2 Hz, 2H, CH₂NPhth), 2.57 (t, *J* = 6.8 Hz, 2H, CH₂SO₃⁻), 2.05-1.95 (m, 4H, CH₂CH₂NPhth, CH₂CH₂SO₃⁻), 1.62 (s, 12H, CyCH₃); **¹³C NMR** (101 MHz, DMSO-*d*₆) δ = 173.8 (C₂, C_{2'}), 172.5 (C₃, C_{3'}), 168.5 (CON), 155.1 (CHCHCN), 154.3 (CHCHCN), 142.6 (C₉/C_{9'}), 142.5 (C₉/C_{9'}), 141.7 (C₄/C_{4'}), 141.5 (C₄/C_{4'}), 134.9 (PhthC₂), 132.3 (PhthC₁), 129.0 (C₇/C_{7'}), 128.9 (C₇/C_{7'}), 126.1 (CHCHCHCN), 125.5 (C₆/C_{6'}), 125.0 (C₆/C_{6'}), 123.6 (PhthC₃), 123.0 (C₅, C_{5'}), 111.9 (C₈/C_{8'}), 111.3 (C₈/C_{8'}), 104.3 (CHCN), 103.3 (CHCN), 48.4 (CH₂SO₃⁻), 43.3 (CH₂CH₂CH₂SO₃⁻), 41.5 (CH₂CH₂CH₂NPhth), 35.6 (CH₂NCO), 27.6 (CyCH₃), 26.5 (CH₂CH₂NPhth), 24.0 (CH₂CH₂SO₃⁻); **HRMS**: *m/z* (ESI⁺) calc. for C₃₉H₄₁N₃O₅S [M+H]⁺: 664.2840; Obs.: 664.2858; **ν_{max}**: (FT-ATR)/cm⁻¹: 3442, 2973, 1770, 1709, 1492, 1455, 1381, 1337, 1132, 1108, 1034, 1017, 927, 795, 721, 530; **m.p.**: 264-269 °C.



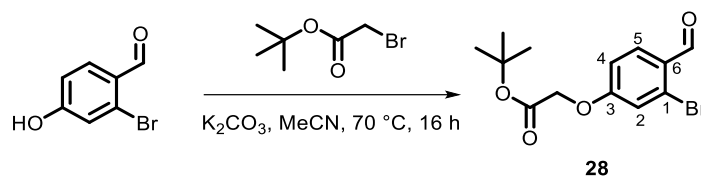
Methylamine (40% in water, 30 mL) was added to a solution of **4** (200 mg, 0.30 mmol) in ethanol (5 mL) and the solution stirred at r.t. for 16 h. The reaction mixture was then concentrated under reduced pressure to ~5 mL, and the remaining solution added dropwise to diethyl ether (400 mL). The resultant precipitate was collected by filtration, washed with diethyl ether (30 mL) and dried in air. The solid was then redissolved in methanol (20 mL) and

concentrated under reduced pressure to give the product as a blue solid (159 mg, 0.298 mmol, 99%).

Nb. Attempts to cleave the phthalimide with traditional hydrazinolysis were unsuccessful, with a loss of colour over a period of 1 h indicating a loss of conjugation/dye structure.

R_f: 0.17 (1:9, MeOH:CH₂Cl₂, visible light active). **¹H NMR** (400 MHz, CD₃OD) δ = 8.21 (d, *J* = 13.2 Hz, 2H, CHCHCN), 7.49-7.43 (m, 2H, H₅, H_{5'}), 7.41-7.34 (m, 3H, H₇, H_{7'}, H₈/H_{8'}), 7.27-7.17 (m, 3H, H₆, H_{6'}, H₈/H_{8'}), 6.69-6.65 (m, 1H, CHCHCHCN), 6.62-6.58 (m, 1H, CHCN), 6.33-6.28 (m, 1H, CHCN), 4.35 (t, *J* = 8.0 Hz, 2H, CH₂CH₂CH₂SO₃⁻), 4.22-4.10 (m, 2H, CH₂CH₂CH₂NH₂), 3.02-2.94 (m, 4H, CH₂NH₂, CH₂SO₃⁻), 2.24-2.18 (m, 2H, CH₂CH₂SO₃⁻), 2.10-2.00 (m, 2H, CH₂CH₂NH₂), 1.66 (s, 12H, CyCH₃); **¹³C NMR** (101 MHz, CD₃OD) δ = 174.7 (C₂, C_{2'}), 170.9 (C₃/C_{3'}), 170.3 (C₃/C_{3'}), 155.1 (CHCHCN), 154.1 (CHCHCN), 142.8 (C₉/C_{9'}), 142.1 (C₉/C_{9'}), 141.4, (C₄, C_{4'}), 128.5 (C₇, C_{7'}), 125.9 (CHCHCHCN), 125.0 (C₆, C_{6'}), 123.3 (C₅, C_{5'}), 122.1 (C₇, C_{7'}), 110.8 (C₈, C_{8'}), 103.4 (CHCN), 102.9 (CHCN), 49.1 (CH₂SO₃⁻), 42.7 (CH₂CH₂CH₂SO₃⁻), 41.7 (CH₂CH₂CH₂NH₂), 36.7 (CH₂NH₂), 28.8 (CyCH₃), 26.6 (CH₂CH₂NH₂), 22.9 (CH₂CH₂SO₃⁻); **HRMS**: *m/z* (ESI⁺) calc. for C₃₁H₃₉N₃O₃S [M+H]⁺: 534.2785; Obs.: 534.2803; **v_{max}**: (FT-ATR)/cm⁻¹: 3438, 2968, 2937, 1573, 1482, 1454, 1381, 1338, 1136, 1105, 1035, 1017, 927, 800, 752, 709, 525; **m.p.**: 252-256 °C.

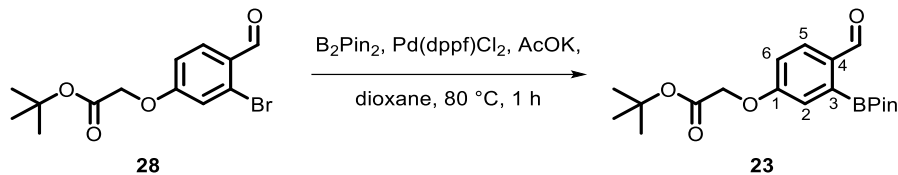
4.3. Synthesis of Reactive Handles



A mixture of 2-bromo-4-hydroxybenzaldehyde (2.07 g, 10.4 mmol), *tert*-butyl bromoacetate (1.53 mL, 10.4 mmol) and potassium carbonate (2.43 g, 17.6 mmol) in acetonitrile (30 mL) was stirred for 16 h at 70 °C. The mixture was then cooled to r.t. and diluted with water (150 mL). The aqueous mixture was extracted with ethyl acetate (3 × 70 mL), and the combined organics washed with brine (2 × 200 mL), dried with MgSO₄, filtered, and concentrated under reduced pressure. The residue was purified via flash column chromatography on silica gel eluting with EtOAc:Petrol (15:85). Fractions containing the product were concentrated under reduced pressure to provide a white solid (3.23 g, 10.3 mmol, 99%). Data were consistent with those previously reported.⁴⁵

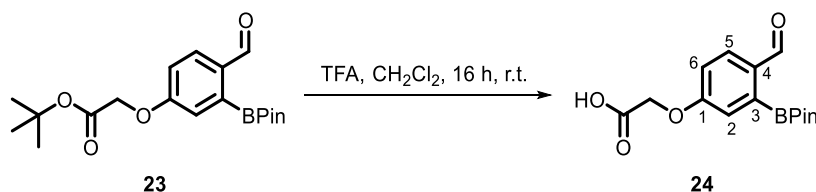
R_f: 0.35 (2:8, EtOAc:Petrol, UV active); **¹H NMR** (400 MHz, CDCl₃) δ = 10.19 (s, 1H, CHO), 7.87 (d, *J* = 8.6 Hz, 1H, PhH₅), 7.11 (d, *J* = 2.5 Hz, 1H, PhH₂), 6.91 (dd, *J* = 8.6, 2.5 Hz, 1H, PhH₄), 4.57 (s, 2H, CH₂O), 1.47 (s, 9H, ^tBu); **¹³C NMR** (101 MHz, CDCl₃) δ = 190.6 (CHO),

166.8 (COO), 162.8 (PhC4), 131.5 (PhC5), 128.7 (PhC1), 127.7 (PhC3), 119.5 (PhC2), 114.5 (PhC6), 83.3 (CMe₃), 65.8 (CH₂O), 28.1 (^tBu); **HRMS**: m/z (ESI⁺) calc. for C₁₃H₁₅⁷⁹BrO₄ [⁷⁹M+Na]⁺: 337.0053; Obs.: 337.0046; **v**_{max}: (FT-ATR)/cm⁻¹: 2979, 2863, 1746, 1685, 1590, 1486, 1368, 1310, 1218, 1152, 1071, 1028, 843, 613; **m.p.**: 87-89 °C.

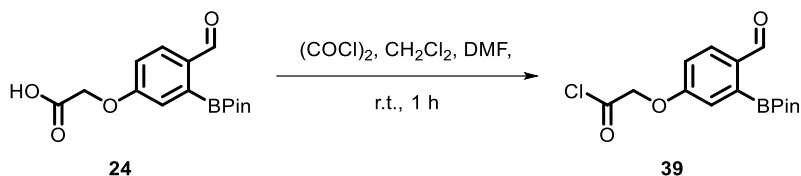


32 (2.15 g, 6.85 mmol), bis(pinacolato)diboron (4.52 g, 17.8 mmol), 1,1'-[bis(diphenylphosphino)ferrocene]dichloropalladium(II) (500 mg, 0.685 mmol) and potassium acetate (3.62 g, 37.0 mmol) were placed under a nitrogen atmosphere, and anhydrous dioxane (25 mL) was added. Nitrogen was bubbled through the reaction mixture for 10 min, which was then stirred at 80 °C for 1 h. After cooling to r.t., the reaction was concentrated under reduced pressure. The residue was purified via flash column chromatography on silica gel, eluting with EtOAc:Petrol (15:85). Fractions containing the product were concentrated under reduced pressure to yield a white solid (1.87 g, 5.16 mmol, 75%). Data were consistent with those previously reported.⁴⁵

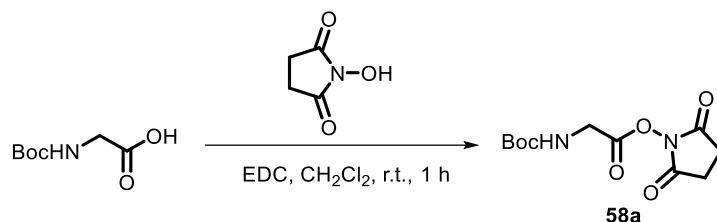
R_f: 0.38 (15:85, EtOAc:Petrol, UV active); **¹H NMR** (400 MHz, CDCl₃) δ = 10.39 (s, 1H, CHO), 7.93 (d, *J* = 8.8 Hz, 1H, PhH5), 7.26 (d, *J* = 2.5 Hz, 1H, PhH2), 7.03 (dd, *J* = 8.8, 2.5 Hz, 1H, PhH6), 4.59 (s, 2H, CH₂O), 1.47 (s, 9H, ^tBu), 1.36 (s, 12H, C(CH₃)₂); **¹³C NMR** (101 MHz, CDCl₃) δ = 193.2 (CHO), 167.4 (COO), 161.5 (PhC1), 135.5 (PhC3), 132.0 (PhC4), 130.4 (PhC5), 120.5 (PhC2), 117.2 (PhC6), 84.6 (OC(CH₃)₂), 82.9 (CMe₃), 65.6 (CH₂O), 28.1 (^tBu), 25.1 (C(CH₃)₂); **HRMS**: m/z (ESI⁺) calc. for C₁₉H₂₇BO₆ [M+H]⁺: 363.1977; Obs.: 363.1977; **v**_{max}: (FT-ATR)/cm⁻¹: 2979, 2933, 1752, 1686, 1589, 1420, 1340, 1323, 1211, 1147, 1123, 1077, 1052, 964, 849, 734; **m.p.**: 80-83 °C.



(CHO), 168.4 (COOH), 161.4 (PhC1), 135.2 (PhC3), 131.3 (PhC4), 130.8 (PhC5), 121.0 (PhC2), 116.7 (PhC6), 85.0 (OC(CH₃)₂), 64.5 (CH₂O), 25.0 (C(CH₃)₂); **HRMS**: m/z (ESI⁺) calc. for C₁₅H₁₈BO₆ [M+H]⁺: 307.1350; Obs.: 307.1350; **v**_{max}: (FT-ATR)/cm⁻¹: 2979, 2937, 1763, 1561, 1418, 1371, 1343, 1283, 1203, 1174, 1125, 1072, 960, 850, 691; **m.p.**: 169-172 °C.

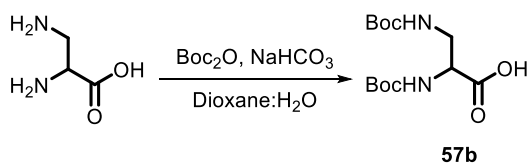


Oxalyl chloride (61 μ L, 0.71 mmol) was added to a solution of **34** (72 mg, 0.24 mmol), dichloromethane (3 mL) and dimethylformamide (1 drop), and stirred at r.t. for 1 h. Excess oxalyl chloride and dichloromethane were removed under reduced pressure to give the crude product as a brown oil, which was carried forward without further purification.



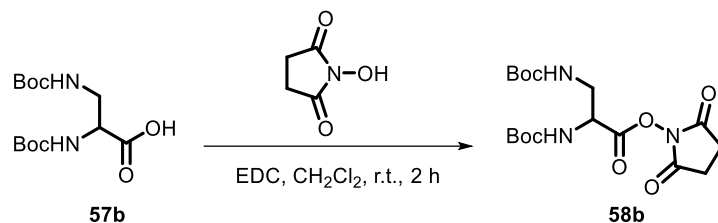
A mixture of *N*-(tert-butoxycarbonyl)glycine (100 mg, 0.571 mmol), *N*-hydroxy succinimide (99 mg, 0.857 mmol), and *N*-(3-dimethylaminopropyl)-*N*-ethylcarbodiimide hydrochloride (164 mg, 0.86 mmol) in dichloromethane (5 mL) was stirred at r.t. for 1 h. Dichloromethane (30 mL) was then added and the organic layer was washed with water (2 \times 20 mL) and brine (2 \times 20 mL), dried with MgSO₄, filtered and concentrated under reduced pressure to give a white solid (165 mg, 0.61 mmol, 75%). Data were consistent with those previously reported.⁴⁶

R_f: 0.27 (2:8, EtOAc:Petrol); **¹H NMR** (400 MHz, CDCl₃) δ = 4.97 (app br s, 1H, NH), 4.28 (d, *J* = 5.9 Hz, 2H, CH₂N), 2.84 (s, 4H, OSu), 1.44 (s, 9H, Boc); **HRMS**: m/z (ESI⁺) calc. for C₁₁H₁₆N₂O₆ [M+Na]⁺: 295.0901; Obs.: 295.0901; **m.p.**: 156-159 °C.



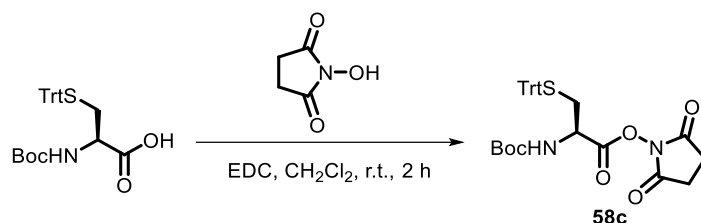
Di-*tert*-butyl dicarbonate (3.05 g, 14 mmol) was added to a solution of 2,3-diaminopropionic acid (500 mg, 3.5 mmol) and sodium bicarbonate (2.94 g, 10 mmol) in a mixture of dioxane (15 mL) and water (15 mL), and the reaction was stirred at r.t. for 18 h. The mixture was then diluted with water (50 mL) and washed with dichloromethane (2 \times 15 mL). The aqueous layer was acidified with hydrochloric acid (1 M) to pH \sim 2, and then extracted with dichloromethane (3 \times 30 mL). The combined organic extracts of the acidified aqueous fraction were combined, dried with MgSO₄, filtered, and concentrated under reduced pressure. The residue was

purified via flash column chromatography on silica gel, eluting with MeOH:CH₂Cl₂ (5:95). Fractions containing the product were concentrated under reduced pressure to yield a colourless oil (210 g, 0.7 mmol, 20%). Data were consistent with those previously reported.⁴⁷ **¹H NMR** (400 MHz, CDCl₃) δ = 6.71 (br s, 1H, NH), 5.19 (br s, 1H, NH), 4.22-4.31 (m, 1H, H_α), 3.46-3.75 (m, 2H, H_β), 1.43 (s, 18H, 2 × Boc).



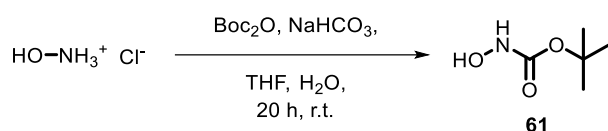
A mixture of **37** (29 mg, 95 μmol), *N*-hydroxysuccinimide (16 mg, 0.143 mmol), and *N*-(3-dimethylaminopropyl)-*N'*-ethylcarbodiimide hydrochloride (28 mg, 0.143 mmol) in dichloromethane (1.0 mL) was stirred at r.t. for 2 h. Dichloromethane (10 mL) was then added and the organics were washed with water (2 × 15 mL) and brine (15 mL), dried with MgSO₄, filtered, and concentrated under reduced pressure to give a pink foam (28 mg, 70 μmol, 74%). The product was used immediately without any further purification or analysis.

R_f: 0.28 (1:9, EtOAc:Petrol); **HRMS**: *m/z* (ESI⁺) calc. for C₁₇H₂₇N₃O₈ [M+H]⁺: 402.1871; Obs.: 402.1874; **¹H NMR** (400 MHz, CDCl₃) δ = 2.82 (m, 4H, NHS-CH₂), 1.42 (s, 18H, 2 × Boc).



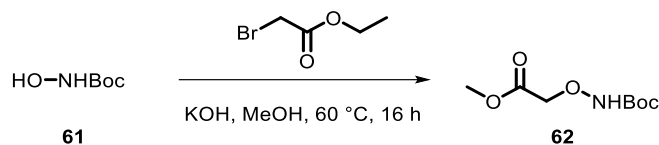
A mixture of Boc-Cys-(Trt)-OH (1.00 g, 2.16 mmol), *N*-hydroxysuccinimide (372 mg, 3.23 mmol), and *N*-(3-dimethylaminopropyl)-*N'*-ethylcarbodiimide hydrochloride (620 mg, 3.23 mmol) in dichloromethane (20 mL) was stirred at r.t. for 2 h. Dichloromethane (30 mL) was then added and the organics were washed with water (2 × 50 mL) and brine (50 mL), dried with MgSO₄, filtered, and concentrated under reduced pressure to give a white foam. (1.16 g, 0.207 mmol, quantitative yield).

R_f: 0.24 (2:8, EtOAc:Petrol, UV active); **¹H NMR** (400 MHz, CDCl₃) δ = 7.43 (dd, *J* = 7.5, 1.7 Hz, 6H, PhH₂), 7.29 (t, *J* = 7.5 Hz, 6H, PhH₃), 7.24-7.18 (t, *J* = 7.5, 1.7 Hz, 3H, PhH₄), 4.86 (d, *J* = 8.3 Hz, 1H, CHNHBoc), 2.79 (s, 4H, OSu), 2.81-2.76 (m, 1H, CH₂STrt), 2.71-2.66 (m, 1H, CH₂STrt), 1.42 (s, 9H, Boc); **HRMS**: *m/z* (ESI⁺) calc. for C₂₉H₃₀N₂O₆S [M+H]⁺: 536.1658; Obs.: 536.1658; **v_{max}**: (FT-ATR)/cm⁻¹: 3426, 2978, 1707, 1491, 1444, 1393, 1368, 1217, 1162, 1052, 852, 744, 700, 675, 620, 505; **m.p.**: 71-74 °C.



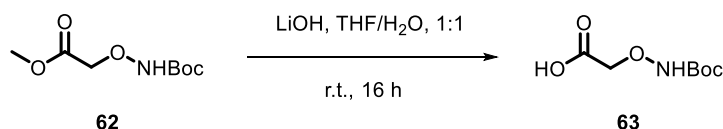
A solution of sodium hydrogen carbonate (2.44 g, 29.0 mmol) in water (30 mL) was added dropwise to a mixture of hydroxylamine hydrochloride (1.00 g, 14.5 mmol) and di-*tert*-butyl dicarbonate (3.16 g, 14.5 mmol) in tetrahydrofuran (20 mL), and the reaction stirred at r.t. for 20 h. Water (150 mL) was then added, and the aqueous was extracted with ethyl acetate (2 × 150 mL). The combined organics were washed with water (30 mL) and brine (2 × 30 mL), dried with MgSO₄, filtered, and concentrated to afford a colourless oil (1.71 g, 12.9 mmol, 89%). Data were consistent with those previously reported.^{48,49}

R_f: 0.30 (1:9, EtOAc:Petrol); **¹H NMR** (400 MHz, CDCl₃) δ = 7.02 (s, 1H, NH), 1.46 (s, 9H, Boc); **¹³C NMR** (101 MHz, CDCl₃) δ = 158.8 (C=O), 82.3 (CMe₃), 28.3 (Boc); **HRMS**: m/z (ESI⁺) calc. for C₅H₁₀NO₃ [M+Na]⁺: 156.0633; Obs.: 156.0633.



A mixture of ethyl bromoacetate (1.40 mL, 12.6 mmol), **UK/NR/037** (1.68 g, 12.6 mmol), and potassium hydroxide (0.71 g, 12.6 mmol) in methanol (15 mL) was stirred at 60 °C for 16 h. The reaction mixture was then concentrated under reduced pressure. Water (30 mL) was added to residue and the aqueous was extracted with dichloromethane (4 × 30 mL). The combined organics were washed with brine (50 mL), dried with MgSO₄, filtered, and concentrated under reduced pressure. The residue was purified via flash column chromatography on silica gel, eluting with EtOAc:petrol (2:8). Pure fractions were concentrated under reduced pressure to provide a yellow solid (1.36 g, 6.63 mmol, 53%). Data were consistent with those previously reported.⁵⁰

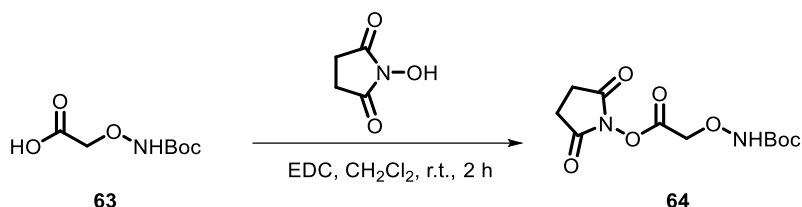
R_f: 0.33 (2:8, EtOAc:Petrol); **¹H NMR** (400 MHz, CDCl₃) δ = 7.75 (s, 1H, NH), 4.43 (s, 2H, CH₂O), 3.77 (s, 3H, OCH₃), 1.48 (s, 9H, Boc); **¹³C NMR** (101 MHz, CDCl₃) δ = 170.2 (CO), 156.3 (COONH), 82.3 (CMe₃), 72.6 (CONH), 52.2 (CH₃O), 28.2 (Boc); **HRMS**: m/z (ESI⁺) calc. for C₈H₁₄NO₅ [M+Na]⁺: 228.0842; Obs.: 228.0841; **v_{max}**: (FT-ATR)/cm⁻¹: 3305, 2979, 1737, 1439, 1368, 1216, 1165, 1117, 995, 848, 776, 713, 589; **m.p.**: 55-57 °C.



Lithium hydroxide (0.40 g, 16.6 mmol) was added to a solution of **41** (1.36 g, 6.63 mmol) in a mixture of tetrahydrofuran (5 mL) and water (5 mL), and the reaction was stirred at r.t. for 16 h. The tetrahydrofuran was then removed under reduced pressure and hydrochloric acid (1 M, 30 mL) was added. The aqueous was extracted with ethyl acetate (3 × 50 mL) and the

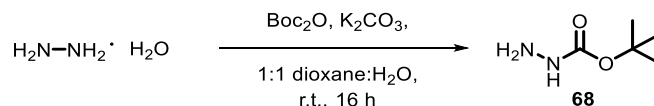
combined organics dried with MgSO₄, filtered, and concentrated under reduced pressure to afford a cream-white solid (972 mg, 5.09 mmol, 77%).

R_f: 0.22 (1:1, EtOAc:Petrol); **¹H NMR** (400 MHz, CDCl₃) δ = 11.02 (s, 1H, OH), 8.21 (s, 1H, NH), 4.46 (s, 2H, CH₂O), 1.47 (s, 9H, Boc); **HRMS**: m/z (ESI⁺) calc. for C₇H₁₁NO₅ [M+H]⁺: 190.0721; Obs.: 190.0716; **v_{max}**: (FT-ATR)/cm⁻¹: 3266, 2981, 2936, 1721, 1479, 1395, 1370, 1251, 1163, 1122, 1054, 979, 847, 777, 675; **m.p.**: 102-105 °C.



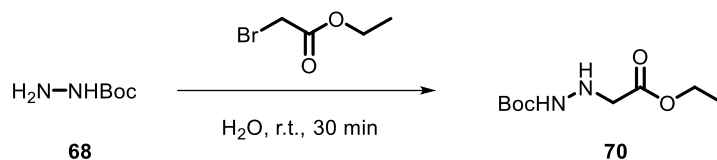
A mixture of **41** (920 mg, 4.82 mmol), *N*-hydroxysuccinimide (831 mg, 7.23 mmol), and *N*-(3-dimethylaminopropyl)-*N*-ethylcarbodiimide hydrochloride (1.39 g, 7.23 mmol) in dichloromethane (20 mL) was stirred at r.t. for 2 h. Dichloromethane (30 mL) was then added and the organics were washed with water (2 × 30 mL) and brine (30 mL), dried with MgSO₄, filtered, and concentrated under reduced pressure to give a colourless oil (1.12 g, 3.89 mmol, 81%).

R_f: 0.35 (2:8, EtOAc:Petrol); **¹H NMR** (400 MHz, CDCl₃) δ = 7.99 (s, 1H, NH), 4.71 (s, 2H, CH₂O), 2.81 (s, 4H, CH₂CO), 1.41 (s, 9H, Boc); **HRMS**: m/z (ESI⁺) calc. for C₁₁H₁₅N₂O₇ [M+Na]⁺: 311.0850; Obs.: 311.0840; **v_{max}**: (FT-ATR)/cm⁻¹: 3230, 2981, 1702, 1395, 1370, 1215, 1162, 1120, 1080, 997, 815, 86, 716, 655; **m.p.**: 110-114 °C.



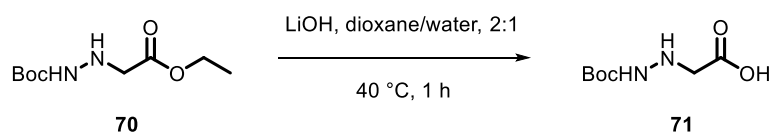
A solution of di-*tert*-butyl dicarbonate (3.52 g, 16.2 mmol) in dioxane (30 mL) was added dropwise to a stirred solution of hydrazine monohydrate (3.20 mL, 66.4 mmol) and potassium carbonate (9.28 g, 66.4 mmol) in water (30 mL), and the mixture stirred at r.t for 16 h. The reaction mixture was then extracted with diethyl ether (3 × 50 mL), and the combined organics dried with MgSO₄, filtered, and concentrated under reduced pressure to give a white solid (2.08 g, 15.8 mmol, 97%).

R_f: 0.18 (8:2, EtOAc:Petrol); **¹H NMR** (400 MHz, CDCl₃) δ = 3.79 (s, 1H, NH), 1.44 (s, 9H, Boc); **¹³C NMR** (101 MHz, CDCl₃) δ = 135.9 (C=O), 80.6 (CMe₃), 28.4 (Boc); **HRMS**: m/z (ESI⁺) calc. for C₅H₁₂N₂O₂ [M+Na]⁺: 155.0791; Obs.: 155.0792; **v_{max}**: (FT-ATR)/cm⁻¹: 3333, 2978, 2933, 1701, 1489, 1366, 1287, 1161, 1061, 870, 768; **m.p.**: 40-43 °C.



Ethyl bromoacetate (840 μL , 7.58 mmol) was added to a stirred solution of **43** (1.50 g, 11.3 mmol) in water (15 mL) and stirred at r.t. for 1 h. The reaction mixture was then extracted with diethyl ether (3 \times 40 mL), and the combined organics were washed with brine (2 \times 50 mL), dried with MgSO_4 , filtered, and concentrated under reduced pressure. The residue was purified via flash column chromatography on silica gel, eluting with EtOAc:Petrol (4:6). Fractions containing the product were concentrated under reduced pressure to provide a colourless oil (1.12 g, 5.14 mmol, 68%).

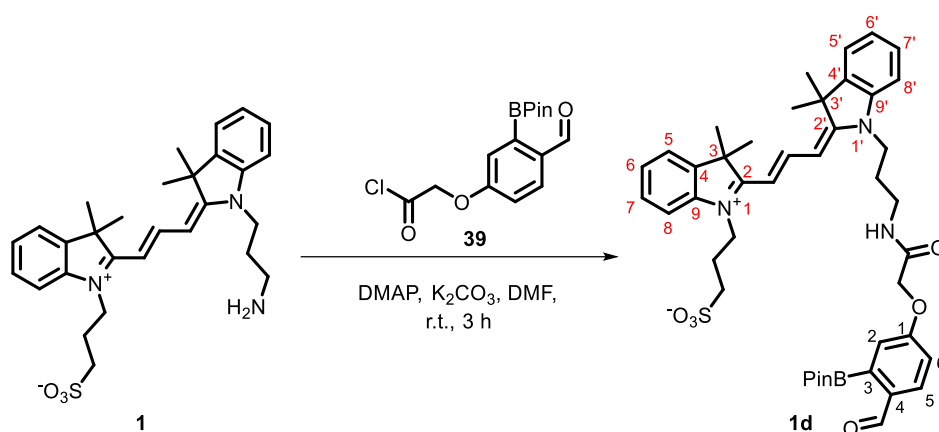
R_f: 0.27 (4:6, EtOAc:Petrol); **¹H NMR** (400 MHz, CDCl_3) δ = 6.47 (s, 1H, NH), 4.23-4.13 (m, 2H, CH₂CH₃), 3.66-3.59 (m, 2H, CH₂O), 1.42 (s, 9H, Boc), 1.25 (t, J = 7.1 Hz, 3H, CH₂CH₃); **¹³C NMR** (101 MHz, CDCl_3) δ = 171.2 (COCH₂), 135.9 (CONH), 80.8 (CMe₃), 61.1 (CH₂CH₃), 52.9 (CH₂NH), 28.4 (Boc), 14.3 (CH₂CH₃); **HRMS**: m/z (ESI⁺) calc. for $\text{C}_9\text{H}_{18}\text{N}_2\text{O}_4$ [M+Na]⁺: 241.1159; Obs.: 241.1160; **v_{max}**: (FT-ATR)/ cm^{-1} : 3290, 2971, 2926, 2854, 1675, 1557, 1456, 1429, 1151, 1114, 795.



A solution of lithium hydroxide (749 mg, 31.2 mmol) in water (5 mL) was added to a solution of **44** (680 mg, 3.12 mmol) in dioxane (10 mL), and the mixture stirred at 40 °C for 1 h. The reaction was then cooled to r.t. and acidified to pH ~4 by addition of potassium bisulphate (1 M). The aqueous mixture was then extracted with dichloromethane (3 \times 20 mL), and the combined organics were washed with brine (40 mL), dried with MgSO_4 , filtered, and concentrated under reduced pressure to give a white solid (256 mg, 1.35 mmol, 43%).

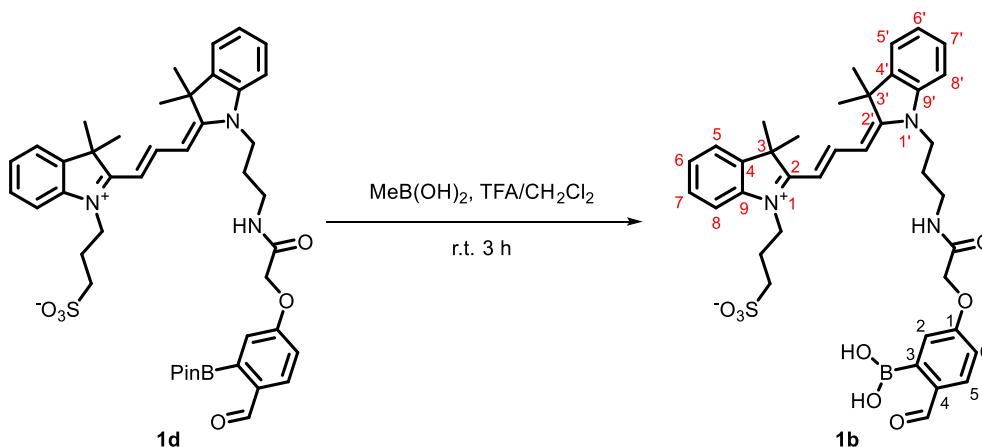
R_f: 0.11 (9:1, EtOAc:Petrol); **¹H NMR** (400 MHz, CD_3OD) δ = 3.34-3.23 (m, 2H, CH₂O), 1.42 (s, 9H, Boc); **¹³C NMR** (101 MHz, CD_3OD) δ = 172.9 (COCH₂), 135.9 (CONH), 83.3 (CMe₃), 51.9 (CH₂), 27.3 (Boc); **HRMS**: m/z (ESI⁺) calc. for $\text{C}_7\text{H}_{14}\text{N}_2\text{O}_4$ [M+Na]⁺: 213.0846; Obs.: 213.0846; **v_{max}**: (FT-ATR)/ cm^{-1} : 3252, 2978, 2964, 1701, 1536, 1368, 1247, 1148, 1058, 803, 736. **m.p.**: 143-145 °C.

4.4. Reactive Dye Synthesis



4-Dimethylaminopyridine (75 mg, 0.62 mmol) was added to a mixture of **1** (104 mg, 0.21 mmol), **35** (77 mg, 0.24 mmol), and potassium carbonate (85 mg, 0.62 mmol) in anhydrous dichloromethane (5 mL) and stirred at r.t. for 2 h. The reaction mixture was then precipitated in diethyl ether (400 mL). The solid was then collected by filtration, washed with diethyl ether (30 mL), and dried in air to give a pink powder. The residue was purified via flash column chromatography on silica gel eluting with MeOH:CH₂Cl₂ (5:95). Fractions containing the product were concentrated under reduced pressure to provide a pink oil, which was redissolved in dichloromethane (30 mL). The organics were washed with hydrochloric acid (0.1 M, 2 × 10 mL), dried with MgSO₄, filtered, and concentrated under reduced pressure, to give a pink oil (30 mg, 38 μmol, 18%).

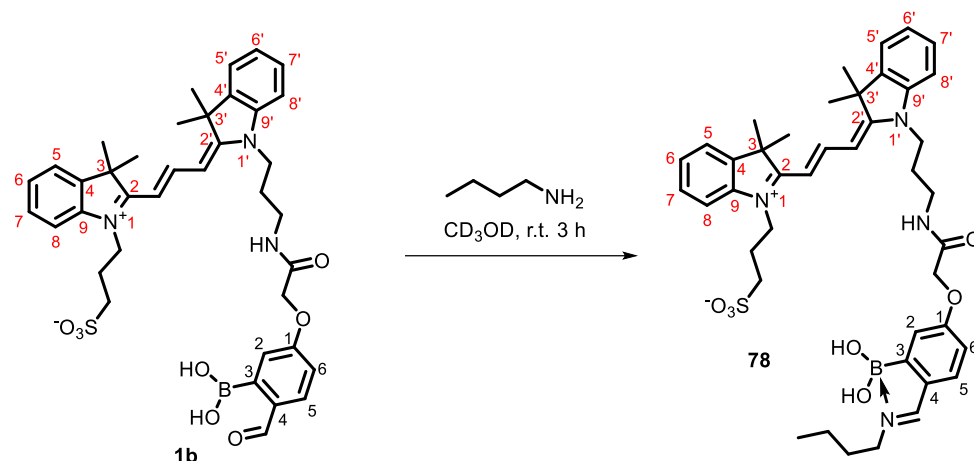
R_f: 0.16 (5:95, MeOH:CH₂Cl₂, visible light active); **¹H NMR** (400 MHz, CD₃OD, NMR data is provided for the acetal) δ = 8.48 (dd, *J*₁ = *J*₂ = 13.4 Hz, 1H, CHCHCN), 7.53-7.48 (m, 2H, H₅, H_{5'}), 7.43-7.36 (m, 3H, H₇, H_{7'}, H₈/H_{8'}), 7.35-7.22 (m, 4H, PhH₅, H₆, H_{6'}, H₈/H_{8'}), 7.00 (dd, *J* = 8.1, 2.6 Hz, 1H, PhH₆), 6.85 (d, *J* = 2.6 Hz, 1H, PhH₂), 6.66 (dd, *J* = 13.4, 5.2 Hz, 1H, CHCN), 6.41 (dd, *J* = 13.4, 5.2 Hz, 1H, CHCN), 5.47 (s, 1H, CH(OR)₂), 4.52 (s, 2H, CH₂O), 4.26 (t, *J* = 7.6 Hz, 2H, CH₂CH₂CH₂SO₃), 4.12 (t, *J* = 7.6 Hz, 2H, CH₂CH₂CH₂NH), 3.45 (t, *J* = 7.6 Hz, 2H, CH₂NH), 2.97 (t, *J* = 7.6 Hz, 2H, CH₂SO₃), 2.25-2.20 (m, 2H, CH₂CH₂SO₃), 2.11-2.01 (m, 2H, CH₂CH₂NH), 1.72 (s, 12H, CyCH₃), 1.21 (s, 12H, C(CH₃)₂); **¹³C NMR** (101 MHz, CD₃OD, NMR data is provided for the acetal) δ = 174.7 (CHCHCN), 174.6 (C₂, C_{2'}), 170.2 (CONH), 157.4 (PhC₁), 150.9 (C₃, C_{3'}), 141.9 (C₉, C_{9'}), 140.8 (C₄, C_{4'}), 134.1 (PhC₄), 130.7 (PhC₅), 128.8 (C₇/C_{7'}), 128.7 (C₇/C_{7'}), 125.5 (C₆, C_{6'}), 125.4 (PhC₃), 122.2 (C₅, C_{5'}), 115.9 (PhC₂), 114.4 (PhC₆), 111.2 (C₈/C_{8'}), 111.0 (C₈/C_{8'}), 102.9 (CHCN), 102.8 (CHCN), 74.5 ((CH₃)₂O), 66.9 (CH₂CO), 49.3 (CH₂SO₃), 42.6 (CH₂CH₂CH₂SO₃), 41.6 (CH₂CH₂CH₂NH), 36.1 (CH₂NH), 27.0 (CyCH₃), 23.9 (CH₂CH₂NH₂), 23.7 (C(CH₃)₂), 22.9 (CH₂CH₂SO₃); **HRMS**: *m/z* (ESI⁺) calc. for C₄₄H₅₄BN₃O₈S [M+Na]⁺: 818.3636; Obs.: 818.3636; **v_{max}**: (FT-ATR)/cm⁻¹: 3415, 3076, 2915, 1645, 1556, 1454, 1427, 1217, 1149, 1113, 1036, 926, 795, 756, 731, 680, 527.



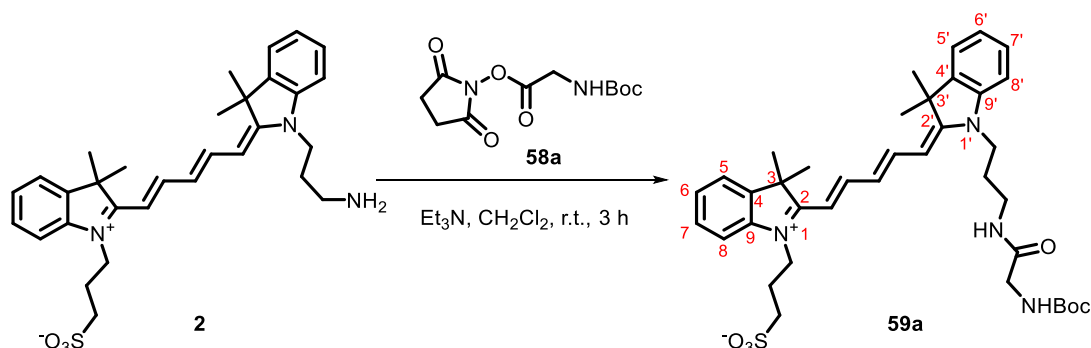
Trifluoroacetic acid (0.5 mL) was added to a solution of **46** (30 mg, 38 μmol) and methylboronic acid (23 mg, 377 μmol) in dichloromethane (5 mL), and the mixture stirred at r.t for 3 h. The reaction was azeotroped with dichloromethane (3 \times 20 mL), and hydrochloric acid (0.1 M, 2 \times 10 mL) was added, and concentrated under reduced pressure. The residue was then suspended in water (10 mL) and lyophilised to yield a pink solid. (26 mg, 38 μmol , quantitative yield).

R_f: 0.12 (5:95, MeOH:CH₂Cl₂, visible light active); **¹H NMR** (400 MHz, CD₃OD, NMR data is provided for the acetal) δ = 8.53 (dd, $J_1 = J_2 = 13.4$ Hz, 1H, CH₂CHCN), 7.55 (dd, $J = 7.4, 2.8$ Hz, 2H, H₅, H_{5'}), 7.47-7.39 (m, 3H, H₇, H_{7'}, H₈/H_{8'}), 7.37-7.27 (m, 4H, PhH₅, H₆, H_{6'}, H₈/H_{8'}), 7.04 (dd, $J = 8.1, 2.7$ Hz, 1H, PhH₆), 6.90 (d, $J = 2.7$ Hz, 1H, PhH₂), 6.62 (d, $J = 13.4$ Hz, 1H, CHCN), 6.46 (d, $J = 13.4$ Hz, 1H, CHCN), 5.41 (s, 1H, CH(OR)₂), 4.57 (s, 2H, CH₂O), 4.39-4.27 (m, 2H, CH₂CH₂CH₂SO₃), 4.16 (t, $J = 7.2$ Hz, 2H, CH₂CH₂CH₂NH), 3.49 (t, $J = 7.2$ Hz, 2H, CH₂NH), 3.02 (t, $J = 6.9$ Hz, 2H, CH₂SO₃), 2.29-2.25 (m, 2H, CH₂CH₂SO₃), 2.10 (tt, $J_1 = J_2 = 7.2$ Hz, 2H, CH₂CH₂NH), 1.77 (s, 12H, CyCH₃); **¹³C NMR** (101 MHz, CD₃OD, NMR data is provided for the acetal) δ = 174.7 (CHCHCN), 174.5 (C₂, C_{2'}), 170.2 (CONH), 157.4 (PhC₁), 150.8 (C₃, C_{3'}), 141.8 (C₉, C_{9'}), 140.8 (C₄, C_{4'}), 134.1 (PhC₄), 130.7 (PhC₅), 128.7 (C₇, C_{7'}), 125.4 (C₆, C_{6'}), 125.3 (PhC₃), 122.1 (C₅, C_{5'}), 115.9 (PhC₂), 114.4 (PhC₆), 111.2 (C₈/C_{8'}), 111.0 (C₈/C_{8'}), 102.9 (CHCN⁺), 102.7 (CHCN), 66.9 ((CH₃)₂O), 49.2 (CH₂CO), 46.8 (CH₂SO₃), 42.6 (CH₂CH₂CH₂SO₃), 41.5 (CH₂CH₂CH₂NH), 36.1 (CH₂NH), 26.9 (CyCH₃), 26.6 (CH₂CH₂NH₂), 22.8 (CH₂CH₂SO₃); **HRMS**: m/z (ESI⁺) calc. for C₃₈H₄₄BN₃O₈S [M+Na]⁺: 736.2834; Obs.: 736.2834; **v_{max}**: (FT-ATR)/cm⁻¹: 3289, 2926, 1676, 1558, 1456, 1429, 1373, 1232, 1151, 1115, 1037, 927, 756, 681; **m.p**: 315-320 °C;

Evidence for the formation of **5** was further provided by incubating 5 mg with 1.5 equiv. of *n*-butylamine in MeOD for 30 min. After this time, exclusive formation of boronimine **47** was observed.



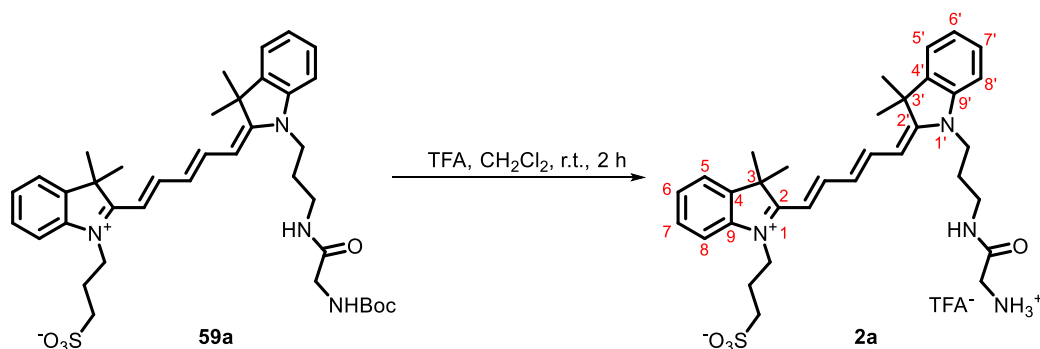
¹H NMR (400 MHz, CD₃OD, NMR data is provided for the acetal) δ = 8.62 (s, 1H, -CHNCH₂), 8.57 (dd, $J_1 = J_2 = 13.4$ Hz, 1H, CHCHCN), 7.63 (d, $J = 8.3$ Hz, 1H, PhH₅), 7.58-7.54 (m, 2H, H₅, H_{5'}), 7.48-7.41 (m, 3H, H₇, H_{7'}, H₈/H_{8'}), 7.35-7.30 (m, 3H, PhH₅, H₆, H_{6'}, H₈/H_{8'}), 7.15 (d, $J = 2.4$ Hz, 1H, PhH₂), 6.99 (dd, $J = 8.3, 2.4$ Hz, 1H, PhH₆), 6.63 (d, $J = 13.4$ Hz, 1H, CHCN), 6.50 (d, $J = 13.4$ Hz, 1H, CHCN), 4.64 (s, 2H, CH₂O), 4.39-4.33 (m, 2H, CH₂CH₂CH₂SO₃), 4.22 (t, $J = 7.5$ Hz, 2H, CH₂CH₂CH₂NH), 3.57 (t, $J = 7.7$ Hz, 2H, CH₂NH), 3.48 (t, $J = 7.0$ Hz, 2H, -CHNCH₂), 3.00 (t, $J = 6.7$ Hz, 2H, CH₂SO₃), 2.29-2.23 (m, 2H, CH₂CH₂SO₃), 2.15-2.10 (m, 2H, CH₂CH₂NH), 1.79 (s, 12H, CyCH₃), 1.52-1.38 (m, 2H, -CHNCH₂CH₂CH₂), 1.01 (t, 3H, -CH₃).



A mixture of **2** (30 mg, 56 μ mol), **36** (31 mg, 0.112 mmol), and triethylamine (39 μ L, 0.280 mmol) in dichloromethane (3 mL) was stirred at r.t. for 3 h. The reaction was then concentrated under reduced pressure and the residue was purified via flash column chromatography on silica gel, eluting with MeOH:CH₂Cl₂ (5:95). Fractions containing the product were concentrated under reduced pressure to provide a blue oil (30 mg, 44 μ mol, 77%).

R_f: 0.38 (5:95, MeOH:CH₂Cl₂, visible light active); **¹H NMR** (400 MHz, CD₃OD) δ = 8.20 (dd, $J_1 = J_2 = 13.5$ Hz, 2H, CHCHCN), 7.43 (dd, $J = 7.9, 2.6$ Hz, 2H, H₅, H_{5'}), 7.37-7.30 (m, 3H, H₇, H_{7'}, H₈/H_{8'}), 7.30-7.27 (m, 1H, H₈/H_{8'}), 7.19 (dd, $J = 7.9, 2.8$ Hz, 2H, H₆, H_{6'}), 6.67 (dd, $J_1 = J_2 = 13.5$ Hz, 1H, CHCHCHCN), 6.38 (d, $J = 13.5$ Hz, 1H, CHCN), 6.27 (d, $J = 13.5$ Hz, 1H, CHCN), 4.34-4.26 (m, 2H, CH₂CH₂CH₂SO₃), 4.08 (t, $J = 7.6$ Hz, 2H, CH₂CH₂CH₂NH), 3.70 (s, 2H, CH₂NHBoc), 3.36 (t, $J = 7.6$ Hz, 2H, CH₂NH), 2.97 (t, $J = 7.5$ Hz, 2H, CH₂SO₃), 2.22

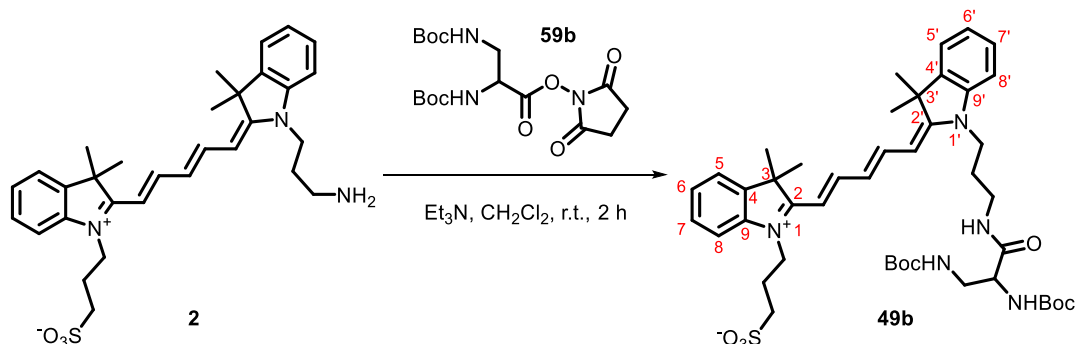
(tt, $J_1 = J_2 = 7.5$ Hz, 2H, $\text{CH}_2\text{CH}_2\text{SO}_3$), 1.95 (tt, $J_1 = J_2 = 7.6$ Hz, 2H, $\text{CH}_2\text{CH}_2\text{NH}$), 1.65 (s, 12H, CyCH_3), 1.42 (s, 9H, Boc); ^{13}C NMR (101 MHz, CD_3OD) $\delta = 173.1$ ($\underline{\text{C}}_2$, $\underline{\text{C}}_2'$), 171.8 ($\underline{\text{C}}_3$, $\underline{\text{C}}_3'$), 169.9 ($\underline{\text{C}}\text{ON}$), 157.2 ($\underline{\text{C}}\text{HCHCN}$), 154.4 ($\underline{\text{C}}\text{HCHCN}$), 142.2 ($\underline{\text{C}}_9/\underline{\text{C}}_9'$), 142.0 ($\underline{\text{C}}_9/\underline{\text{C}}_9'$), 141.3 ($\underline{\text{C}}_4/4'$), 141.2 ($\underline{\text{C}}_4/\underline{\text{C}}_4'$), 130.1 ($\underline{\text{C}}_7$, $\underline{\text{C}}_7'$), 129.9 ($\underline{\text{C}}_7$, $\underline{\text{C}}_7'$), 126.0 ($\underline{\text{C}}\text{HCHCHCN}$), 124.9 ($\underline{\text{C}}_6/\underline{\text{C}}_6'$), 124.8 ($\underline{\text{C}}_6/\underline{\text{C}}_6'$), 122.1 ($\underline{\text{C}}_5$, $\underline{\text{C}}_5'$), 110.8 ($\underline{\text{C}}_8/\underline{\text{C}}_8'$), 110.7 ($\underline{\text{C}}_8/\underline{\text{C}}_8'$), 103.3 ($\underline{\text{C}}\text{HCN}$), 103.1 ($\underline{\text{C}}\text{HCN}$), 79.4 ($\underline{\text{C}}\text{H}_2\text{NHBoc}$), 79.1, ($\underline{\text{C}}\text{Me}_3$), 49.2 ($\underline{\text{C}}\text{H}_2\text{SO}_3$), 42.4 ($\underline{\text{C}}\text{H}_2\text{CH}_2\text{CH}_2\text{SO}_3$), 41.5 ($\underline{\text{C}}\text{H}_2\text{CH}_2\text{CH}_2\text{NH}$), 36.4 ($\underline{\text{C}}\text{H}_2\text{NH}$), 27.4 (Boc), 26.9 ($\underline{\text{C}}\text{H}_2\text{CH}_2\text{NH}$), 26.6 ($\text{Cy}\underline{\text{C}}\text{H}_3$), 22.8 ($\underline{\text{C}}\text{H}_2\text{CH}_2\text{SO}_3$); **HRMS**: m/z (ESI⁺) calc. for $\text{C}_{38}\text{H}_{50}\text{N}_4\text{O}_6$ $[\text{M}+\text{Na}]^+$: 713.3343; Obs.: 713.3351; ν_{max} : (FT-ATR)/ cm^{-1} : 3300, 2968, 2924, 2852, 1702, 1659, 1492, 1482, 1453, 1378, 1338, 1216, 1138, 1102, 1035, 925, 709, 522.



Trifluoroacetic acid (1.0 mL) was added to a solution of **48** (30 mg, 44 μmol) in dichloromethane (5 mL) and stirred at r.t. for 2 h. The reaction mixture was then concentrated under reduced pressure to ~ 5 mL, and the remaining solution added dropwise to diethyl ether (200 mL). The resultant precipitate was collected by filtration, washed with diethyl ether (30 mL), and dried in air. The solid was then dissolved in methanol (30 mL) and concentrated under reduced pressure to give a blue oil (19 mg, 32 μmol , 73%).

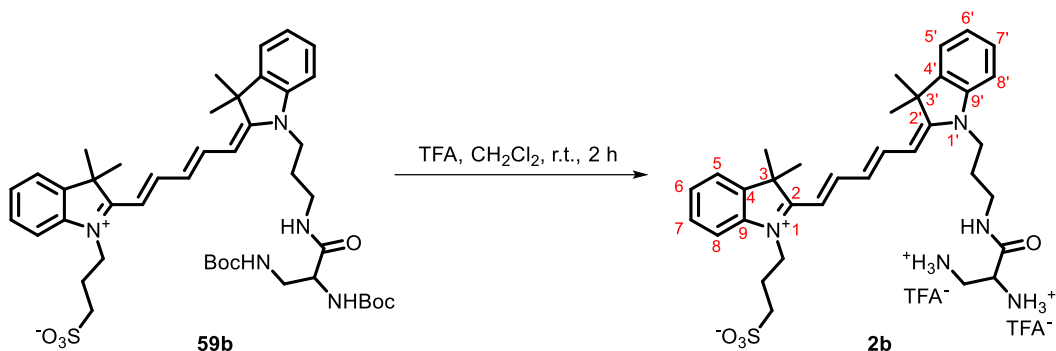
R_f: 0.21 (5:95, CH_2Cl_2 :MeOH, visible light active); ^1H NMR (400 MHz, CD_3OD) $\delta = 8.10$ (d, $J = 13.6$ Hz, 2H, $\underline{\text{C}}\text{HCHCN}$), 7.40 (dd, $J_1 = J_2 = 7.5$ Hz, 2H, $\underline{\text{H}}_5$, $\underline{\text{H}}_5'$), 7.34 (t, $J = 7.5$ Hz, 2H, $\underline{\text{H}}_7$, $\underline{\text{H}}_7'$), 7.29 (dd, $J = 7.9$, 2.5 Hz, 2H, $\underline{\text{H}}_8$, $\underline{\text{H}}_8'$), 7.15 (dd, $J_1 = J_2 = 7.5$ Hz, 2H, $\underline{\text{H}}_6$, $\underline{\text{H}}_6'$), 6.61 (dd, $J_1 = J_2 = 13.6$ Hz, 1H, $\underline{\text{C}}\text{HCHCHCN}$), 6.48 (d, $J = 13.6$ Hz, 1H, $\underline{\text{C}}\text{HCN}$), 6.17 (d, $J = 13.6$ Hz, 1H, $\underline{\text{C}}\text{HCN}$), 4.32 (t, $J = 7.5$ Hz, 2H, $\underline{\text{C}}\text{H}_2\text{CH}_2\text{CH}_2\text{SO}_3$), 4.13 (t, $J = 7.4$ Hz, 2H, $\underline{\text{C}}\text{H}_2\text{CH}_2\text{CH}_2\text{NH}$), 3.81 (s, 2H, $\underline{\text{C}}\text{H}_2\text{NH}_3^+$), 3.42 (t, $J = 7.4$ Hz, 2H, $\underline{\text{C}}\text{H}_2\text{NH}$), 3.03 (t, $J = 7.5$ Hz, 2H, $\underline{\text{C}}\text{H}_2\text{SO}_3$), 2.23 (tt, $J_1 = J_2 = 7.5$ Hz, 2H, $\underline{\text{C}}\text{H}_2\text{CH}_2\text{SO}_3$), 1.96 (tt, $J_1 = J_2 = 7.4$ Hz, 2H, $\underline{\text{C}}\text{H}_2\text{CH}_2\text{NH}$), 1.59 (s, 12H, CyCH_3); ^{13}C NMR (101 MHz, CD_3OD) $\delta = 173.5$ ($\underline{\text{C}}_2$, $\underline{\text{C}}_2'$), 172.7 ($\underline{\text{C}}_3$, $\underline{\text{C}}_3'$), 166.4 ($\underline{\text{C}}\text{O}$), 154.2 ($\underline{\text{C}}\text{HCHCN}$), 153.7 ($\underline{\text{C}}\text{HCHCN}$), 142.0 ($\underline{\text{C}}_9$, $\underline{\text{C}}_9'$), 141.3 ($\underline{\text{C}}_4$, $\underline{\text{C}}_4'$), 128.4 ($\underline{\text{C}}_7$, $\underline{\text{C}}_7'$), 126.1 ($\underline{\text{C}}\text{HCHCHCN}$), 125.0 ($\underline{\text{C}}_6$, $\underline{\text{C}}_6'$), 122.1 ($\underline{\text{C}}_5$, $\underline{\text{C}}_5'$), 110.7 ($\underline{\text{C}}_8$, $\underline{\text{C}}_8'$), 103.9 ($\underline{\text{C}}\text{HCN}$), 49.1 ($\underline{\text{C}}\text{H}_2\text{NH}_3$), 47.5 ($\underline{\text{C}}\text{H}_2\text{SO}_3$), 45.3, 41.4 ($\underline{\text{C}}\text{H}_2\text{CH}_2\text{CH}_2\text{SO}_3$), 40.4 ($\underline{\text{C}}\text{H}_2\text{CH}_2\text{CH}_2\text{NH}$), 36.5 ($\underline{\text{C}}\text{H}_2\text{NH}$), 26.9 ($\underline{\text{C}}\text{H}_2\text{CH}_2\text{NH}$), 26.6 ($\text{Cy}\underline{\text{C}}\text{H}_3$), 22.8 ($\underline{\text{C}}\text{H}_2\text{CH}_2\text{SO}_3$); **HRMS**: m/z (ESI⁺) calc.

for $C_{33}H_{42}N_4O_4S$ $[M+H]^+$: 591.3014; Obs.: 591.3000; ν_{\max} : (FT-ATR)/ cm^{-1} : 2918, 2856, 1683, 1495, 1461, 1388, 1145, 1106, 1034, 928, 799, 752, 710.

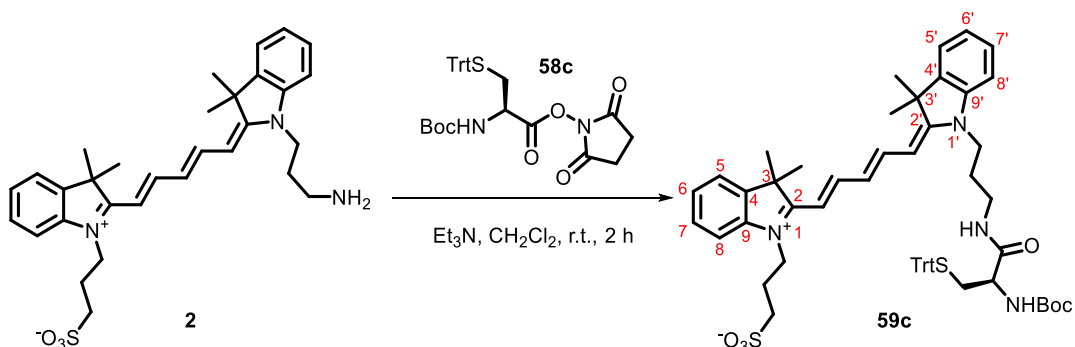


A mixture of **2** (19 mg, 36 μ mol), **38** (28 mg, 70 μ mol), and triethylamine (24 μ L, 0.18 mmol) in dichloromethane (1 mL) was stirred at r.t. for 2 h. The reaction mixture was then concentrated under reduced pressure, and the residue was purified via flash column chromatography on silica gel, eluting with MeOH:CH₂Cl₂ (5:95). Fractions containing the product were concentrated under reduced pressure to provide a blue oil. (11 mg, 13 μ mol, 38%).

R_f: 0.32 (5:95, MeOH:CH₂Cl₂, visible light active); **¹H NMR** (400 MHz, CD₃OD) δ = 8.22 (dd, J = 13.0 Hz, 2H, 2 \times CHCHCN), 7.44 (d, J = 7.3 Hz, 2H, H5, H5'), 7.40-7.36 (m, 2H, H7, H7'), 7.36-7.28 (m, 2H, H8, H8'), 7.20 (dd, $J_1 = J_2 = 7.3$ Hz, 2H, H6, H6'), 6.67 (dd, $J_1 = J_2 = 13.0$ Hz, 1H, CHCHCHCN), 6.38 (d, J = 13.0 Hz, 1H, CHCN), 6.29 (t, J = 13.0 Hz, 1H, CHCN), 4.40-4.24 (m, 2H, CH₂CH₂CH₂SO₃), 4.13-4.07 (m, 3H, CH₂CH₂CH₂NH, CHCO), 3.40-3.33 (m, 2H, CH₂NH), 3.30-3.23 (m, 2H, CH₂NHBoc), 2.98 (t, J = 6.9 Hz, 2H, CH₂SO₃), 2.23 (tt, $J_1 = J_2 = 6.9$ Hz, 2H, CH₂CH₂SO₃), 1.97 (tt, $J_1 = J_2 = 7.0$ Hz, 2H, CH₂CH₂NH), 1.66 (s, 12H, CyCH₃), 1.40 (s, 18H, 2 \times Boc); **¹³C NMR** (101 MHz, CD₃OD) δ = 173.1 (C2, C2'), 172.2 (C3, C3'), 167.8 (CON), 157.4 (CHCHCN), 156.5 (CHCHCN), 142.2 (C9/C9'), 142.1 (C9/C9'), 141.3 (C4/C4'), 141.2 (C4/C4'), 128.5 (C7, C7'), 126.1 (CHCHCHCN), 124.8 (C6, C6'), 122.1 (C5, C5'), 110.8 (C8, C8'), 103.1 (CHCN), 103.4 (CHCN), 80.9 (CMe₃), 80.6 (CMe₃), 56.0 (CH₂NHBoc), 49.3 (CHCO), 48.3 (CH₂SO₃), 42.7 (CH₂CH₂CH₂SO₃), 41.5 (CH₂CH₂CH₂NH), 36.6 (CH₂NH), 27.4 (CyCH₃), 26.6 (Boc), 26.6 (CH₂CH₂NH), 22.8 (CH₂CH₂SO₃); **HRMS**: m/z (ESI⁺) calc. for $C_{44}H_{61}N_5O_8S$ $[M+H]^+$: 820.4314; Obs.: 820.4341; ν_{\max} : (FT-ATR)/ cm^{-1} : 3655, 2981, 2927, 1707, 1481, 1453, 1381, 1138, 1101, 1035, 926, 803, 753, 709, 552; **m.p.**: 168-171 °C.



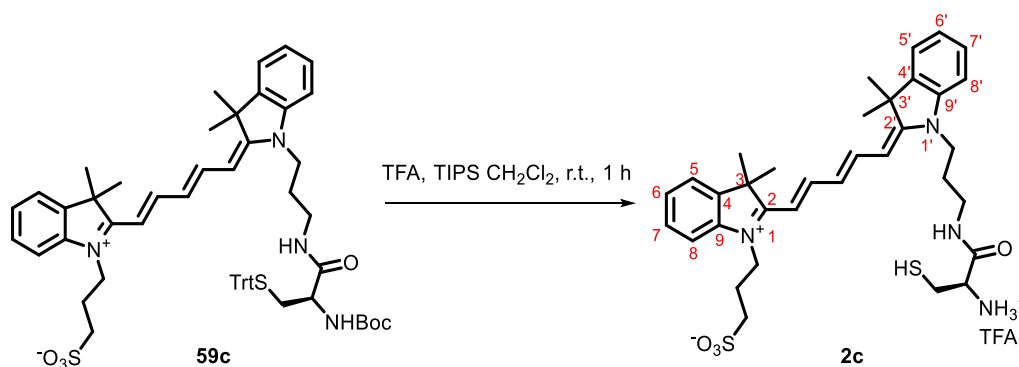
Trifluoroacetic acid (1 mL) was added dropwise to a stirred solution of **49** (11 mg, 13 μ mol) in dichloromethane (9 mL) and the mixture was stirred at r.t. for 2 h. The reaction was then concentrated under reduced pressure to \sim 5 mL, and the remaining solution added dropwise to diethyl ether (200 mL). The resultant precipitate was collected by filtration, washed with diethyl ether (30 mL), and dried in air. The solid was then dissolved in methanol (10 mL) and concentrated under reduced pressure to afford a blue oil. (10 mg, 13 μ mol, quantitative yield). **R_f**: 0.15 (1:9, MeOH:CH₂Cl₂, visible light active); **¹H NMR** (400 MHz, CD₃OD) δ = 8.13 (dd, $J_1 = J_2 = 13.6$ Hz, 2H, 2 \times CHCHCN), 7.48-7.40 (m, 2H, H₅, H_{5'}), 7.38-7.34 (m, 2H, H₇, H_{7'}), 7.32-7.25 (m, 2H, H₈, H_{8'}), 7.25-7.12 (m, 2H, H₆, H_{6'}), 6.66 (dd, $J_1 = J_2 = 13.6$ Hz, 1H, CHCHCHCN), 6.52 (d, $J = 13.6$ Hz, 1H, CHCN), 6.21 (d, $J = 13.6$ Hz, 1H, CHCN), 4.36-4.32 (m, 3H, CH₂CH₂CH₂SO₃/CHCO), 4.19-4.15 (m, 2H, CH₂CH₂CH₂NH), 3.60-3.54 (m, 2H, CH₂NH), 3.44-3.38 (m, 2H, CH₂SO₃), 3.08 (t, $J = 7.0$ Hz, 2H, CH₂NH₃⁺), 2.24 (tt, $J_1 = J_2 = 7.5$ Hz, 2H, CH₂CH₂SO₃), 2.02 (tt, $J_1 = J_2 = 7.0$ Hz, 2H, CH₂CH₂NH), 1.62 (s, 12H, CyCH₃); **¹³C NMR** (101 MHz, CD₃OD) δ = 174.9 (C₂, C_{2'}), 174.2 (C₃, C_{3'}), 168.5 (C_{ON}), 155.5 (CHCHCN), 154.9 (CHCHCN), 143.4 (C₉, C_{9'}), 142.7 (C₄, C_{4'}), 129.3 (C₇, C_{7'}), 126.9 (CHCHCHCN), 126.3 (C₆, C_{6'}), 123.6, (C₅, C_{5'}), 111.9 (C₈, C_{8'}), 105.5 (CHCN), 104.4 (CHCN), 57.4 (CH₂NH₃⁺), 50.6 (CHCO), 50.5 (CH₂SO₃), 44.3 (CH₂CH₂CH₂SO₃), 42.8 (CH₂CH₂CH₂NH), 38.4 (CH₂NH), 28.4 (CyCH₃), 24.5, (CH₂CH₂NH), 24.2 (CH₂CH₂SO₃); **HRMS**: m/z (ESI⁺) calc. for C₃₄H₄₅N₅O₄S [M+H]⁺: 620.3265; Obs.: 620.3265; **v_{max}**: (FT-ATR)/cm⁻¹: 2978, 2929, 1680, 1488, 1456, 1384, 1145, 1038 1018, 995, 926, 800; **m.p.**: 178-181 °C.



A mixture of **2** (30 mg, 56 μ mol), **39** (90 mg, 0.169 mmol), and triethylamine (29 μ L, 0.280 mmol) in dichloromethane (2 mL) was stirred at r.t. for 2 h. The reaction mixture was then

concentrated under reduced pressure and the residue was purified via flash column chromatography on silica gel, eluting with MeOH:CH₂Cl₂ (5:95). Fractions containing the product were concentrated under reduced pressure to provide a blue solid (45 mg, 46 μmol, 84%). The product was carried into the next step without further characterisation.

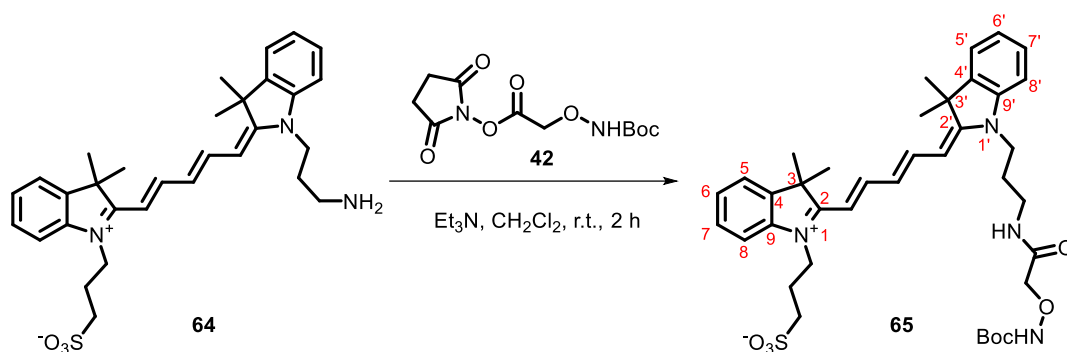
R_f: 0.32 (5:95, MeOH:CH₂Cl₂, visible light active); **¹H NMR** (400 MHz, CD₃OD) δ = 8.24 (dd, *J* = 13.5, 13.0 Hz, 2H, 2 × CHCHCN), 7.45 (dd, *J* = 7.3, 2.2 Hz, 2H, H₅, H_{5'}), 7.42-7.38 (m, 2H, H₇, H_{7'}), 7.34 (d, *J* = 7.7 Hz, 6H, TrtPhH₂), 7.31-7.26 (m, 2H, H₈, H_{8'}), 7.26-7.20 (m, 8H, TrtPhH₃ / H₆, H_{6'}), 7.17 (t, *J* = 7.7 Hz, 3H, TrtPhH₄), 6.63 (dd, *J*₁ = *J*₂ = 13.0 Hz, 1H, CHCHCHCN), 6.34 (d, *J* = 13.5 Hz, 1H, CHCN), 6.25 (d, *J* = 13.5 Hz, 1H, CHCN), 4.30 (t, *J* = 8.3 Hz, 2H, CH₂CH₂CH₂SO₃), 4.04 (t, *J* = 6.9 Hz, 2H, CH₂CH₂CH₂NH), 3.96 (t, *J* = 6.9 Hz, 1H, CHCO), 3.33 (d, *J* = 6.9 Hz, 2H, CH₂NH), 2.95 (t, *J* = 7.0 Hz, 2H, CH₂STrt), 2.57-2.42 (m, 2H, CH₂SO₃), 2.24-2.17 (m, 2H, CH₂CH₂SO₃), 1.99-1.92 (m, 2H, CH₂CH₂NH), 1.68 (s, 12H, CyCH₃), 1.40 (s, 9H, Boc); **HRMS**: *m/z* (ESI⁺) calc. for C₅₈H₆₆N₄O₆S₂ [M+H]⁺: 979.4497; Obs.: 979.4542; **v_{max}**: (FT-ATR)/cm⁻¹: 3419, 2925, 2859, 1711, 1489, 1455, 1382, 1338, 1216, 1140, 1104, 1036, 1018, 926, 750, 707; **m.p.**: 167-154 °C.



Trifluoroacetic acid (2 mL) was added dropwise to a stirred solution of **50** (40 mg, 41 μmol) and triisopropylsilane (43 μL, 0.210 mmol) in dichloromethane (10 mL), and the mixture stirred at r.t. for 1 h. The reaction was then concentrated under reduced pressure to ~5 mL, and the remaining solution added dropwise to diethyl ether (200 mL). The resultant precipitate was collected by filtration, washed with diethyl ether (30 mL), and dried in air. The solid was then dissolved in methanol (10 mL) and concentrated under reduced pressure to afford a blue oil. (22 mg, 35 μmol, 86%).

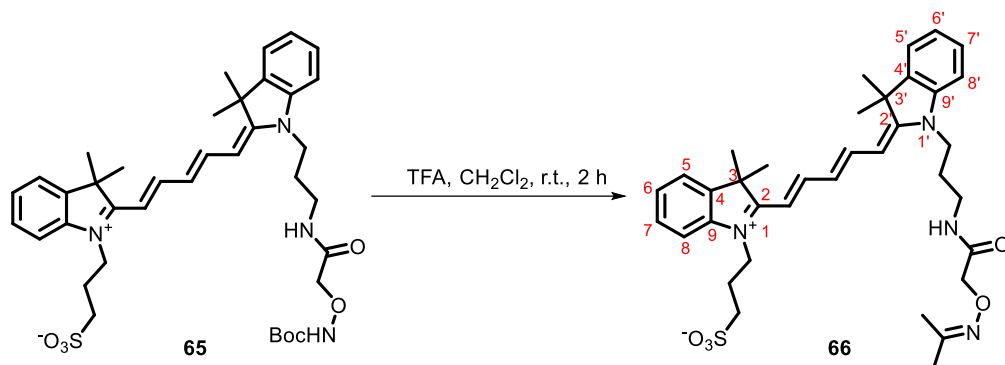
R_f: 0.29 (1:9, MeOH:CH₂Cl₂, visible light active); **¹H NMR** (400 MHz, CD₃OD) δ = 8.13 (dd, *J* = 13.5, 13.0 Hz, 2H, 2 × CHCHCN), 7.41 (dd, *J* = 7.4, 1.1 Hz, 2H, H₅, H_{5'}), 7.38-7.33 (m, 2H, H₇, H_{7'}), 7.33-7.26 (m, 2H, H₈, H_{8'}), 7.17 (ddd, *J*₁ = *J*₂ = 7.5, *J*₃ = 1.0 Hz, 2H, H₆, H_{6'}), 6.64 (dd, *J*₁ = *J*₂ = 13.0 Hz, 1H, CHCHCHCN), 6.48 (d, *J* = 13.5 Hz, 1H, CHCN), 6.21 (d, *J* = 13.5 Hz, 1H, CHCN), 4.34 (t, *J* = 7.4 Hz, 2H, CH₂CH₂CH₂SO₃), 4.18-4.10 (m, 3H, CH₂CH₂CH₂NH, CHCO), 3.53-3.40 (m, 2H, CH₂NH), 3.17-3.11 (m, 1H, CH₂SH), 3.09-3.00 (m, 3H, CH₂SO₃,

CH₂SH), 2.26-2.20 (m, 2H, CH₂CH₂SO₃), 2.05-1.93 (m, 2H, CH₂CH₂NH), 1.61 (s, 12H, CyCH₃); ¹³C NMR (101 MHz, CD₃OD) δ = 173.5 (C₂, C_{2'}), 172.7 (C₃, C_{3'}), 167.5 (CONH), 154.3 (CHCHCN), 153.7 (CHCHCN), 142.0 (C₉/C_{9'}), 141.3 (C₉/C_{9'}), 142.0 (C₄/C_{4'}), 141.3 (C₄/C_{4'}), 128.4 (C₇, C_{7'}), 126.2 (CHCHCHCN), 125.0 (C₆/C_{6'}), 124.8 (C₆/C_{6'}), 122.1 (C₅, C_{5'}), 110.7 (C₈/C_{8'}), 110.4 (C₈/C_{8'}), 103.9 (CHCN), 102.9 (CHCN), 54.9 (CH₂SH), 49.1 (CHCO), 48.3 (CH₂SO₃), 42.6 (CH₂CH₂CH₂SO₃), 41.5 (CH₂CH₂CH₂NH), 36.8 (CH₂NH), 26.9 (CyCH₃), 26.6 (CH₂CH₂NH), 22.8 (CH₂CH₂SO₃); **HRMS**: m/z (ESI⁺) calc. for C₃₄H₄₄N₄O₄S₂ [M+H]⁺: 637.2877; Obs.: 637.2873; ν_{max}: (FT-ATR)/cm⁻¹: 3412, 2966, 1677, 1490, 1455, 1381, 1338, 1202, 1139, 1101, 1035, 1016, 925, 798, 751, 709; **m.p.**: 194-197 °C.



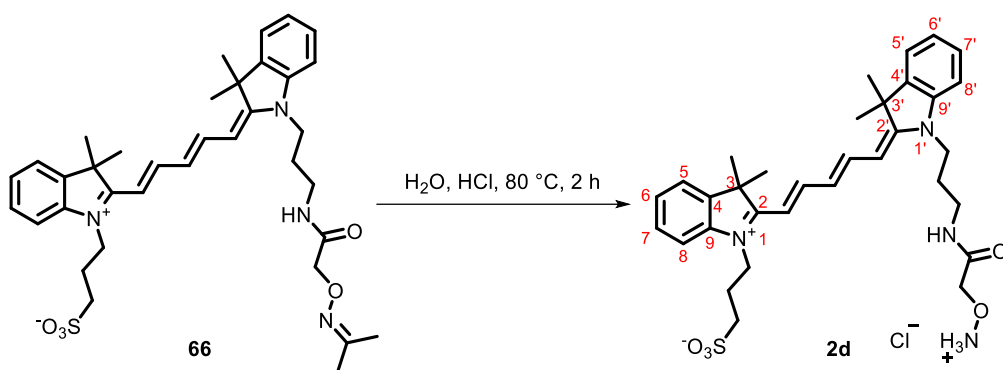
A mixture of **2** (30 mg, 56 μmol), **42** (49 mg, 0.170 mmol), and triethylamine (29 μL, 0.28 mmol) in dichloromethane (2 mL) was stirred for at r.t. for 2 h. The reaction mixture was then concentrated under reduced pressure and the residue was purified via flash column chromatography on silica gel, eluting with MeOH:CH₂Cl₂ (5:95). Fractions containing the product were concentrated under reduced pressure to provide a blue oil (15 mg, 21 μmol, 38%).

R_f: 0.24 (1:9, MeOH:CH₂Cl₂, visible light active); ¹H NMR (400 MHz, CDCl₃) δ = 9.00 (s, 1H, NH_{Boc}), 7.86-7.78 (m, 2H, 2 × CHCHCN) 7.39-7.32 (m, 2H, H₅, H_{5'}), 7.31 (d, J = 7.8 Hz, 2H, H₇, H_{7'}), 7.24-7.18 (m, 1H, H₈/H_{8'}), 7.20-7.12 (m, 2H, H₈/H_{8'}, H₆/H_{6'}), 7.10 (d, J = 7.8 Hz, 1H, H₆/H_{6'}), 7.08-7.03 (m, 1H, CHCN), 6.92-6.66 (m, 1H, 2 × CHCN), 6.05 (dd, J₁ = J₂ = 13.4 Hz, 1H, CHCHCHCN), 4.48 (s, 2H, CH₂O), 4.46-4.40 (m, 2H, CH₂CH₂CH₂SO₃), 4.07 (t, J = 7.8 Hz, 2H, CH₂CH₂CH₂NH), 3.45 (t, J = 7.8 Hz, 2H, CH₂NH), 3.03 (t, J = 7.5 Hz, 2H, CH₂SO₃), 2.32-2.21 (m, 2H, CH₂CH₂SO₃), 2.09-1.98 (m, 2H, CH₂CH₂NH), 1.64 (s, 12H, CyCH₃), 1.37 (s, 9H, Boc); ¹³C NMR (101 MHz, CDCl₃) δ = 174.7 (C₂/C_{2'}), 174.3 (C₂/C_{2'}), 172.3 (C₃/C_{3'}), 172.1 (C₃/C_{3'}), 160.6 (CON), 155.3 (CHCHCN), 155.0 (CHCHCN), 143.5 (C₉, C_{9'}), 142.2 (C₄, C_{4'}), 130.4 (C₇/C_{7'}), 130.3 (C₇/C_{7'}), 128.9 (CHCHCHCN), 126.8 (C₆/C_{6'}), 126.4 (C₆/C_{6'}), 123.7 (C₅/C_{5'}), 123.6 (C₅/C_{5'}), 112.3 (C₈/C_{8'}), 111.9 (C₈/C_{8'}), 104.6 (CHCN), 104.5 (CHCN), 80.8 (CMe₃), 77.5 (CH₂O), 48.9 (CH₂SO₃⁻), 47.6 (CH₂CH₂CH₂SO₃⁻), 43.3 (CH₂CH₂CH₂NH), 37.2 (CH₂NH), 29.7 (Boc), 29.0 (CH₂CH₂NH), 26.8 (CyCH₃), 24.9 (CH₂CH₂SO₃⁻); **HRMS**: m/z (ESI⁺) calc. for C₃₈H₅₀N₄O₇S [M+H]⁺: 707.3473; Obs.: 707.3492.



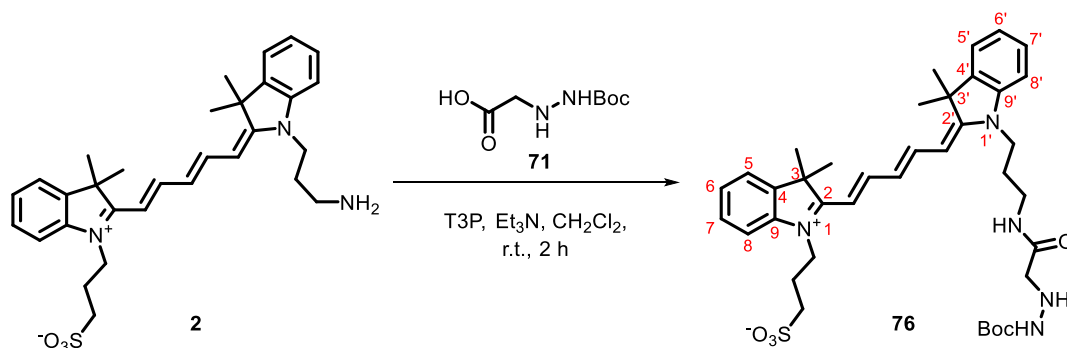
Trifluoroacetic acid (4 mL) was added dropwise to a stirred solution of **51** (30 mg, 42 μ mol) in dichloromethane (4 mL) and the mixture was stirred at r.t. for 2 h. The reaction was then concentrated under reduced pressure to \sim 5 mL, and the remaining solution added dropwise to diethyl ether (400 mL). The resultant precipitate was collected by filtration, washed with diethyl ether (30 mL), and dried in air. The solid was dissolved in methanol (10 mL) and concentrated under reduced pressure to afford a blue oil (20 mg, 31 μ mol, 74%).

R_f: 0.21 (1:9, MeOH:CH₂Cl₂, visible light active); **¹H NMR** (400 MHz, CD₃OD) δ = 8.24 (dd, $J_1 = J_2 = 13.5$ Hz, 2H, 2 \times CHCHCN), 7.98 (t, $J = 6.1$ Hz, 1H, NHCO), 7.45 (d, $J = 7.5$ Hz, 2H, H₅, H_{5'}), 7.41-7.33 (m, 3H, H₇, H_{7'}, H₈/H_{8'}), 7.31-7.17 (m, 3H, H₆, H_{6'}, H₈/H_{8'}), 6.64 (dd, $J_1 = J_2 = 13.0$ Hz, 1H, CHCHCHCN), 6.40 (d, $J = 13.5$ Hz, 1H, CHCN), 6.26 (d, $J = 13.5$ Hz, 1H, CHCN), 4.43 (s, 2H, CH₂O), 4.32 (t, $J = 7.2$ Hz, 2H, CH₂CH₂CH₂SO₃), 4.09 (t, $J = 7.6$ Hz, 2H, CH₂CH₂CH₂NH), 3.43-3.36 (m, 2H, CH₂NH), 2.97 (t, $J = 7.2$ Hz, 2H, CH₂SO₃), 2.22 (tt, $J_1 = J_2 = 7.2$ Hz, 2H, CH₂CH₂SO₃), 2.01 (tt, $J_1 = J_2 = 7.6$ Hz, 2H, CH₂CH₂NH), 1.94 (s, 3H, CH₃), 1.83 (s, 3H, CH₃), 1.68 (s, 12H, CyCH₃). **¹³C NMR** (101 MHz, CD₃OD) δ = 174.5 (C₂/C_{2'}), 173.7 (C₂/C_{2'}), 173.5 (C₃/C_{3'}), 173.1 (C₃/C_{3'}), 172.0 (CON), 157.8 (CHCHCN), 154.6 (CHCHCN), 142.2 (C₉/C_{9'}), 142.1 (C₉/C_{9'}), 141.3 (C₄/C_{4'}), 141.2 (C₄/C_{4'}), 128.5 (C₇/C_{7'}), 128.4 (C₇/C_{7'}), 125.8 (CHCHCHCN), 125.0 (C₆/C_{6'}), 124.8 (C₆/C_{6'}), 122.1 (C₅/C_{5'}), 122.1 (C₅/C_{5'}), 110.8 (C₈/C_{8'}), 110.5 (C₈/C_{8'}), 103.4 (CHCN), 102.9 (CHCN), 71.8 (CH₂O), 49.3 (C=N), 49.2 (CH₂SO₃), 42.7 (CH₂CH₂CH₂SO₃), 41.3 (CH₂CH₂CH₂NH), 36.2 (CH₂NH), 27.6 (CyCH₃), 26.9 (CH₂CH₂NH), 26.6 (CH₃), 26.5 (CH₃), 22.8 (CH₂CH₂SO₃); **HRMS**: m/z (ESI⁺) calc. for C₃₆H₄₅N₄O₅S [M+H]⁺: 647.3261; Obs.: 647.3261;



52 (15 mg, 23 μmol) was dissolved in hydrochloric acid (0.1 M 3 mL) and stirred at 80 °C for 2 h. The reaction mixture was then lyophilised to give the product as a blue oil (14 mg, 23 μmol , 99%). Due to the reactivity of the hydroxylamine, the product was used directly in the next experiments without further analysis.

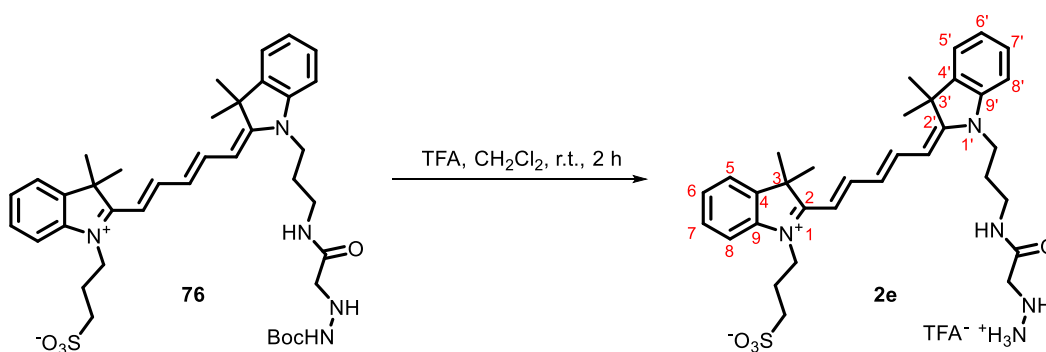
R_f: 0.14 (1:9, MeOH:CH₂Cl₂, visible light active); **¹H NMR** (400 MHz, CD₃OD) δ = 8.30-8.24 (m, 2H, 2 \times CHCHCN), 7.49-7.43 (m, 2H, H5, H5'), 7.46-7.39 (m, 3H, H7, H7', H8/H8'), 7.33-7.24 (m, 3H, H6, H6', H8/H8'), 6.68 (dd, $J_1 = J_2 = 12.4$ Hz, 1H, CHCHCHCN), 6.59 (d, $J = 13.7$ Hz, 1H, CHCN), 6.24 (d, $J = 13.7$ Hz, 1H, CHCN), 4.64 (s, 2H, CH₂O), 4.41-4.35 (m, CH₂CH₂CH₂SO₃), 4.18-4.10 (m, 2H, CH₂CH₂CH₂NH), 3.46-3.42 (m, 2H, CH₂NH), 3.05-2.98 (m, 2H, CH₂SO₃), 2.24-2.30 (m, 2H, CH₂CH₂SO₃), 2.10-2.02 (m, 2H, CH₂CH₂NH), 1.76 (s, 12H, CyCH₃); **HRMS**: m/z (ESI⁺) calc. for C₃₃H₄₂N₄O₅S [M+H]⁺: 607.2949; Obs.: 607.2964.



Propylphosphonic anhydride solution (50% w/w in EtOAc, 44 μL , 140 μmol) was added to a stirred solution of **2** (30 mg, 56 μmol), **45** (21 mg, 112 μmol), and triethylamine (39 μL , 281 μmol) in dichloromethane (3 mL) dropwise at 0 °C. The solution was then stirred at r.t. for 16 h. The reaction was concentrated under reduced pressure and the residue purified via flash column chromatography on silica gel, eluting with MeOH:CH₂Cl₂ (5:95). Fractions containing the product were concentrated under reduced pressure to provide a blue oil (18 mg, 18 μmol , 45%).

R_f: 0.28 (5:95, MeOH:CH₂Cl₂, visible light active); **¹H NMR** (400 MHz, CD₃OD) δ = 8.18 (dd, $J = 13.3, 12.5$ Hz, 2H, 2 \times CHCHCN), 7.43 (dd, $J = 7.6, 2.3$ Hz 2H, H5, H5'), 7.39-7.31 (m, 3H, H7, H7', H8/H8'), 7.31-7.25 (m, 1H, H8/H8'), 7.25-7.16 (m, 2H, H6, H6'), 6.60 (dd, $J_1 = J_2 = 12.5$ Hz, 1H, CHCHCHCN), 6.52 (d, $J = 13.3$ Hz, 1H, CHCN), 6.16 (d, $J = 13.3$ Hz, 1H, CHCN),

5.47 (s, 1H, CH₂NH), 4.34 (t, *J* = 7.6 Hz, 2H, CH₂CH₂CH₂SO₃), 4.14 (t, *J* = 7.8 Hz, 2H, CH₂CH₂CH₂NH), 3.54 (s, 2H, CH₂NHNHBoc), 3.38 (t, *J* = 7.8 Hz 2H, CH₂NH), 2.98 (t, *J* = 7.6 Hz, 2H, CH₂SO₃), 2.22 (tt, *J*₁ = *J*₂ = 7.6 Hz, 2H, CH₂CH₂SO₃), 2.00 (tt, *J*₁ = *J*₂ = 7.8 Hz, 2H, CH₂CH₂NH), 1.64 (s, 12H, CyCH₃), 1.45 (s, 9H, Boc); ¹³C NMR (101 MHz, CD₃OD) δ = 172.9 (C₂, C_{2'}), 172.8 (C₃, C_{3'}), 163.5 (CON), 154.3 (CHCHCN), 153.7 (CHCHCN), 142.0 (C₉, C_{9'}), 141.3 (C₄/C_{4'}), 141.2 (C₄/C_{4'}), 128.5 (C₇/C_{7'}), 128.4 (C₇/C_{7'}), 125.0 (CHCHCHCN), 124.8 (C₆, C_{6'}), 122.1 (C₅, C_{5'}), 110.8 (C₈/C_{8'}), 110.5 (C₈/C_{8'}), 103.8 (CHCN), 102.9 (CHCN), 79.3, (CMe₃), 54.9 (CH₂NHNHBoc), 46.5 (CH₂SO₃), 42.6 (CH₂CH₂CH₂SO₃), 41.2 (CH₂CH₂CH₂NH), 36.2 (CH₂NH), 27.3 (Boc), 26.9 (CyCH₃), 26.6 (CH₂CH₂NH), 22.7 (CH₂CH₂SO₃); HRMS: *m/z* (ESI⁺) calc. for C₃₈H₅₁N₅O₆S [M+Na]⁺: 728.3488,; Obs.: 728.3488; *v*_{max}: (FT-ATR)/cm⁻¹: 3267, 2974, 2929, 1705, 1658, 1492, 1456, 1338, 1141, 1104, 1018, 926, 802, 756.

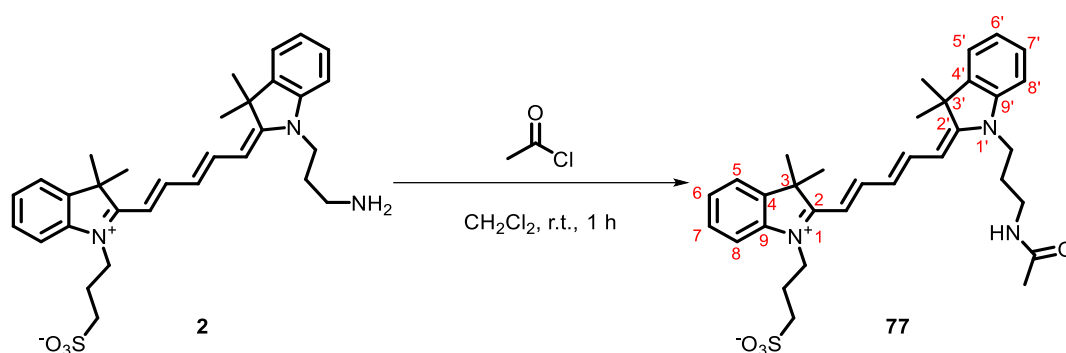


Trifluoroacetic acid (1 mL) was added to a solution of **53** (13 mg, 18 μmol) in dichloromethane (5 mL) and stirred at r.t. for 2 h. The reaction mixture was then added dropwise into diethyl ether (400 mL). The resultant precipitate was collected by filtration, washed with diethyl ether (30 mL), and dried in air. The solid was then dissolved in methanol (30 mL) and concentrated under reduced pressure to give a blue oil (11 mg, 18 μmol, quantitative yield).

*R*_f: 0.13 (5:95, MeOH:CH₂Cl₂, visible light active); ¹H NMR (400 MHz, CD₃OD) δ = 8.19 (dd, *J* = 13.3, 12.5 Hz, 2H, 2 × CHCHCN), 7.44 (dd, *J* = 7.3, 2.0 Hz, 2H, H₅, H_{5'}), 7.41-7.33 (m, 3H, H₇, H_{7'}, H₈/H_{8'}), 7.28 (d, *J* = 7.9 Hz, 1H, H₈/H_{8'}) 7.25-7.16 (m, 2H, H₆, H_{6'}), 6.63 (dd, *J*₁ = *J*₂ = 12.5 Hz, 1H, CHCHCHCN), 6.52 (d, *J* = 13.3 Hz, 1H, CHCN), 6.18 (d, *J* = 13.3 Hz, 1H, CHCN), 4.35 (t, 2H, *J* = 7.0 Hz, CH₂CH₂CH₂SO₃), 4.13 (t, *J* = 6.9 Hz, 2H, CH₂CH₂CH₂NH), 3.75 (s, 2H, CH₂NHNH₂), 3.39 (t, *J* = 6.9 Hz, 2H, CH₂NH), 3.01 (t, *J* = 7.0 Hz, 2H, CH₂SO₃), 2.23 (tt, *J*₁ = *J*₂ = 7.0 Hz, 2H, CH₂CH₂SO₃), 1.99 (tt, *J*₁ = *J*₂ = 6.9 Hz, 2H, CH₂CH₂NH), 1.66 (s, 12H, CyCH₃); ¹³C NMR (101 MHz, CD₃OD) δ = 173.6 (C₂, C_{2'}), 172.8 (C₃, C_{3'}), 163.2 (CON), 154.4 (CHCHCN), 153.8 (CHCHCN), 142.0 (C₉, C_{9'}), 141.2 (C₄, C_{4'}), 128.5 (C₇, C_{7'}), 125.0 (CHCHCHCN), 124.8 (C₆, C_{6'}), 122.1 (C₅, C_{5'}), 110.7 (C₈/C_{8'}), 110.4 (C₈/C_{8'}), 104.0 (CHCN), 102.6 (CHCN), 49.2 (CH₂NHNH₂), 47.2 (CH₂SO₃), 42.4 (CH₂CH₂CH₂SO₃), 41.2 (CH₂CH₂CH₂NH), 36.3 (CH₂NH), 26.9 (CyCH₃), 26.6 (CH₂CH₂NH), 22.7 (CH₂CH₂SO₃);

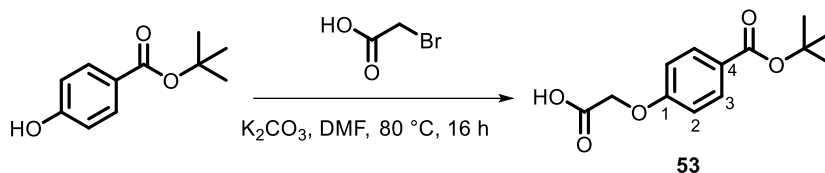
HRMS: m/z (ESI⁺) calc. for C₃₃H₄₃N₅O₄S [M+H]⁺: 606.3109; Obs.: 606.3122; ν_{\max} : (FT-ATR)/cm⁻¹: 3294, 2923, 2853, 1678, 1495, 1458, 1385, 1338, 1144, 1105, 1038, 926, 751.

4.5. Synthesis of Control Substrates for FRET Studies



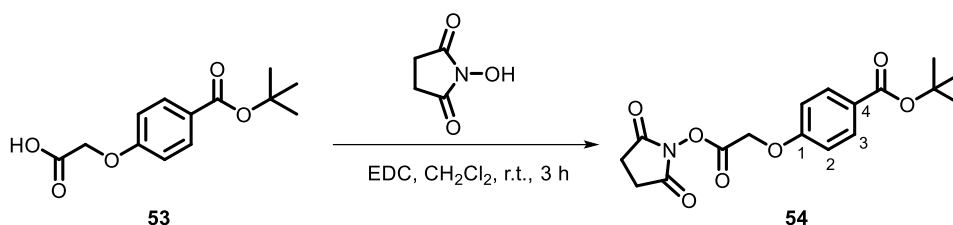
Acetyl chloride (7 μ L, 99 μ mol) was added to a solution of **2** (10 mg, 19 μ mol) in dichloromethane (3 mL) and stirred at r.t. for 1 h. The reaction mixture was then concentrated under reduced pressure and the residue was purified via flash column chromatography on silica gel, eluting with MeOH:CH₂Cl₂ (5:95). Fractions containing the product were concentrated under reduced pressure to provide a blue oil (7 mg, 12 μ mol, 64%).

R_f: 0.29 (5:95, MeOH:CH₂Cl₂, visible light active); **¹H NMR** (400 MHz, CD₃OD) δ = 8.30 (dd, $J_1 = J_2 = 13.1$ Hz, 2H, CHCHCN), 7.53-7.47 (m, 2H, H₅, H_{5'}), 7.45-7.41 (m, 3H, H₇, H_{7'}, H₈/H_{8'}), 7.31-7.25 (m, 3H, H₆, H_{6'}, H₈/H_{8'}), 6.68 (dd, $J_1 = J_2 = 13.1$ Hz, 1H, CHCHCHCN), 6.47 (d, $J = 13.1$ Hz, 1H, CHCN), 6.30 (d, $J = 13.1$ Hz, 1H, CHCN), 4.37 (t, $J = 7.5$ Hz, 2H, CH₂CH₂CH₂SO₃), 4.15 (t, $J = 7.5$ Hz, 2H, CH₂CH₂CH₂NH₂), 3.34-3.30 (m, 2H, CH₂NH₂), 3.01 (t, $J = 7.5$ Hz, 2H, CH₂SO₃), 2.27 (tt, $J_1 = J_2 = 7.5$ Hz, 2H, CH₂CH₂SO₃), 2.03 (tt, $J_1 = J_2 = 7.5$ Hz, 2H, CH₂CH₂NH₂), 1.99 (s, 3H, COCH₃), 1.74 (s, 12H, CyCH₃); **¹³C NMR** (101 MHz, CD₃OD) δ = 173.5 (C₂, C_{2'}), 172.9 (C₃/C_{3'}), 172.2 (C₃/C_{3'}), 164.7 (CON), 154.6 (CHCHCN), 154.1 (CHCHCN), 142.1 (C₉, C_{9'}), 141.3 (C₄, C_{4'}), 128.4 (C₇, C_{7'}), 125.8 (CHCHCHCN), 125.0 (C₆, C_{6'}), 122.0 (C₅, C_{5'}), 110.6 (C₈, C_{8'}), 103.1 (CHCN), 102.8 (CHCN), 49.2 (CH₂SO₃), 46.5 (CH₂CH₂CH₂SO₃), 41.9 (CH₂CH₂CH₂NH₂), 36.5 (CH₂NH), 26.7 (CyCH₃), 26.4 (CH₃), 26.5 (CH₂CH₂NH₂), 22.7 (CH₂CH₂SO₃); **HRMS:** m/z (ESI⁺) calc. for C₃₃H₄₁N₃O₄S [M+H]⁺: 576.2891; Obs.: 576,2905; ν_{\max} : (FT-ATR)/cm⁻¹: 3288, 3054, 2921, 2850, 1657, 1492, 1452, 1377, 1337, 1217, 1137, 1099, 1016, 926, 796, 708, 593.



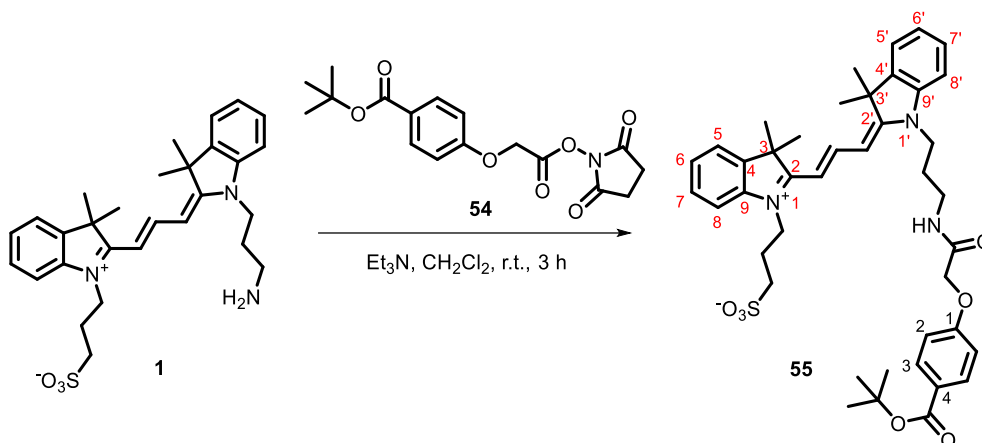
A mixture of *tert*-butyl 4-hydroxybenzoate (1.00 g, 5.15 mmol), bromoacetic acid (1.08 g, 7.73 mmol) and potassium carbonate (1.92 g, 13.9 mmol) in dimethylformamide (10 mL) was stirred for 16 h at 80 °C. The mixture was then cooled to r.t. and diluted with water (100 mL). The aqueous was extracted with ethyl acetate (3 × 70 mL) and the combined organic layers washed with brine (2 × 70 mL), dried with MgSO₄, filtered and concentrated under reduced pressure. The residue was purified via flash column chromatography on silica gel eluting with EtOAc:Petrol (15:85). Fractions containing the product were concentrated under reduced pressure to provide a white foam (77 mg, 0.31 mmol, 6%).

R_f: 0.22 (15:85, EtOAc:petrol, UV active); **¹H NMR** (400 MHz, CD₃OD) δ = 7.82 (d, *J* = 8.4 Hz, 2H, PhH₃), 6.80 (d, *J* = 8.4 Hz, 2H, PhH₂), 4.45 (s, 2H, CH₂), 1.52 (s, 9H, ^tBu); **¹³C NMR** (101 MHz, CD₃OD) δ = 166.1 (C=O_{OH}) 165.5 (C=O_{OC}), 160.8 (PhC₄), 131.7 (PhC₃), 131.5 (PhC₃), 125.5 (PhC₁), 115.2 (PhC₂), 114.2 (PhC₂), 81.0 (CCH₃), 65.1 (CH₂), 28.3 (^tBu); **HRMS**: *m/z* (ESI⁺) calc. for C₁₃H₁₆O₅ [M+H]⁺: 253.1080; Obs.: 253.1080; **v_{max}**: (FT-ATR)/cm⁻¹: 3296, 2979, 2932, 1674, 1605, 1589, 1514, 1442, 1317, 1280, 1226, 1154, 1102, 849, 774, 700, 618, 520, 499; **m.p.**: 185-204 °C.



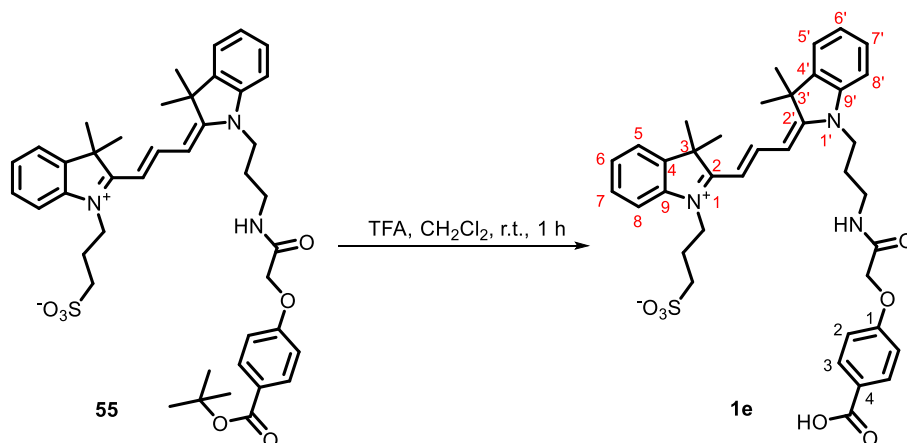
A mixture of **54** (77 mg, 0.31 mmol), *N*-hydroxysuccinimide (53 mg, 0.46 mmol) and *N*-(3-dimethylaminopropyl)-*N'*-ethylcarbodiimide hydrochloride (88 mg, 0.46 mmol) in dichloromethane (3 mL) was stirred at r.t. for 3 h. Dichloromethane (20 mL) was then added and the organics were washed with water (2 × 30 mL) and brine (30 mL), dried with MgSO₄, filtered, and concentrated under reduced pressure to give a colourless oil (61 mg, 0.18 mmol, 56%).

R_f: 0.31 (1:9, EtOAc:petrol, UV active); **¹H NMR** (400 MHz, CD₃OD) δ = 7.95-7.91 (m, 2H, PhH₃), 6.94-6.90 (m, 2H, PhH₂), 4.99 (s, 2H, CH₂O), 2.82 (s, 4H, OSu), 1.54 (s, 9H, ^tBu); **¹³C NMR** (101 MHz, CD₃OD) δ = 169.3 (CON), 168.8 (CON), 165.3 (C=O^tBu), 164.3 (C=O_{ON}), 160.4, (PhC₄), 131.6 (PhC₃), 131.4 (PhC₃), 126.3 (PhC₁), 114.2, (PhC₂), 114.2 (PhC₂), 80.8 (CCH₃), 65.2 (CH₂O), 28.3 (^tBu), 25.6 (OSu), 25.5 (OSu); **HRMS**: *m/z* (ESI⁺) calc. for C₁₇H₁₉NO₇ [M+Na]⁺: 372.1054; Obs.: 372.1054.



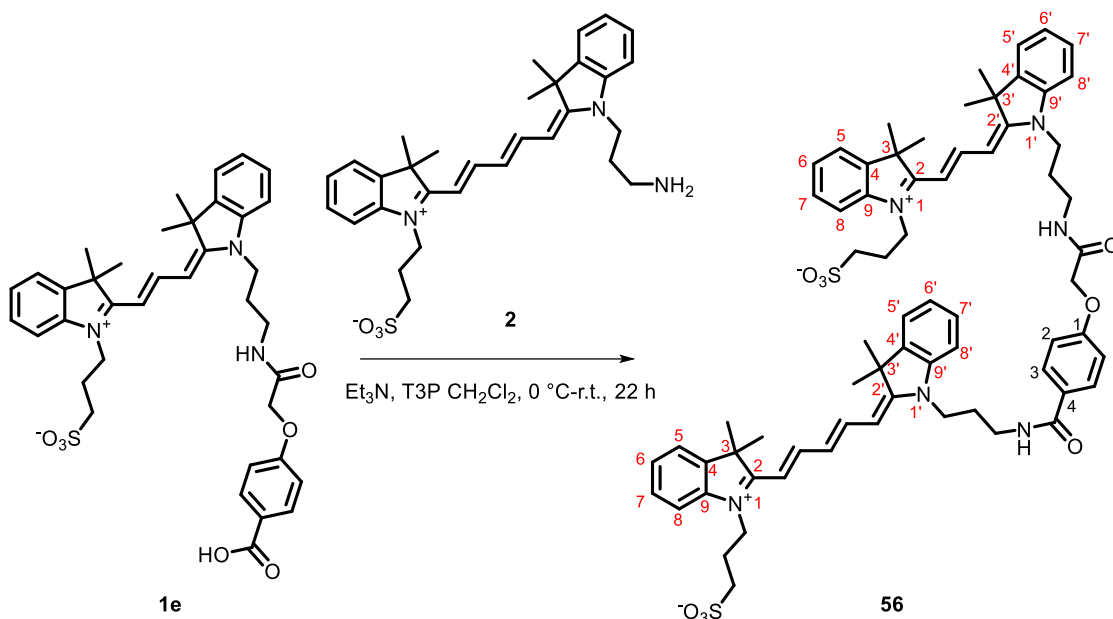
A mixture of **1** (67 mg, 0.13 mmol), **55** (60 mg, 0.17 mmol) and triethylamine (91 μ L, 0.66 mmol) in dichloromethane (3 mL) was stirred for 3 h. The reaction mixture was then concentrated under reduced pressure, and the residue purified via flash column chromatography on silica gel eluting with MeOH:CH₂Cl₂ (5:95). Fractions containing the product were concentrated under reduced pressure to provide a pink oil (29 mg, 39 μ mol, 30%).

R_f: 0.36 (5:95, MeOH:CH₂Cl₂, visible light active); **¹H NMR** (400 MHz, CD₃OD) δ = 8.51 (dd, $J_1 = J_2 = 13.5$ Hz, 1H, CHCHCN), 7.92-7.84 (m, 2H, PhH₃), 7.53-7.49 (m, 2H, H₅, H_{5'}), 7.46-7.34 (m, 3H, H₇, H_{7'}, H₈/H_{8'}), 7.34-7.19 (m, 3H, H₆, H_{6'}, H₈/H_{8'}), 7.09-7.00 (m, 2H, PhH₂), 6.60 (dd, $J = 13.5, 3.6$ Hz, 1H, CHCN), 6.44 (dd, $J = 13.5, 3.6$ Hz, 1H, CHCN), 4.61 (s, 2H, CH₂O), 4.30 (t, $J = 7.2$ Hz, 2H, CH₂CH₂CH₂SO₃), 4.14 (t, $J = 7.4$ Hz, 2H, CH₂CH₂CH₂NH), 3.45 (t, $J = 7.0$ Hz, 2H, CH₂NH), 2.96 (t, $J = 7.2$ Hz, 2H, CH₂SO₃), 2.21 (tt, $J_1 = J_2 = 7.2$ Hz, 2H, CH₂CH₂SO₃), 2.06 (tt, $J_1 = J_2 = 7.4$ Hz, 2H, CH₂CH₂NH), 1.74 (s, 12H, CyCH₃), 1.52 (s, 9H, ^tBu); **¹³C NMR** (101 MHz, CD₃OD) δ = 176.3 (CONH), 176.1 (CHCHCN), 171.0 (C₂, C_{2'}), 165.4 (COO^tBu), 162.2 (PhC₄), 152.4 (C₃, C_{3'}), 143.4 (C₉, C_{9'}), 142.6 (C₄, C_{4'}), 132.6 (PhC₃), 130.2 (C₇/C_{7'}), 130.1 (C₇/C_{7'}), 127.1 (C₆/C_{6'}), 126.9 (C₆/C_{6'}), 125.5 (PhC₁), 123.8 (C₅/C_{5'}), 123.6 (C₅/C_{5'}), 115.4 (PhC₂), 112.6 (C₈/C_{8'}), 112.4 (C₈/C_{8'}), 104.5 (CHCN), 104.2 (CHCN), 81.0 (CCH₃), 68.4 (CH₂CO), 50.8 (CH₂SO₃), 44.1 (CH₂CH₂CH₂SO₃), 43.1 (CH₂CH₂CH₂NH), 37.7 (CH₂NH), 28.5 (CyCH₃), 28.3 (^tBu), 28.3 (CH₂CH₂NH₂), 24.3 (CH₂CH₂SO₃); **HRMS**: m/z (ESI⁺) calc. for C₄₂H₅₀N₃O₇S [M+H]⁺: 742.3530; Obs.: 742.3530; **ν_{\max}** : (FT-ATR)/cm⁻¹: 3410, 2979, 2934, 1752, 1686, 1589, 1450, 1339, 1211, 1145, 1076, 964, 850, 734, 674.



Trifluoroacetic acid (1 mL) was added dropwise to a stirred solution of **56** (15 mg, 20 μ mol) in dichloromethane (4 mL) and the mixture stirred at r.t. for 1 h. The reaction was then added dropwise to diethyl ether (200 mL). The precipitate was collected by filtration, washed with diethyl ether (30 mL), and dried in air. The solid was redissolved in methanol (10 mL) and concentrated under reduced pressure to afford a pink oil (10 mg, 15 μ mol, 73%).

R_f: 0.23 (1:9, MeOH:CH₂Cl₂, visible light active); **¹H NMR** (400 MHz, CD₃OD) δ = 8.51 (dd, J = 13.5, 4.3 Hz, 1H, CHCHCN), 7.95 (d, J = 8.4 Hz, 2H, PhH₃), 7.54-7.48 (m, 2H, H₅, H_{5'}), 7.45-7.34 (m, 3H, H₇, H_{7'}, H₈/H_{8'}), 7.30-7.22 (m, 3H, H₆, H_{6'}, H₈/H_{8'}), 7.06 (d, J = 8.4 Hz, 2H, PhH₂), 6.58 (dd, J = 13.5, 4.3 Hz 1H, CHCN), 6.41 (dd, J = 13.5, 4.3 Hz, 1H, CHCN), 4.62 (s, 2H, CH₂O), 4.37-4.26 (m, 2H, CH₂CH₂CH₂SO₃), 4.15-4.11 (m, 2H, CH₂CH₂CH₂NH), 3.52-3.39 (m, 2H, CH₂NH), 3.01-2.94 (m, 2H, CH₂SO₃), 2.25-2.31 (m, 2H, CH₂CH₂SO₃), 2.09-2.03 (m, 2H, CH₂CH₂NH), 1.73 (s, 12H, CyCH₃); **¹³C NMR** (101 MHz, CD₃OD) δ = 176.4 (CONH), 176.1 (CHCHCN), 171.1 (C₂, C_{2'}), 169.5 (COOH), 163.1 (PhC₄), 152.4 (C₃, C_{3'}), 143.4 (C₉/C_{9'}), 143.3 (C₉/C_{9'}), 142.4 (C₄, C_{4'}), 133.1 (PhC₃), 130.2 (C₇/C_{7'}), 130.1 (C₇/C_{7'}), 127.0 (C₆/C_{6'}), 126.9 (C₆/C_{6'}), 125.4 (PhC₁), 123.7 (C₅/C_{5'}), 123.6 (C₅/C_{5'}), 115.8 (PhC₂), 112.7 (C₈/C_{8'}), 112.4 (C₈/C_{8'}), 104.5 (CHCN), 104.2 (CHCN), 68.4 (CH₂CO), 50.8 (CH₂SO₃), 44.1 (CH₂CH₂CH₂SO₃), 43.1 (CH₂CH₂CH₂NH), 37.7 (CH₂NH), 28.5 (CyCH₃), 28.3 (CH₂CH₂NH₂), 24.3 (CH₂CH₂SO₃); **HRMS**: m/z (ESI⁺) calc. for C₃₈H₄₂N₃O₇S [M+H]⁺: 686.2917; Obs.: 686.2917; **ν_{\max}** ; (FT-ATR)/cm⁻¹: 2979, 2929, 1709, 1558, 1457, 1430, 1275, 1153, 1114, 928, 750.

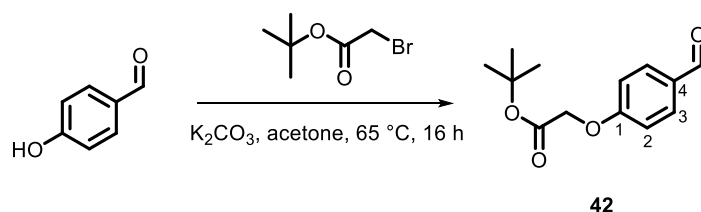


To a solution of **57** (10 mg, 15 μmol), **2** (12 mg, 22 μmol), and triethylamine (10 μL , 73 μmol) in dichloromethane (5 mL), was added propylphosphonic anhydride solution (50% w/w in EtOAc, 13 μL , 37 μmol) at 0 $^{\circ}\text{C}$ and the mixture stirred at r.t. for 16 h. The reaction was then concentrated under reduced pressure. The residue was purified via flash column chromatography on silica gel eluting with MeOH:CH₂Cl₂ (5:95). Fractions containing the product were concentrated under reduced pressure to provide a purple oil (12 mg, 10 μmol , 10, 66%).

R_f: 0.32 (5:95, MeOH:CH₂Cl₂, visible light active); **¹H NMR** (400 MHz, CD₃OD) δ = 8.50 (dd, $J_1 = J_2 = 13.5$ Hz, 1H, Cy3-CH₂CHCN), 8.22-8.16 (m, 2H, CH₂CHCN), 7.89-7.84 (m, 2H, PhH₃), 7.52-7.48 (m, 2H, H₇, H_{7'}), 7.48-7.44 (m, 2H, H₇, H_{7'}), 7.42-7.35 (m, 6H, H₅, H_{5'}, H₅, H_{5'}, H₈, H_{8'}), 7.30-7.21 (m, 6H, H₈, H_{8'}, 2 \times H₆, 2 \times H_{6'}), 7.19-7.15 (m, 2H, PhH₂), 6.57 (d, $J = 13.5$ Hz, 1H, Cy3-CH₂CN), 6.46 (d, $J = 13.5$ Hz, 1H, Cy3-CH₂CN), 6.40 (t, $J = 12.5$ Hz, 1H, CH₂CH₂CHCN), 6.31 (d, $J = 13.5$ Hz, 1H, Cy5-CH₂CN), 6.18 (d, $J = 13.5$ Hz, 1H, Cy5-CH₂CN), 4.65 (s, 2H, CH₂O), 4.36-4.26 (m, 4H, CH₂CH₂CH₂SO₃), 4.21-4.11 (m, 4H, CH₂CH₂CH₂NH), 3.44-3.50 (m, 4H, CH₂NH), 3.01-2.95 (m, 4H, CH₂SO₃), 2.19-2.11 (m, 4H, CH₂CH₂SO₃), 2.16-2.04 (m, 4H, CH₂CH₂NH), 1.80-1.56 (m, 24H, CyCH₃); **¹³C NMR** (101 MHz, CD₃OD) δ = 176.3 (Cy3-C₂/C_{2'}), 176.1 (Cy3-C₂/C_{2'}), 174.9 (Cy3-CH₂CHCN), 174.6 (Cy3-C₃/C_{3'}), 174.4 (Cy3-C₃/C_{3'}), 171.1 (Cy5-C₂, C_{2'}), 169.8 (Cy3-CON), 162.1, 155.8, 152.4, 143.6 (C₉, C_{9'}), 143.3 (C₉/C_{9'}), 142.8 (C₉/C_{9'}), 142.7 (C₄/C_{4'}), 142.4 (C₄/C_{4'}), 130.6 (PhC₂), 130.2 (PhC₁), 130.0 (PhthC₃), 129.9 (C₇/C_{7'}), 128.8 (C₇/C_{7'}), 126.9 (C₇/C_{7'}), 126.9 (C₇/C_{7'}), 126.4 (C₆, C_{6'}), 126.4 (CH₂CH₂CHCN), 124.2 (C₆/C_{6'}), 123.7 (C₆/C_{6'}), 123.6 (PhthC₃), 123.6 (C₅, C_{5'}), 116.1 (C₅, C_{5'}), 112.7 (C₈/C_{8'}), 112.5 (C₈/C_{8'}), 112.3 (C₈/C_{8'}), 112.1 (C₈/C_{8'}), 104.4 (CH₂CN), 104.2 (CH₂CN), 71.6 (CH₂O), 50.1 (CH₂SO₃⁻), 48.1 (CH₂SO₃⁻), 44.1 (CH₂CH₂CH₂SO₃⁻), 43.1

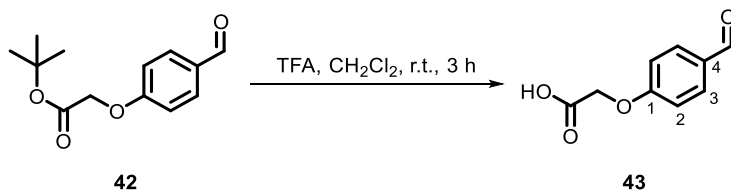
($\text{CH}_2\text{CH}_2\text{CH}_2\text{SO}_3^-$), 42.8 ($\text{CH}_2\text{CH}_2\text{CH}_2\text{NCO}$), 38.3 ($\text{CH}_2\text{CH}_2\text{CH}_2\text{NCO}$), 37.7 (CH_2NCO), 28.5 (CyCH_3), 28.4 (CyCH_3), 28.2 ($\text{CH}_2\text{CH}_2\text{NCO}$), 28.1 ($\text{CH}_2\text{CH}_2\text{NCO}$), 24.8 ($\text{CH}_2\text{CH}_2\text{SO}_3^-$), 24.4 ($\text{CH}_2\text{CH}_2\text{SO}_3^-$); **HRMS**: m/z (ESI⁺) calc. for $\text{C}_{69}\text{H}_{80}\text{N}_6\text{O}_9\text{S}_2$ [M+Na]⁺: 1223.5320; Obs.: 1223.5322; ν_{max} : (FT-ATR)/ cm^{-1} : 3358, 2922, 2852, 1659, 1633, 1556, 1487, 1429, 1454, 1377, 1140, 1035, 925, 797, 750, 708, 552.

4.6. Synthesis of Cy3 Negative Controls



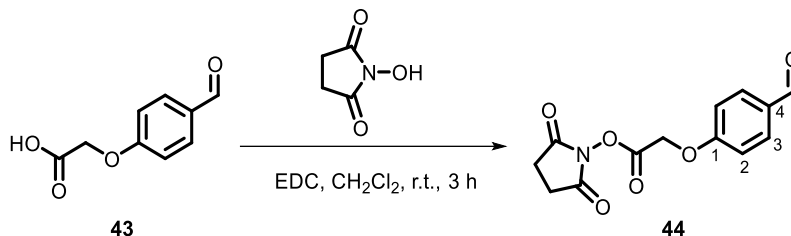
A mixture of *tert*-butyl bromoacetate (1.20 mL, 8.20 mmol), 4-hydroxybenzaldehyde (1.00 g, 8.20 mmol), and potassium carbonate (1.92 g, 14.0 mmol) in acetone (15 mL) was stirred at 65 °C for 16 h. The mixture was then cooled to r.t. and diluted with water (100 mL). The aqueous layer was extracted with ethyl acetate (3 × 70 mL), and the combined organics washed with brine (2 × 70 mL), dried with MgSO_4 , filtered, and concentrated under reduced pressure. The residue was purified via flash column chromatography on silica gel, eluting with EtOAc:petrol (15:85). Fractions containing the product were concentrated under reduced pressure to provide a colourless oil (1.43 g, 6.06 mmol, 74%). Data were consistent with those previously reported.⁵¹

R_f: 0.26 (15:85, EtOAc:petrol, UV active); **¹H NMR** (400 MHz, CDCl_3) δ = 9.91 (s, 1H, CHO), 7.86 (d, J = 8.0 Hz, 2H, PhH_3), 7.04 (d, J = 8.0 Hz, 2H, PhH_2), 4.77 (s, 2H, CH_2), 0.06 (s, 9H, tBu); **HRMS**: m/z (ESI⁺) calc. for $\text{C}_{13}\text{H}_{16}\text{O}_4$ [M+H]⁺: 237.1121; Obs.: 237.1119; ν_{max} : (FT-ATR)/ cm^{-1} : 2980, 1748, 1691, 1598, 1509, 1368, 1308, 1216, 1148, 1071, 944, 831, 746, 608, 513; **m.p.**: 191-194 °C.



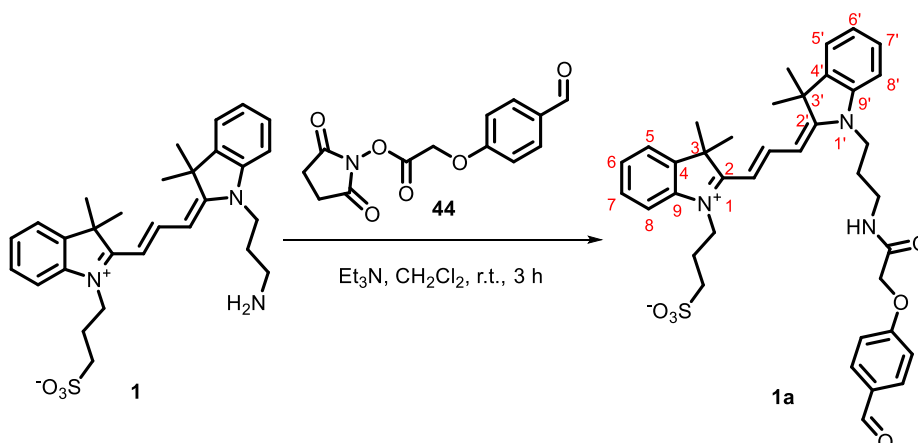
Trifluoroacetic acid (10 mL) was added dropwise to a stirred solution of **58** (1.43 g, 6.06 mmol) in dichloromethane (10 mL) and the mixture was stirred at r.t. for 1 h. The reaction mixture was then concentrated under reduced pressure and the residue was azeotroped with dichloromethane (3 × 10 mL) to afford a yellow powder (1.08 g, 6.00 mmol, 99%). Data were consistent with those previously reported.⁵²

R_f: 0.28 (2:8, EtOAc:petrol, UV active); **¹H NMR** (400 MHz, DMSO-*d*₆) δ = 13.13 (s, 1H, OH), 9.83 (s, 1H, CHO), 7.82 (d, *J* = 7.9 Hz, 2H, PhH₃), 7.06 (d, *J* = 7.9 Hz, PhH₂), 4.79 (s, 2H, CH₂); **HRMS**: *m/z* (ESI⁺) calc. for C₉H₈O₄ [M-H]⁻: 179.0350; Obs.: 179.0351; **v_{max}**: (FT-ATR)/cm⁻¹: 3660, 2982, 1598, 1385, 1259, 1166, 1074, 954, 750; **m.p.**: 191-194 °C;



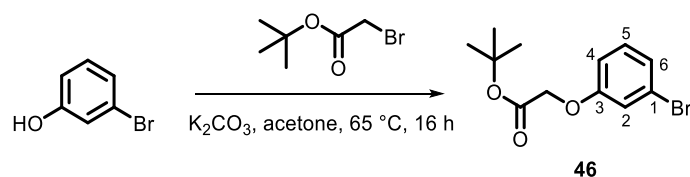
A reaction mixture of **59** (100 mg, 0.56 mmol), *N*-hydroxysuccinimide (96 mg, 0.83 mmol), and *N*-(3-dimethylaminopropyl)-*N*-ethylcarbodiimide hydrochloride (150 mg, 0.83 mmol) in dichloromethane (2 mL) was stirred at r.t. for 2 h. Dichloromethane (20 mL) was then added and the organic layer was washed with water (2 × 30 mL) and brine (30 mL), dried with MgSO₄, filtered, and concentrated under reduced pressure to give a pink foam which was used in the subsequent step without further analysis or purification (72 mg, 0.26 mmol, 46%).

R_f: 0.29 (1:9, EtOAc:petrol, UV active); **¹H NMR** (400 MHz, CD₃OD for aldehyde) δ = 9.90 (s, 1H, CHO), 7.87 (d, *J* = 8.0 Hz, 2H, PhH₃), 7.05 (d, *J* = 8.0 Hz, 2H, PhH₂), 6.08 (s, CH₂O), 2.87 (s, 4H, OSu); **HRMS**: *m/z* (ESI⁺) calc. C₁₃H₁₁NO₆ [M+H]⁺: 278.0652; Obs.: 278.0652; **v_{max}**: (FT-ATR)/cm⁻¹: 2978, 1824, 1785, 1737, 1600, 1508, 1427, 1207, 1165, 1074, 834, 646; **m.p.**: 142-146 °C.



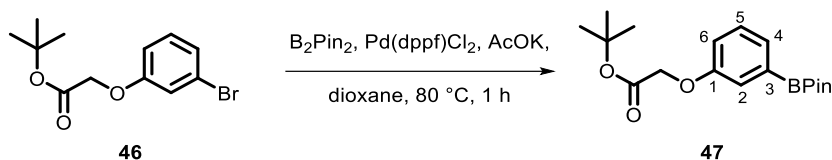
A reaction mixture of **1** (40 mg, 79 μmol), **60** (22 mg, 79 μmol), and triethylamine (42 μL, 0.395 μmol) in dichloromethane (2 mL) was stirred at r.t. for 3 h. The reaction mixture was then concentrated under reduced pressure. The residue was purified via flash column chromatography on silica gel, eluting with MeOH:CH₂Cl₂ (5:95). Fractions containing the product were concentrated under reduced pressure to provide a pink oil (18 mg, 27 μmol, 45%).

R_f: 0.17 (5:95, MeOH:CH₂Cl₂, visible light active); **¹H NMR** (400 MHz, CD₃OD; in this solvent, a mix of aldehyde and methanol hemi-acetal were formed. Data is provided for the aldehyde form) δ = 9.82 (s, 1H, CHO), 8.53 (dd, *J*₁ = *J*₂ = 13.4 Hz, 1H, CHCHCN), 7.86 (d, *J* = 8.5 Hz, 2H, PhH₃), 7.54-7.50 (m, 2H, H₅, H_{5'}), 7.45-7.33 (m, 3H, H₇, H_{7'}, H₈/H_{8'}), 7.31-7.25 (m, 3H, H₈/H_{8'}, H₆, H_{6'}), 7.17 (d, *J* = 8.5 Hz 2H, PhH₂), 6.60 (d, *J* = 13.4 Hz, 1H, CHCN), 6.44 (d, *J* = 13.4 Hz, 1H, CHCN), 4.55 (s, 2H, CH₂O), 4.32 (t, *J* = 7.1 Hz, 2H, CH₂CH₂CH₂SO₃), 4.16 (t, *J* = 7.3 Hz, 2H, CH₂CH₂CH₂NH), 3.45 (t, *J* = 7.3 Hz, 2H, CH₂NH), 2.96 (t, *J* = 7.1 Hz, 2H, CH₂SO₃), 2.27-2.21 (m, 2H, CH₂CH₂SO₃), 2.11-2.07 (m, 2H, CH₂CH₂NH), 1.76 (s, 12H, CyCH₃); **¹³C NMR** (101 MHz, CD₃OD) δ = 192.8 (CHO), 176.3 (CONH), 176.0 (PhC₁), 175.9 (CHCHCN), 171.4 (C₂, C_{2'}), 159.3 (PhC₄), 152.3 (C₃, C_{3'}), 143.2 (C₉, C_{9'}), 142.2 (C₄, C_{4'}), 133.1 (PhC₃), 130.1 (PhC₃), 129.3 (C₇, C_{7'}), 126.8 (C₆, C_{6'}), 123.5 (C₅, C_{5'}), 116.4 (PhC₂), 115.5 (PhC₂), 112.6 (C₈/C_{8'}), 112.3 (C₈/C_{8'}), 104.3 (CHCN), 104.1 (CHCN), 68.3 (CH₂CO), 48.0 (CH₂SO₃), 44.0 (CH₂CH₂CH₂SO₃), 42.9 (CH₂CH₂CH₂NH), 37.5 (CH₂NH), 28.1 (CH₂CH₂NH₂), 26.3 (CyCH₃), 24.2 (CH₂CH₂SO₃); **HRMS**: *m/z* (ESI⁺) calc. for C₃₈H₄₃N₃O₆S [M+H]⁺ requires 670.2945, found 670.2928; **v_{max}**: (FT-ATR)/cm⁻¹: 3378, 2925, 2854, 1713, 1600, 1557, 1457, 1430, 1373, 1218, 1153, 1115, 1037, 928, 795.



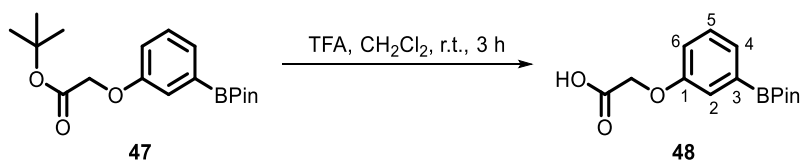
A mixture of 3-bromophenol (2.00 g, 11.6 mmol), *tert*-butyl bromoacetate (1.71 mL, 11.6 mmol), and potassium carbonate (2.71 g, 19.7 mmol) in acetone (20 mL) was stirred at 65 °C for 16 h. After cooling to r.t., water (100 mL) was added, and the aqueous was extracted with ethyl acetate (3 × 70 mL). The combined organics were washed with brine (2 × 70 mL), dried with MgSO₄, filtered and concentrated under reduced pressure. The residue was purified via flash column chromatography on silica gel eluting with EtOAc:petrol (1:9). Fractions containing the product were concentrated under reduced pressure to provide a red oil. (3.32 g, 11.5 mmol, 99%).

R_f: 0.23 (1:9, EtOAc:petrol, UV active); **¹H NMR** (400 MHz, CDCl₃) δ = 7.14-7.10 (m, 1H, PhH₅), 7.11-7.08 (m, 1H, PhH₄), 7.03 (d, *J* = 2.1 Hz, 1H, PhH₂), 6.81 (dd, *J* = 7.8, 2.1, 1H, PhH₆), 4.48 (s, 2H, CH₂O), 1.47 (s, 9H, ^tBu); **¹³C NMR** (101 MHz, CDCl₃) δ = 167.6 (C=O), 158.7 (PhC₁), 130.7 (PhC₅), 124.8 (PhC₄), 122.9 (PhC₃), 118.1 (PhC₂), 113.7 (PhC₆), 82.8 (CMe₃), 65.8 (CH₂O), 28.1 ^tBu); **HRMS**: *m/z* (ESI⁺) calc. for C₁₂H₁₅⁷⁹BrO₃ [M+Na]⁺: 309.0097; Obs.: 309.0096; **v_{max}**: (FT-ATR)/cm⁻¹: 2979, 2933, 1750, 1575, 1474, 1368, 1304, 1215, 1150, 1078, 834, 767.



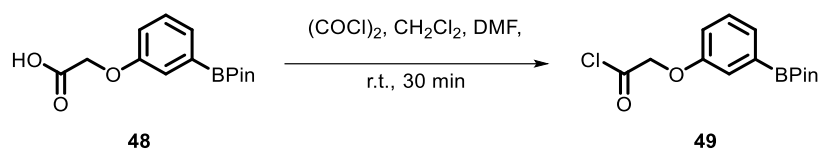
62 (1.77 g, 6.17 mmol), bis(pinacolato)diboron (2.35 g, 9.25 mmol), 1,1'-bis(diphenylphosphino)ferrocene]dichloropalladium (II) (452 mg, 0.617 mmol) and potassium acetate (3.26 g, 33.3 mmol) were placed under a nitrogen atmosphere, and anhydrous dioxane (5 mL) was added. Nitrogen was bubbled through the reaction mixture for 10 min, which was then stirred at 80 °C for 1 h. After cooling to r.t., water (70 mL) was added, and the aqueous was extracted with ethyl acetate (3 × 50 mL). The combined organics were washed with brine (2 × 50 mL), dried with MgSO₄, filtered, and concentrated under reduced pressure. The residue was purified via flash column chromatography on silica gel eluting with EtOAc:petrol (15:85). Fractions containing the product were concentrated under reduced pressure to provide a white solid (1.76 g, 5.27 mmol, 88%).

R_f: 0.22 (15:85, EtOAc:petrol, UV active); **¹H NMR** (400 MHz, CDCl₃) δ = 7.41 (dd, *J*₁ = *J*₂ = 8.2 Hz, 1H, PhH₅), 7.29 (d, *J* = 8.2 Hz, 1H, PhH₄), 7.27 (d, *J* = 2.8 Hz, 1H, PhH₂), 7.03 (dd, *J* = 8.2, 2.8 Hz, 1H, PhH₆), 4.53 (s, 2H, CH₂O), 1.47 (s, 9H, ^tBu), 1.31 (s, 12H, C(CH₃)₂); **¹³C NMR** (101 MHz, CDCl₃) δ = 168.2 (C=O), 157.4 (PhC₁), 129.1 (PhC₄), 128.1 (PhC₅), 120.0 (PhC₃), 119.4 (PhC₂), 118.9 (PhC₆), 83.9 (C(CH₃)₂), 82.3 (CMe₃), 65.8 (CH₂O), 28.1 (^tBu), 24.9 (C(CH₃)₂); **HRMS**: *m/z* (ESI⁺) calc. for C₁₈H₂₇BO₅ [M+Na]⁺: 357.1855; Obs.: 357.1844; **ν_{max}**: (FT-ATR)/cm⁻¹: 2979, 2993, 1754, 1576, 1428, 1355, 1317, 1213, 1147, 1085, 065, 852, 775, 705, 673, 599; **m.p.**: 65-69 °C.

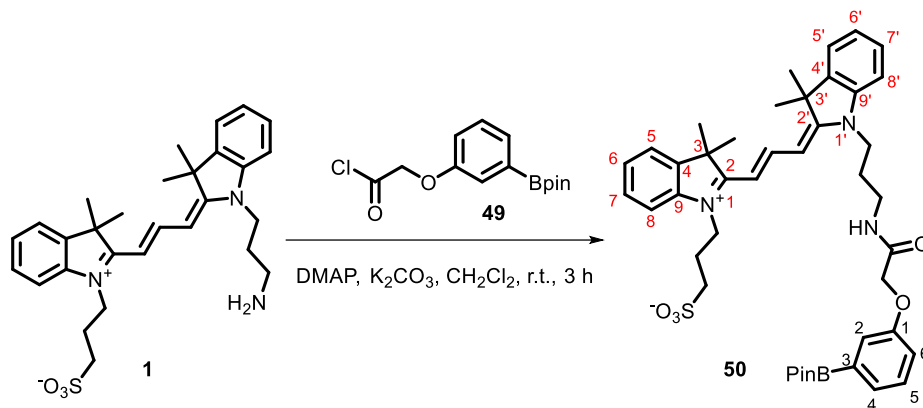


Trifluoroacetic acid (5 mL) was added dropwise to a solution of **63** (500 mg, 1.50 mmol) in dichloromethane (15 mL) and the mixture was stirred at r.t. for 3 h. The reaction mixture was then concentrated under reduced pressure and azeotroped with dichloromethane (3 × 20 mL) to afford a white powder. (344 mg, 1.24 mmol, 83%).

R_f: 0.22 (1:9, EtOAc:petrol, UV active); **¹H NMR** (600 MHz, DMSO-*d*₆) δ = 7.32 (dd, *J* = 8.1, 7.2 Hz, 1H, PhH₅), 7.27 (ddd, *J* = 7.2, 2.8, 1.2 Hz, 1H, PhH₄), 7.11 (dd, *J* = 2.8, 1.2 Hz, 1H, PhH₂), 7.05 (ddd, *J* = 8.1, 2.8, 1.2 Hz, 1H, PhH₆), 4.69 (s, 2H, CH₂O), 1.30 (s, 12H, C(CH₃)₂); **¹³C NMR** (101 MHz, DMSO-*d*₆) δ = 170.7 (C=O), 157.8 (PhC₁), 129.7 (PhC₅), 127.7 (PhC₄), 120.0 (PhC₃), 119.6 (PhC₂), 118.6 (PhC₆), 84.2 (C(CH₃)₂), 64.8 (CH₂O), 25.1 (C(CH₃)₂); **HRMS**: *m/z* (ESI) calc. for C₁₄H₁₈BO₅ [M-H]⁻: 277.1263; Obs.: 277.1263; **ν_{max}**: (FT-ATR)/cm⁻¹: 3059, 2979, 2932, 1737, 1575, 1428, 1356, 1143, 1064, 964, 705; **m.p.**: 155-158 °C.



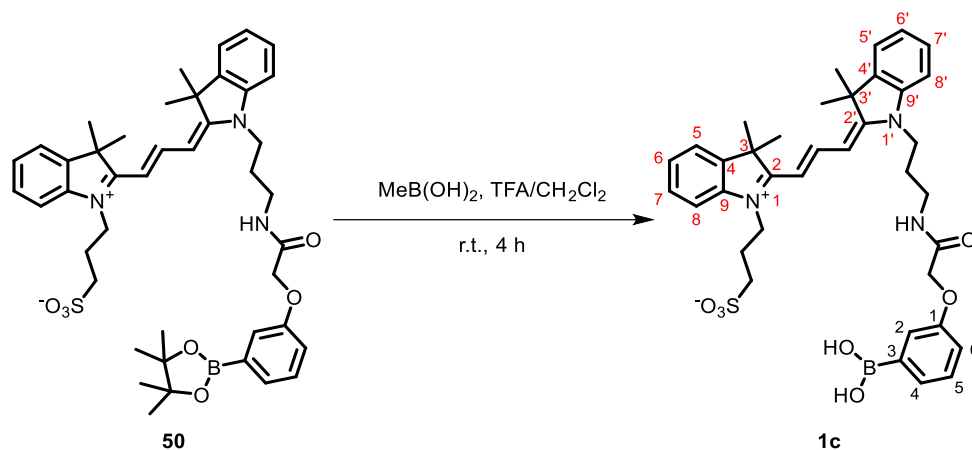
Oxalyl chloride (46 μL , 0.540 mmol) was added to a solution of **64** (50 mg, 0.180 mmol), and dimethylformamide (1 drop) in dichloromethane (3 mL), and the mixture was stirred at r.t. for 30 min. Excess oxalyl chloride and dichloromethane were removed under reduced pressure to give the crude product as an orange oil, which was carried forward without further purification.



4-Dimethylaminopyridine (75 mg, 0.62 mmol) was added to a mixture of **1** (77 mg, 0.15 mmol), **65** (77 mg, 0.24 mmol), and potassium carbonate (62 mg, 0.44 mmol) in anhydrous dichloromethane (5 mL) and the reaction stirred at r.t. for 3 h. The reaction mixture was then added dropwise to diethyl ether (400 mL), and the resultant precipitate was collected by filtration, washed with diethyl ether (30 mL), and dried in air to give a pink powder. The precipitate was then purified via flash column chromatography on silica gel eluting with MeOH:CH₂Cl₂ (5:95). Fractions containing the product were concentrated under reduced pressure to provide a pink oil. The residue was then redissolved in dichloromethane (30 mL), and the organics were washed with hydrochloric acid (0.1 M, 2 × 10 mL) to remove coordinating 4-dimethylaminopyridine, dried with MgSO₄, filtered, and concentrated under reduced pressure, to give a pink oil (5 mg, 6 μmol , 4%).

R_f: 0.34 (5:95, MeOH:CH₂Cl₂, visible light active); **¹H NMR** (400 MHz, CD₃OD) δ = 8.54 (d, $J_1 = J_2 = 13.5$ Hz, 1H, CHCHCN), 7.57-7.53 (m, 2H, H5, H5'), 7.49-7.37 (m, 4H, H7, H7', H8, H8'), 7.34-7.31 (m, 2H, H6, H6'), 7.31-7.25 (m, 2H, PhH5, PhH4), 7.25-7.21 (m, 1H, PhH6), 7.11-7.07 (m, 1H, PhH2), 6.57 (d, $J = 13.5$ Hz, 1H, CHCN), 6.46 (d, $J = 13.5$ Hz, 1H, CHCN), 4.56 (s, 2H, CH₂O), 4.33-4.26 (m, 2H, CH₂CH₂CH₂SO₃), 4.18 (t, $J = 7.5$ Hz, 2H, CH₂CH₂CH₂NH), 3.47 (t, $J = 7.5$ Hz, 2H, CH₂NH), 3.00 (t, $J = 7.8$ Hz, 2H, CH₂SO₃), 2.25 (tt, $J_1 = J_2 = 7.8$ Hz, 2H, CH₂CH₂SO₃), 2.11 (tt, $J_1 = J_2 = 7.5$ Hz, 2H, CH₂CH₂NH), 1.79 (s, 12H, CyCH₃); **¹³C NMR** (151 MHz, CD₃OD) δ = 176.3 (CONH), 174.7 (CHCHCN), 170.2 (C2, C2'), 157.2 (PhC1), 150.8 (C3, C3'), 141.8 (C9, C9'), 140.8 (C4, C4'), 129.8 (PhC5), 128.7 (C7,

$\underline{C}7'$), 127.1 (Ph $\underline{C}4$), 126.5 (Ph $\underline{C}3$), 125.4 ($\underline{C}6$, $\underline{C}6'$), 122.1 ($\underline{C}5$, $\underline{C}5'$), 119.1 (Ph $\underline{C}2$), 116.0 (Ph $\underline{C}6$), 111.2 ($\underline{C}8/\underline{C}8'$), 110.9 ($\underline{C}8/\underline{C}8'$), 102.7 ($\underline{C}HCN$), 102.6 ($\underline{C}HCN$), 66.9 ($\underline{C}H_2CO$), 46.8 ($\underline{C}H_2SO_3$), 42.5 ($\underline{C}H_2CH_2CH_2SO_3$), 41.4 ($\underline{C}H_2CH_2CH_2NH$), 36.0 ($\underline{C}H_2NH$), 26.9 (Cy $\underline{C}H_3$), 26.6 ($\underline{C}H_2CH_2NH_2$), 22.8 ($\underline{C}H_2CH_2SO_3$); **HRMS**: m/z (ESI⁺) calc. for C₄₃H₅₄BN₃O₇S [M+Na]⁺: 790.3668; Obs.: 790.3712; ν_{max} : (FT-ATR)/cm⁻¹: 3378, 2921, 2850, 1558, 1457, 1430, 1372, 1152, 1114, 749.



A solution of **66** (5 mg, 6.5 μ mol) and methylboronic acid (4 mg, 65.3 μ mol) in a mixture of dichloromethane (5 mL) and trifluoroacetic acid (0.5 mL) was stirred at r.t. for 4 h. The reaction mixture was then concentrated under reduced pressure. The residue was azeotroped with hydrochloric acid (0.1 M, 2 \times 10 mL) to give a pink oil (4 mg, 6.5 μ mol, quantitative yield).

R_f: 0.29 (5:95, MeOH:CH₂Cl₂, visible light active); **¹H NMR** (600 MHz, CD₃OD) δ = 8.54 (dd, $J_1 = J_2 = 13.4$ Hz, 1H, $\underline{C}HCHCN$), 7.57-7.53 (m, 2H, $\underline{H}5$, $\underline{H}5'$), 7.49-7.40 (m, 3H, $\underline{H}7$, $\underline{H}7'$, $\underline{H}8/\underline{H}8'$), 7.34 – 7.27 (m, 3H $\underline{H}6$, $\underline{H}6'$, $\underline{H}8/\underline{H}8'$), 6.62-6.52 (m, 1H, $\underline{C}HCN$), 6.48-6.42 (m, 1H, $\underline{C}HCN$), 4.56 (s, 2H, $\underline{C}H_2O$), 4.29 (d, $J = 7.2$ Hz, 2H, $\underline{C}H_2CH_2CH_2SO_3$), 4.18 (t, $J = 7.5$ Hz, 2H, $\underline{C}H_2CH_2CH_2NH$), 3.48 (t, $J = 7.5$ Hz, 2H, $\underline{C}H_2NH$), 2.99 (t, $J = 7.2$ Hz, 2H, $\underline{C}H_2SO_3$), 2.25 (tt, $J_1 = J_2 = 7.2$ Hz, 2H, $\underline{C}H_2CH_2SO_3$), 2.11 (tt, $J_1 = J_2 = 7.5$ Hz, 2H, $\underline{C}H_2CH_2CH_2NH$), 1.78 (s, 12H, Cy $\underline{C}H_3$); **¹³C NMR** (151 MHz, CD₃OD) δ = 174.6 ($\underline{C}ONH$), 174.5 ($\underline{C}HCHCN$), 157.3 ($\underline{C}2$, $\underline{C}2'$), 150.8 ($\underline{C}3$, $\underline{C}3'$), 141.8 ($\underline{C}9$, $\underline{C}9'$), 140.8 ($\underline{C}4$, $\underline{C}4'$), 128.7 (Ph $\underline{C}5$), 128.6 ($\underline{C}7$, $\underline{C}7'$), 125.4 (Ph $\underline{C}4$), 125.3 (Ph $\underline{C}3$), 122.1 ($\underline{C}6$, $\underline{C}6'$), 122.1 ($\underline{C}5$, $\underline{C}5'$), 119.1 (Ph $\underline{C}2$), 116.7 (Ph $\underline{C}6$), 111.2 ($\underline{C}8/\underline{C}8'$), 110.9 ($\underline{C}8/\underline{C}8'$), 102.9 ($\underline{C}HCN$), 102.7 ($\underline{C}HCN$), 66.9 ($\underline{C}H_2CO$), 49.2 ($\underline{C}H_2SO_3$), 42.5 ($\underline{C}H_2CH_2CH_2SO_3$), 41.4 ($\underline{C}H_2CH_2CH_2NH$), 36.0 ($\underline{C}H_2NH$), 27.0 (Cy $\underline{C}H_3$), 26.9 ($\underline{C}H_2CH_2NH_2$), 22.7 ($\underline{C}H_2CH_2SO_3$); **HRMS**: m/z (ESI⁺) calc. for C₃₇H₄₄BN₃O₇S [M+Na]⁺: 708.2882; Obs.: 708.2885; ν_{max} : (FT-ATR)/cm⁻¹: 3321, 2923, 1663, 1559, 1429, 1373, 1229, 1151, 1113, 1039, 756.

5. References

1. L. Wu, C. Huang, B. P. Emery, A. C. Sedgwick, S. D. Bull, X.-P. He, H. Tian, J. Yoon, J. L. Sessler and T. D. James, *Chem. Soc. Rev.*, 2020, **49**, 5110–5139.
2. M. Levitus and S. Ranjit, *Quart. Rev. Biophys.*, 2011, **44**, 123–151.
3. D. Wu, A. C. Sedgwick, T. Gunnlaugsson, E. U. Akkaya, J. Yoon and T. D. James, *Chem. Soc. Rev.*, 2017, **46**, 7105–7125.
4. J. Fan, M. Hu, P. Zhan and X. Peng, *Chem. Soc. Rev.*, 2013, **42**, 29–43.
5. L. Yuan, W. Lin, K. Zheng and S. Zhu, *Chem. Soc. Rev.*, 2013, **42**, 622–661.
6. H. Faustino, M. J. S. A. Silva, L. F. Veiros, G. J. L. Bernardes and P. M. P. Gois, *Chem. Sci.*, 2016, **7**, 5052–5058.
7. A. Bandyopadhyay, S. Cambray and J. Gao, *Chem. Sci.*, 2016, **7**, 4589–4593.
8. T. Förster, *Energiewanderung und Fluoreszenz*, **33**, 166–175.
9. W. R. Algar, *Nature Methods*, 2019, **16**, 15–23.
10. C. E. Rowland, C. W. B. Iii, I. L. Medintz and J. B. Delehanty, *Methods Appl. Fluoresc.*, 2015, **29**, 17–25.
11. N. Hildebrandt and D. Geißler, *J. Biomed. Nanotechnol.*, 2012, **733**, 75–86.
12. Stryer L, Haugland R.P., *Proc. Natl. Acad. Sci.*, 1967, **58**, 719–726
13. Guo, Q. Li, J. Xiang, M. Liu, A. Guan, Y. Tang and H. Sun, *Anal. Chim. Acta.*, 2021, **1165**, 3385–3394.
14. Y. Zhang, J. Bi, S. Xia, W. Mazi, S. Wan, L. Mikesell, R. L. Luck and H. Liu, *Molecules*, 2018, **23**, 2679–2681.
15. E. Herbst and D. Shabat, *Org. Biomol. Chem.*, 2016, **14**, 3715–3728.
16. X. Jia, Q. Chen, Y. Yang, Y. Tang, R. Wang, Y. Xu, W. Zhu and X. Qian, *J. Am. Chem. Soc.*, 2016, **138**, 10778–10781.
17. X. Ma, L. Shi, B. Zhang, L. Liu, Y. Fu and X. Zhang, *Anal. Bioanal. Chem.*, 2022, **414**, 4551–4573.
18. O. Dilek, Z. Lei, K. Mukherjee and S. Bane, *Chem. Comm.*, 2015, **51**, 16992–16995.
19. G. S. Han and D. W. Domaille, *Org. Biomol. Chem.*, 2021, **19**, 4986–4991.
20. D. Gillingham, *Org. Biomol. Chem.*, 2016, **14**, 7606–7609.
21. P. Schmidt, C. Stress and D. Gillingham, *Chem. Sci.*, 2015, **6**, 3329–3333.
22. H. Faustino, M. J. S. A. Silva, L. F. Veiros, G. J. L. Bernardes and P. M. P. Gois, *Chem. Sci.*, 2016, **7**, 5052–505.
23. R. Liu, D. Liu, F. Meng, W. Li, L. Wang and X. Zhou, *Dyes Pigm.*, 2021, **187**, 109–118.
24. J. D. Scott and R. M. Williams, *J. Am. Chem. Soc.*, 2002, **124**, 2951–2956.
25. M. Kaneda, S. Inuki, H. Ohno and S. Oishi, *J. Org. Chem.*, 2018, **83**, 3047–3060.

26. W. S. Fernando, A. F. Martins, P. Zhao, Y. Wu, G. E. Kiefer, C. Platas-Iglesias and A. D. Sherry, *Inorg. Chem.*, 2016, **55**, 3007–3014.
27. S. Chaves, S. Resta, F. Rinaldo, M. Costa, R. Josselin, K. Gwizdala, L. Piemontese, V. Capriati, A. R. Pereira-Santos, S. M. Cardoso and M. A. Santos, *Molecules*, 2020, **25**, 985.
28. F. Scheidt, C. Thiehoff, G. Yilmaz, S. Meyer, C. G. Daniliuc, G. Kehr and R. Gilmour, *Beilstein J. Org. Chem.*, 2018, **14**, 1021–1027.
29. Y. Xu, M. Scipioni, H. Blevins and S. Zhang, *Med. Chem. Res.*, 2021, **30**, 473–482.
30. X. Li, J. Hou, C. Wang, X. Liu, H. He, P. Xu, Z. Yang, Z. Chen, Y. Wu and L. Zhang, *Molecules*, 2013, **18**, 13957–13978.
31. Y.-H. Shi, D.-F. Dai, J. Li, Y.-W. Dong, Y. Jiang, H.-G. Li, Y. Gao, C.-K. Chong, H.-Y. Li, X.-Q. Chu, C. Yang, Q. Zhang, Z.-S. Tong, C.-G. Bai and Y. Chen, *Molecules*, 2016, **21**, 514–523.
32. L. Brunetti, R. Leuci, A. Carrieri, M. Catto, S. Occhineri, G. Vinci, L. Gambacorta, H. Baltrukovich, S. Chaves, A. Laghezza, C. D. Altomare, P. Tortorella, M. A. Santos, F. Loidice and L. Piemontese, *Euro. J. Med. Chem.*, 2022, **237**, 1143–1158.
33. B. Xiao, B. Jiang, R. Yan, J. Zhu, K. Xie, X. Gao, Q. Ouyang, W. Du and Y. Chen, *J. Am. Chem. Soc.* 2021, **43**, 17989–17994
34. R. A. Aitken, P. K. G. Hodgson, J. J. Morrison and A. O. Oyewale, *J. Chem. Soc.*, 2002, **1**, 402–415.
35. M. Manenti, S. Gusmini, L. Lo Presti and A. Silvani, *Eur. J. Org. Chem.*, 2022, **43**, 175–189.
36. P. M. S. D. Cal, J. B. Vicente, E. Pires, A. V. Coelho, L. F. Veiros, C. Cordeiro and P. M. P. Gois, *J. Am. Chem. Soc.*, 2012, **134**, 10299–10305.
37. N. C. Rose, A. V. Sanchez, E. F. Tipple, J. M. Lynam and C. D. Spicer, *Chem. Sci.*, 2022, **13**, 12791–12798.
38. L. Fernandes, F. L. Fischer, C. W. Ribeiro, G. P. Silveira, M. M. Sá, F. Nome and H. Terenzi, *Bioorg. Med. Chem. Lett.*, 2008, **18**, 4499–4502.
39. H. Pfeiffer, T. Sowik and U. Schatzschneider, *J. Organometal. Chem.*, 2013, **734**, 17–24.
40. Y. Seno, T. Matsushita, H. M. Mahbulul, M. I. Ali, M. M. Mahmud, T. Mandai and H. Nemoto, *Tetrahedron*, 2022, **110**, 1326–1340.
41. A. Rahim, B. Sahariah, K. Baruah, J. K. R. Deka and B. K. Sarma, *J. Org. Chem.*, 2020, **85**, 2927–2937.
42. A. Rahim, B. Sahariah and B. K. Sarma, *Org. Lett.*, 2018, **20**, 5743–5746.
43. Z. Shi, P. Peng, D. Strohecker and Y. Liao, *J. Am. Chem. Soc.*, 2011, **133**, 14699–14703.
44. X. Duan, Q. Ruan, Q. Gan, X. Song, S. Fang, X. Zhang and J. Zhang, *J. Organometal. Chem.*, 2018, **868**, 154–163.
45. K. Li, C. Weidman and J. Gao, *Org. Lett.*, 2018, **20**, 20–23.

46. K. K. H. Vong, S. Maeda and K. Tanaka, *Chem. A Eur. J.*, 2016, **22**, 18865–18872.
47. M. K. Islam, S. Kim, H. K. Kim, S. Park, G. H. Lee, H. J. Kang, J. C. Jung, J. S. Park, T. J. Kim and Y. Chang, *J. Med. Chem.*, 2017, **60**, 2993–3001.
48. R. K. Varshnaya and P. Banerjee, *Eur. J. Org. Chem.*, 2016, **2016**, 4059–4066.
49. L. Bollans, J. Bacsa, J. A. Iggo, G. A. Morris and A. V. Stachulski, *Org. Biomol. Chem.*, 2009, **7**, 4531–4538.
50. A. Weickgenannt, J. Mohr and M. Oestreich, *Tetrahedron*, 2012, **68**, 3468–3479.
51. J. Gao, B. Zhao, M. Wang, M. A. C. Serrano, J. Zhuang, M. Ray, V. M. Rotello, R. W. Vachet and S. Thayumanavan, *J. Am. Chem. Soc.*, 2018, **140**, 2421–2425.
52. S. Nazreen, M. S. Alam, H. Hamid, M. S. Yar, A. Dhulap, P. Alam, M. A. Q. Pasha, S. Bano, M. M. Alam, S. Haider, C. Kharbanda, Y. Ali and K. Pillai, *Archiv. Pharm.*, 2015, **348**, 421–432.

Chapter Three

FRET-Based Binding Assay

Contents

1. FRET Binding Assay of oBIDS	119
1.1. Calculation of Cyanine Dye Concentration	119
1.2. Plate Reader Studies	122
1.2.1. Initial Screening of Photobleaching.....	122
1.2.2. Preliminary Fluorescence Measurements.....	123
1.2.3. Disulphide Reduction with TCEP	129
1.3. Fluorimeter FRET Measurements	133
1.3.1. Preliminary FRET Measurements.....	133
1.3.2. Second-Order Fluorimeter Measurements.....	137
1.4. Lack of Cy5 Emission at 641 nm	142
1.5. Extrapolation of Conversions	144
1.6. pH Dependency of oBID Formation	147
1.6.1 pH 6	147
1.6.2. pH 8.....	149
1.6.3. pH 4.....	150
1.7. Reaction Additives	151
2. Conclusion	155
3. Experimental	156
3.1. Determination of Substrate Concentration via UV/Vis Analysis	156
3.2. Initial Screening of Cy3 Quenching	156
3.3. FRET Studies	157
4. References	159

1. FRET Binding Assay of oBIDS

In this Chapter, we develop a sensitive and versatile Förster resonance energy transfer (FRET)-assay to probe rapid *ortho*-boronoimines, and related derivatives (collectively oBID) formation, stability, and cleavage in detail under complex media across a pH range of 6-8 using a plate reader and fluorimeter. Cy3 and Cy5 dyes synthesised in Chapter 2 were used here to determine the reaction kinetics of oBID formation.

1.1. Calculation of Cyanine Dye Concentration

As detailed in Chapter 2, FRET analysis could be used to measure the formation rates and dissociation constants for the reactions of an *ortho*-boronoaldehyde (oBA) with amine-based nucleophiles to form *ortho*-boronoimine conjugates. The FRET platform needed to be operational at low concentrations (100 nM-50 μ M) to study the kinetics of oBID formation and to determine reaction parameters due to the rapid nature of these reactions. As a result, the syntheses described in Chapter 2 were scaled appropriately to form 2-100 mg of each material to prevent waste. This low amount of material could result in high inaccuracies in the mass measured due to errors during weighing, and subsequently, this would affect the exact concentrations of solutions to be used in FRET studies, which is a highly sensitive technique. Therefore, masses with errors ± 0.5 mg of a total sample which is 2.0 mg, could cause significant discrepancies in the subsequent FRET analysis. To minimise this error, the concentrations of stock solutions of each dye were calculated by correlating the UV-Vis absorbance of the Cy3/Cy5 chromophore to standards of known concentrations. The reactive handles required for *ortho*-boronoimine formation are sufficiently distal to the cyanine chromophore and therefore have a negligible effect on the absorbance of the dye.¹ A calibration curve could therefore be set up using known concentrations of the cyanine dyes **1** and **2** (Fig. 1), and used to calculate the concentrations of unknown samples.

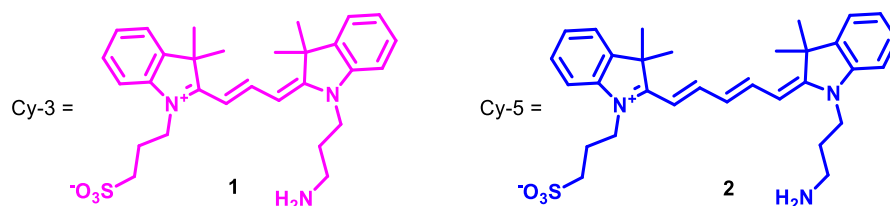


Figure 1: Cy3 **1** and Cy5 **2** dyes used to measure accurate concentrations in UV studies.

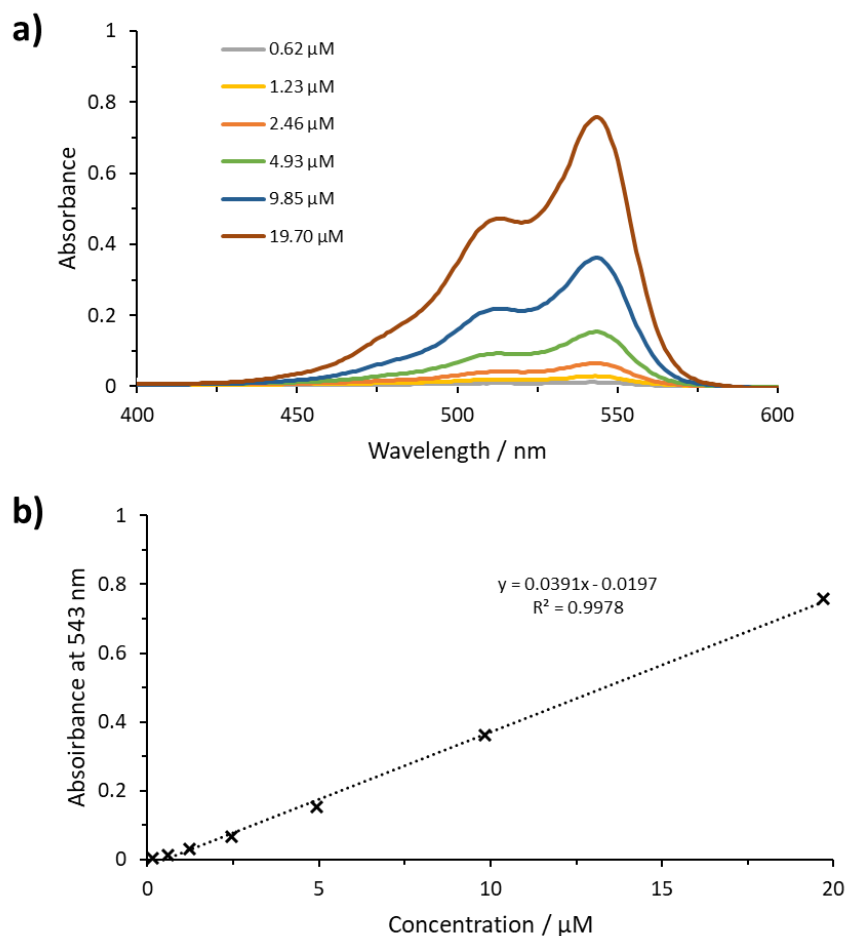


Figure 2: a) Absorbance spectra of solutions of known concentrations of Cy3 dye 1; b) Plot of the absorption at 543 nm across varying concentrations of 0.15-19.70 μM of 1 and linear fitting.

A calibration curve was set up of known concentrations of Cy3 dye 1 (0.5-19.7 μM). The absorption maxima were found to be at 543 nm (Fig. 2a). A plot of absorbance at 543 nm against concentration yielded a linear fit with an $R^2 = 0.9978$ (Fig. 2b). This R^2 value was very close to one, indicating reliability in this linear fit. The absorbance (y) of samples of unknown concentration could then be measured, and Equation 3 could be used to calculate the concentration (x) of the sample.

$$(1) \quad y = 0.0391x - 0.0197$$

$$(2) \quad x = \frac{y+0.0197}{0.0391}$$

Analogous data was obtained for known concentrations of amino Cy5 dye **2** (0.3-9.4 μM). The absorption maxima were found to be at 641 nm (Fig. 3a). A plot of absorbance at 641 nm against concentration yielded a linear fit with an $R^2 = 0.99325$ (Fig. 3b). The exact concentration of stock solutions of the synthesised dye targets **1a-e** and **2a-e** (Fig. 4) could then be calculated using these calibrations.

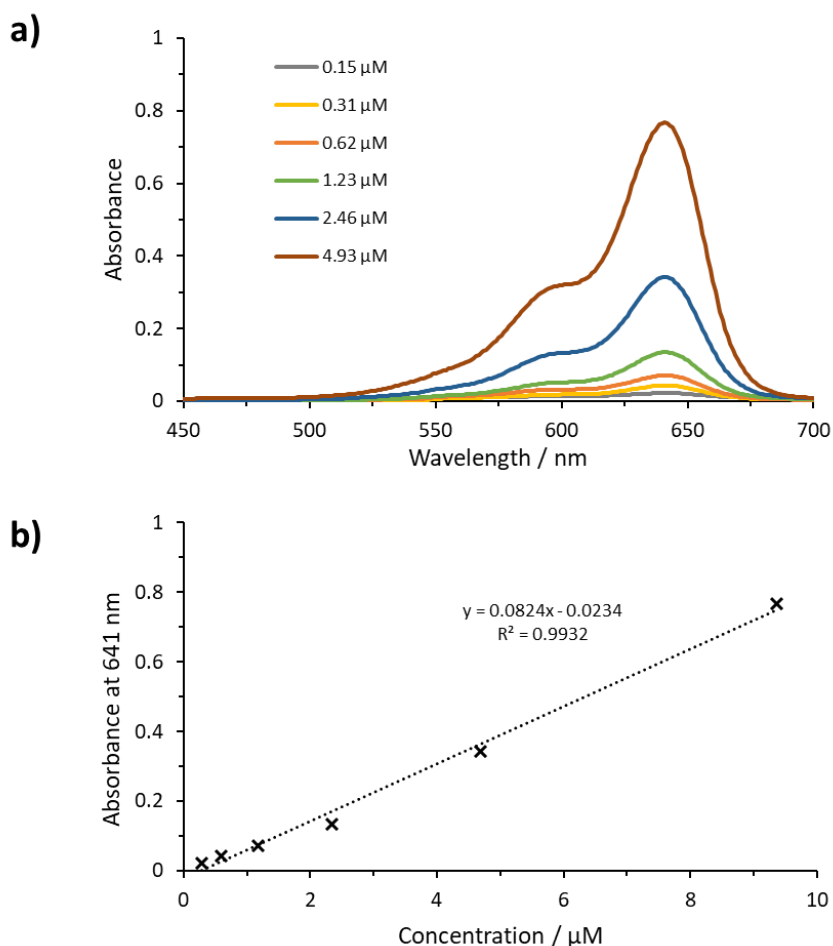


Figure 3: a) Absorbance spectra of solutions of known concentrations of Cy5 dye **2**; b) Plot of the absorption at 641 nm across varying concentrations of 0.29-9.38 μM of amino Cy5 dye and linear fitting.

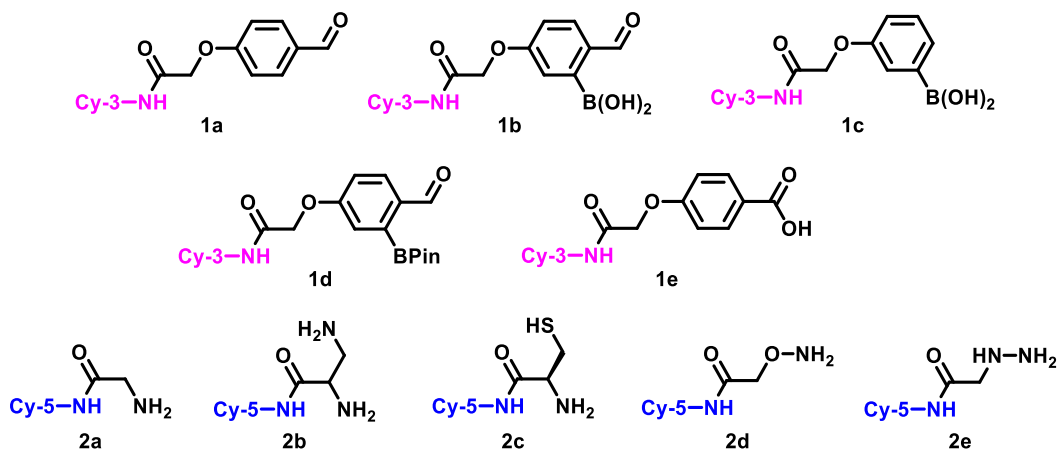
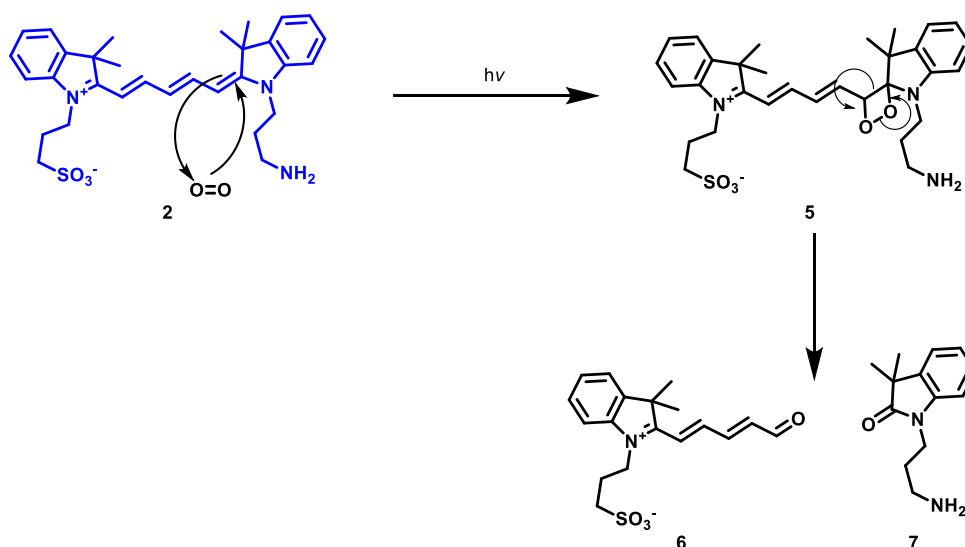


Figure 4: Cy3 dyes (**1a-e**) and Cy5 dyes (**2a-e**), which are analysed in this work.

1.2. Plate Reader Studies

1.2.1. Initial Screening of Photobleaching

We first undertook fluorescence measurements of cyanine dye samples over a broad range of concentrations (1 μM to 12 mM) to find the optimum dye concentration for FRET measurements and to see if any photobleaching occurred. Photobleaching is the degradation process of light sensitive compounds, such that the dye is permanently unable to fluoresce. This is caused by the cleavage of covalent bonds or non-specific reactions between the fluorophore and surrounding molecules.² If photobleaching did occur over time, this would lead to a loss of cyanine fluorescence, which would subsequently cause discrepancies in the FRET measurements. James *et al.* investigated the mechanism of photobleaching of cyanine dyes, which reported the reduction of singlet state oxygen in the presence of light (Scheme 1).³ This photobleaching process occurs between the different transition states of oxygen with highly conjugated cyanine dyes in the presence of light. These highly conjugated systems are suggested to have reactive alkene bonds, which can react with oxygen under light irradiation to form intermediate **5**, which is then cleaved to form compounds **6** and **7**. Therefore, the susceptibility of our dyes to bleaching was monitored over time. Aliquots of both the Cy3 **1** and Cy5 **2** dyes were diluted to various concentrations and excited at 480 nm every 10 mins over 6 h with the emission monitored at 580 nm. This timeframe was suitable as the dyes would not be irradiated for more than 3 h for any measurement. There was no significant change in the emission data for either cyanine dye, showing that the dyes were photostable under these conditions. This experiment gave us confidence that photobleaching would not affect subsequent FRET measurements, which were carried out over 3 h.



Scheme 1: Mechanism of photobleaching of Cy5 dye with singlet oxygen.³

1.2.2. Preliminary Fluorescence Measurements

oBID formation was initially screened in a 96-well format under pseudo-first order conditions, to allow optimal timeframes for reaction monitoring to be established. These preliminary reactions were performed using a plate reader, which allowed for high throughput screening of multiple different conditions in parallel to collate a library of data, which could then be optimised for reaction monitoring. Although the plate reader we used had many limitations in versatility due to its limited range of wavelength filters, it was used here as it allowed high throughput parallel monitoring of multiple reactions. The rate at which measurements could be taken was slow, which meant that often high levels of conversion were achieved by the first measurement. Additionally, the accuracy of measurements on the plate reader was hindered by potential crosstalk between different wells, and the use of parallel emission detection, which is significantly less accurate than perpendicular measurements. Therefore, these results were used solely as a guide to determine which reaction parameters to probe in more detail. Initial fluorescence studies were performed under pseudo-first order conditions, with the reduction in Cy3 emission upon oBID formation being monitored. Pseudo first order conditions were achieved by using the Cy5 dye in excess 10 equivalents, which meant the effective concentration of Cy5 would be approximately constant.

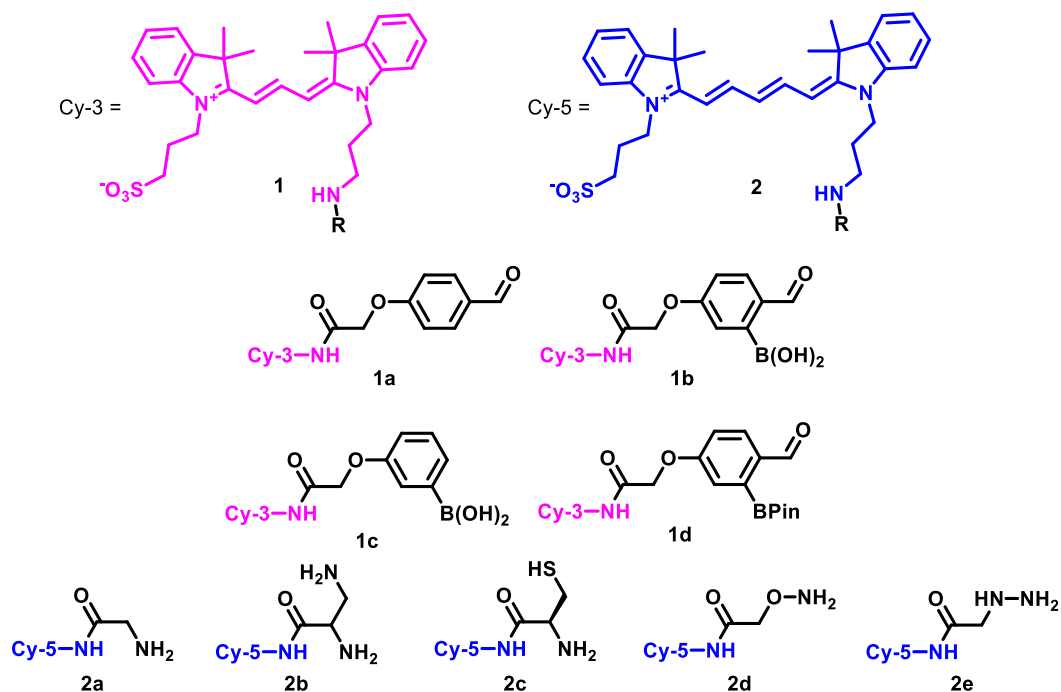


Figure 3: Target molecules of Cy3 dyes (1a-d) and Cy5 dyes (2a-e) that were synthesised for FRET assay studies.

The following graphs show the emission of the Cy3 dye at 580 nm, after excitation at 480 nm in a mixture of a single Cy3 (**1a-d**) and amine derivatives (**2a-e**) at 5 μM and 50 μM respectively (Fig. 5). The emission observed is a composite of fluorescence from bound Cy3-Cy5, the remaining unreacted Cy3, and background signal from the excess Cy5. If the Cy3 and Cy5 dyes are conjugated, we would expect to see a drop in emission at 580 nm after excitation at 480 nm, as a result of FRET from Cy3 to Cy5. The conjugates were excited at 480 nm, as although this is not the λ_{max} of the Cy3 chromophore, the Cy5 has a negligible absorbance at 480 nm, which minimises background signals of the system. An adjusted emission at 641 nm was taken here to account for any possible background fluorescence from the Cy5 dye which normalises the noise of the system. Preliminary fluorescence measurements using a plate reader were taken every 10 min for a 3 h period. A decrease in adjusted Cy3 emission resulting from FRET was seen between 0-20 min for all of the Cy5 derivatives (Fig. 6-10) with the Cy3 *ortho*-boronoaldehyde **1b** or pinacol ester **1d**. Importantly, no significant drop in Cy3 emission was observed for the control reactions using Cy3 substrate lacking either the boronic acid (**1a**) or aldehyde (**1c**) functional groups, confirming the importance of the B-N stabilisation of the resultant imine derivative. Though benzaldehyde can form non-stabilised thiazolidines, oximes and hydrazones in aqueous conditions, reactions are slow at neutral pH in the absence of catalysts ($k_1 < 1 \text{ M}^{-1} \text{ s}^{-1}$) and therefore would not be expected to form over the timeframe of these studies.^{4,5} The *ortho*-boronopinacol aldehyde (**1b**) shows a slight reduction in Cy3 emission, indicating some stabilisation is offered from either binding to the pinacol ester, or through hydrolysis to the boronic acid (**1b**) in the PBS solution during the reaction. The biggest drops in emission were the *o*BA **1b** in combination with the 1,2-diamine **2b** (Fig. 7), hydroxylamine **2d** (Fig. 9) and hydrazine **2e** (Fig. 10) functionalised Cy5 dyes.

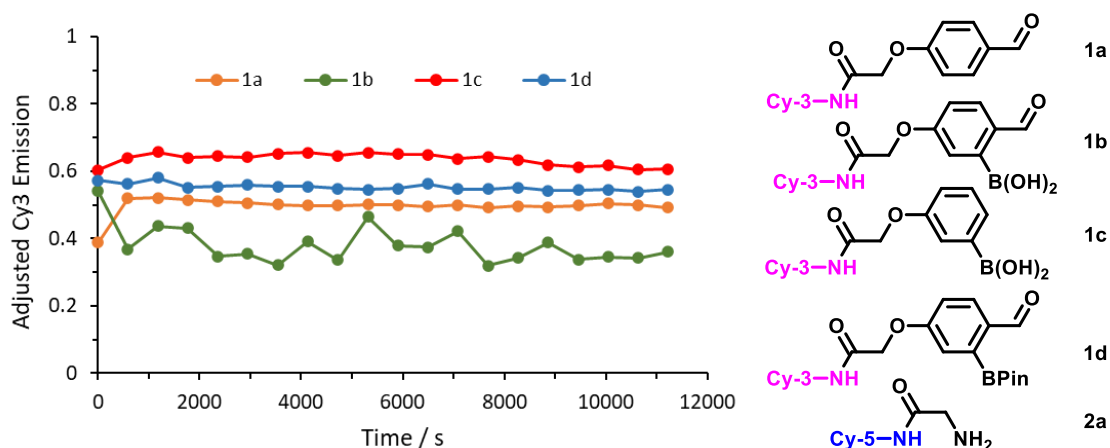


Figure 4: Adjusted Cy3 emission against time after mixing Cy3 (**1a-d**) derivative with the amine-Cy5 **2a**. Adjusted emission negates negative control reactions and background from the system.

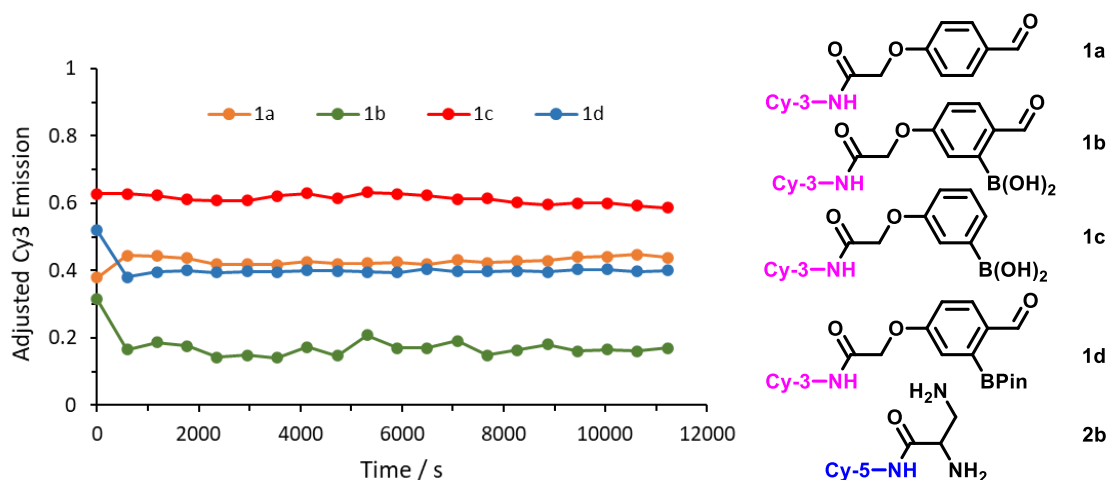


Figure 5: Adjusted Cy3 emission against time after mixing Cy3 (1a-d) derivative with the diamine-Cy5 2b. Adjusted emission negates negative control reactions and background from the system.

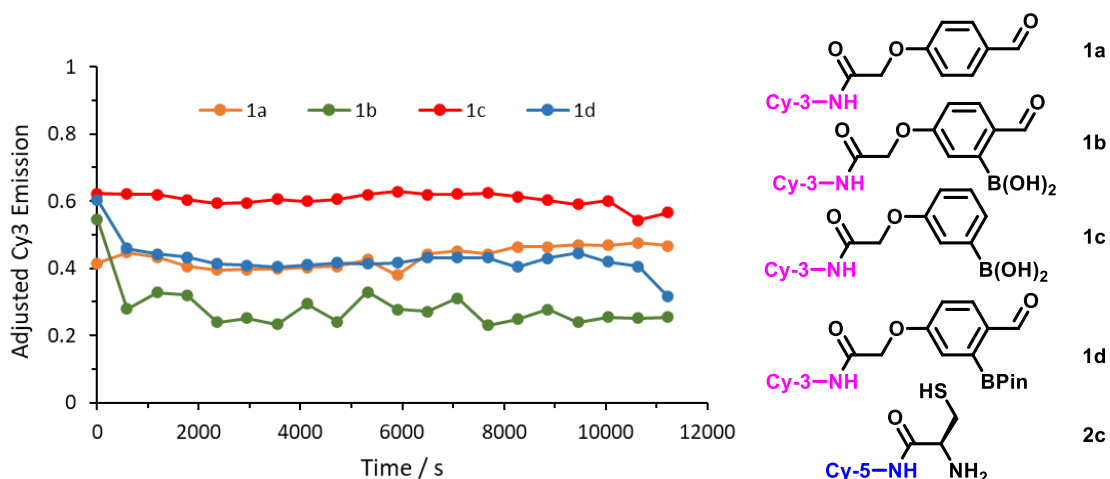


Figure 6: Adjusted Cy3 emission against time after mixing Cy3 (1a-d) derivative with the aminothiols-Cy5 2c. Adjusted emission negates negative control reactions and background from the system.

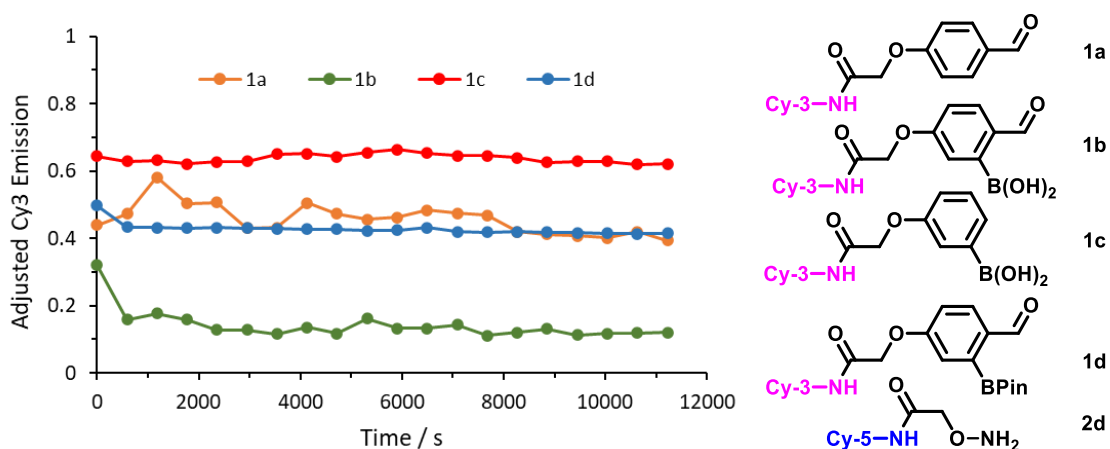


Figure 7: Adjusted Cy3 emission against time after mixing Cy3 (1a-d) derivative with the hydroxylamine-Cy5 2d. Adjusted emission negates negative control reactions and background from the system.

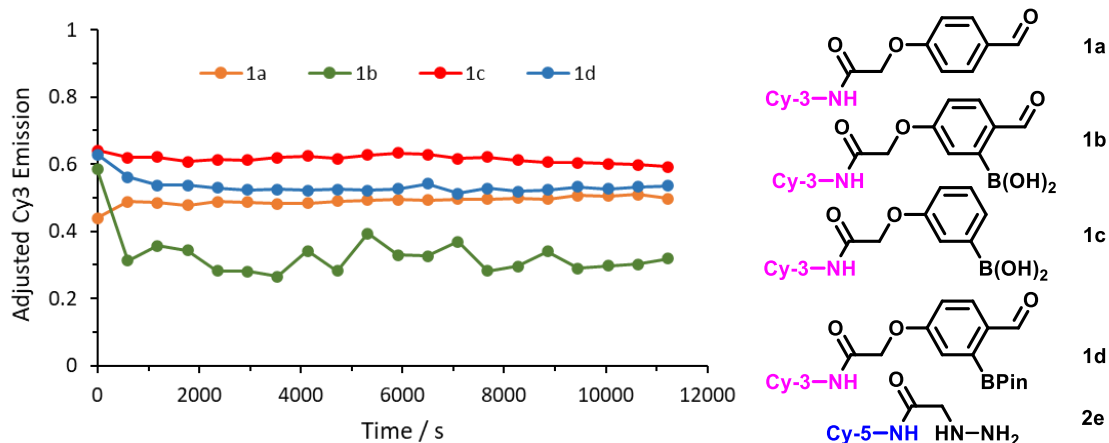


Figure 8: Adjusted Cy3 emission against time after mixing Cy3 (**1a-d**) derivative with the hydrazine-Cy5 **2e**. Adjusted emission negates negative control reactions and background from the system.

An additional discussion point is the fluctuation in the data shown in Fig. 11, which are consistent between all of the measurements. This suggests that there was a consistent error in the plate reader, which propagates throughout the measurements. As this error was consistent across all of the measurements, and the plate reader is used solely as a guide for more precise and accurate future measurements, the fluctuations in the data were not concerning.

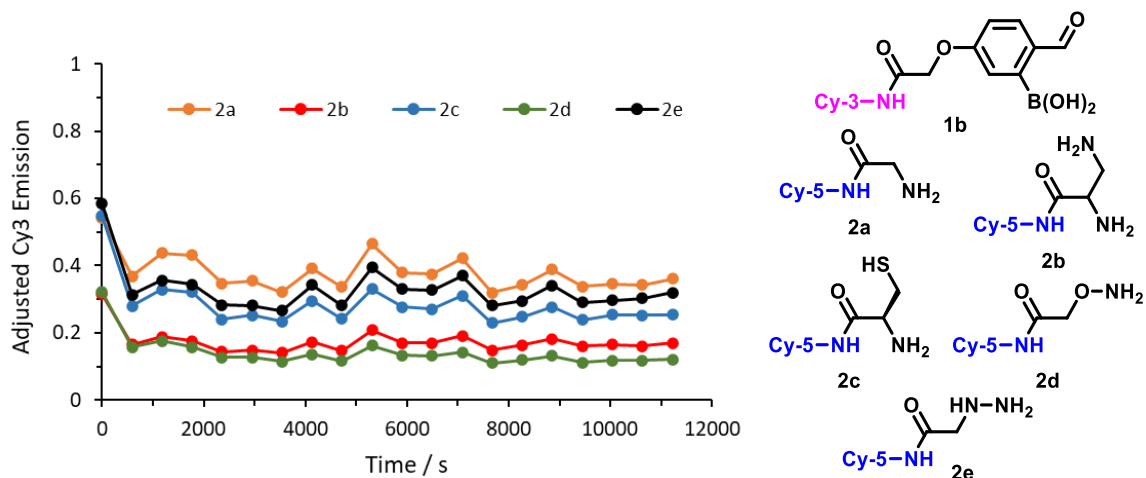


Figure 9 Adjusted Cy3 emission against time to monitor the interactions with the Cy3 oBA **1b** with the Cy5 amine (**2a-e**) functionalities. Adjusted emission negates negative control reactions and background from the system.

This data showed promising signs of FRET taking place upon oBID formation with reduced Cy3 emission as a result of conjugation, for reactions with *ortho*-boronobenzaldehydes **1b**. However, as these measurements were taken every 10 min, it appeared that high levels of conversion had already been reached by the time of the first measurement was taken. Therefore, reaction monitoring had to be performed on a much shorter timescale. Thus, we expanded this study, repeating the FRET measurements of each of the synthesised Cy3 (**1a-d**) dyes in combination with each Cy5 amine (**2a-e**) dyes. We then aimed to record the emission following excitation every 1 minute over 100 cycles in the hope of observing

a gradual decrease in Cy3 emission over a relevant timeframe. Reactions on the plate reader were measured in triplicate, and an average was taken to ensure reproducibility of data and account for error. The following graphs (Fig. 12-16) show Cy3 emission at 580 nm following excitation at 480 nm of Cy3 dyes (**1a-d**) at 5 μM concentration, and Cy5 dyes (**2a-e**) at 50 μM concentration. These concentrations of dye analogues ensured pseudo-first order conditions were obeyed as described above.

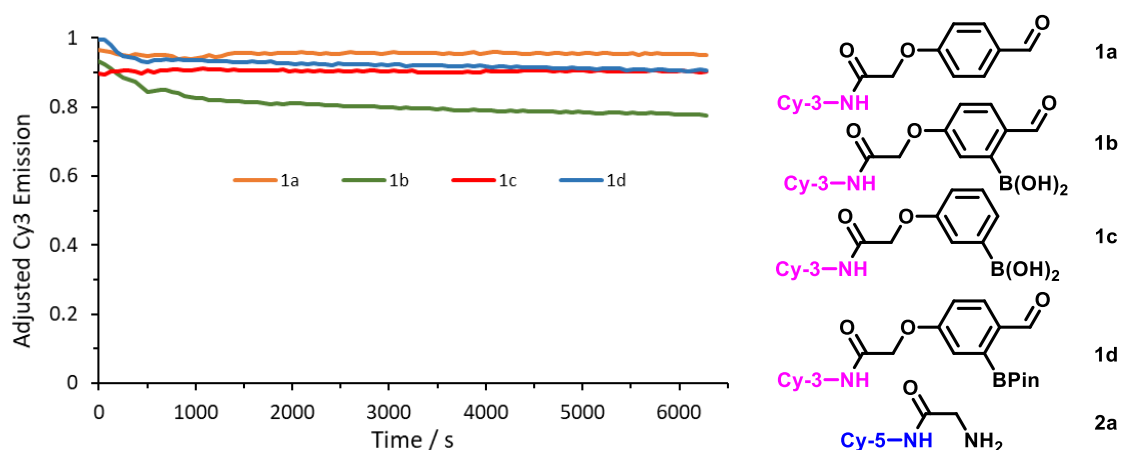


Figure 10 Adjusted Cy3 emission against time to monitor the Cy3 (**1a-d**) derivative interactions with the amine **2a** functionality. Adjusted emission negates negative control reactions and background from the system.

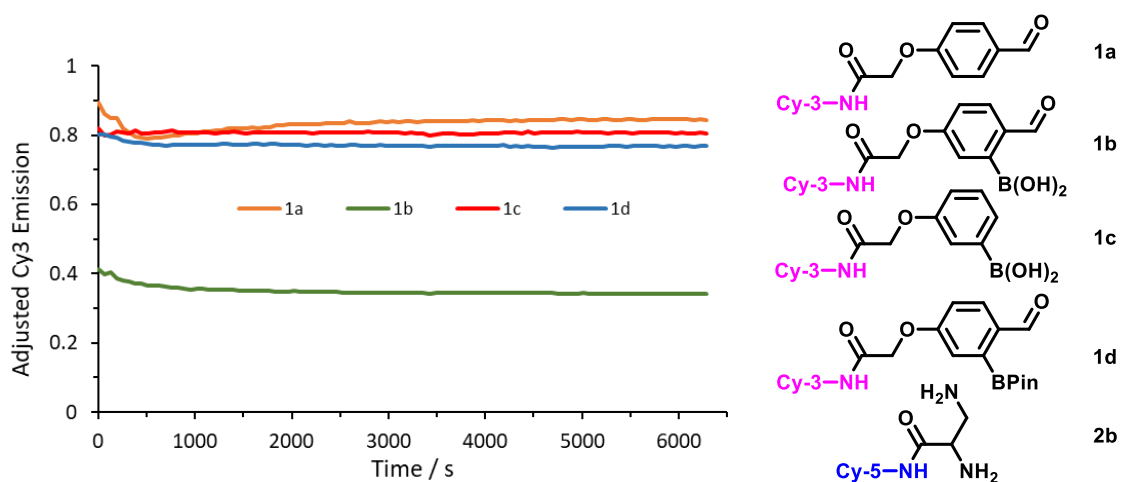


Figure 11: Adjusted Cy3 emission against time to monitor the Cy3 (**1a-d**) derivative interactions with the 1,2-diamine **2b** functionality. Adjusted emission negates negative control reactions and background from the system.

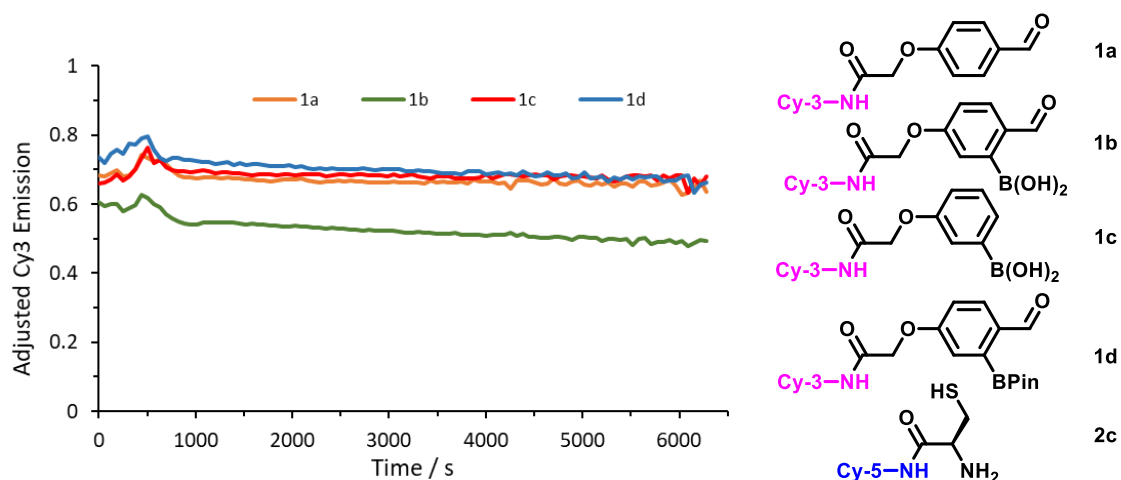


Figure 12: Adjusted Cy3 emission against time to monitor the Cy3 (1a-d) derivative interactions with the 1,2-aminothiol 2c functionality. Adjusted emission negates negative control reactions and background from the system.

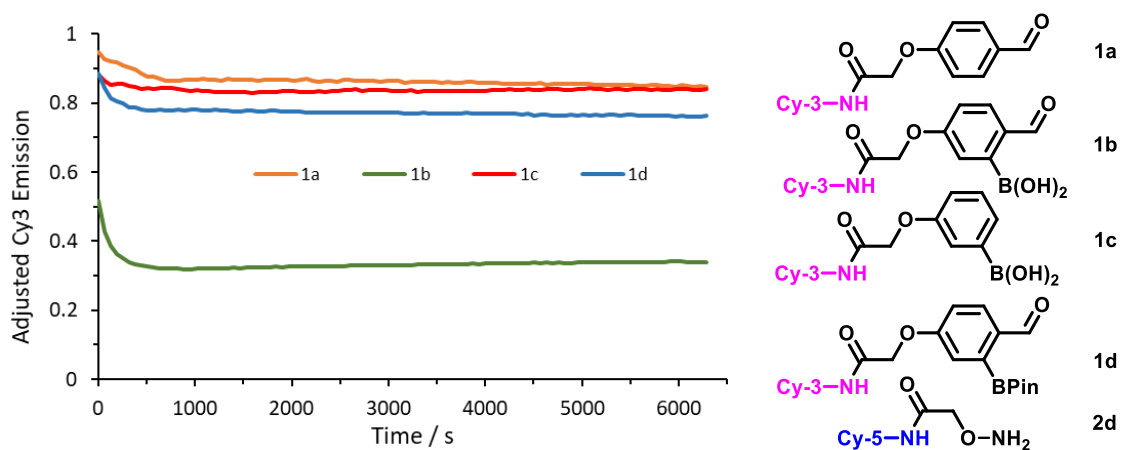


Figure 13: Adjusted Cy3 emission against time to monitor the Cy3 (1a-d) derivative interactions with the hydroxylamine 2d functionality. Adjusted emission negates negative control reactions and background from the system.

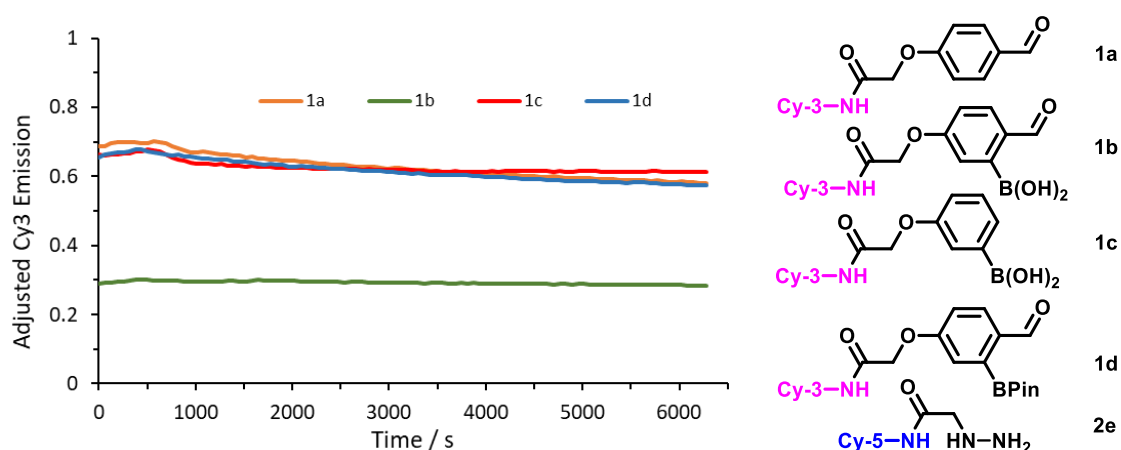


Figure 14: Adjusted Cy3 emission against time to monitor the Cy3 (1a-d) derivative interactions with the hydrazine 2e functionality. Adjusted emission negates negative control reactions and background from the system.

As shown by these results (Fig. 12-16) there was a clear decrease in adjusted Cy3 emission for the *ortho*-boronobenzaldehyde 1b when combined with most of the Cy5

amine derivatives **2b-e** indicating the formation of oBIDs. This contrasts with the control molecules, with little change in emission at 580 nm observed for aldehyde **1a**, boronic acid **1c** or *ortho*-boronopinacol ester aldehyde **1d** over the time course of the experiment, which suggests that both the boronic acid group and aldehyde in combination are required to stabilise the imine product. These results validated our assay design, and the lack of binding in negative control reactions of **1a**, **1c** and **1d**. The three combinations that caused the biggest drop in adjusted Cy3 emission, were the *ortho*-boronobenzaldehyde **1b** in combination with 1,2-diamine **2b** (Fig. 13), hydroxylamine **2d** (Fig. 15) and hydrazine **2e** (Fig. 16), which was predicted before the measurements were taken, due to their increased electron densities.⁶⁻¹⁰ Fig 17 shows *ortho*-boronobenzaldehyde **1b** in combination with the five amine-based nucleophiles (**2a-e**), which all show some drop in Cy3 emission over time, and gave us confidence to move forward with more accurate and detailed studies using a fluorimeter as described later.

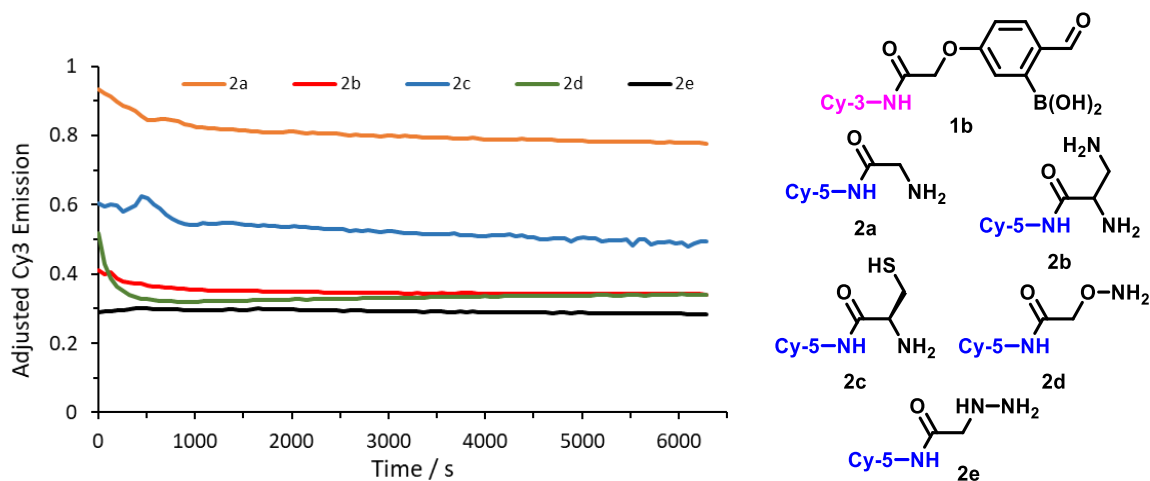
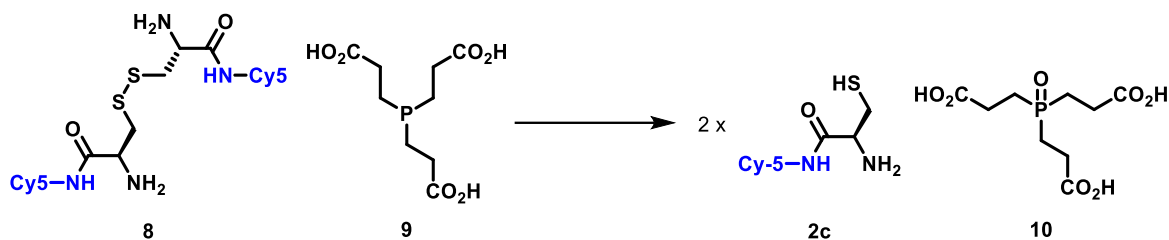


Figure 15: Adjusted Cy3 emission against time to monitor the interactions with the Cy3 oBA **1b** with the Cy5 amine (**2a-e**) functionalities. Adjusted emission negates negative control reactions and background from the system.

1.2.3. Disulphide Reduction with TCEP

The Cy5 1,2-aminothiol derivative **2c** did not show significant reductions in Cy3 emission intensity in the preliminary data described above despite what we had expected based on literature rates of reaction and dissociation constants.^{11,12} We therefore reasoned that the thiol handle in the molecule could be forming disulphides leading to dimerization of the dyes to form **8** (Scheme 2). Disulphide formation from cysteine residues containing thiols, similar to our reactive handle, are common rendering the sulphur group unreactive.^{10,11,13-16} We hypothesised that these disulphide bridges could be broken up by pre-treatment with a reducing agent such as tris(2-carboxyethyl)phosphine (TCEP) or dithiothreitol (DTT). Although both of these reducing agents have been used to cleave disulphide

linkages, TCEP (**9**) was used in this work as a result of fast reduction in aqueous conditions, driven by the thermodynamics of a strong P=O bond formation **10** (Scheme 2).



Scheme 2: The use of TCEP **9** to break up disulphide bridges to reinstate the active aminothiols which could then form more effective oBID linkages.

Therefore, measurements with **2c** were repeated with prior treatment with TCEP to reduce the disulfide bonds and form monomeric dyes (Fig 18-22). The reaction was repeated with TCEP concentrations of 50 μ M, 100 μ M and 500 μ M (1, 2 and 10 equivalents to **2c** respectively). Cy5 1,2-aminothiol **2c** was incubated and shaken for ~30 secs with various concentrations of TCEP prior to the addition of the Cy3 dyes. Upon addition of the Cy3 dyes, the measurements were taken immediately. The results obtained were compared alongside control reactions to allow for the elucidation of the adjusted Cy3 emission. All data was measured in triplicates and show averages of all 3 data series.

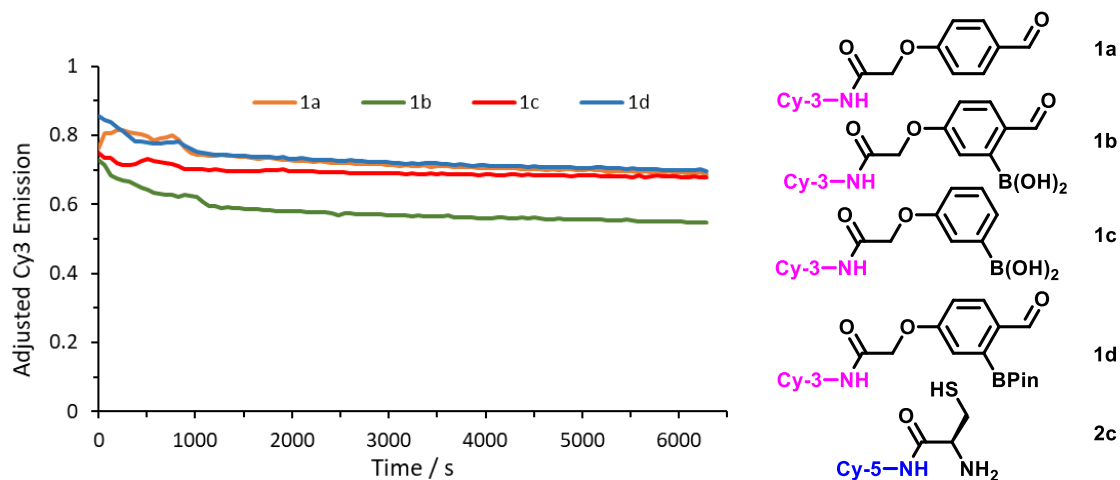


Figure 16: Adjusted Cy3 emission against time to monitor the Cy3 (**1a-d**) derivative interactions with the 1,2-aminothiol **2c** functionality in PBS with no prior treatment with TCEP.

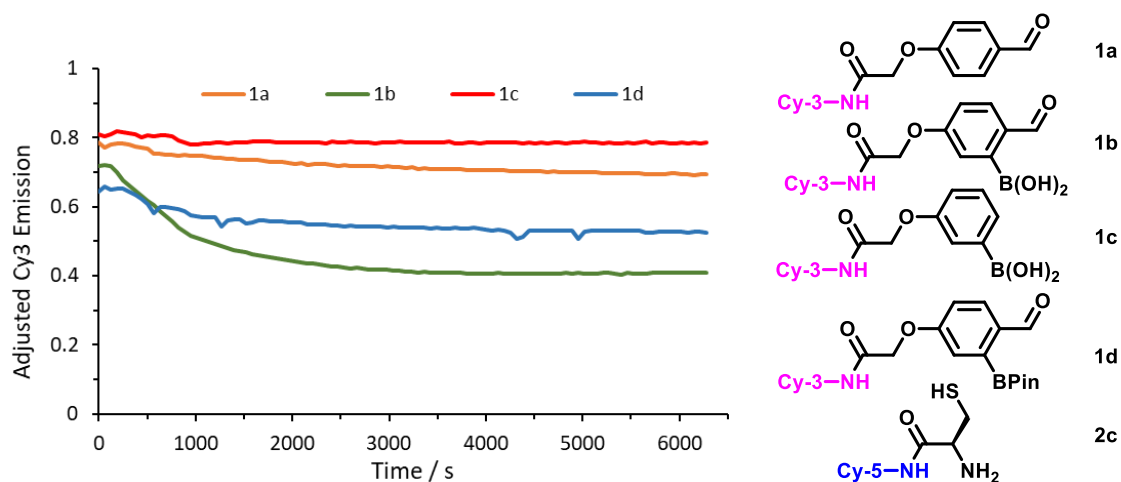


Figure 17: Adjusted Cy3 emission against time to monitor the Cy3 (1a-d) derivative interactions with the 1,2-aminothiol **2c** functionality with 50 μM TCEP.

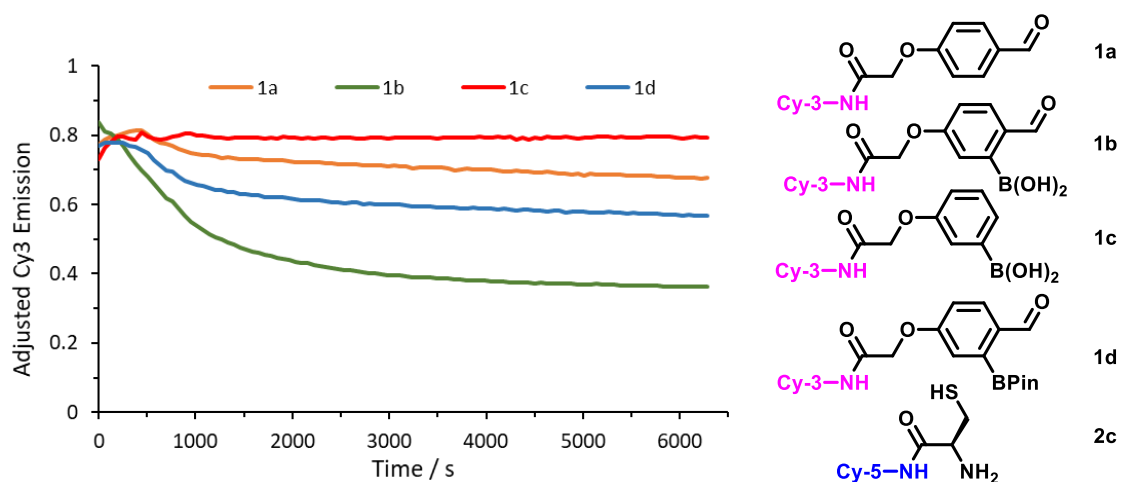


Figure 18: Adjusted Cy3 emission against time to monitor the Cy3 (1a-d) derivative interactions with the 1,2-aminothiol **2c** functionality with 100 μM TCEP.

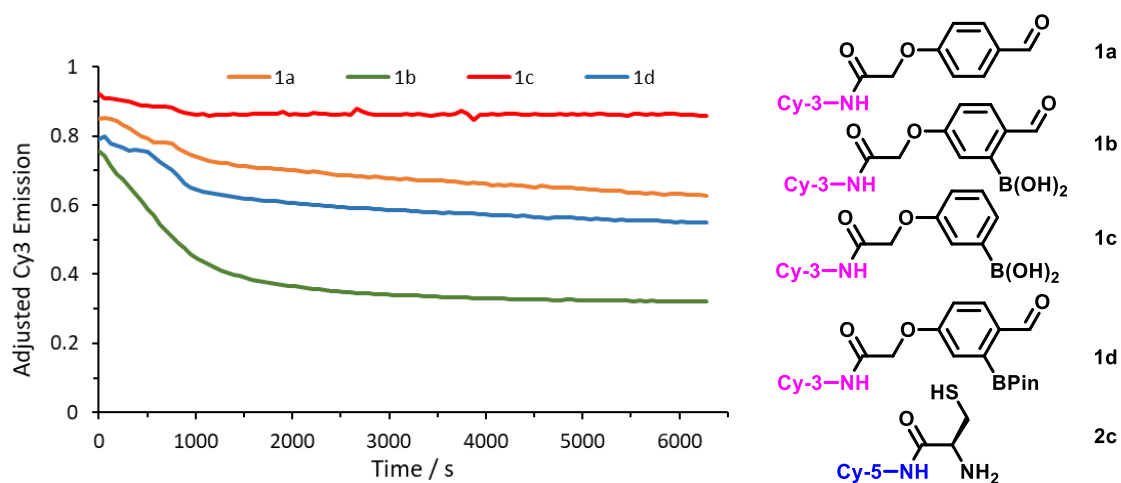


Figure 19: Adjusted Cy3 emission against time to monitor the Cy3 (1a-d) derivative interactions with the 1,2-aminothiol **2c** functionality with 500 μM TCEP.

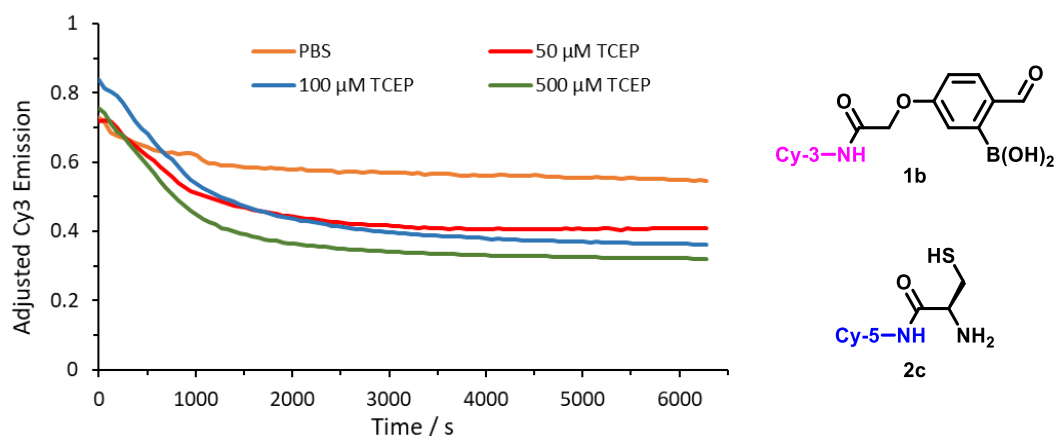


Figure 20: Adjusted Cy3 emission against time to monitor the Cy3 (**1a-d**) derivative interactions with the 1,2-aminothiols **2c** functionality with prior treatment of varying amounts (0-500 μM) of TCEP.

Using Fig. 18-22, it could be concluded that TCEP has a significant effect on the adjusted Cy3 emission of *ortho*-boronobenzaldehyde **1b** and pinacol ester **1d** in the presence of the Cy5 aminothiols **2c**, as there was a drop in adjusted Cy3 emission with increasing concentration of TCEP. For aldehyde **1a**, there was no appreciable drop in emission, even in the presence of TCEP, which was expected at a neutral pH in the absence of catalysts over these timeframes. This is because the rate of formation of the imine (k_1) is slow, which therefore favoured the equilibrium to lie towards the aldehyde and aminothiols counterparts, with long reaction times needed to form an appreciable drop in Cy3 emission intensity. The emission intensity of the boronic acid **1c** surprisingly increased slightly, which could be due to drift in the system. The *ortho*-boronobenzaldehyde **1b** seems to exhibit the most effective binding, as the electron density of the 1,2-aminothiols moiety could be donated into the empty p-orbital of the boron centre to form a thiazolidino-boronate (TzB) complex. Therefore, it was demonstrated that the controls are not forming effective Cy3-Cy5 conjugates using initial plate reader measurements and did not need to be studied further via more accurate fluorimeter measurements. Fig. 22 shows a gradual decrease in adjusted Cy3 emission with increasing concentration of TCEP. A significant difference between the 50 μM and 500 μM concentrations was observed, with a continued fall in adjusted Cy3 emission at the highest concentration, therefore a 500 μM (10 equivalents) solution of TCEP was chosen and carried forward in subsequent fluorescence measurements.

1.3. Fluorimeter FRET Measurements

High throughput data obtained from the plate reader allowed us to move forward and perform more detailed studies with the *ortho*-boronobenzaldehyde **1b** using a fluorimeter, which gave much more accurate and quantitative results. **1b** was mixed in a cuvette with Cy5 amino derivatives (**2a-e**), and measurements were taken as close to $t=0$ as possible (~3 secs) and then every 15 seconds, to allow the initial burst in conjugation previously unseen in the literature to be monitored. It should be noted that we were unable to take measurements at exactly $t = 0$ due to the impracticalities of the fluorimeter. However, we were able to extrapolate the data back to find our $t = 0$ using the control reactions. Additionally, we used the negative control (**1b + 3**) to account for drift in the unconjugated molecules to increase accuracy of the system. The fluorimeter is able to take measurements every 15 sec, and provides emission spectra, rather than taking a single point measurement at a particular wavelength.

1.3.1. Preliminary FRET Measurements

The following spectra (Fig. 23-29) show the change in emission over time for the reactions of Cy3-Cy5 dyes between 520-700 nm in phosphate buffered saline (pH 7.4) following excitation at 480 nm. Reactions were undertaken with a mixture of *ortho*-boronobenzaldehyde **1b**, in combination with each of the Cy5 amine derivatives (**2a-e**) under pseudo first order conditions at 5 μ M and 50 μ M concentrations respectively. Upon mixing the dyes, a gradual drop in the intensity of Cy3 emission over the repeated cycles was expected. In addition, two reference samples were measured, using a Cy5 dye with an acetate cap **3** as a negative control, incapable of forming an *o*BID unit to give a 0% conjugation reference. We also measured a positive control, which was an irreversibly covalently conjugated Cy3-Cy5 dye **4**. This kept the dyes in constant close proximity allowing maximum FRET to occur 100% of the time. Using these two controls, numerous *o*BID linkages could be studied with FRET ratios which were expected to fall in between the two controls. These control compounds were used as references to translate FRET to conversion as detailed in the experimental. The following graphs (Fig. 23-29) show the emission spectra of Cy3 *ortho*-boronobenzaldehyde **1b**, in combination with each Cy5 analogue (**2a-e**).

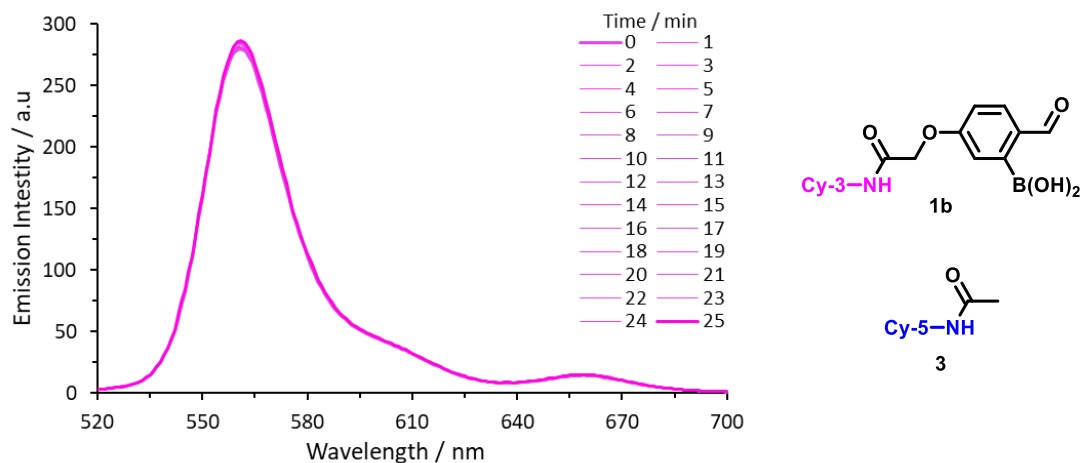


Figure 21: Emission spectra between 520-700 nm, following excitation of a mixture of Cy3 oBA **1b** with the Cy5 acetate cap (**3**) at 480 nm at $t \sim 3$ sec.

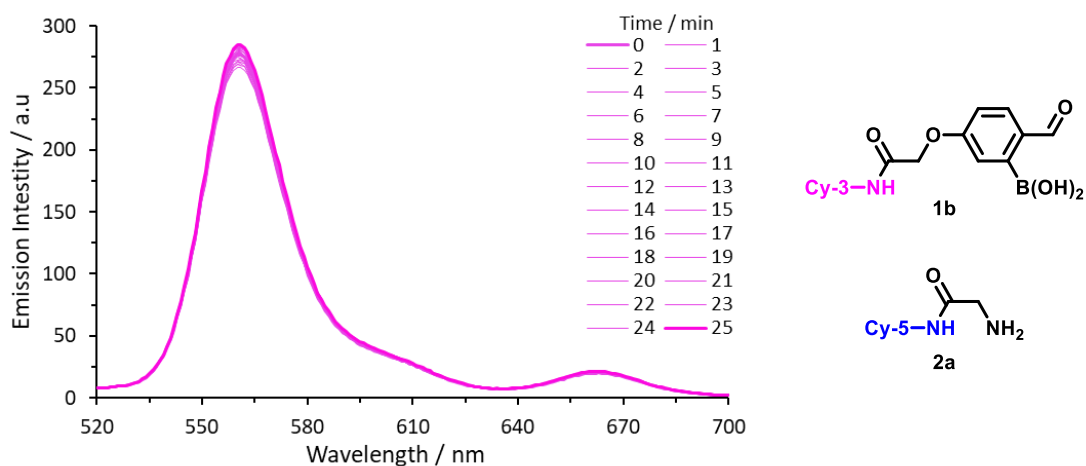


Figure 22: Emission spectra between 520-700 nm, following excitation of a mixture of Cy3 oBA **1b** with the Cy5 amine **2a** at 480 nm at $t \sim 3$ sec.

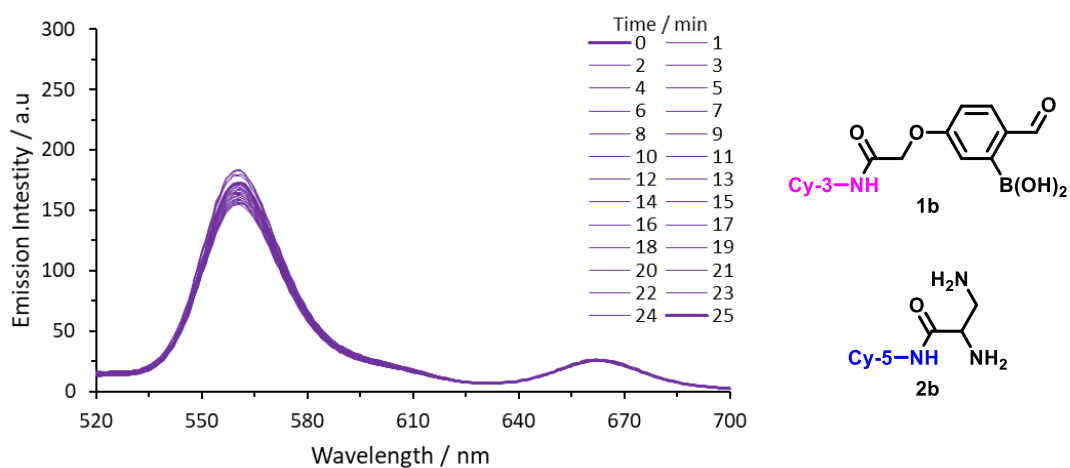


Figure 23: Emission spectra between 520-700 nm, following excitation of a mixture of Cy3 oBA **1b** with the Cy5 1,2-diamine **2b** at 480 nm at $t \sim 3$ sec.

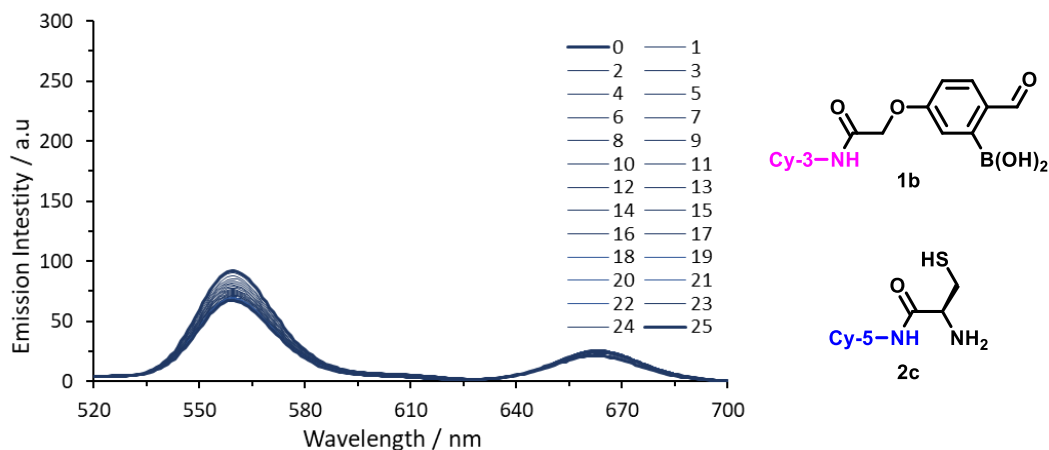


Figure 24: Emission spectra between 520-700 nm, following excitation of a mixture of Cy3 oBA **1b** with the Cy5 aminothiols **2c** at 480 nm at $t \sim 3$ sec.

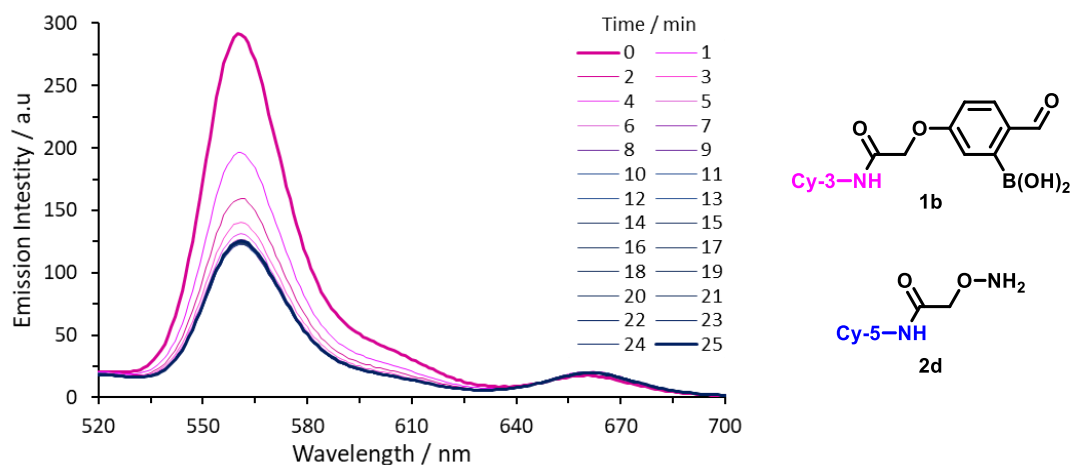


Figure 25: Emission spectra between 520-700 nm, following excitation of a mixture of Cy3 oBA **1b** with the Cy5 hydroxylamines **2d** at 480 nm at $t \sim 3$ sec.

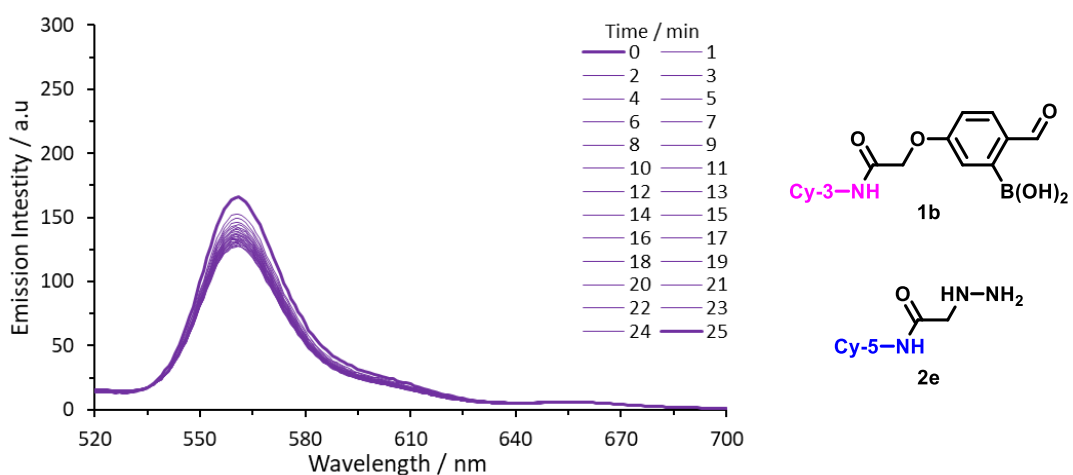


Figure 26: Emission spectra between 520-700 nm, following excitation of a mixture of Cy3 oBA **1b** with the Cy5 hydrazines **2e** at 480 nm at $t \sim 3$ sec.

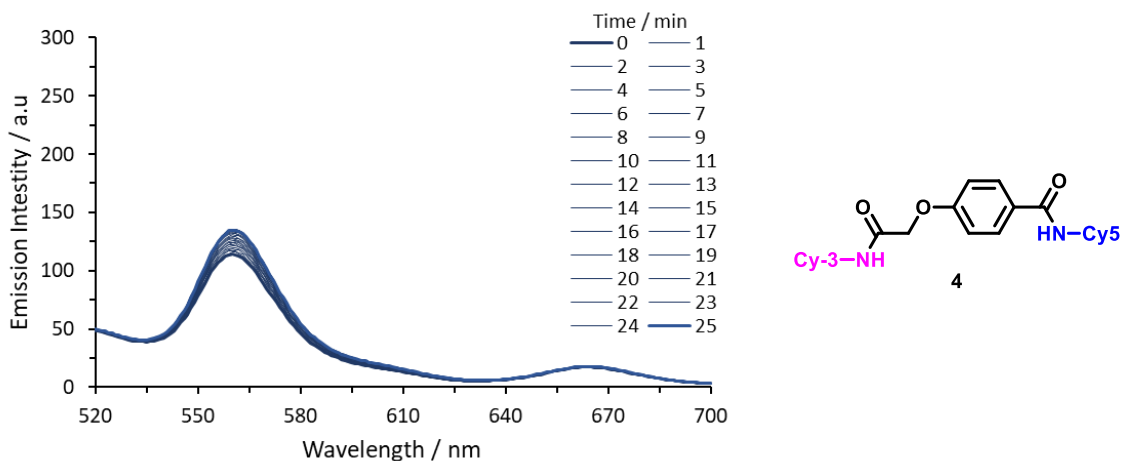


Figure 27: Emission spectra between 520 - 700 nm, following excitation of a covalently conjugated Cy3-Cy5 positive control **4** for this reaction at 480 nm at $t \sim 3$ sec.

The fluorescence data show an array of different extents of binding to form the desired Cy3-Cy5 conjugates. All data was measured in triplicates, showing averages of all three data series. The initial measurement of the negative control with *ortho*-boronobenzaldehyde **1b** in combination with the Cy5 acetate cap **3** shows a high Cy3 emission intensity (Fig. 23), which did not change over time. In contrast the covalently bound reference **4** showed a low Cy3 emission intensity (Fig. 29), which served as the 100% bound reference. Measurements with a combination of *ortho*-boronobenzaldehyde **1b** in combination with the Cy5 amine **2a** showed very little conjugation occurring, whereby the Cy3 emission intensity only dropped slightly (Fig. 24). This indicated minimal amine conjugation to form an *o*BID at this specific concentration, and that the position of equilibrium lies significantly towards the starting materials. *o*BA **1b** in combination with the Cy5 1,2-diamine **2b** shows much more significant conjugation with a significant drop in Cy3 emission intensity (Fig. 25) after 100 cycles (~ 25 min). This is a result of the known lower dissociation constant for the diamine relative to a standard amine.¹² The Cy5 1,2-aminothiol derivative **2c** shows a similar result to the 1,2-diamine **2b** species, with a significant drop in Cy3 emission intensity (Figure 26), which also shows significant conjugation at these concentrations. The result of the hydroxylamine **2d** in combination with *o*BA **1b** showed similar promise to the early FRET data recorded on the plate reader. The hydroxylamine proves to form a very effective *o*BID over 100 cycles, with the stepwise drop in Cy3 emission from an emission intensity from high Cy3 emission to low Cy3 emission over 100 cycles (Figure 27), recorded 15 seconds apart. The hydrazine component **2e** in combination with *o*BA **1b** showed similar results to the others, but Cy3 emission did not drop as much as those for **2c** and **2d** after 100 cycles (Fig. 28).

Although this preliminary data showed promising results with a drop in emission intensity for each conjugate, we were unable to accurately quantify the gradual reduction in this emission intensity at these concentrations. These reactions were performed with 5 μM of the Cy3-oBA **1b**, and 50 μM of Cy5 amine derivatives **2a-e**, under pseudo first order conditions. It was observed that at these concentrations, the reaction was reaching equilibrium too fast with only the tail end of the data being recorded, and therefore the kinetics of the system were hard to analyse. For more precise and conclusive results, we aimed to reduce the rate of reaction leading to a more gradual decrease in emission intensity. This was done by screening a range of concentrations, between 100 nM-25 μM under both pseudo-first order and second order conditions. Using pseudo first order conditions, the conjugation reaction was complete before the first measurement was taken, and therefore was unsuitable. Using second order conditions at 2.5 μM Cy3 dye and 2.5 μM Cy5 dye, we observed a gradual decrease in emission intensity over the first 1000 sec of the reactants. This result highlighted the need to monitor these interactions using FRET when considering such small changes in concentrations could affect these results significantly, due to the high k_1 values. The concentrations necessary are too small to be monitored by alternative techniques such as NMR. In light of how rapid these oBID linkages were anticipated to form, we therefore opted that future measurements would be conducted with 2.5 μM concentrations, to track this conjugation.

1.3.2. Second-Order Fluorimeter Measurements

Subsequent FRET studies were carried out under second-order conditions where Cy3-oBA **1b** was mixed in a cuvette with Cy5 amine-based nucleophiles **2a-e** at a concentration of 2.5 μM each in PBS (pH 7.4, experiments run in triplicate). The cuvette was excited at 480 nm, and the emission was monitored between 520-700 nm every 15 sec for ~25 mins. Fig 30-36 show the raw data of the emission intensities from a fluorimeter, which can be used to show the extent of oBID formation, by monitoring a drop in Cy3 emission.

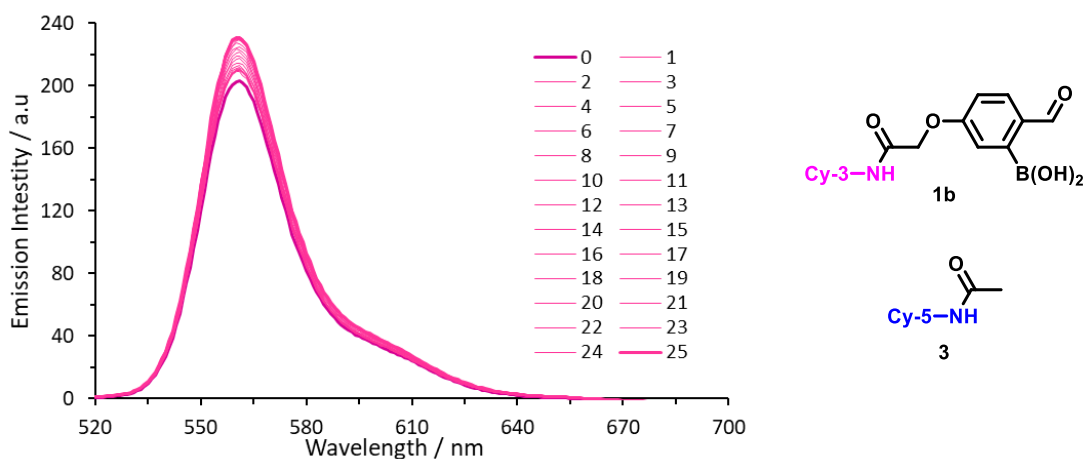


Figure 28: Emission spectra between 520-700 nm, following excitation of a mixture of Cy3 oBA **1b** with the negative control Cy5 acetate capped **3** at 480 nm at $t \sim 3$ sec.

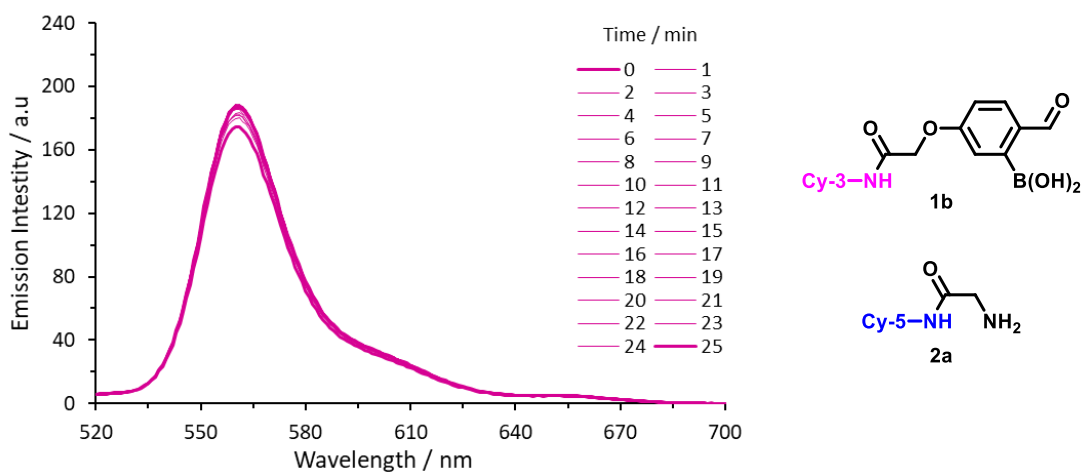


Figure 29: Emission spectra between 520-700 nm, following excitation of a mixture of Cy3 oBA **1b** with the Cy5 amine **2a** at 480 nm at $t \sim 3$ sec.

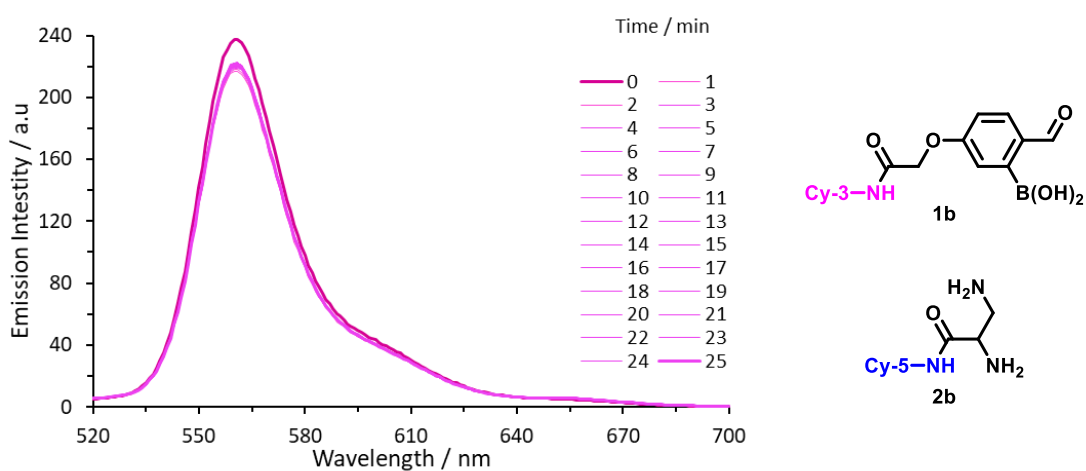


Figure 30: Emission spectra between 520-700 nm, following excitation of a mixture of Cy3 oBA **1b** with the Cy5 1,2-diamine **2b** at 480 nm at $t \sim 3$ sec.

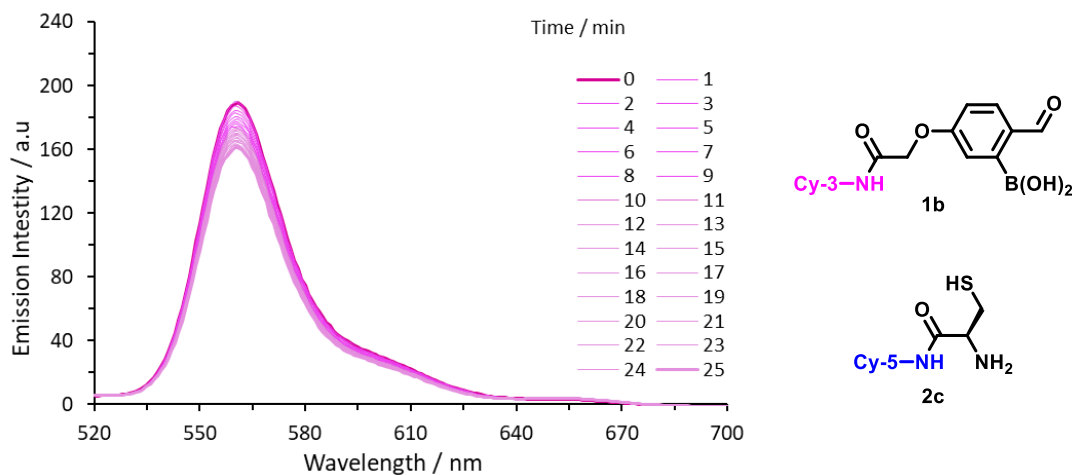


Figure 31: Emission spectra between 520-700 nm, following excitation of a mixture of Cy3 oBA **1b** with the Cy5 1,2-aminothiol **2c** at 480 nm at $t \sim 3$ sec.

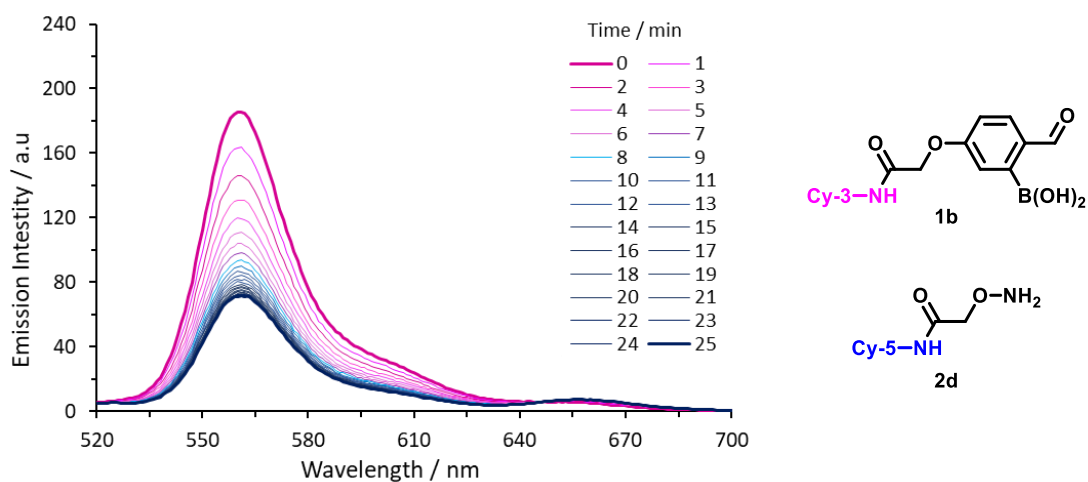


Figure 32: Emission spectra between 520-700 nm, following excitation of a mixture of Cy3 oBA **1b** with the Cy5 hydroxylamine **2d** at 480 nm at $t \sim 3$ sec.

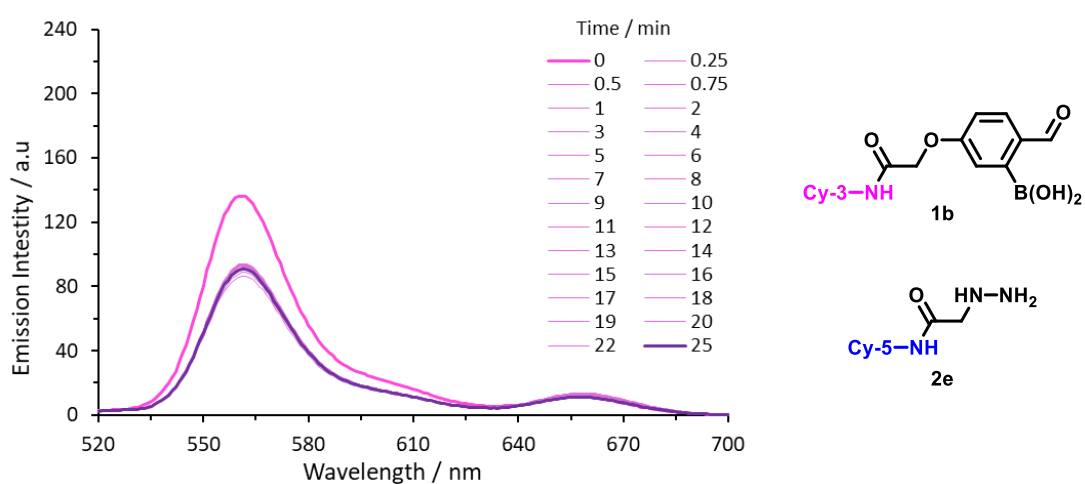


Figure 33: Emission spectra between 520-700 nm, following excitation of a mixture of Cy3 oBA **1b** with the Cy5 hydrazine **2e** at 480 nm at $t \sim 3$ sec.

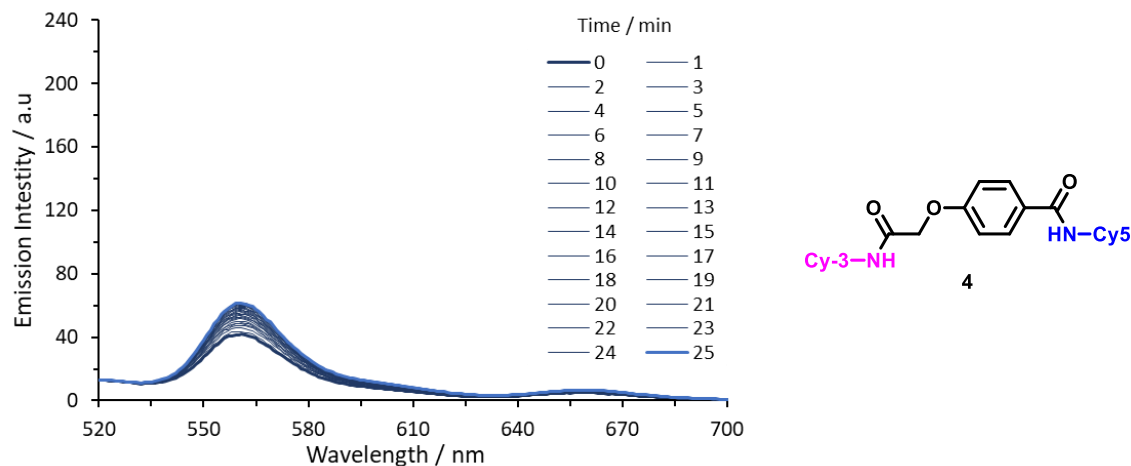
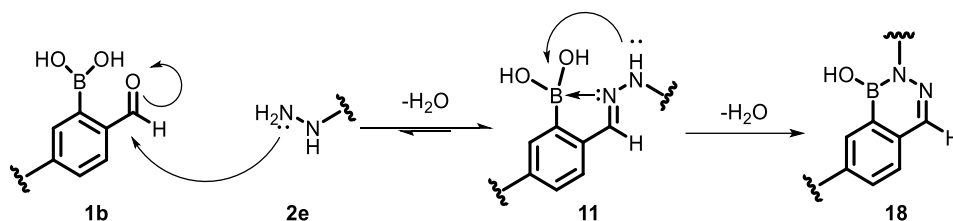


Figure 34: Emission spectra between 520 - 700 nm, following excitation of a covalently conjugated Cy3-Cy5 positive control **4** for this reaction at 480 nm at $t \sim 3$ sec.

For the 0% reference high emission intensity was observed. Conversely, Fig. 34 shows the 100% bound reference of the covalently linked conjugate **4**, for which the Cy3 emission was very low, indicating that FRET was constantly occurring. Fig. 29 shows the amine **2a**, which in combination with oBA **1b**, would form a primary iminoboronate. However, as expected given reports of $K_d \sim 10$ mM,¹⁷ a primary iminoboronate was not found to form to an appreciable extent at at 2.5 μ M concentration over a 25 min period. Therefore, in order to drive the equilibrium towards the iminoboronate formation higher concentrations would be required. Fig. 30 and 31 show the reaction of Cy3-oBA **1b** with 1,2-diamine **2b** and 1,2-aminothiols **2c** respectively. These both exhibit drops in Cy3 emission in comparison to the negative control. TzB formation (Fig. 31) was performed in the presence of TCEP as described above. Fig. 32 shows the reaction of Cy3-oBA **1b**, with hydroxylamine **2d**, which shows a gradual reduction in Cy3 emission intensity indicating oxime formation. This binding was significant, with a reduced emission intensity after 25 min. Finally, Fig. 33 showed the reaction of Cy3-oBA **1b** and the Cy5-hydrazine **2e**, which react together to form a hydrazone/diazaboronate (DAB) conjugate. From this raw data, we see a rapid reaction of hydrazine, even at these very low concentrations of reagents. Fig. 33 shows the reduction in Cy3 emission intensity every 15 sec, rather than every min shown for **2a-d** (Fig. 35-37) due to slower conjugation. This was due to the rapid formation of the hydrazine/DAB complex, with a reduction in emission intensity upon completion. In the first 30 sec, this reaction had already reached equilibrium exhibiting rapid kinetics. This was in line with previous reports, which had only an approximate range of rate constants ($k_1 > 10^4$ M⁻¹ s⁻¹) for hydrazone formation. In order to probe the kinetics of these systems, the reaction of **1b** and **2e** was repeated at 2.5 μ M, however the fluorimeter could still not capture the initial burst in conjugation quick enough. Therefore, the measurements were repeated, this time at 750 nm. At these reduced concentrations, a more gradual though

still fast reduction in Cy3 emission intensity was observed in Fig. 36. The reaction of the Cy3-oBA **1b** with Cy5 hydrazine **2e** shows astonishingly rapid reactions in an aqueous environment. Upon formation of the conjugate, a hydrazone structure is formed, which can subsequently cyclise to form a very stable 6-membered DAB ring **18** (Scheme 3). As shown by Fig. 36, the reaction of Cy3-oBA **1b** and hydrazine **2e** has reached equilibrium with hydrazone **11** and DAB **18** formation within 2 mins, as shown by the plateau data, even at concentrations as low as 750 nM. The significance of this data will be shown in the following section.



Scheme 3: Reaction of oBA **1b** with hydrazine **2e** to form stabilised 6-membered DAB **18** ring via a hydrazone intermediate **11**.

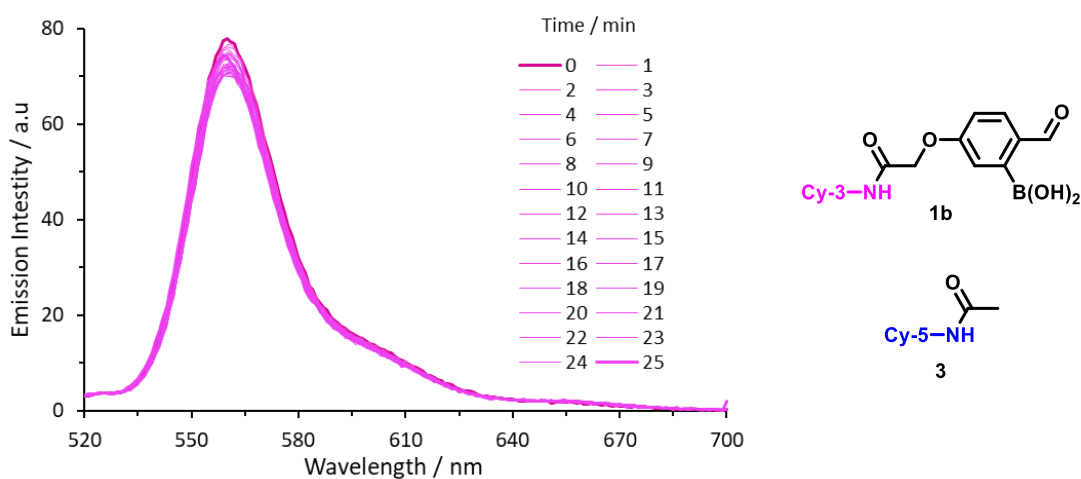


Figure 35: Reduced concentration at 750 nM of each Cy3 and Cy5 dye to show the emission spectra between 520-700 nm, following excitation of a mixture of Cy3 oBA **1b** with the acetate capped negative control Cy5 **3** at 480 nm at $t \sim 3$ sec.

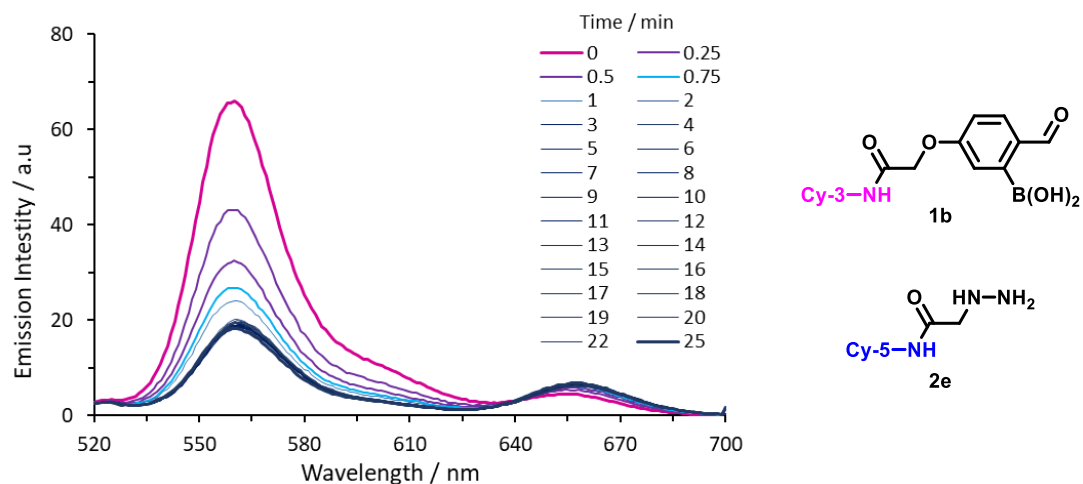


Figure 36: Reduced concentration at 750 nM of each Cy3 and Cy5 dye to show the emission spectra between 520-700 nm, following excitation of a mixture of Cy3 oBA **1b** with the Cy5 hydrazine **2e** at 480 nm at $t \sim 3$ sec.

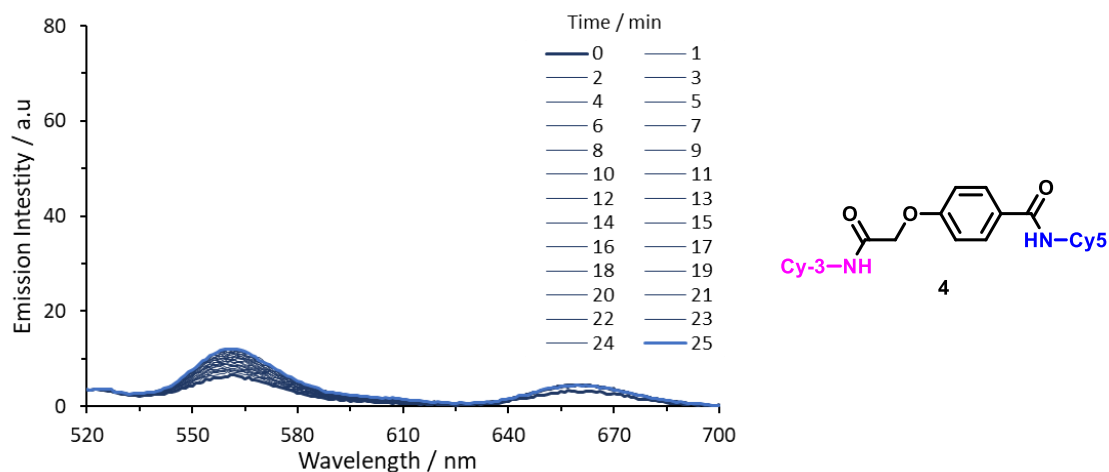


Figure 37: Reduced concentration at 750 nM of each Cy3 and Cy5 dye to show the emission spectra between 520-700 nm, following excitation of a covalently conjugated Cy3-Cy5 positive control **4** for this reaction at 480 nm at $t \sim 3$ sec.

1.4. Lack of Cy5 Emission at 641 nm

As detailed in Chapter 2, Section 1.1, FRET is a non-radiative energy transfer that occurs through dipole-dipole coupling from an excited donor fluorophore to a ground state acceptor.¹⁸ When a donor moiety (Cy3) absorbs light of a particular wavelength, it becomes excited, and would normally release radiative emission energy at a corresponding wavelength (543 nm). However, during FRET a non-radiative energy transfer occurs which excites the acceptor (Cy5), resulting in emission of the acceptor moiety with a maximum of 641 nm (Fig. 38).

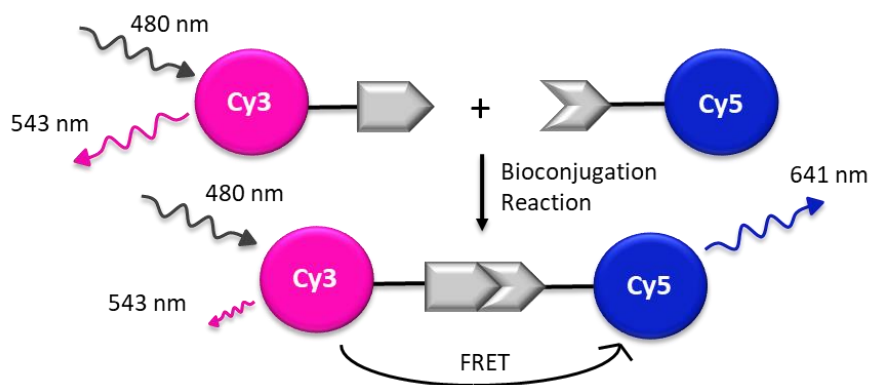


Figure 38: Mechanism to show how FRET works between a donor and acceptor with a proximity dependency.

Whilst we observed a significant decrease in Cy3 emission intensity at 543 nm in the fluorimeter studies, we did not observe a significant increase in the corresponding Cy5 emission channel upon oBID formation. It is noteworthy that the emission of the Cy5 channel did proportionally increase as the Cy3 emission decreased, however this emission intensity was small when compared to the drop in Cy3 emission. This lack of emission intensity at 641 nm could be due to radiative quenching of the excited Cy5 energy state.^{3,11} It is likely that this quenching was due to solvent effects, which would almost completely quench the Cy5 excited state due to the large excess of solvent.¹⁹ Therefore, the reaction was repeated in water, dichloromethane and methanol but no increase in emission at 641 nm was observed under any conditions. It is unlikely that this quenching in emission intensity is due to the free amine of the nucleophile, as the reaction is performed under second order conditions, which reach >95% conversion for the oxime and DAB conjugates and therefore has <5% of amine derivative to quench the emission intensity. Despite this lack of increase in emission intensity at 641 nm, we are confident that the conjugation reactions proceed, which subsequently result in the FRET process occurring. Many control reactions were set up during the course of the FRET studies, which showed that reaction between oBA **1b** and nucleophiles that were not functionalised with a Cy5 acceptor moiety did not lead to a change in Cy3 emission. Cy3 oBA **1b** was reacted with a hydroxylamine **12** and hydrazine **13** moiety, which had a propyl group substituted for a Cy5 group, to analyse if they affected Cy3 emission intensity (Fig. 39). Hydroxylamine **12** and hydrazine **13** nucleophiles were selected as there were considered to be the strongest nucleophiles in the reaction series.

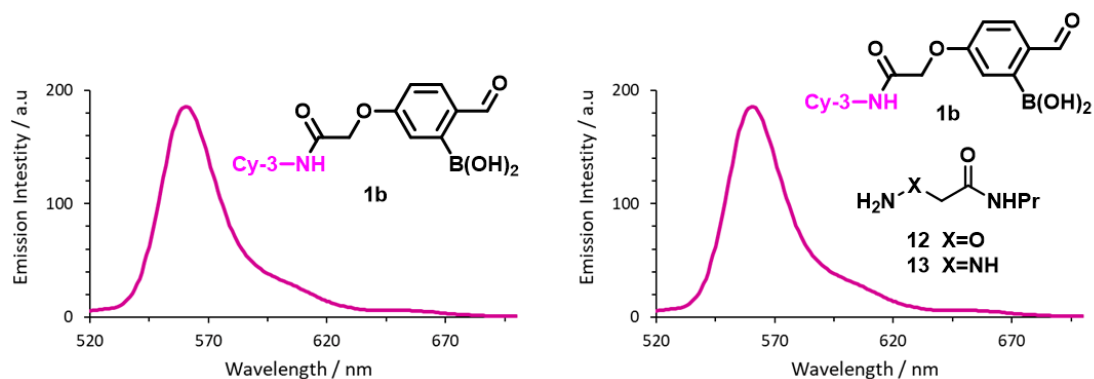


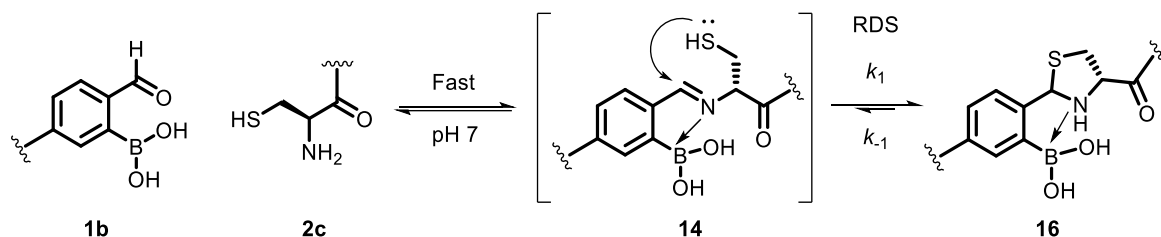
Figure 39: Experiment to show that hydroxylamine **12** and hydrazine **13** has no effect on Cy3 oBA **1b** emission intensity.

The emission intensity in the Cy3 channel remained constant upon the addition of hydroxylamine and hydrazine nucleophiles, which proved that the Cy3 dye was not simply breaking down, which confirmed that energy transfer was taking place between the two dyes specifically upon conjugation. Crucially, for the positive control reaction containing an irreversibly bound reference sample **4**, we observed a similar emission at 641 nm as we did for reactions with the oxime or DAB conjugates, indicating that fluorescence quenching of the Cy3 channel is happening in both instances. Therefore, we can be confident that the drop in Cy3 emission at 543 nm that we observe during these studies is as a result of conjugation and subsequent FRET, despite the lack of increase in emission at 641 nm.

1.5. Extrapolation of Conversions

Using the raw fluorescence data from the fluorimeter recorded above, as well as the positive and negative controls, the data could be converted from Cy3: Cy5 emission ratios to conversions over time. A ratio between the Cy3 and Cy5 emission was calculated to give a FRET ratio, which was then converted into conversion as detailed in the experimental. Conversion plots are shown below (Fig. 40). The data was fitted using second order reversible or irreversible models,^{7,20} and the errors were calculated from the standard deviation of experiments run in triplicate. As a result of a lack of binding a conversion plot could not be generated for the amine (**2a**) conjugate at 2.5 μM concentration over a 25 min period, as the conversion was within the error of the system. The formation of IzB (**15**, orange fit,) and TzB (**16**, green fit) were found to fit a reversible second-order kinetic model, allowing us to extrapolate k_1 and k_{-1} and thus K_d .²¹ Although the overall position of equilibrium for both IzB and TzB was similar ($K_d \sim 4\text{-}5 \mu\text{M}$), IzB **15** was found to form at an order of magnitude higher rate than TzB **16** ($\sim 9900 \text{ M}^{-1} \text{ s}^{-1}$ vs. 610

$M^{-1} s^{-1}$), highlighting the thiol cyclisation as rate-limiting for the formation of a stable TzB conjugate **16** via a rapidly forming intermediate **14** (Scheme 4).



Scheme 4: Thiazolidino boronate **16** formation through a rate-determining cyclisation step.²²

Despite the need to use 100 equiv. of TCEP for TzB formation, the errors between triplicate measurements remain very small indicating accurate and reproducible measurements. The practicality issue of requiring 100 equiv. TCEP in future applications is something which should be considered when choosing between oBIDs. This could hinder TzB chemistry *in vitro* as it requires high concentration of TCEP to break up disulphide linkages which may not be biocompatible. Though our results are in line with previous reports on TzB **16** formation,¹² the rate of IzB **15** formation was found to be accelerated by a factor of 10, relative to literature precedent.²³ This difference could be attributed to the use of functionalised 2-borono-4-alkoxy-benzaldehyde handles within our studies, in contrast to the FPBA model used in the previous reports. This result therefore highlights the critical importance of studying derivatised oBIDs which more accurately reflect the substrates used in real-world applications. Moreover, our measurements were insensitive to the mixtures of diastereoisomers which complicate NMR analysis of IzB and TzB formation, providing further benefit over previous analyses.^{5,23}

The formations of oxime (**17**, red fit) and hydrazone/DAB (**18**, blue fit) were found to fit an irreversible second-order model, and so k_1 was calculated from plots of inverse reagent concentration against time.^{7,20} Calculation of k_{-1} and K_d values via alternative methods are detailed in Chapter 4 Section 1, but are included in Table 1 for completeness. The rate of oxime formation and dissociation constant ($k_1 \sim 5000 M^{-1} s^{-1}$; $K_d \sim 10$ nM) is in line with previous reports by Schmidt et al. ($k_1 \sim 1100 M^{-1} s^{-1}$; $K_d \sim 25$ nM). Interestingly, this previous work studied the reactivity of 2-borono-5-alkoxy analogues that are also used in this work, again highlighting the contributions of stereoelectronic arrangements to oBA reactivity. Experimental data (grey points) deviate slightly from the irreversible kinetic model which could suggest some reversibility of oxime formation, which was investigated further in Chapter 4, Section 1.5.

The reactivity of hydrazine with FPBA has been extensively studied by previous groups, which report hydrazone intermediates can form before an eventual DAB **18** thermodynamic product, but have failed to report precise rates of formation and dissociation constants.¹⁹⁻²¹ These reports which use alternative approaches to probe DAB formation such as UV/Vis titration and NMR experiments are unable to provide kinetic resolution of such exceedingly rapid reactions.^{6,24,26} This shortcoming further highlights the benefit of analysing all conjugated products collectively, rather than individual structures which may complicate or be neglected using other techniques. We report a rate of formation ($k_1 = 169030 \pm 6962 \text{ M}^{-1} \text{ s}^{-1}$) which is amongst the fastest bioconjugation reactions known in the literature. The large error in this study is noteworthy, with large standard deviations in studies with high conversion, causing the hydrazine study to exceed 100% conversion. All measurements, including positive and negative control measurements were measured in triplicate. For the reference molecules **3** and **4**, FRET ratios were very low, and therefore even small variations in the data, leads to large margins of error at >95% conversion. This is particularly exacerbated for exceptionally fast reactions which near conversion in ~50 seconds as seen for DAB **18**. Thus, these errors are minimised by conducting measurements in triplicate and at lower concentrations of 750 nM, which meant that the conversions remain at <100% as expected. With these remarkably rapid reactions, this opens many avenues of applications in bioconjugation chemistry, which could be used to covalently attach two biomolecules together selectively.

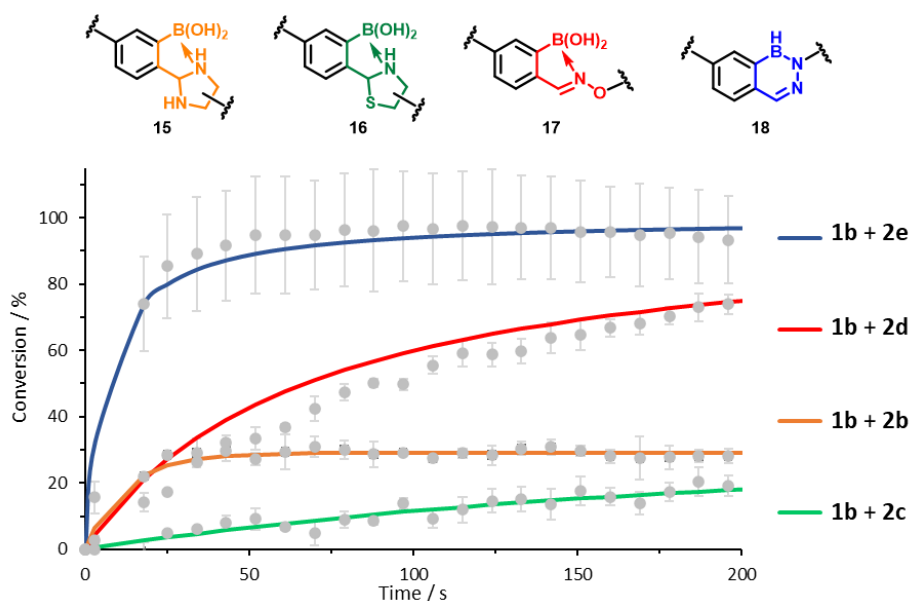


Figure 40: Plot of reaction conversion against time for the formation of 9-12 from Cy3-oBA **1b** with Cy5 amine derivatives **2b-e** in PBS solution at 2.5 μM under second order conditions using fluorimeter data. Fits are based on second-order reversible (**9** and **10**) or irreversible (**11** and **12**) model, with errors based on the standard deviation of experiments run in triplicate.

Table 1: Tabulated dissociation (K_d) and rate (k_1 , k_{-1}) constants for the formation of oBIDs **9-12** in PBS solution

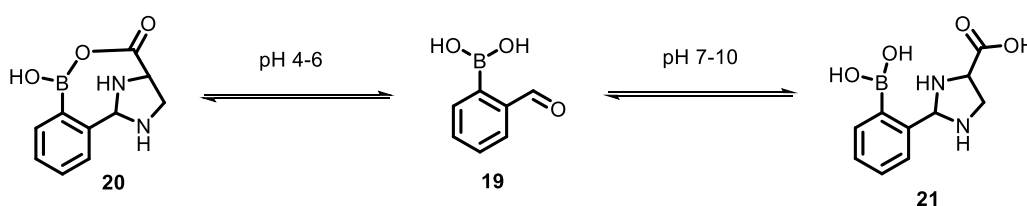
	pH	$k_1 / M^{-1} s^{-1}$	k_{-1} / s^{-1}	K_d
1b + 2a	7.4	-	-	-
1b + 2b	7.4	9883 ± 978	$4.02 \pm 0.45 \times 10^{-2}$	4.3 μ M
1b + 2c	7.4	613 ± 16	$3.01 \pm 0.11 \times 10^{-3}$	4.9 μ M
1b + 2d	7.4	4370 ± 164	$5.61 \pm 1.28 \times 10^{-5}$	12 nM
1b + 2e	7.4	169030 ± 6962	$2.60 \pm 0.55 \times 10^{-6}$	15 pM

1.6. pH Dependency of oBID Formation

We next went on to study the reaction kinetics of oBID formation across pH 6-8 to analyse the effect pH might have on the rate of formation, and corresponding dissociation constants. Many groups have independently studied the pH dependency of oBID formation, but as mentioned previously, these singular and incomplete measurements may lead to significant discrepancies between literature values. Performing these studies under exactly the same conditions allowed us to standardise measurements. As oBIDs contain a series of protonated intermediates at pH 7.4, each with various pK_a values, the change in pH is known to have a significant effect on the rate of formation as well as the dissociation constants. When applying these systems in real-life applications, changes in pH could be used as a switch to associate and dissociate these dynamic linkages.

1.6.1 pH 6

Conducting these studies at pH 6 meant that the studies were conducted under more acidic conditions than those at neutral pH (Fig. 41). The formation of IzB **15** showed no conversion at pH 6 when accounting for error and noise within our calculations. It is noteworthy that Li *et al.* previously reported that the carboxylic acid of diamino propionic acid was able to cyclise to form a mixed boron-carbon anhydride structure **20** which was actually favoured at pH 6 and stabilised by IzB formation (Scheme 5).



Scheme 5: imidazolidino boronate conjugation at varied pH, to show standard IzB formation between pH 8-10 and further cyclisation between pH 4-6.²⁷

However, when the 1,2-diamine **2b** is conjugated to a functional cargo, as in our system, no such interactions are possible. This demonstrates further the importance of studying models relevant to real-world functional applications.²³ The rate of formation of TzB **16** at pH 6 ($\sim 250 \text{ M}^{-1} \text{ s}^{-1}$) was slightly slower than that at pH 7.4 ($\sim 600 \text{ M}^{-1} \text{ s}^{-1}$), which owes itself to the thiol cyclisation rate-limiting step, which would be partially deprotonated at pH 7.4 and plays a key role in TzB formation. For the formation of oxime **17** conjugate, k_1 at pH 6 ($\sim 3000 \text{ M}^{-1} \text{ s}^{-1}$) was slightly slower than k_1 at pH 7.4 ($\sim 4300 \text{ M}^{-1} \text{ s}^{-1}$) but showed similar dissociation constants (12 nM vs. 19 nM). Hydrazone/DAB **18** formation rates were severely reduced at pH 6 ($\sim 23000 \text{ M}^{-1} \text{ s}^{-1}$) versus pH 7.4 ($\sim 170000 \text{ M}^{-1} \text{ s}^{-1}$) by more than an order of magnitude. In a more acidic environment, the NH_2 group of the hydrazine could become protonated, with the protonated NH_3^+ group being a weaker nucleophile, leading to a slower rate of formation of DAB **18**. This leads to a corresponding increase in K_d , from $\sim 10 \text{ pM}$ at pH 7.4 to $\sim 300 \text{ pM}$ at pH 6. Despite this reduced rate of formation, DAB formation remains rapid comparatively, necessitating measurements at lowered concentrations (750 nM) to allow sufficient data points for analysis.

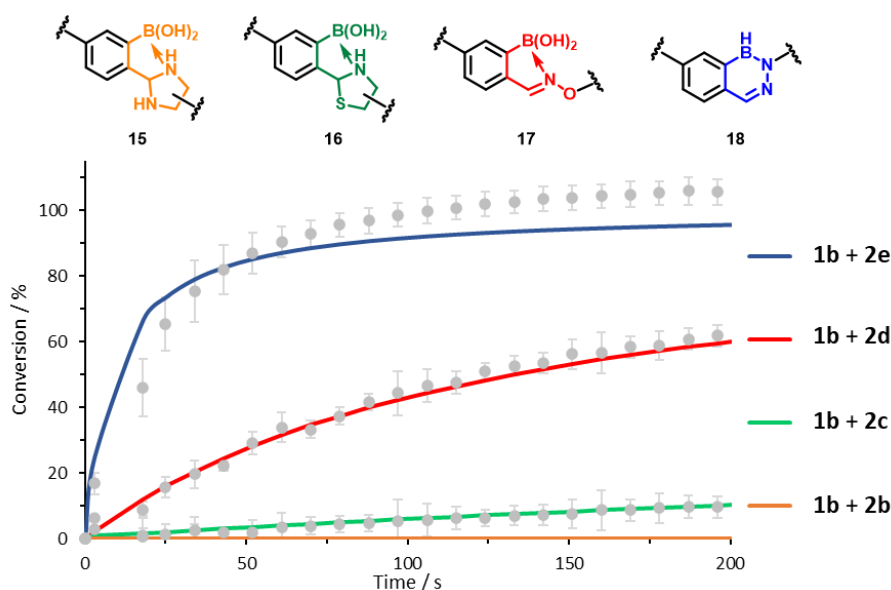


Figure 41: Plot of reaction conversion against time for the formation of **9-12** from Cy3-oBA **1b** with Cy5 amine derivatives **2b-e** at pH = 6 at $2.5 \mu\text{M}$ under second order conditions using fluorimeter data. Fits are based on second-order reversible (**9** and **10**) or irreversible (**11** and **12**) model, with errors based on the standard deviation of experiments run in triplicate.

Table 2: Tabulated dissociation (K_d) and rate (k_1 , k_{-1}) constants for the formation of oBIDs **9-12** at pH 6.

	pH	$k_1 / M^{-1} s^{-1}$	k_{-1} / s^{-1}	K_d
1b + 2a	6	-	-	-
1b + 2b	6	-	-	-
1b + 2c	6	250 ± 3	$1.13 \pm 0.04 \times 10^{-3}$	4.5 μ M
1b + 2d	6	3034 ± 27	$6.04 \pm 1.08 \times 10^{-5}$	19 nM
1b + 2e	6	22920 ± 839	$8.07 \pm 0.29 \times 10^{-6}$	352 pM

1.6.2. pH 8

These dynamic linkages were then tested at pH 8, to provide a slightly more alkali environment. Firstly, IzB **15** formation was significantly accelerated at pH 8 ($k_1 \sim 17500 M^{-1} s^{-1}$), with a corresponding small increase in stability. This increase in formation may have been due to the increase in rate of formation of the imidazole ring, which is a rate-limiting step. Similarly, TzB **16** saw a large increase in the rate in formation from $\sim 600 M^{-1} s^{-1}$ at pH 7.4 in PBS, to $\sim 21000 M^{-1} s^{-1}$. This means that TzB **16** formation is significantly quicker at pH 8, presumably due to the accelerated cyclisation of the deprotonated thiolate that forms at higher pH. The stability of the TzB was also increased by a substantial 2-orders of magnitude ($K_d \sim 50$ nM vs. 5 μ M). This exciting result offers possibilities of using the pH changes as a switch to associate and dissociate the oBID linkages. The rate of formation of oxime **17** was reduced slightly, but contributions from accelerated oxime hydrolysis (k_{-1}) on K_d were far more significant leading to K_d s ~ 200 nM. These results are in line with recent work by Han and Domaille,⁷ as well as prior studies from Schmidt *et. al.* showing that borono-oxime stability is highly pH dependent.⁹ Similar to previous studies at pH 6, the rate of DAB formation was slowed slightly at pH 8 when compared to that at pH 7.4, but remains remarkably fast, nonetheless. This also meant that lowered concentrations (750 nM) were necessary to allow sufficient data points for analysis as mentioned previously.

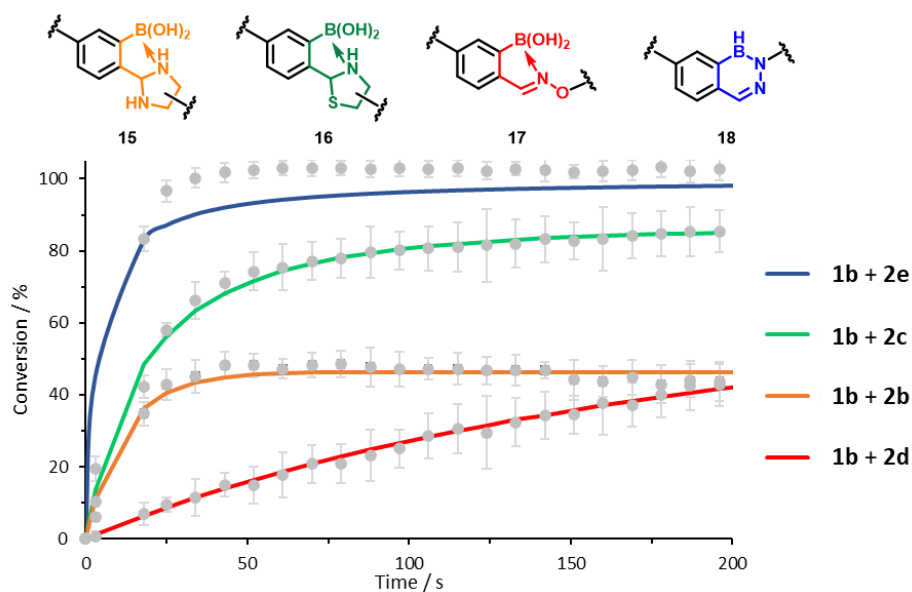


Figure 42: Plot of reaction conversion against time for the formation of **9-12** from Cy3-oBA **1b** with Cy5 amine derivatives **2b-e** at pH = 8 at 2.5 μM under second order conditions using fluorimeter data. Fits are based on second-order reversible (**9** and **10**) or irreversible (**11** and **12**) model, with errors based on the standard deviation of experiments run in triplicate.

Table 3: Tabulated dissociation (K_d) and rate (k_1 , k_{-1}) constants for the formation of oBIDs **9-12** at pH 8.

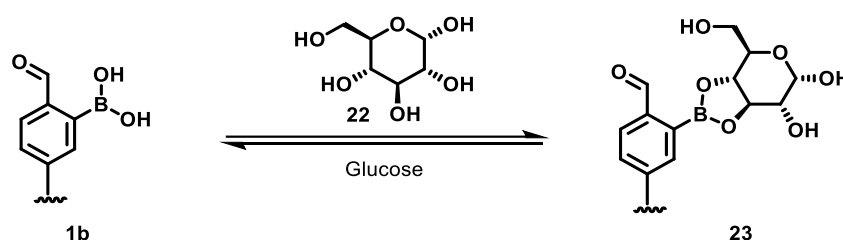
	pH	$k_1 / \text{M}^{-1} \text{s}^{-1}$	k_{-1} / s^{-1}	K_d
1b + 2a	8	-	-	-
1b + 2b	8	17521 ± 1211	2.72×10^{-3}	1.5 μM
1b + 2c	8	21261 ± 591	1.22×10^{-3}	57 nM
1b + 2d	8	1528 ± 10	$3.56 \pm 0.11 \times 10^{-5}$	233 nM
1b + 2e	8	37471 ± 1238	$8.05 \pm 0.26 \times 10^{-6}$	215 pM

1.6.3. pH 4

Studies were performed at pH 4, to further test the hypothesis of a pH switch, as well as considering drug delivery systems which are tested at pH 4 (Fig, 43 and 44). Drugs are taken up into the lysosome of cells where the pH is more acidic (\sim pH 4), before being released into the cytoplasm as the active drug. Therefore, it is necessary to analyse how these oBID linkages form in acidic conditions. Oxime **17** and DAB **18** conjugation were the most stable oBIDs formed from the series and are therefore the most likely drug candidates. Interestingly, despite the significantly lower pH, the oxime conjugate had a $K_d \sim 34$ nM, indicating that acidic pH did not have a detrimental impact on oxime conjugate stability (Fig. 43 Table 4). Conversely, hydrazone/DAB formation at pH 4 was significantly decreased ($k_1 \sim 850 \text{ M}^{-1} \text{ s}^{-1}$), with conjugate stability showing an even more dramatic 6-orders of magnitude drop (K_d 40 μM vs. 15 pM in PBS, Fig. 44, Table 4).

1.7. Reaction Additives

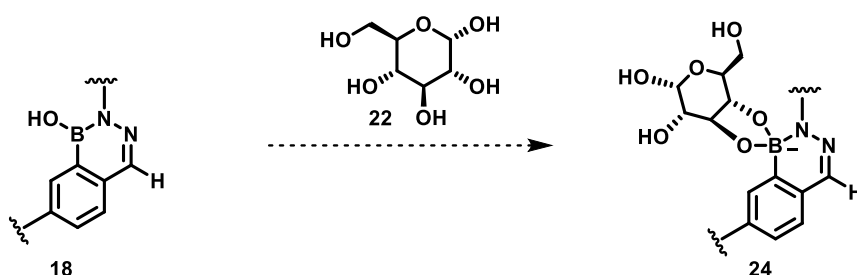
The dynamicity of oBID chemistry provides an exciting prospect for *in vitro* studies, and therefore testing these linkages in the presence of additives that exist in biological systems and buffers are an important factor to explore to implement this chemistry. The presence of biological media or monosaccharides could result in the formation of competing interactions with the nucleophilic amine or the electrophilic aldehyde to prevent oBID formation. The ability to study oBID formation in the presence of such additives, which would otherwise complicate absorbance measurements is a major benefit of our FRET-based platform. Glucose and fructose covalently bind to boronic acids (Scheme 6) stronger than any other naturally abundant sugar and there are many applications in chemical biology based on these interactions.^{28–32} In order for these oBID linkages to be used *in vitro*, they must be tested with biocompatible additives such as sugars, amongst other nutrients needed for the growth of living cells. In a number of reports it has been shown that pre-formed oBIDs are relatively stable to the addition of both glucose ($K_d \sim 10$ mM with phenylboronic acid) and fructose ($K_d \sim 500$ μ M with phenylboronic acid), but less is known about how these sugars affect oBID formation.³³ As oBID formation could be hindered by competing sugars at the boronic acid moiety, then it is important to understand how these sugars bind to oBID complexes. This would also give an insight into how stable these linkages are with respect to small molecule competitors, or if they are reversible to these stimuli. Binding studies were necessary for both the oxime **17** and DAB **18** as these oBIDs show very strong and stable binding across pH ranges 6–8. These reactions were monitored in PBS solution containing 100 mM of either glucose or fructose.



Scheme 6: Glucose reversibly binding to a boronic acid of the oBA moiety (**1b**) to form **23**.

The rates of conjugation were found to be slowed for both oxime **17** and DAB **18** formation, with fructose having a more significant influence in accordance with its higher boronic acid binding ability ($\sim \times 10$ reduction in k_1 for both hydroxylamine and hydrazine reactivity). In the case of the oxime conjugate **17** with fructose, the rate of formation significantly dropped by 2-orders of magnitude (Table 4), which translated to $\sim 10\%$ conversion after 25 min at 2.5 μ M, which reached $>95\%$ conversion after 3h. A corresponding increase in K_d from 12

nM to 571 nM was calculated, which is an overall significant effect on both oBID formation and stability (Fig. 43). This is in contrast to previous reports that suggest minimal influence of sugar additives on the stability of pre-formed oximes.²⁶ This contrast could have been due to the increased sensitivity of our FRET-based platform which gives a further insight into not only the rate, but also the reversibility of the reaction, which was not previously observed by the Gillingham lab, due to the use of high reagent concentrations. Furthermore, it is possible that sugar complexation after oxime formation is no longer favoured, and so tests of stability could give contrasting results to reactions that study formation in the presence of the additive. Hydrazone/DAB formation also has a suppressed rate of formation in fructose by a factor of $\times 10$ (Fig. 44). However, both glucose and fructose showed no effect on k_1 , which suggests that sugars do not complex to DAB **18** after formation (Table 4). This hypothesis seems logical due to the large steric repulsion required for the sugars to bind to the p-orbital of boron in a tetrahedral geometry, following DAB cyclisation **24**. This interaction with the monosaccharides is further unfavoured as a negative charge would have to reside on the boron, further destabilising this species (Scheme 7).



Scheme 7: Proposed binding of glucose with pre-formed DAB oBID conjugate **24**.

To further validate oBID chemistry for *in vitro* and *in vivo* applications, we next studied the formation and stability of oxime and hydrazone/DAB conjugates in 10% bovine serum (Fig, 43 and 44). Bovine serum creates an environment similar to the composition of blood, which has a highly complex composition of proteins, carbohydrates and lipids. Understanding functionalised oBID formation and stability under these conditions is imperative when considering their potential use in drug delivery systems.^{17,34} However, studying conjugation chemistry within serum is highly challenging due to its complex composition with various potential nucleophiles. The limited number of previous studies into oBID formation have relied on high concentrations of reagents that may not truly reflect the end application.^{35,36} In contrast, as background fluorescence within the 520-700 nm window is minimal and can be accounted for, FRET provides us with an ideal means to monitor oBID formation in serum at low μM concentrations. The rate of oxime formation was slowed significantly in the presence of 10% bovine serum ($k_1 \sim 60 \text{ M}^{-1} \text{ s}^{-1}$ vs. 4000

$M^{-1} s^{-1}$ in PBS), and the conjugates were also found to be highly dynamic, with a $K_d \sim 15$ mM being calculated (Table 4). The decrease in reaction rate was even more significant for hydrazine **18**, with a three order of magnitude reduction in k_1 being recorded ($\sim 150 M^{-1} s^{-1}$). Furthermore, conjugation was also found to be dynamic with a $K_d \sim 20$ mM. Since the rate of DAB **18** formation is significantly slower than initial hydrazone formation (Table 4), this data may indicate that the intermediate hydrazone is dynamic in the presence of serum, with implications for oBID formation in complex medias. This result is unsurprising when considering the complex composition of serum, which maybe have many competing side reactions with either of the two orthogonal reactive handles, significantly slowing down the rate of oBID formation. In contrast, when DAB **18** was pre-formed in PBS prior to dilution in 10% serum, the FRET ratio was found to stay unchanged over a period of 25 min. This supports previous reports that DABs are stable in serum, with exciting opportunities for future *in vivo* applications.³⁵ Interestingly, oximes pre-formed in PBS were also observed to undergo minimal change in FRET ratio upon addition of 10% serum, pointing towards a potential role for serum complexation to the oBA precursors *in vitro*, leading to the observed slow formation of **18**. Cumulatively, these results highlight the potential of our platform to give far greater insight into oBID chemistry under relevant conditions to their translational applications, and efforts to explore such factors in high throughput are of high importance to explore the full potential of oBID chemistry.

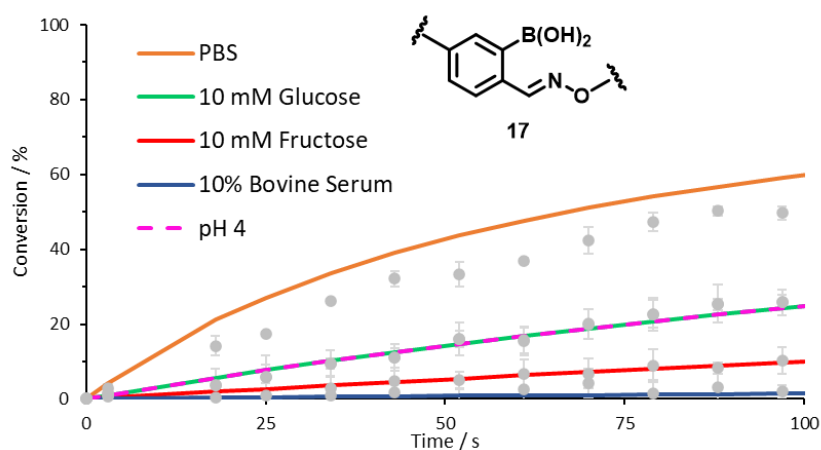


Figure 43: Plot of reaction conversion against time for the formation of **17** from Cy3-oBA **1b** with Cy5 hydroxylamine **2d** in PBS, 10 mM glucose, 10 mM fructose, 10% bovine serum and at pH = 4 using fluorimeter data. Fits are based on second-order irreversible model, with errors based on the standard deviation of experiments run in triplicate. NB: data between 10 mM glucose (green line) and studies at pH = 4 (pink dashed line) are very similar leading to overlap.

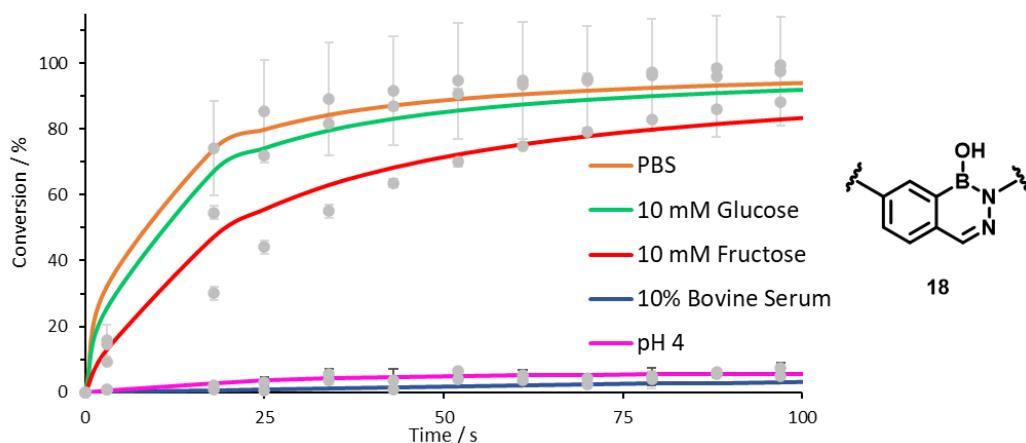


Figure 44: Plot of reaction conversion against time for the formation of **18** from Cy3-oBA **1b** with Cy5 hydrazine **2e** in PBS, 10 mM glucose, 10 mM fructose, 10% bovine serum and at pH = 4 using fluorimeter data. Fits are based on second-order irreversible model, with errors based on the standard deviation of experiments run in triplicate.

Table 4: Tabulated dissociation (K_d) and rate (k_1 , k_{-1}) constants for the formation of oBIDs **9-12** in PBS, 10 mM glucose, 10 mM fructose, 10% bovine serum and at pH = 4

	Additive	$k_1 / M^{-1} s^{-1}$	k_{-1} / s^{-1}	K_d
1b + 2d	-	4370 ± 164	$5.61 \pm 1.28 \times 10^{-5}$	12 nM
1b + 2d	Glucose	1340 ± 10	$2.04 \pm 0.12 \times 10^{-4}$	152 nM
1b + 2d	Fructose	446 ± 4	$2.54 \pm 0.20 \times 10^{-4}$	571 nM
1b + 2d	pH = 4	1517 ± 81	$5.23 \pm 0.56 \times 10^{-5}$	34 nM
1b + 2d	10% Serum	64.0 ± 4.4	$9.03 \pm 2.22 \times 10^{-4}$	14.1 μ M
1b + 2e	-	169030 ± 6962	$2.60 \pm 0.55 \times 10^{-6}$	15 pM
1b + 2e	Glucose	45750 ± 6614	$2.36 \pm 0.50 \times 10^{-6}$	51 pM
1b + 2e	Fructose	16549 ± 1338	$2.35 \pm 0.50 \times 10^{-6}$	142 nM
1b + 2e	pH = 4	876 ± 163	$3.36 \pm 0.70 \times 10^{-2}$	38 μ M
1b + 2e	10% Serum	153 ± 6	$2.93 \pm 0.20 \times 10^{-3}$	19.2 μ M

2. Conclusion

In this Chapter, we have developed a novel FRET-based assay to provide key new insights into the reactivity and stability of *ortho*-boronaldehydes with a series of different amine nucleophiles. This assay has allowed us to quantify conjugation with unprecedented accuracy and sensitivity under standardised conditions. These results therefore highlight the previous discrepancies in the literature which were performed and analysed under various conditions including nucleophiles, analytical techniques and environmental conditions. We found a range in dissociation constants spanning six orders of magnitude in physiological pH, from a IzB conjugate to a stabilised DAB six-membered ring between 4.3 μM and 15 pM respectively. We next went on to conduct standardised studies to show the effects of pH changes from pH 4-8, which too saw a staggering range in dissociation constants. It was found that particular amine-based nucleophiles form stabilised oBIDs between the different pH ranges, due to the varied pK_a values of protonated intermediates. The dissociation constant of the oxime conjugate remained largely unchanged across pH ranges 6-8, with a variation between 12-34 nM which is in contrast to both TzB and DAB conjugates, which were significantly affected by pH. TzB stability ranged greatly with $K_d \sim 5 \mu\text{M}$ between pH 6-7.4, with a two-order increase in stability at pH 8 showing $K_d = 57 \text{ nM}$, highlighting the importance of changes in pH for oBID complexes. DAB complexes suffer a decrease in K_d from pH 7.4 to 8 ($K_d \sim 15 \text{ pM}$ and 38 μM respectively), further consolidating the staggering effect that pH has on oBID formation. The FRET-based assay also displayed its versatility in measurements to track conjugation in the presence of glucose and fructose monosaccharides, as well as studies conducted in 10% bovine serum. oBID formation was observed to proceed in both glucose and fructose, albeit at a slightly reduced rate of formation and subsequently larger K_d values. Monosaccharides were seen to have a limited effect on oBID formation and stability, better suiting oBID chemistry for studies performed in vitro, which would involve monosaccharides as well as other nutrients which could form competing interactions. Boronoimine linkages were seen to be stable in 10% serum when pre-formed but did have a severely reduced rate of formation and stability when performed in serum. This information better suits oBID chemistry for applications in chemical biology, with knowledge in which dynamic linkages are better for a particular application.

3. Experimental

3.1. Determination of Substrate Concentration via UV/Vis Analysis

Due to the low amounts of Cy3 and Cy5 substrates synthesised, and the potential for errors in mass calculations, the concentrations of stock solutions of each substrate were calculated from a calibration curve of **1** or **2** of known concentrations. Briefly, stock dilutions of **1** or **2** were made in water to concentrations in the range of 0.1-400 μM (at least 6 data points). Absorbance spectra were then recorded in the range 400-600 nm, and the absorbance at the λ_{max} plotted as a function of concentration (Cy3: 543 nm; Cy5: 641 nm).

Aliquots of each Cy3 dyes (**1a-e**) and Cy5 dye (**2a-e**) were then serially diluted in water to generate samples for measurement. Concentrations were then determined for appropriately dilute samples for which absorbance at λ_{max} fell within the linear range of the calibration curves.

3.2. Initial Screening of Cy3 Quenching

General procedure: A solution of Cy5-nucleophile (50 μL , 100 μM) in PBS buffer was added to a solution Cy3-oBA **5** (50 μL , 10 μM) in PBS buffer in a 96-well plate, to give final Cy3 and Cy5 concentrations of 5 μM and 50 μM respectively (pseudo-first order). Single-point fluorescence emission intensities ($\lambda_{\text{excitation}} = 480 \text{ nm}$; $\lambda_{\text{emission}} = 580 \text{ nm}$) in the Cy3 channel were then recorded every 1 min for a period of 100 min.

Negative control: Run as for the general procedure, using Cy5-NHAc **16** (50 μL , 100 μM)

Positive control: The emission of a solution of Cy3-Cy5 covalent control **17** (100 μL , 5 μM) was recorded over time as described above.

Data processing: Emission at 580 nm was plotted as a function of time, relative to the negative (100%) and positive (0%) controls.

Cy3 controls: Run as for the general procedure, using either Cy3-benzaldehyde **61** or Cy3-phenylboronic acid **67** (50 μL , 10 μM).

Controls to validate quenching via FRET: Run as for the general procedure, using PrNH-capped nucleophiles **26**, **77**, **79**, **81**, or **83** (50 μL , 100 μM) in place of the Cy5-nucleophile.

3.3. FRET Studies

General procedure: FRET studies were performed in a 700 μL fluorescence cuvette under second-order conditions. A solution of Cy5-nucleophile (300 μL , 5 μM) in the stated buffer was added to a solution of Cy3-oBA **5** (300 μL , 5 μM) in the same buffer and rapidly mixed by pipetting up and down. Fluorescence emission spectra between 520-700 nm were recorded immediately after mixing, and then subsequently every 15 seconds for a total of 100 measurements. The delay between mixing and the measurement of the first spectra was \sim 3 seconds. All measurements were performed in triplicate.

Negative control: Run as for the general procedure, using Cy5-NHAc **16** (300 μL , 5 μM).

Positive control: The emission of a solution of Cy3-Cy5 covalent control **17** (600 μL , 2.5 μM) was recorded over time as described above.

Data processing: The ratio of the emission at the λ_{max} of Cy3 (Emiss_{560}) and Cy5 (Emiss_{657}) was used to determine the FRET ratio ($\text{Emiss}_{560}/\text{Emiss}_{657}$). As the initial spectra were recorded at $t = 3$ sec, a plot of $1/[\text{Emiss}_{560/657}]$ against time and linear regression analysis was used to determine $\text{Emiss}_{560/657}$ at $t = 0$ (intercept of linear regression). A minimum of 4 data points that lay within the initial linear region of this plot were included in this analysis. Emiss_{700} was used as a background measurement and subtracted from $\text{Emiss}_{560/657}$ prior to analysis.

Conversion of FRET ratios to conversion: Data from the positive and negative controls was used to account for drift in the system and to calculate the expected FRET ratio for 0% and 100% conjugation at $t = x$, averaged across three triplicates:

i) *0% conjugation:* Changes in $\text{Emiss}_{560/657}$ from the negative control over the period of the measurement were fitted to a linear regression analysis, generating the gradients of drift $a_{560/657}$. The 0% conjugation FRET reference, A , then equals:

$$A = \frac{{}^0\text{Emiss}_{560} + (a_{560} \times x)}{{}^0\text{Emiss}_{657} + (a_{657} \times x)}$$

ii) *100% conjugation:* Changes in $\text{Emiss}_{560/657}$ from the positive control over the period of the measurement were fitted to a linear regression analysis, generating the gradients of drift $b_{560/657}$ and the emissions at $t = 0$, ${}^0c_{560/657}$. The 100% conjugation FRET reference, B , then equals:

$$B = \frac{{}^0c_{560} + (b_{560} \times x)}{{}^0c_{657} + (b_{657} \times x)}$$

Conversion can then be calculated from:

$$Conversion = \frac{A - FRET}{A - B} \times 100$$

Conversions over time were then averaged over the three triplicates and standard deviations at each time point calculated.

Data fitting: Data were fit to a second order reversible kinetic model in Copasi 4.34.251. k_1 and k_{-1} were estimated using the evolutionary programming method built into the software, with 200 generations and a population size of 20. Parameters were restricted within the confines of: k_1 10^{-6} - 10^7 $M^{-1} s^{-1}$; k_{-1} 10^{-8} - 10^3 s^{-1} .

4. References

1. M. Levitus and S. Ranjit, *Quart. Rev. Biophys.*, 2011, **44**, 123–151.
2. A. P. Demchenko, *Methods Appl. Fluoresc.*, 2020, **8**, 22–41.
3. N. S. James, R. R. Cheruku, J. R. Missert, U. Sunar and R. K. Pandey, *Molecules*, 2018, **23**, 1842–1853.
4. D. K. Kölmel and E. T. Kool, *Chem. Rev.*, 2017, **117**, 10358–10376.
5. D. Bermejo-Velasco, G. N. Nawale, O. P. Oommen, J. Hilborn and O. P. Varghese, *Chem. Commun.*, 2018, **54**, 12507–12510.
6. O. Dilek, Z. Lei, K. Mukherjee and S. Bane, *Chem. Comm.*, 2015, **51**, 16992–16995.
7. G. S. Han and D. W. Domaille, *Org. Biomol. Chem.*, 2021, **19**, 4986–4991.
8. D. Gillingham, *Org. Biomol. Chem.*, 2016, **14**, 7606–7609.
9. P. Schmidt, C. Stress and D. Gillingham, *Chem. Sci.*, 2015, **6**, 3329–3333.
10. H. Faustino, M. J. S. A. Silva, L. F. Veiros, G. J. L. Bernardes and P. M. P. Gois, *Chem. Sci.*, 2016, **7**, 5052–5058.
11. E. Herbst and D. Shabat, *Org. Biomol. Chem.*, 2016, **14**, 3715–3728.
12. S. Cambray and J. Gao, *Acc. Chem. Res.*, 2018, **51**, 2198–2206.
13. K. A. McCarthy, M. A. Kelly, K. Li, S. Cambray, A. S. Hosseini, T. van Opijnen and J. Gao, *J. Am. Chem. Soc.*, 2018, **140**, 6137–6145.
14. L. Raynal, N. C. Rose, J. R. Donald and C. D. Spicer, *Chem. Eur. J.*, 2021, **27**, 69–88.
15. T. M. S. Tang, D. Cardella, A. J. Lander, X. Li, J. S. Escudero, Y.-H. Tsai and L. Y. P. Luk, *Chem. Sci.*, 2020, **11**, 5881–5888.
16. P. M. S. D. Cal, J. B. Vicente, E. Pires, A. V. Coelho, L. F. Veiros, C. Cordeiro and P. M. P. Gois, *J. Am. Chem. Soc.*, 2012, **134**, 10299–10305.
17. S. Chatterjee, E. V. Anslyn and A. Bandyopadhyay, *Chem. Sci.*, 2021, **12**, 1585–1599.
18. T. Förster. Zwischenmolekulare Energiewanderung und Fluoreszenz. *Ann. P.*, 1948, **437**, 55-75
19. A. H. Gore, M. B. Kale, P. V. Anbhule, S. R. Patil and G. B. Kolekar, *RSC Adv.*, 2014, **4**, 683–692.
20. N. C. Rose, A. V. Sanchez, E. F. Tipple, J. M. Lynam and C. D. Spicer, *Chem. Sci.*, 2022, **13**, 12791–12798.
21. A. Dirksen, S. Dirksen, T. M. Hackeng and P. E. Dawson, *J. Am. Chem. Soc.*, 2006, **128**, 15602–15603.
22. A. Bandyopadhyay, S. Cambray and J. Gao, *Chem. Sci.*, 2016, **7**, 4589–4593.
23. K. Li, C. Weidman and J. Gao, *Org. Lett.*, 2018, **20**, 20–23.
24. H. Gu, T. I. Chio, Z. Lei, R. J. Staples, J. S. Hirschi and S. Bane, *Org. Biomol. Chem.*, 2017, **15**, 7543–7548.
25. H. Gu, S. Ghosh, R. J. Staples and S. L. Bane, *Bioconjugate Chem.*, 2019, **30**, 2604–2613
26. C. J. Stress, P. J. Schmidt and D. G. Gillingham, *Org. Biomol. Chem.*, 2016, **14**, 5529–5533
27. K. Li, C. Weidman and J. Gao, *Org. Lett.*, 2018, **20**, 20–23.
28. K. Sugita, Y. Suzuki, Y. Tsuchido, S. Fujiwara, T. Hashimoto and T. Hayashita, *RSC Adv.*, 2022, **12**, 20259–20263.
29. D. B. Cordes, S. Gamsey and B. Singaram, *Angew. Chem. Int. Ed.*, 2006, **45**, 3829–3832.
30. K. Unger and A. M. Coclite, *Biomacromolecules*, 2022, **23**, 4289–4295.
31. J. Ren, H. Hu, S. Wang, Y. He, Y. Ji, Y. Chen, K. Wang, H. Zhang, Y. Zhao and F. Dai, *ACS Appl. Mater. Interfaces*, 2022, **14**, 23182–23193.
32. H. Fang, G. Kaur and B. Wang, *J. Fluoresc.*, 2004, **14**, 481–489.
33. X. Wu, Z. Li, X.-X. Chen, J. S. Fossey, T. D. James and Y.-B. Jiang, *Chem. Soc. Rev.*, 2013, **42**, 8032–8039.
34. J. P. M. António, R. Russo, C. P. Carvalho, P. M. S. D. Cal and P. M. P. Gois, *Chem. Soc. Rev.*, 2019, **48**, 3513–3536.

35. A. Bandyopadhyay, S. Cambray and J. Gao, *J. Am. Chem. Soc.*, 2017, **139**, 871–878.
36. P. Schmidt, C. Stress and D. Gillingham, *Chem. Sci.*, 2015, **6**, 3329–3333.

Chapter Four

Reversibility and Isomeric Studies

Contents

1. Reversibility Studies	164
1.1. Synthesis of non-labelled Nucleophile Derivatives	166
1.1.1. Propyl-Amine Synthesis	166
1.1.2. Propyl-Hydroxylamine Synthesis.....	166
1.1.3. Propyl-Hydrazine Synthesis	167
1.2 Plate Reader Studies	167
1.3. Mechanism of oBID Formation	173
1.4. Fluorimeter Studies	174
1.5. LC-MS Reversibility Studies	175
1.5.1 Synthesis of Methyl–Amine Competitors	176
1.5.2. LC-MS Assay.....	177
2. Alternative <i>ortho</i>-Boronoaldehyde Structures	179
2.1. Synthesis of Cy3-oBA Isomers	180
2.1 1. Synthesis of <i>para</i> -BA, 27a.....	182
2.1.2. Synthesis of <i>para</i> -carboxy oBA, 27b.....	183
2.1.3. Synthesis of <i>meta</i> -phenoxy oBA, 27c	184
2.1.4. Synthesis of <i>ortho</i> -boronoketone, 27d	185
2.2. Plate Reader Isomer Studies	186
2.3. Fluorimeter Isomer Studies	189
2.4. NMR Competition Studies	190
2.5. NMR Kinetic Isomer Studies	197
3 Additional Studies	200
3.1 DAB-Hydrazone pH Study	200
3.2. Glucose and Fructose Binding Study	202
4. Conclusion	207
5. Future Works	208
6. Experimental	209
6.1. Synthesis of Nucleophiles for NMR, LC-MS studies and FRET Controls ...	209
6.2. Synthesis of oBA Substrates for NMR and LC-MS Studies	217
6.3. Initial Screening of Cy3 Quenching	224

6.4. LC-MS Reversibility Studies	225
6.5. NMR Studies of pH Dependent DAB-Hydrazone Exchange.....	226
6.6. NMR Studies of Sugar Binding.....	226
7. References.....	228

1. Reversibility Studies

In this Chapter, we determine the reversibility of oBID linkages, and find how different reaction additives might influence the formation and stability of oBIDs. These studies exploited both FRET, NMR and LC-MS based experiments to determine dissociation (K_d) and rate (k_1 , k_{-1}) constants. We next went on to study the effects of oBA structure on oBID formation, by tuning the electronic and steric configurations of the system.

It would be highly desirable in chemical biology to form covalent bonds which are stable but also reversible under applied stimuli at physiological pH. This would provide a very powerful tool for protein modifications, bioconjugation, bioactive labelling, and functionalisation of materials. For example, it would allow the reversible attachment of a biomolecule to a biomaterial to undergo a function, which can later be detached in a user defined manner. The work described in Chapter 3 demonstrated rapid, covalent and strong oBI bond formation in aqueous media, with a staggering 9-order magnitude range in K_d from 5 pM-300 mM. The tuneable stability of these oBI linkages potentially allows us to alter the dynamic linkages to suit many functions in chemical biology. Therefore, the ability to cleave these bonds is very important to explore.

In Chapter 3, the sensitive and versatile FRET assay we developed allowed us to calculate k_{-1} and K_d for many of the oBIDs studied across the pH range 4-8, as well as in glucose and fructose containing buffers, and in 10% bovine serum. However, for those reactions which went to near completion such as the oxime conjugate, k_{-1} could not be determined by the FRET measurements and therefore further reversibility studies were needed to deduce these values accurately. We first proposed to study reversibility via a fluorescence assay in a 96-well plate format. Initially, oBID linkages would be formed under analogous conditions to those used previously in Chapter 3 Section 1, and then an excess of a competitive nucleophile would be added to see how this affected the emission intensity (Fig. 1). If the Cy3 emission intensity was restored to the levels seen prior to oBID formation this would indicate that the oBID was being cleaved and then trapped by the excess nucleophile and was therefore reversible. Cy3-oBA **1b** could therefore be reacted with each Cy5-amine derivative **2a-e** for 25 mins, at which point an excess of non-labelled nucleophile, 1,2-diamino, 1,2-aminothiols, hydroxylamine and hydrazine could be added (**3a-e**) (Fig. 1).

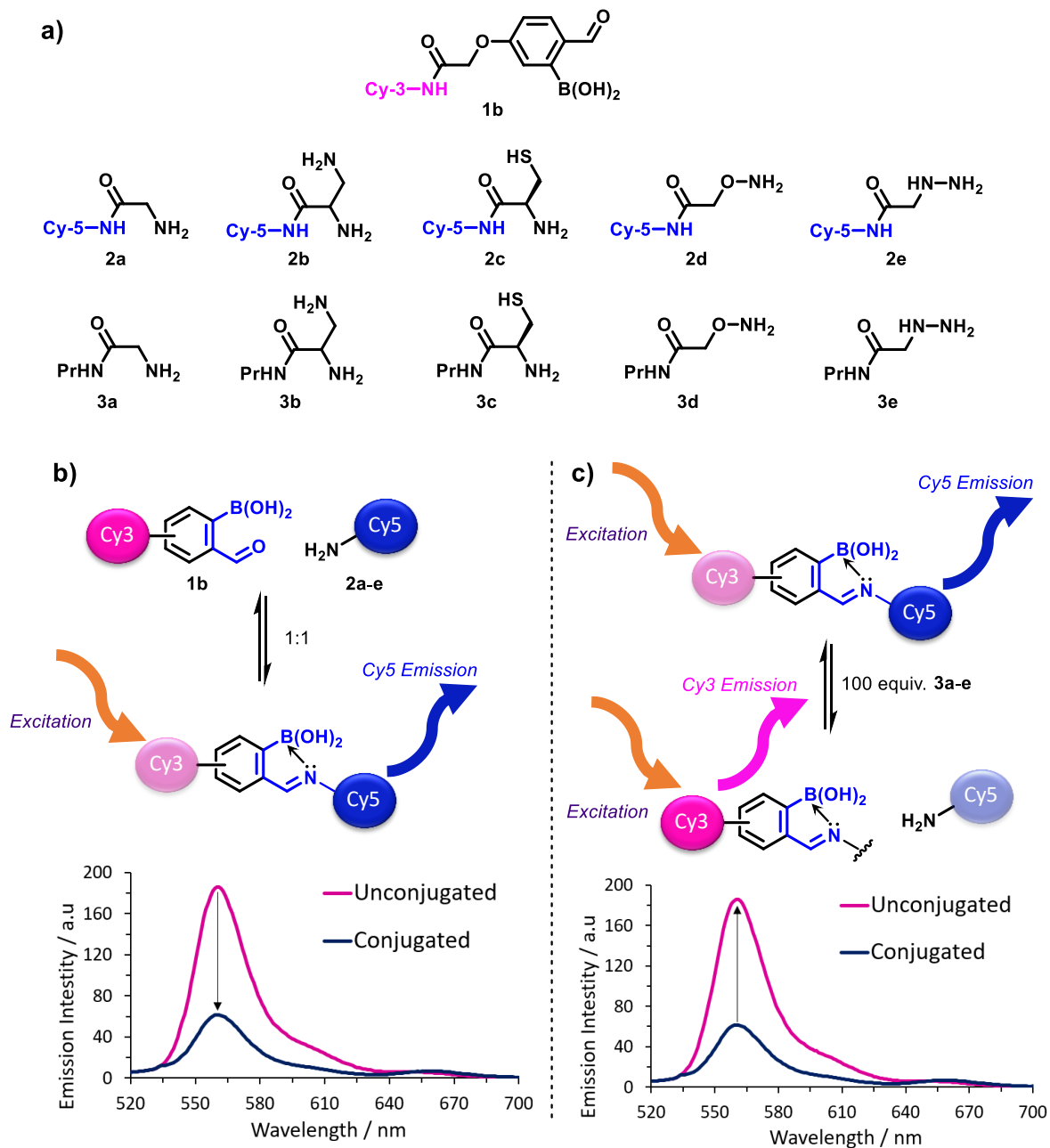


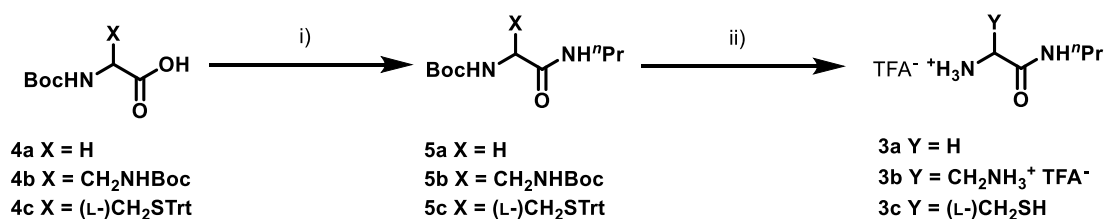
Figure 1: **a)** Synthesised dyes and small molecule derivatives with propyl amide handles to act as trapping agents; **b)** Schematic representation of a drop in Cy3 emission intensity following oBID formation; **c)** Competition assay using a non-labelled nucleophile which does not exhibit FRET, expected to cause an increase in Cy3 emission intensity.

1.1. Synthesis of non-labelled Nucleophile Derivatives

In order to conduct these cleavage studies, non-labelled amine, 1,2-diamino, 1,2-aminothiol, hydroxylamine and hydrazine (**3a-e**) reactive moieties were synthesised, bearing an *n*-propylamide chain rather than a Cy5 dye. Much of the synthesis of the small molecule nucleophile derivatives had similar reaction conditions to Chapter 2 Section 2.2.5.

1.1.1. Propyl-Amine Synthesis

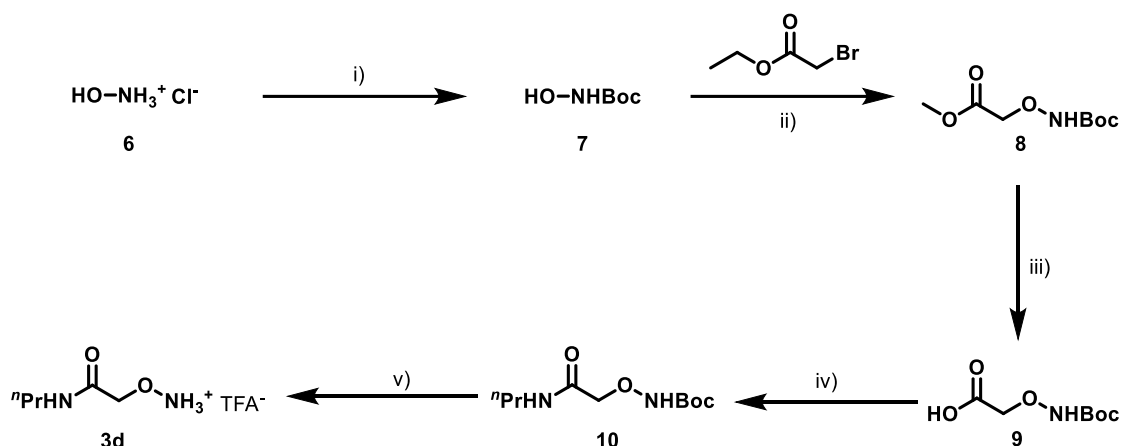
Synthesis of the amine series began with a protected amino acid derivative, whereby the acid groups of **4a-c** were coupled with *n*-propylamine using the optimised amide coupling conditions from Chapter 2 Section 2.5.3, which used T3P, to form **5a-c**. These substrates were then subsequently deprotected in acidic conditions to give the free amine, 1,2-diamino and 1,2-aminothiol compounds **3a-c** as the trifluoroacetate salts (Scheme 1).



Scheme 1: Synthesis of **3a**, **3b** and **3c** for cleavage studies. *Reagents and conditions:* i) Propylamine, T3P, Et₃N, CH₂Cl₂, 0°C-r.t., 16 h, **5a**) 67% **b**) 59% **c**) 63% ii) TFA, CH₂Cl₂, r.t. 3 h, **3a**) quantitative yield; **b**) quantitative yield; **c**) quantitative yield.

1.1.2. Propyl-Hydroxylamine Synthesis

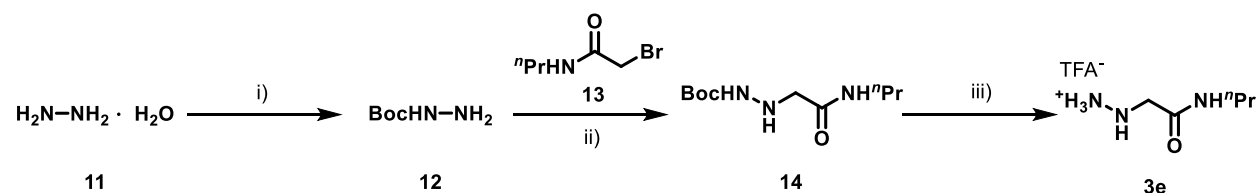
The synthesis of **3d** began with commercially available hydroxylamine hydrochloride **6**, which was protected with Boc anhydride to form **7** and alkylated to form **8**. The methyl ester **8** group which was formed in methanol was then hydrolysed with lithium hydroxide to yield **9**, which was then coupled with *n*-propyl amine to give **10**, before deprotection in acidic conditions to yield the small molecule hydroxylamine compound **3d** (Scheme 2).



Scheme 2: Synthesis of hydroxylamine **3d**. *Reagents and conditions:* i) Boc_2O , NaHCO_3 , $\text{THF}:\text{H}_2\text{O}$ (1:1), r.t., 20 h, 89% ii) KOH , MeOH , 60°C , 16 h, 53%, iii) LiOH , $\text{THF}:\text{H}_2\text{O}$ (1:1), r.t., 16 h, 77%; iv) Propylamine, T3P, Et_3N , CH_2Cl_2 , 0°C -r.t., 16 h, 46% v) TFA , CH_2Cl_2 , r.t. 3 h, quantitative yield.

1.1.3. Propyl-Hydrazine Synthesis

Synthesis of hydrazine **3e** began with commercially available hydrazine monohydrate **11**, which was transformed into hydrazine **3e** in a three-step synthesis. Hydrazine monohydrate **11** was first reacted with Boc anhydride to afford carbamate **12**. **12** then underwent an alkylation reaction with compound **13** to form amide **14** before deprotection in acidic conditions to give hydrazine **3e** (Scheme 3).



Scheme 3: Synthesis of hydrazine small molecule **3e**. *Reagents and conditions:* i) Boc_2O , K_2CO_3 , dioxane and water 1:1, r.t., 16 h, 66%; ii) K_2CO_3 , CH_2Cl_2 , r.t., 16 h, 53%; iii) TFA , CH_2Cl_2 , r.t. 3 h, quantitative yield.

1.2 Plate Reader Studies

With the synthesis of these non-dye labelled nucleophilic trapping agents (**3a-e**) completed (Fig. 2), fluorescence studies could be carried out analogous to those previously described in Chapter 3 Section 2. This time, after formation of the respective oBID's, we hypothesised that the small molecule trapping agents could be added to induce an increase in emission of the Cy3 channel, indicating reversibility. When Cy3 oBA **1b** binds to a non-labelled nucleophile **3a-e**, this essentially occupies the binding site of the Cy3 oBA, which means

it would be unable to bind to the Cy5-amines **2a-e**. Additionally, as the Cy3-Cy5 oBID could be reversible, the small molecule could trap any free oBA as it formed. Therefore, the Cy3-oBA emission at 580 nm would not be quenched by FRET, and we expect to see an increase in Cy3 emission if the oBID linkage is reversible.

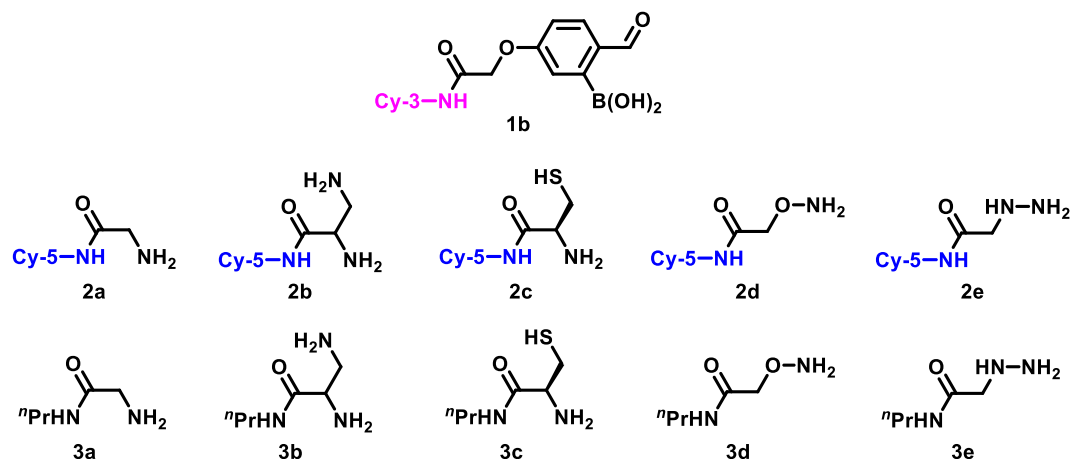


Figure 2: Synthesised Cy3 dye **1b** and Cy5 dyes **2a-e** and small molecule derivatives with propyl amide handles **3a-e** to act as trapping agents.

A 96-well plate assay was initially used to screen which nucleophile was the most effective trapping agent. Initially, Cy3 oBA **1b** was mixed with Cy5 amine-based nucleophiles (**2b-e**), under second order conditions at a concentration 2.5 μ M each. Measurements were taken approximately every 60 sec, for 25 min, which resulted in a gradual decrease in Cy3 emission intensity as a result of oBID formation, as previously observed (**15-19**). After 25 min, when the Cy3 emission had reduced, 10 equivalents (25 μ M) of non-labelled nucleophile competitor (**3a-e**) were added, and further measurements were taken (every 60 sec for 25 mins). The following graphs (Figures 3-7) show the emission at 580 nm (Cy3 channel), after excitation at 480 nm, following the addition of competitor. Only the Cy3 channel was monitored here due to the plate readers limited ability to record single point measurements as covered in Chapter 3 Section 1.2.

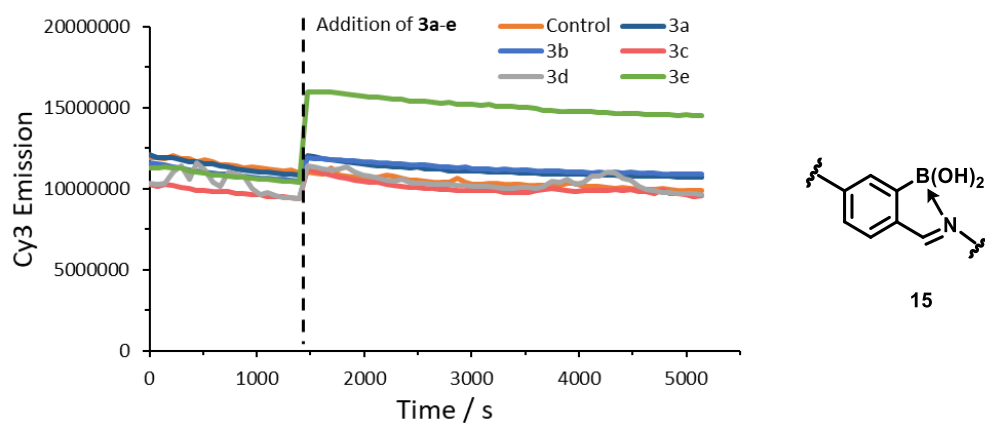


Figure 3: Emission at 580 nm after excitation at 480 nm for Cy3 oBA **1b** with Cy5 amine **2a** reaction for 25 min, followed by addition of non-labelled nucleophile trapping agents (**3a-e**).

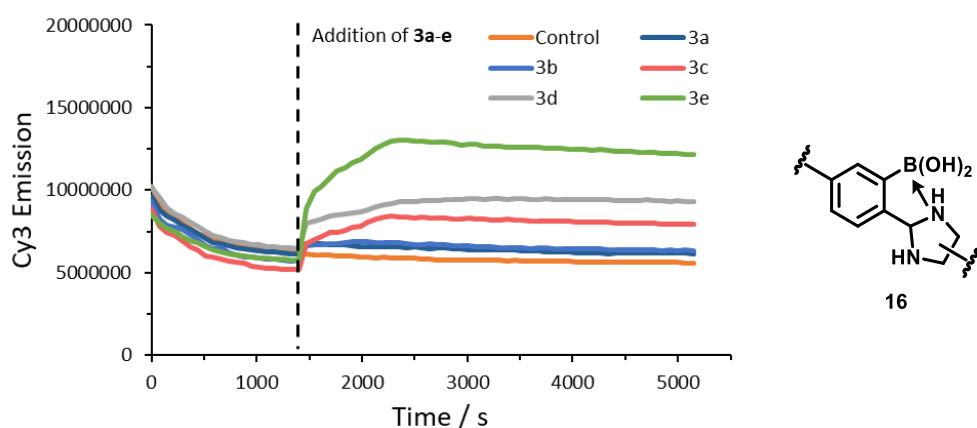


Figure 4: Emission at 580 nm after excitation at 480 nm for Cy3 oBA **1b** with Cy5 1,2-diamine **2b** reaction for 25 min, followed by addition of non-labelled nucleophile trapping agents (**3a-e**).

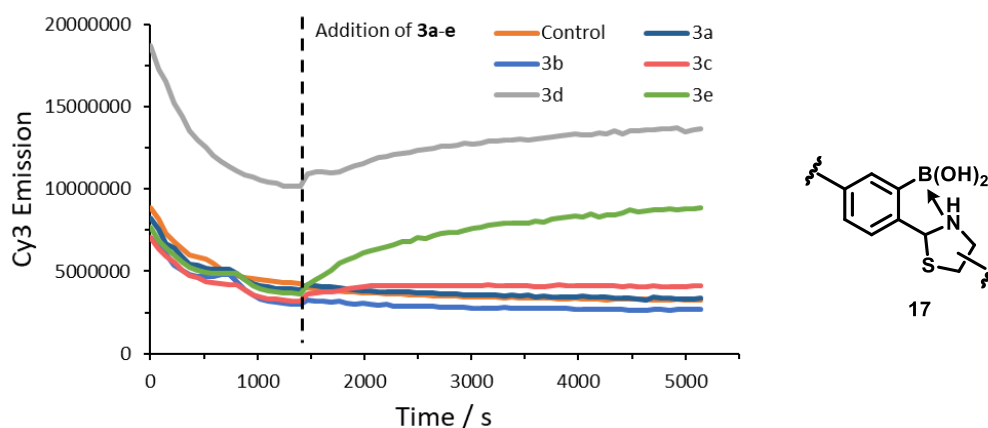


Figure 5: Emission at 580 nm after excitation at 480 nm for Cy3 oBA **1b** with Cy5 1,2-aminothiol **2c** reaction for 25 min, followed by addition of non-labelled nucleophile trapping agents (**3a-e**).

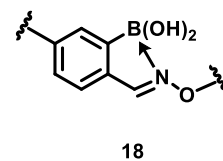
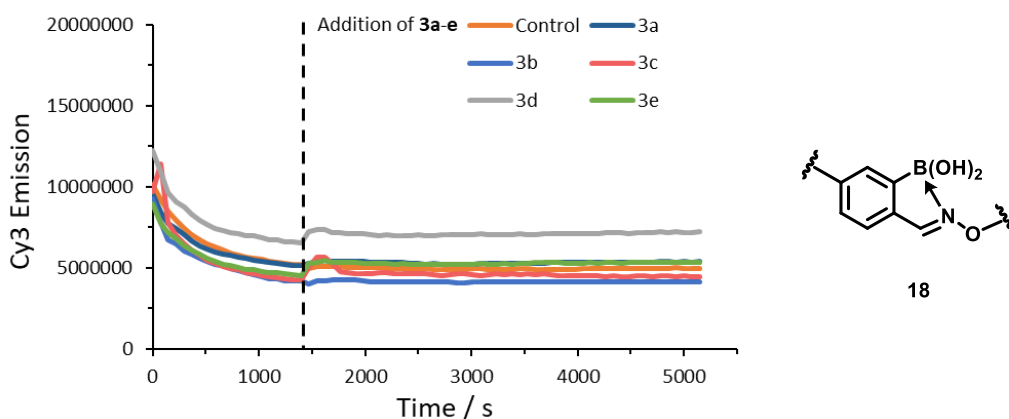


Figure 6: Emission at 580 nm after excitation at 480 nm for Cy3 oBA **1b** with Cy5 hydroxylamine **2d** reaction for 25 min, followed by addition of non-labelled nucleophile trapping agents (**3a-e**).

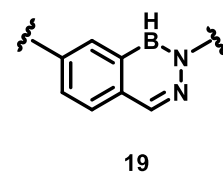
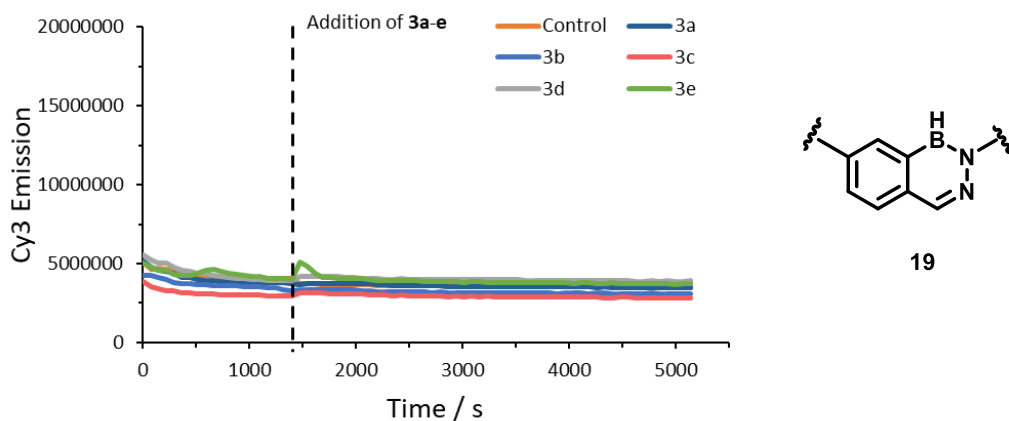


Figure 7: Emission at 580 nm after excitation at 480 nm for Cy3 oBA **1b** with Cy5 hydrazine **2e** reaction for 25 min, followed by addition of non-labelled nucleophile trapping agents (**3a-e**).

Preliminary reversibility studies using the plate reader yielded a mixture of results. It can be concluded that when using 2.5 μM concentration of reagents, the IzB **16** and TzB **17** both show significant reversibility (Fig. 4 and 5). Some restoration of Cy3 emission occurred following the addition of the small molecule hydrazine and hydroxylamine competitor in particular (Fig. 4-7). With respect to the oxime conjugate **18**, there is a very slight increase in Cy3 emission following the addition of the hydroxylamine **3d** and hydrazine **3e** small molecules. This result may have indicated that the oxime conjugate (**1b** + **2d**) exhibited some reversibility, but with the low accuracy of the plate reader, this result could also simply be due to drift in the system. When forming the DAB conjugate **19**, no reversibility was observed, even with the addition of 10 equiv. of hydrazine or hydroxylamine small molecule competitors. On the basis of these results, the cleavage of the IzB **16** and TzB **17** conjugates was further investigated using even higher concentrations (100 and 200 equiv.) of the non-labelled hydroxylamine **3d** and hydrazine **3e** trapping agents to see full reversibility (Fig. 8-12). As these propyl-capped small

molecules **3d** and **3e** were the quickest and most effective competitors for displacement of the respective Cy5 dyes, we chose to focus on these two small molecule competitors. A large excess of **3d** and **3e** was therefore used in the hope to see a restoration of Cy3 emission intensity.

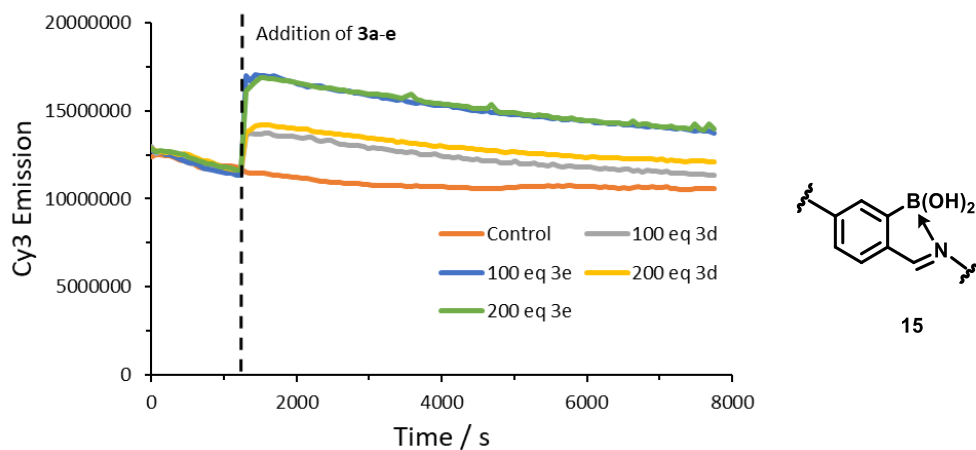


Figure 8: Emission at 580 nm after excitation at 480 nm for Cy3 oBA **1b** with Cy5 amine **2a** reaction for 25 min, followed by addition of 100-200 equivalents of hydroxylamine **3d** or hydrazine **3e** trapping agent.

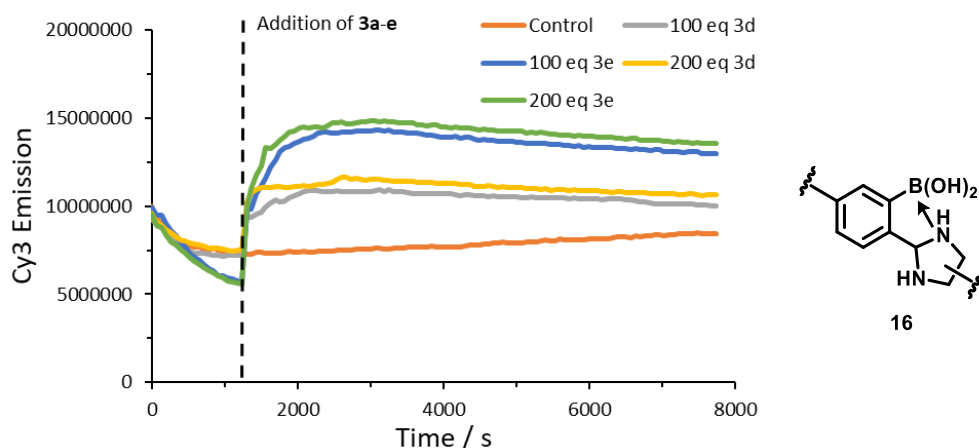


Figure 9: Emission at 580 nm after excitation at 480 nm for Cy3 oBA **1b** with Cy5 1,2-diamine **2b** reaction for 25 min, followed by addition of 100-200 equivalents of hydroxylamine **3d** or hydrazine **3e** trapping agent.

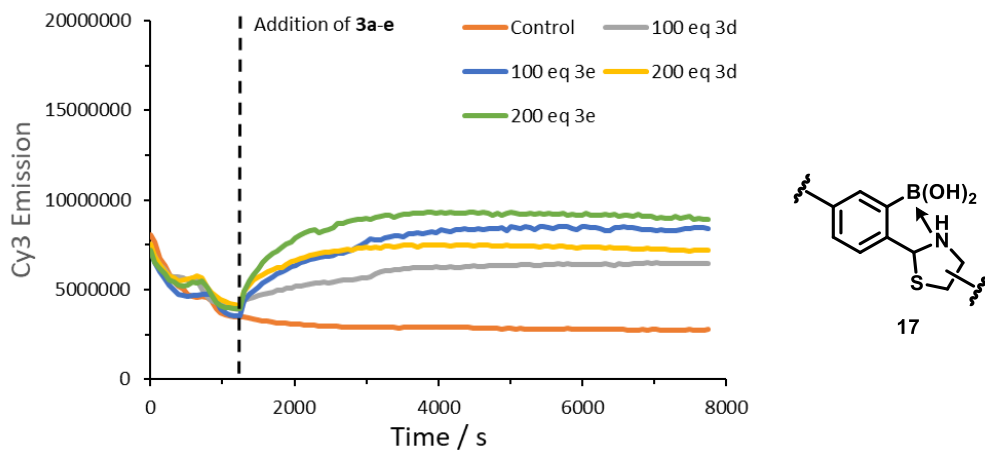


Figure 10: Emission at 580 nm after excitation at 480 nm for Cy3 oBA **1b** with Cy5 1,2-aminothioliol **2c** reaction for 25 min, followed by addition of 100-200 equivalents of hydroxylamine **3d** or hydrazine **3e** trapping agent.

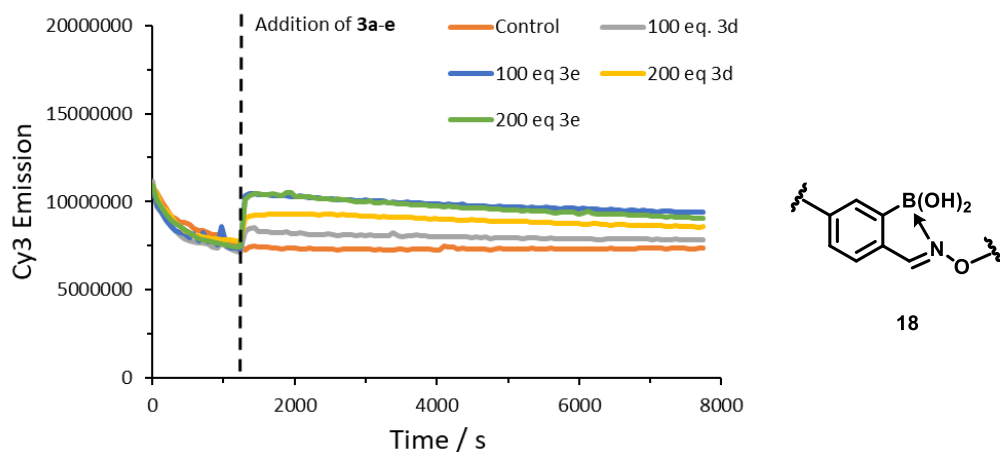


Figure 11: Emission at 580 nm after excitation at 480 nm for Cy3 oBA **1b** with Cy5 hydroxylamine **2d** reaction for 25 min, followed by addition of 100-200 equivalents of hydroxylamine **3d** or hydrazine **3e** trapping agent.

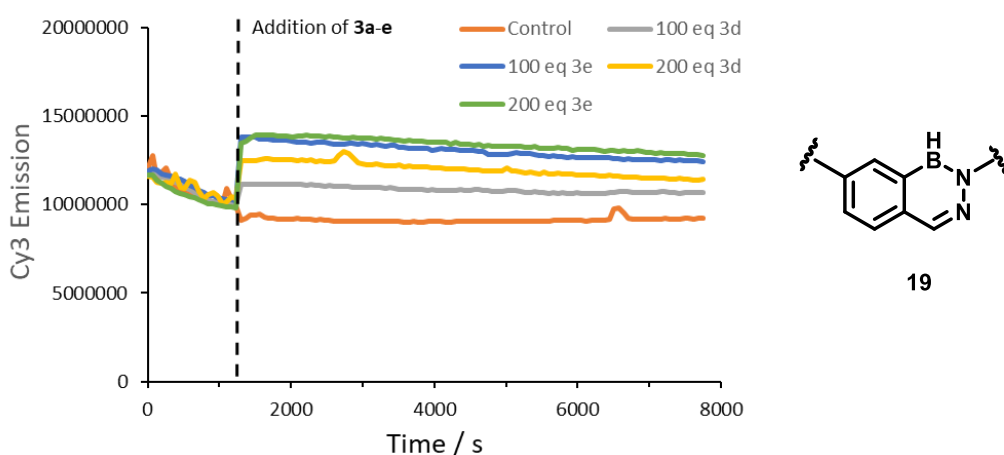


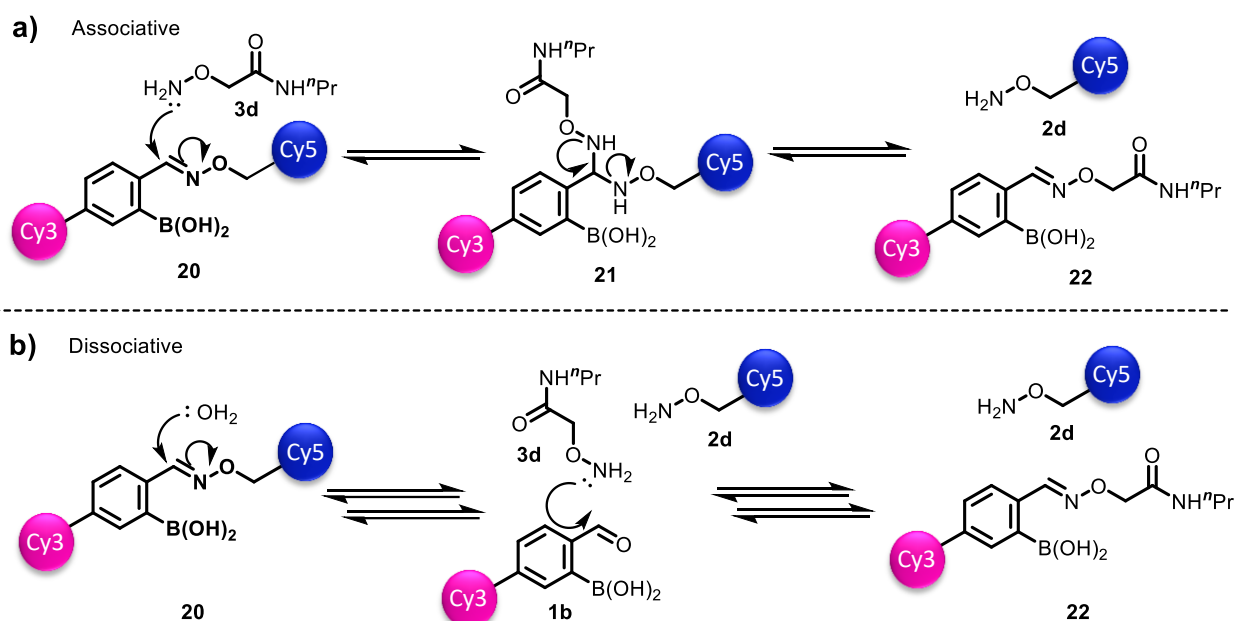
Figure 12: Emission at 580 nm after excitation at 480 nm for Cy3 oBA **1b** with Cy5 hydrazine **2e** reaction for 25 min, followed by addition of 100-200 equivalents of hydroxylamine **3d** or hydrazine **3e** trapping agent.

As seen in Fig. 8-12, with the addition of 200 equiv. of hydrazine **3e**, each of the conjugates shows some increase in Cy3 emission intensity. For the primary amine iminoboronate **15** (Fig. 8), and IzB **16** (Fig. 9), these results suggest that complete reversibility is achieved at these concentrations, as indicated by full restoration of the Cy3 emission intensity. Although the Cy3 emission intensity was not totally restored for TzB **17** (Fig. 10) due to inherent low reproducibility of the plate reader, this preliminary data fit well with the reversibility trend found for these oBIDs in Chapter 3. The hydroxylamine trapping agent **3d** seemed to have slightly slower reaction rates compared to the hydrazine trapping agent **3e**, potentially due to a lower k_1 value as calculated in Chapter 3, which means conducting these studies over a longer period of time may be beneficial for the hydroxylamine trapping agent. In the case of the oxime **18** and DAB **19** conjugates, we did see a small degree of reversibility for both conjugates with excess competitor (Fig. 11 and 12), indicated by the slight increase in Cy3 emission after 25 mins. As larger concentrations of the hydrazine were used, we saw slightly larger increases in the Cy3 emission intensity. Although these results appear promising, the data is caveated by a low reproducibility and some of the variation could be due to experimental error. Nonetheless, these preliminary results suggest that some reversibility was achieved, and further studies were done using a fluorimeter to gain more accurate quantitative results to draw more solid conclusions on the reversibility of these systems.

1.3. Mechanism of oBID Formation

Having analysed the plate reader studies using 10 equiv. of the amine-based trapping agents **3a-e**, it was observed that conjugates with a high rate of hydrolysis resulted in an increase in Cy3 emission intensity. The primary iminoboronate **15**, IzB **16** and TzB **17** all show rapid rates of hydrolysis (k_1), which allows the reformation of an oBA which can then react with a different amine-based trapping agent. Oxime **18** and DAB **19** in contrast seemed to not hydrolyse over the time course of the fluorescence studies. Cleavage of the oBID could either occur via an associative or a dissociative mechanism. In an associative mechanism (Scheme 4a), propyl amide-capped hydroxylamine **3d** would attack at the electrophilic C=N bond of **20** in a reversible reaction. This nucleophilic amine group of **21** then pushes through its electrons, causing the release of the original nucleophile **22** in an associative mechanism. The other possibility is a dissociative mechanism (Scheme 4b), whereby iminoboronate **20** is hydrolysed in water first, followed by the nucleophilic attack of the propyl amide-capped hydroxylamine **3d** to form the subsequent iminoboronate **22**.

An associative cleavage mechanism is linearly dependent on the concentration of the competitor, as it is involved in a cleavage step, and therefore directly impacts the rate of reaction (Scheme 4a). Dissociative cleavage is largely independent of the concentration as the competitor is not involved in the cleavage step (Scheme 4b). Our results using the plate reader and fluorimeter showed that in the case of oxime and hydrazine conjugates, there were no significant changes to the rate of cleavage when using 10, 100 or 200 equivalents of competitor, suggesting cleavage was occurring via a dissociative mechanism.



Scheme 4: Possible mechanism of iminoboronate reaction showing **a)** associative mechanism and **b)** dissociative mechanism.

1.4. Fluorimeter Studies

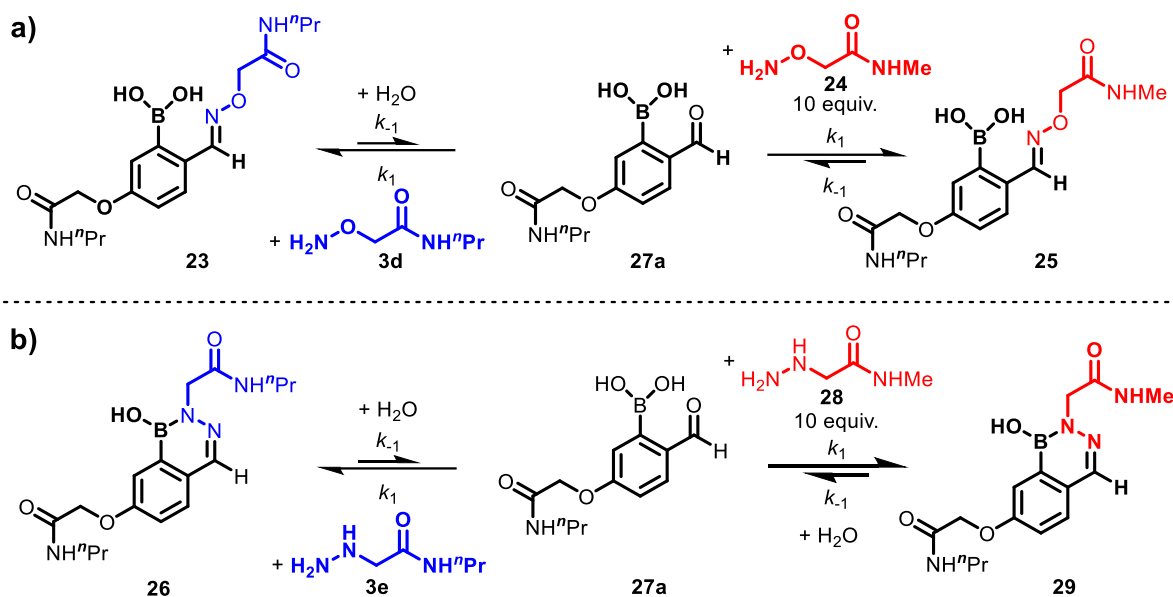
Having performed all of the studies described above using a plate reader in Section 1.3, the results showed a significant degree of reversibility for the primary iminoboronate **15**, IzB **16** and TzB **17** upon addition of trapping agents **3a-e**. We therefore attempted to test the reversibility using a fluorimeter. We first mixed Cy3 oBA **1b**, with Cy5 amine-based nucleophiles **2a-e**. As expected, we saw a drop in Cy3 emission intensity similar to those seen in Chapter 3 Section 1.3 under second order binding conditions. Emission was measured over 520-700 nm following excitation at 480 nm and data was collected every 15 seconds for ~25 min. Following this conjugation, 100 equiv. of hydroxylamine **3d** or

hydrazine **3e** trapping agents were added to induce a restoration of Cy3 emission intensity. If cleavage of oBIDs was occurring, the emission of the Cy3 channel at 580 nm would be expected to be restored following the addition of the trapping agent.

However, despite efforts to measure reversibility using the fluorimeter, the results were irreproducible. Using the results of both the plate reader and the fluorimeter, we could see general trends showing fluorescence could be restored upon addition of a trapping agent in some cases, but this decrease in Cy3 quenching was not directly proportional to the concentration of trapping agent used, nor did we see complete reversibility. As a result of using 100 equiv. of trapping agent, though **3d** and **3e** were not dye-labelled, the significant excess of the small molecule was likely interfering with the fluorescence and therefore we were not able to obtain quantitative data. Additionally, as the oxime and hydrazine conjugates are known to be stable over extended periods in the literature,¹⁻³ monitoring cleavage over extended time periods was not feasible via FRET. Conversely, these results could be interpreted as showing the stability of oxime and hydrazine conjugates even in the presence of large excess of hydroxylamine and hydrazine competitive inhibitors. Overall, it can be concluded that FRET is not well-equipped test cleavage via direct competition. Alternative approaches were therefore investigated.

1.5. LC-MS Reversibility Studies

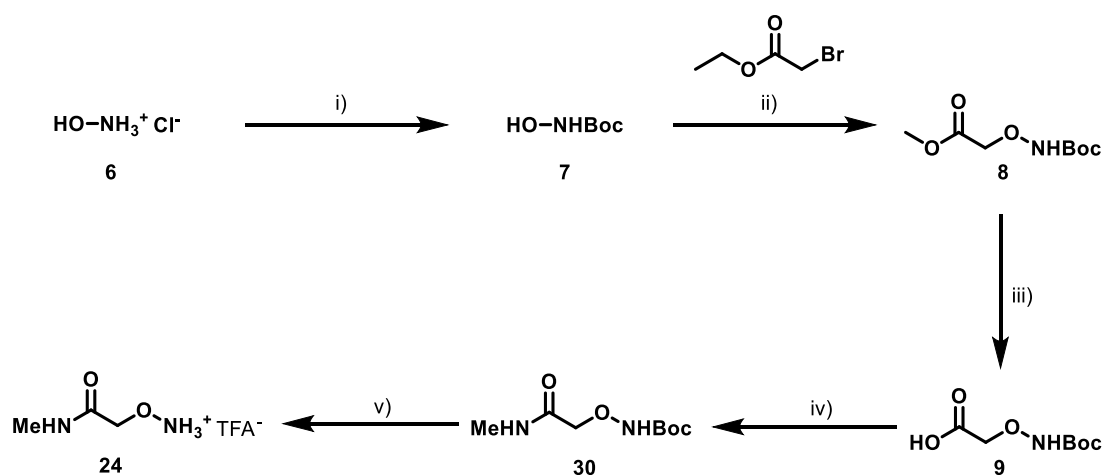
In light of the cleavage studies using the plate reader and fluorimeter, a dissociative mechanism for the reaction of oBID cleavage could be rationalised. No significant reversibility was observed for the oxime and DAB conjugates over 25 min, but we wanted to know if reversibility could happen over a longer period and so needed to adjust the analytical approach. FRET analysis was not suitable to test reversibility, due to impracticalities in the instrument. Liquid chromatography – mass spectrometry (LC-MS) could provide a way to monitor reversibility for the oxime and DAB conjugates, as it could be run over extended time periods. Due to the dissociative mechanism, we could attempt to cleave oxime or DAB linkages using hydroxylamine or hydrazine nucleophiles in excess. A reaction was proposed using a pre-formed propyl-amine functionalised oxime **23** or DAB **26**, followed by addition of excess methyl-amine functionalised hydroxylamine **24** or hydrazine **28**. By monitoring the exchange of the two species we would be able to determine k_1 and thus K_d for these systems. The UV absorbance of the system could be measured periodically over extended time periods until equilibrium was established.



Scheme 5: Equilibration of (a) propylamine-oxime **23** becoming hydrolysed to form **27a**, followed by an excess of methylamine-functionalised hydroxylamine **25**; and (b) propylamine-DAB **26** becoming hydrolysed to form **27a**, followed by an excess of methylamine-functionalised hydrazine **29**; allowing k_{-1} to be calculated over extended periods of time via LC-MS analysis.

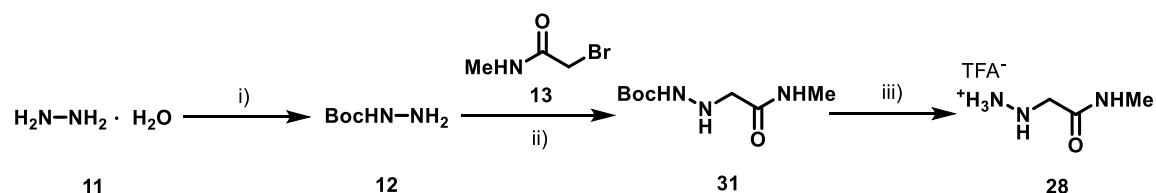
1.5.1 Synthesis of Methyl–Amine Competitors

Methyl hydroxylamine synthesis began with commercially available hydroxylamine hydrochloride (**6**), which was protected with Boc anhydride (**7**) and alkylated (**8**) as described for **3d**. The ester group was then hydrolysed with lithium hydroxide to yield **9** and then coupled with methyl amine to give **30**, which was then deprotected with TFA to yield methyl amide hydroxylamine compound **24** (Scheme 6).



Scheme 6: Synthesis of hydroxylamine small molecule **24**. *Reagents and conditions:* i) Boc_2O , $NaHCO_3$, THF:H₂O (1:1), r.t, 20 h, 89% ii) KOH , MeOH, 60 °C, 16 h, 53%, iii) $LiOH$, THF:H₂O (1:1), r.t, 16 h, 77% iv) methylamine, T3P, Et₃N, CH₂Cl₂, 0°C-r.t, 16 h, 46% v) TFA, CH₂Cl₂, r.t. 3 h, quantitative yield.

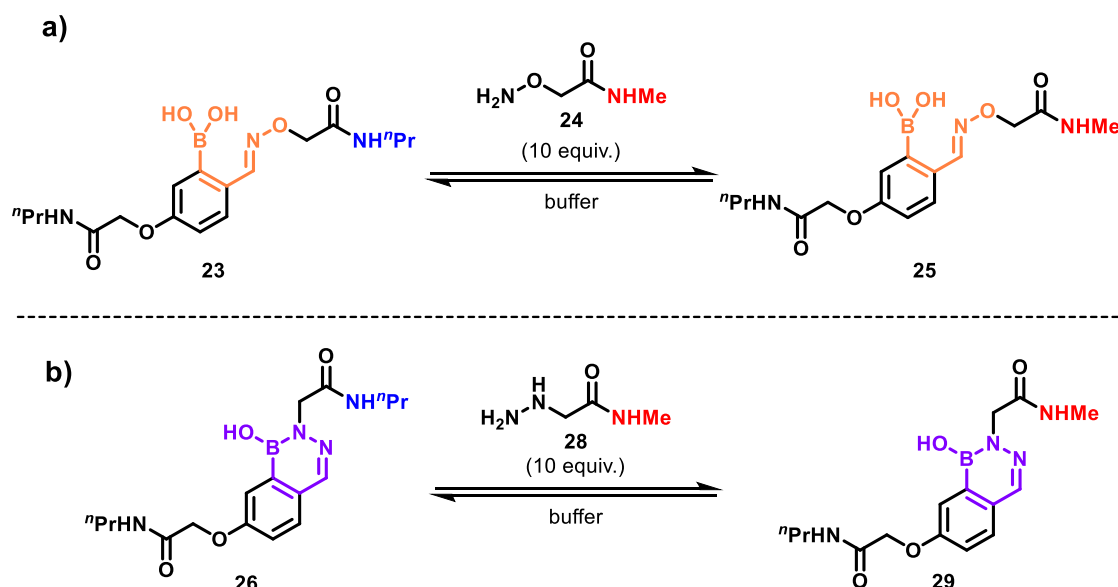
Synthesis of the hydrazine small molecule began with commercially available hydrazine monohydrate **11**, which was transformed into the hydrazine **28** in a three-step synthesis. Hydrazine monohydrate **11** was first reacted with Boc anhydride to afford mono-Boc protected hydrazine **12**. Hydrazine **12** then underwent an alkylation reaction with compound **13** to form amide **31** before deprotection in acidic conditions to give methyl hydrazine **28** (Scheme 7).



Scheme 7: Synthesis of hydrazine small molecule **28**. *Reagents and conditions:* i) Boc_2O , K_2CO_3 , dioxane and water 1:1, r.t, 16 h, 66%; ii) K_2CO_3 , CH_2Cl_2 , r.t, 16 h, 53%; iii) TFA, CH_2Cl_2 , r.t. 3 h, quantitative yield.

1.5.2. LC-MS Assay

An LC-MS assay was run whereby pre-formed propyl oxime **23** was incubated with an excess of methylamide-hydroxylamine **24** (10 equiv.), as the k_1 values could not be determined via FRET analysis. Pre-formed propyl DAB oBID **26** was set up in parallel with analogous addition of methylamide-hydrazine **28** (10 equiv. Scheme 8). The degree of interchange between the propyl- and methyl- functionalised oBIDs was performed every 24 h over the course of a week, and the integration of UV peaks corresponding to the products were calculated. The experiments were measured at pH 6.0, 7.4 and 8.0 to calculate dissociation (K_d) and rate of hydrolysis (k_{-1}) constants.



Scheme 8: Equilibration of propylamine-oxime **23**, with excess methylamine- functionalised hydroxylamine **24**, allowing oxime **25** formation and therefore k_1 to be calculated over extended period via LC-MS analysis.

Analogous experiments were performed with propylamine-hydrazine **26** and methylamine-functionalised hydrazine **28** to form DAB **29**.

Table 1: Tabulated dissociation (K_d) and rate (k_1 , k_{-1}) constants for the formation of oxime and DAB oBIDs in PBS solution via LC-MS studies. Data shown is copied from Chapter 3.

	pH	$k_1 / \text{M}^{-1} \text{s}^{-1}$	k_{-1} / s^{-1}	K_d
Oxime	6.0	3034 ± 27	$6.04 \pm 1.08 \times 10^{-5}$	19 nM
Oxime	7.4	4370 ± 164	$5.61 \pm 1.28 \times 10^{-5}$	12 nM
Oxime	8.0	1528 ± 10	$3.56 \pm 0.11 \times 10^{-5}$	233 nM
DAB	6.0	22920 ± 839	$8.07 \pm 0.29 \times 10^{-6}$	352 pM
DAB	7.4	169030 ± 6962	$2.60 \pm 0.55 \times 10^{-6}$	15 pM
DAB	8.0	37471 ± 1238	$8.05 \pm 0.26 \times 10^{-6}$	215 pM

Over the course of a week, the data obtained from these studies for the rates of dissociation, allowed the calculation of the dissociation constant for oxime **18** ($k_1 = 4370 \pm 164 \text{ M}^{-1} \text{ s}^{-1}$; $k_{-1} = 5.61 \pm 1.28 \times 10^{-5} \text{ s}^{-1}$; $K_d = 12 \text{ nM}$) at neutral pH, which was in line with previous reports by Schmidt et al. ($k_1 \sim 11000 \text{ M}^{-1} \text{ s}^{-1}$; $K_d \sim 25 \text{ nM}$). Interestingly, this previous work studied the reactivity of 2-borono-5-alkoxy benzaldehydes, in contrast to the 4-alkoxy analogues used in this study. LC-MS studies also showed that the DAB was dynamic, with **19** undergoing hydrolysis with a rate of $\sim 10^{-6} \text{ s}^{-1}$ leading to a K_d for hydrazone/DAB formation of $\sim 10 \text{ pM}$. This represents the lowest K_d recorded for a dynamic oBID to date at physiological pH.

The rates of oBID formation and dissociation are less well studied at pH 6-8, and therefore were explored here. The oxime conjugates **18** showed similar stability between pH 6-7.4 with $K_d = 19$ vs. 12 nM respectively, but as the pH was raised to 8, the dissociation constant increased by an order of magnitude, to 233 nM. Despite having a decreased k_1 value, the rate of oBID formation drops significantly, potentially due to the NH_2 group in the hydroxylamine nucleophile becoming protonated at pH 8 to form NH_3^+ and therefore make it a weaker nucleophile. Therefore, the rate of formation is significantly suppressed. The optimum rate of formation and stability for DAB conjugates **19** was found to be at pH 7.4. The dissociation constant increased by an order of magnitude when at either pH 6 or pH 8. The rate of formation also drops significantly, which shows that pH 7.4 is the optimum pH for both the rate of formation and stability.

2. Alternative *ortho*-Boronoaldehyde Structures

Much of the current research on oBIDs in the literature is based on data from 2-formylphenylboronic acid (2-FPBA, **32**) and 2-acetylphenylboronic acid (2-APBA, **33**).^{4-8,1,2} These are the most simplified aromatic aldehyde and ketone *ortho*-boronic acids, with no influence by substituted groups attached to the aromatic ring. These studies were very important in the initial exploration of oBID formation, as the key *ortho*-boronoimine was probed, with no interference from external electronic or steric factors which may affect binding. However, in order to employ these linkages in the real world, substitution effects around the aromatic rings must be explored to analyse the electronic and steric effects on oBID linkages. Phenolic *ortho*-boronoaldehydes have been loosely explored in the literature to allow for some functionalisation of the 2-FPBA/APBA systems substituted either *meta*- or *para*- to the aldehyde structure, as to not interfere with the subsequent B–N binding interactions but acts as an easily functionalised handle.^{6,9}

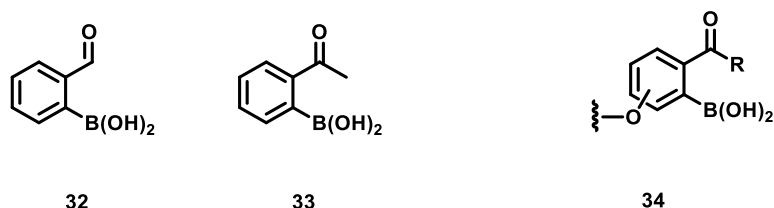


Figure 13: 2-FPBA **32** and 2-APBA **33** explored extensively in literature, as well as oBA **34**, which was explored in our studies.

In our work, we have focused on compound **1b**, whereby the *ortho*-boronoaldehyde is functionalised with a phenolic oxygen at the *para*- position relative to the electrophilic aldehyde functionality. When considering the electronics of this system, the electrons can be donated from the phenolic oxygen, through the aromatic ring and up onto the aldehyde group (Fig. 15b). This donation of electron density would decrease the electrophilicity of the aldehyde, and therefore make this aldehyde less susceptible to nucleophilic attack. Though this may decrease the reactivity, it might also increase the stability of the resultant oBID construct. Therefore, different isomers of boronobenzaldehydes could be generated (Fig 15a), to tune the electronics of the system and generate linkages with different properties. One example could be synthesised where the electron-donating group could be removed altogether and replaced with an electron withdrawing group *para*- to the aldehyde (Fig. 15b), thus making the aldehyde more electrophilic, and more susceptible to nucleophilic attack. This could be done by installing a carbonyl group *para*- to the aldehyde (**27b**). Another isomer could position the phenolic oxygen *meta*- to the aldehyde. In this position the phenolic oxygen would not mesomerically donate electron density into

the aldehyde (**27c**). As well as interfering with the electrophilicity of the aldehyde to form a subsequent imine, the position of the phenolic oxygen also has a significant effect on the Lewis acidity of the system. Positioning a boronic acid moiety *para*- to a phenolic oxygen would decrease the Lewis acidity of the boron, as there would be an increase of electron density at the boron centre via a mesomeric effect, which therefore could weaken the B–N interactions formed (**27d**). Converse effects occur if an electron withdrawing group was *para*- to the boronic acid, as the electron density would be inductively drawn out of the boron centre, and therefore leaving a stronger Lewis acid for B–N interaction. As the *ortho*-boronoaldehyde has a carbonyl group and a boronic acid *ortho*- to each other, the effect of electrophilicity vs. Lewis acidity must be considered when forming different isomers to analyse the electronic effects of the oBID systems. Additionally, the aldehyde group could be replaced by a ketone functionality, similar to 2-APBA in literature, which alters the electronics as well as the sterics of the resultant oBID formed. Therefore, through studying these isomers (Fig. 24a) with different electronic effects on the aldehyde, we proposed to form a library of different oBID linkages, which could be suited to many applications in bioconjugation and material chemistry.

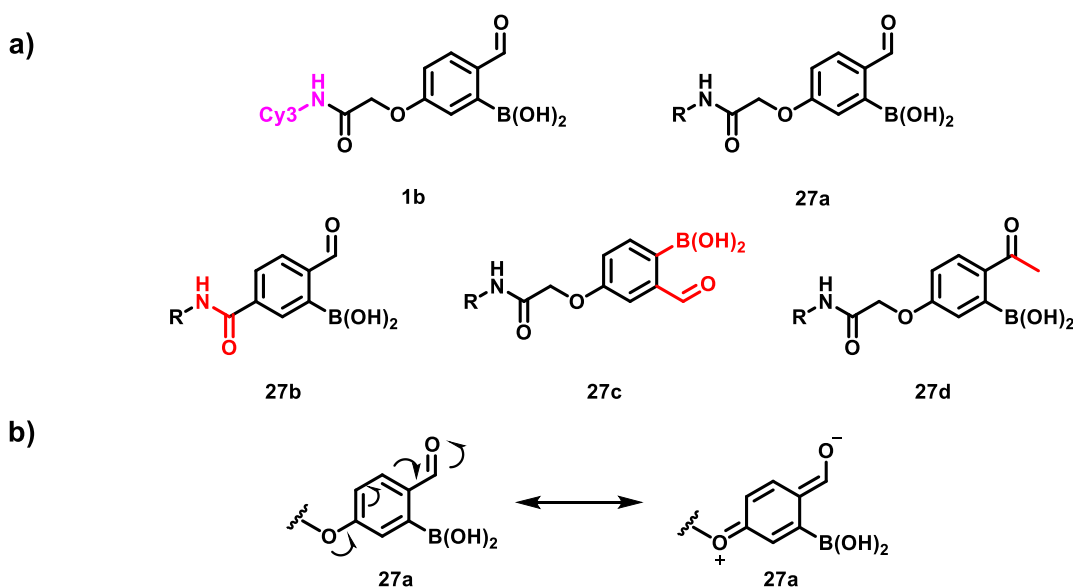
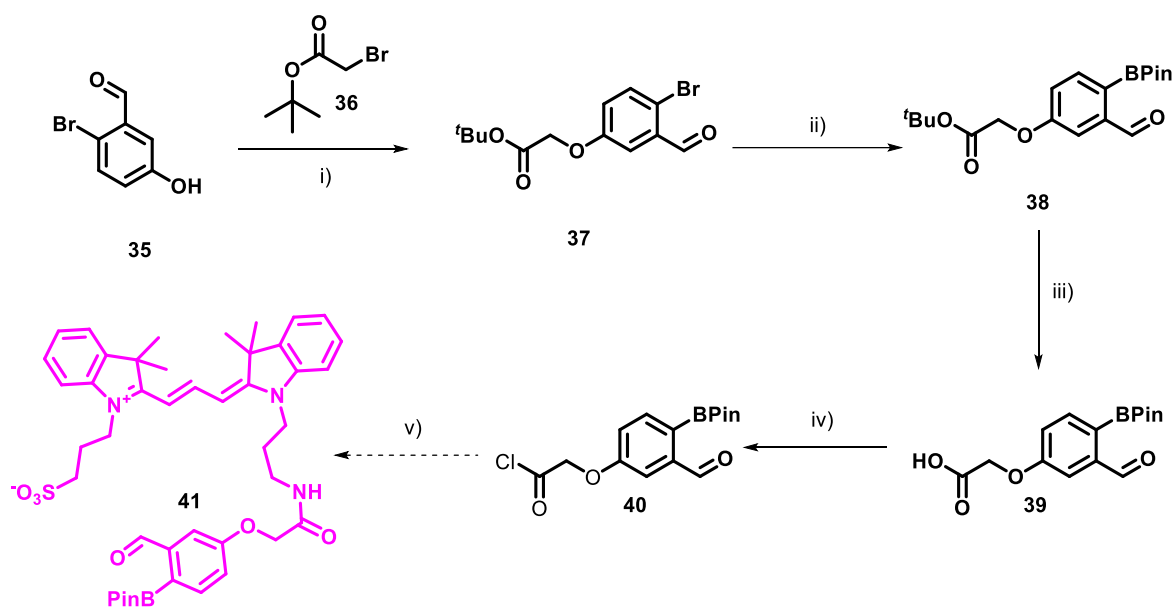


Figure 14: a) Target oBA/BK isomers for synthesis **27a-d**; b) Resonance forms of electron donating group and effects of electronics on the aldehyde.

2.1. Synthesis of Cy3-oBA Isomers

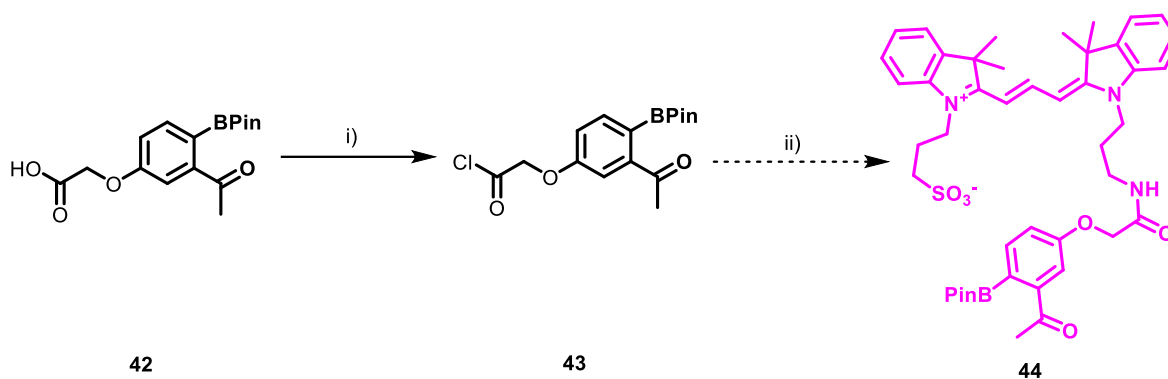
We initially envisaged forming dye labelled isomers of the Cy3-oBA **1b**, which could subsequently be reacted with the five combinations of Cy5-amine derivatives previously synthesised and used for FRET studies. Therefore, the synthesis of these cyanine oBA

isomers began, following the pathway optimised for the synthesis of **1b** in Chapter 2 Section 2.2. Synthesis of the *meta*-phenoxy analogue **41** began with 2-bromo-4-hydroxybenzaldehyde **35**, which was first alkylated with *tert*-butyl bromoacetate **36** to form ester **37**. **37** then underwent a Miyaura borylation reaction to form the pinacol ester **38**, which was then reacted with TFA, which removed the *tert*-butyl group to form carboxylic acid **39**. This was then activated to form acyl chloride **40**, and coupling was attempted to the deprotected Cy3 dye **1** to yield the pinacol ester **41** (Scheme 9).



Scheme 9: Proposed synthesis of the *ortho*-boronobenzaldehyde **41** isomer. *Reagents and conditions:* i) K_2CO_3 , MeCN, 65 °C, 16 h, 96%; ii) TFA, CH_2Cl_2 , r.t., 3 h, 97%; iii) EDC, NHS, CH_2Cl_2 , r.t., 3 h, 80%, iv) $(COCl)_2$, DMF, r.t., 2 h, quantitative yield; v) **1**, DMAP, K_2CO_3 , anhydrous DMF, r.t., 3 h.

Despite using the same conditions used to form the previously mentioned Cy3-*o*BA **1b**, the coupling reaction between the acyl chloride **40** and Cy3 free amine dye **1** was unsuccessful, with similar problems to those observed in Chapter 2 Section 2.2. Many spots were present via TLC, which made chromatography and separation challenging. We reasoned that methanol, which was used as the eluent due to its high polarity, had reacted with the boronic ester to form various adducts, but there was no indication that the product was present. This synthesis was repeated numerous times with various conditions fusing DMAP, triethyl amine and potassium carbonate bases, however the synthesis was unsuccessful, with the recovery of only starting material. An analogous synthesis was attempted, this time with an *ortho*-boronoketone (Scheme 10). Carboxylic acid **42** was activated using an acyl chloride to form **43**, but the coupling reaction was again unsuccessful, and **44** could not be isolated. Rather than using more of the valuable unprotected Cy3 dye **1**, Alternative methods were explored to investigate the chemistry of these *o*BA isomers.



Scheme 10: Proposed synthesis of *ortho*-boronoketone, **44** through activation of acyl chloride. Reagents and conditions: i) (COCl)₂, DMF, r.t., 2 h, quantitative yield; ii) DMAP, K₂CO₃, anhydrous DMF, r.t., 3 h.

It was recognised that having run FRET studies between the Cy3-*o*BA **1b** and Cy5 amine derivatives **2a-e** previously, the rate of formation of *para*-phenoxy *o*BIDs as well as the K_d s established could be used to determine rate and dissociation constants for each of the isomers through NMR competition experiments. Therefore, we could synthesise simpler propylamide analogues rather than relying on the complex synthesis of dye-linked-*o*BAs (Fig. 16). Therefore, synthesis was pursued for these *o*BA isomers **27a-d**, along with the amine derivatives with a *n*-propylamine chain substituted.

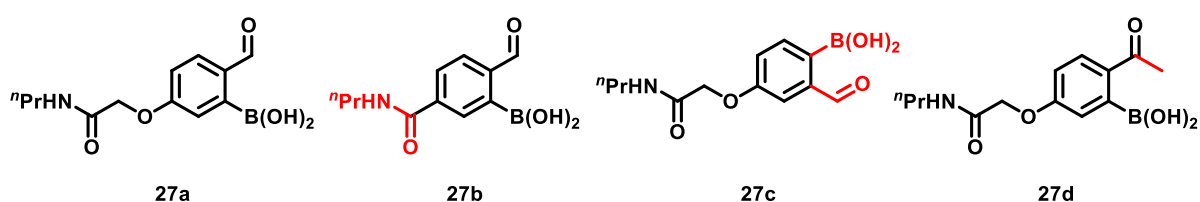
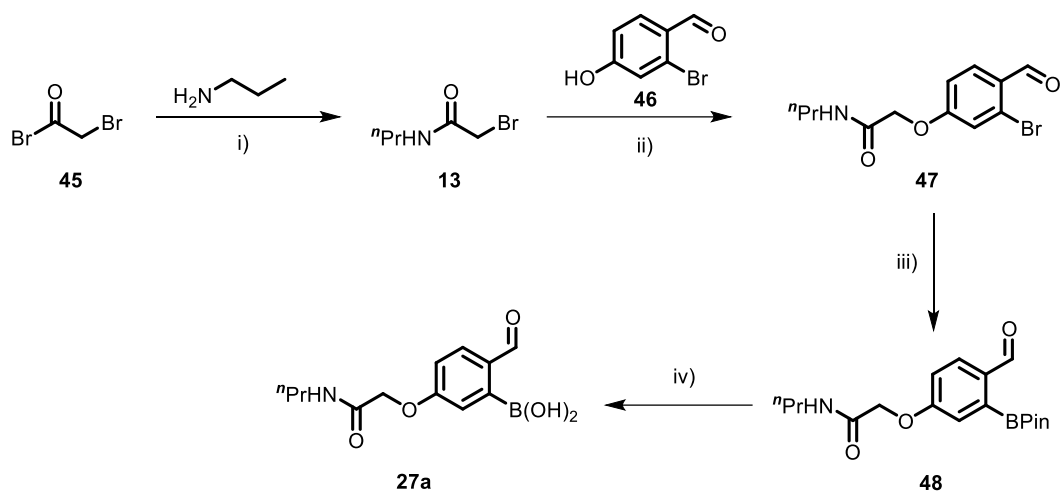


Figure 15: Target isomers **27a-d** with Cy3 dye substituted for propylamine chain.

2.1 1. Synthesis of *para*-BA, **27a**

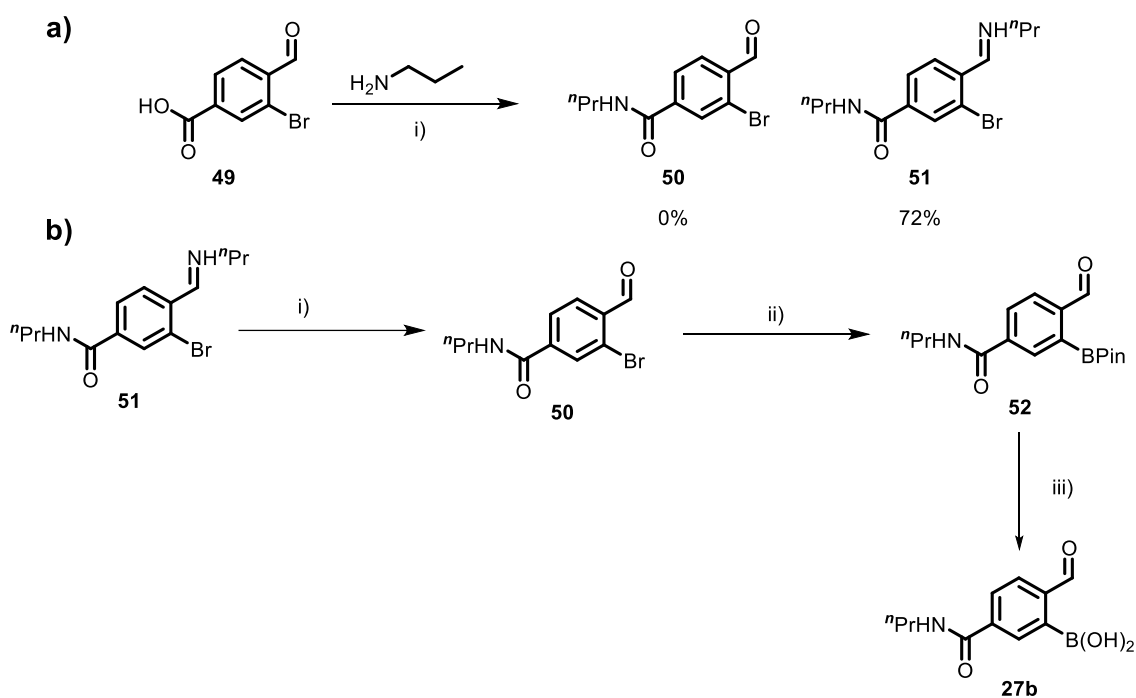
We began by synthesising a model of the *para*-phenoxy isomer previously used in our FRET studies. The synthesis began by first synthesising amide **13**, by reaction of bromo acetyl bromide **45** with propyl amide. This was subsequently coupled to commercially available aldehyde **46** to form aryl bromide **47** which underwent a Miyaura borylation reaction to give pinacol ester **48**. The pinacol ester **48** was then deprotected with methyl boronic acid in TFA, to give the final boronic acid **27a** (Scheme 11). The synthesis was achieved with an overall 52% yield. The propyl *ortho*-boronoaldehyde has analogous reactivity to the Cy3-*o*BA and therefore served as a reference for the other isomers.



Scheme 11: Synthesis of *para*-oxygen oBA (**27a**). Reagents and conditions: i) propyl amine, CH₂Cl₂, r.t., 30 min, 91%; ii) K₂CO₃, acetonitrile, 75 °C, 16 h, 86%; iii) B₂Pin₂, Pd(dppf)Cl₂, AcOK, anhydrous dioxane, 80 °C, 1 h, 67%; iv) MeB(OH)₂, TFA, CH₂Cl₂, r.t., 16 h, quantitative yield.

2.1.2. Synthesis of *para*-carboxy oBA, **27b**

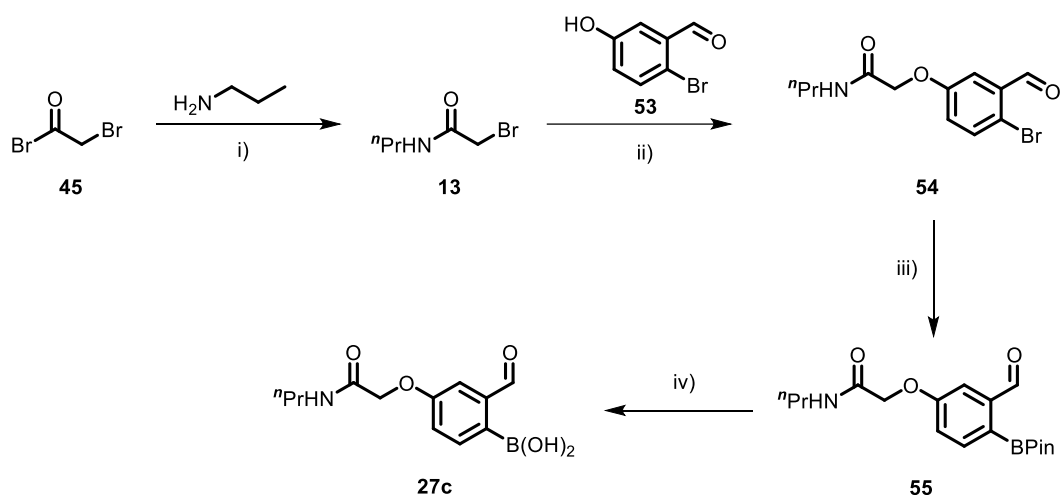
Synthesis of compound **27b** began with an amide coupling reaction between propylamine and commercial carboxylic acid **49** with T3P. However, as well as forming the amide, propylamine also reacted with the aldehyde, to give imine **51** (Scheme 12a). This imine was hydrolysed with citric acid in THF to reinstate the aldehyde functionality in **50**. Aldehyde **50** then underwent a Miyaura borylation to form pinacol ester **52**, before deprotection with methyl boronic acid and TFA to give boronic acid **27b** in an overall yield of 23% (Scheme 12b).



Scheme 12: **a)** Amide coupling followed by formation of imine side product to give **51**. *Reagents and conditions:* i) T3P (50% w/w/ EtOAc), Et₃N, CH₂Cl₂, r.t., 16 h. **b)** Synthesis of electron withdrawing aldehyde (**27b**). *Reagents and conditions:* i) Citric acid, THF (1:1), 70 °C, 16 h, 81%; ii) B₂Pin₂, Pd(dppf)Cl₂, AcOK, anhydrous dioxane, 80 °C, 1 h, 28%; iii) MeB(OH)₂, TFA, CH₂Cl₂, r.t., 16 h, quantitative yield.

2.1.3. Synthesis of *meta*-phenoxy *o*BA, **27c**

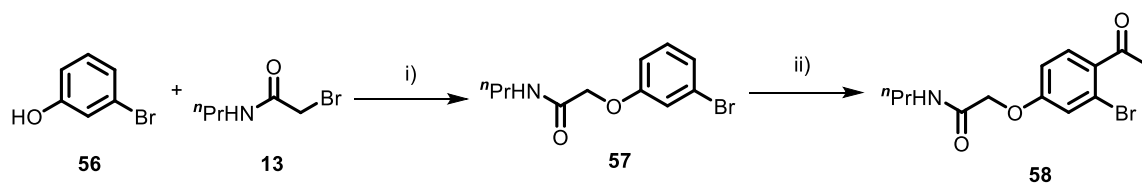
The synthesis of the *meta*-phenoxy *o*BA isomer **27c** is analogous to that described in Chapter 2 Section 1.3. for the standard *o*BA, this time with 2-bromo-5-hydroxybenzaldehyde **53**. The *o*BA isomer **27c** was synthesised over a four-step synthesis, with an overall yield of 22%. Synthesis began by first synthesising amide **13**, by reaction of bromoacetyl bromide **45** with propyl amine. This was subsequently used to alkylate commercially available aldehyde **53** to form aryl bromide **54** before a Miyaura borylation reaction to give pinacol ester **55**. The pinacol ester **55** was then deprotected with methyl boronic acid with TFA, to give the final boronic acid **27c** (Scheme 13).



Scheme 13: Synthesis of compound **27c**. *Reagents and conditions:* i) propyl amine, CH₂Cl₂, r.t., 30 min, 91%; ii) K₂CO₃, acetonitrile, 75 °C, 16 h, 74%; iii) B₂Pin₂, Pd(dppf)Cl₂, AcOK, anhydrous dioxane, 80 °C, 1 h, 32%; iv) MeB(OH)₂, TFA, CH₂Cl₂, r.t., 16 h, quantitative yield.

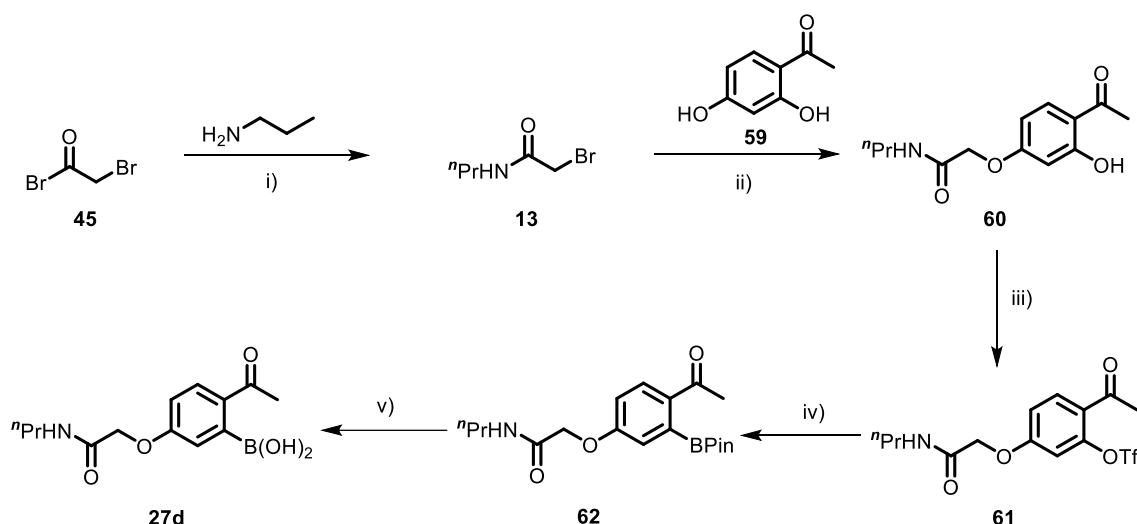
2.1.4. Synthesis of *ortho*-boronoketone, **27d**

The synthesis of the *ortho*-boronoketone began with 3-bromophenol **56** which underwent an alkylation with the synthesised amide **13**, which gave compound **57**. Friedel-Crafts acylation with acetyl chloride was attempted to install the ketone in **58** (Scheme 14). However, although the reaction was successful, it was very low yielding, and therefore new methods were put in place to synthesise the *ortho*-boronoketone, which avoided the use of a Friedel-Crafts reactions.



Scheme 14: Synthesis of *ortho*-boronoketone **52**. *Reagents and conditions:* i) K₂CO₃, acetonitrile, 75 °C, 16 h, 54%; ii) AcCl, AlCl₃, CH₂Cl₂, 0 °C -r.t., 2 h, 12%.

Alternatively, 2,4-dihydroxybenzaldehyde **59** was used in slight excess during an alkylation with **13** to generate the mono-alkylated amide **60**. This alkylation favoured the *para*-OH due to the sterics of the ring and was isolated in a good yield. The *ortho*-OH group was then activated to form triflate **61** and borylated via a Miyaura borylation to form pinacol ester **62**. Finally, **62** was deprotected with methyl boronic acid and TFA to give the boronic acid **27d** (Scheme 15).



Scheme 15: Synthesis of acyl chloride (**27d**). *Reagents and conditions:* i) propyl amine, CH₂Cl₂, r.t., 30 min, 91%; ii) K₂CO₃, acetonitrile, 75 °C, 16 h, 54%; iii) (CF₃SO₂)₂O, Et₃N, CH₂Cl₂, -78 °C, 30 min, 92%; iv) B₂Pin₂, Pd(dppf)Cl₂, AcOK, anhydrous dioxane, 80 °C, 1 h, 44%; v) MeB(OH)₂, TFA, CH₂Cl₂, r.t., 16 h, quantitative yield.

2.2. Plate Reader Isomer Studies

With the newly synthesised *ortho*-boronoaldehydes and *ortho*-boronoketone now in hand, we envisage combining these with our Cy3-*o*BA and Cy5-amine derivatives in competition assays, to compare the reactivity of the isomers. From the previous FRET studies for the standard *o*BA **1b**, we had calculated the dissociation constant and rate constants for *o*BID formation with each nucleophile. We made the assumption that the rate and dissociation constants for the propyl amide derivative (**27a**) would be the same as the Cy3-*o*BA **1b**. On this basis, FRET studies were performed as before (Fig. 16a), but with the addition of a propyl amide *o*BA **27a** small molecule as a competitor (Fig. 16b). **1b**, **27a** and a Cy5 amine-based nucleophiles **2a-e** were added in a 1:1:1 ratio at 2.5 μM, at the same time. Mixtures of Cy3-*o*BA, Cy5-amine derivative and propyl *o*BA **27a** were excited at 480 nm, and the emission at 580 nm was recorded over time. With the addition of the propyl *o*BA **27a**, we expected to see a reduction in Cy3 emission channel, as some of the Cy5-amine would be bound to **27a**. Ideally, when dye and non-labelled *o*BAs were mixed in a 1:1:1 ratio, we would expect to see 50% drop in Cy3 emission channel relative to when **27a** was absent. 96-well plate studies were performed in the first instance to see general trends for 1, 10 and 100 equivalents of competing propyl *o*BA **27a**, with the aim of seeing a relatively smaller drop in Cy3 emission (Fig. 16b).

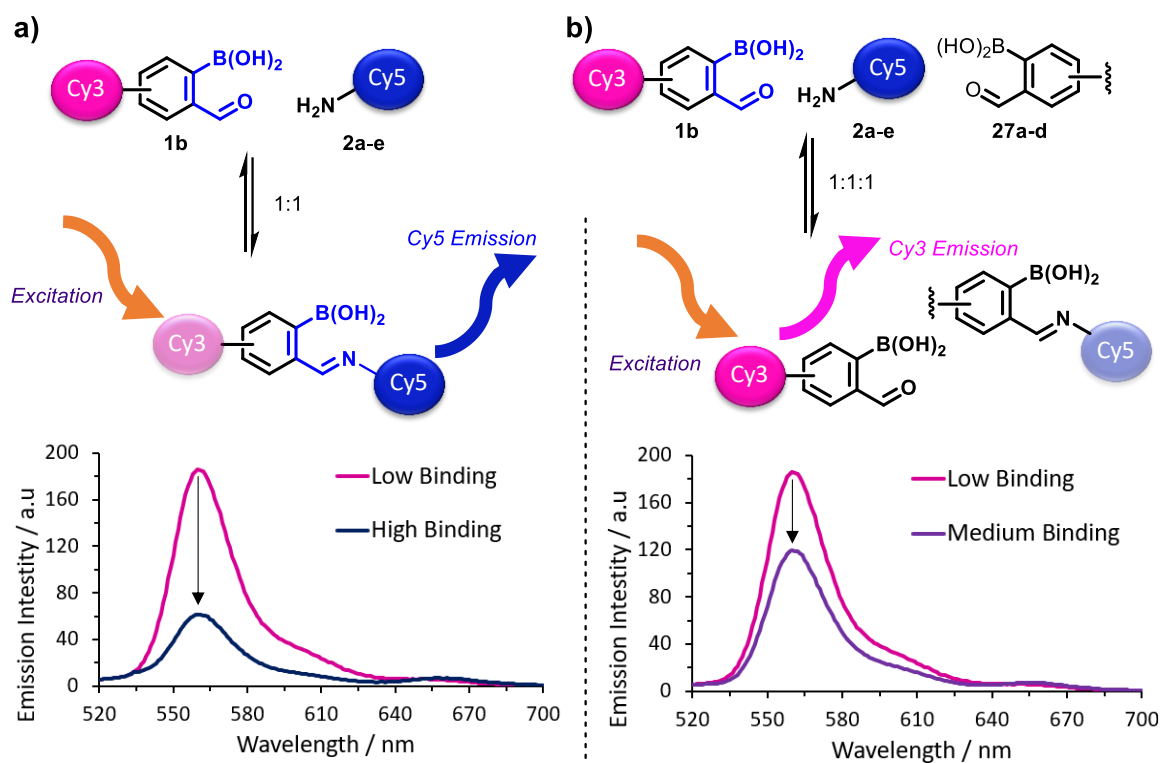


Figure 16: a) Schematic representation of drop in Cy3 emission intensity dropping over time via forming oBID to bring cyanine dyes in close spatial proximity for FRET; b) Competition assay using isomers **27a-d** which bind to Cy5 dye and therefore, the Cy3 excitation is not quenched, indicated by a Cy3 emission in the Cy3 channel.

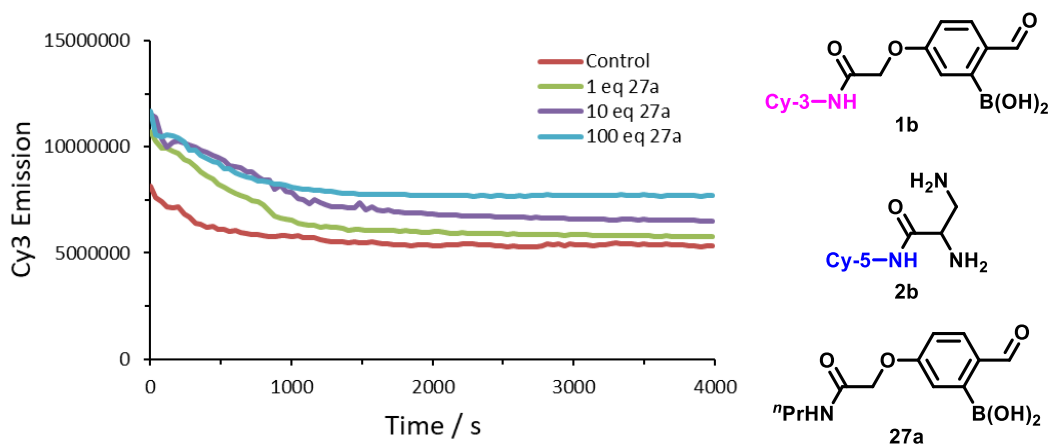


Figure 17: Emission at 580 nm after excitation at 480 nm for Cy3 oBA **1b** with Cy5 1,2-diamine **2b** with varying concentrations (1-100 equiv.) of propyl oBA **27a** trapping agents.

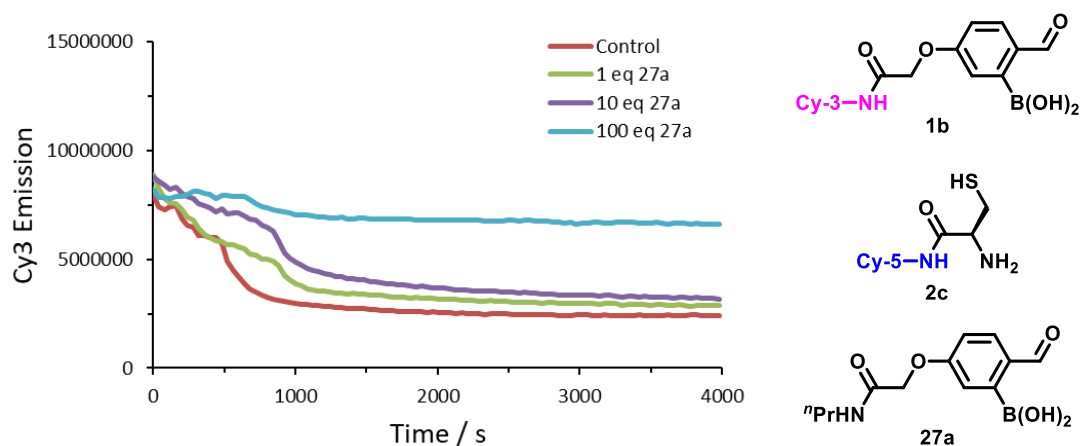


Figure 18: Emission at 580 nm after excitation at 480 nm for Cy3 oBA **1b** and Cy5 1,2-aminothiol **2c** reaction with TCEP, with varying concentrations (1-100 equiv.) of propyl oBA **27a** trapping agents.

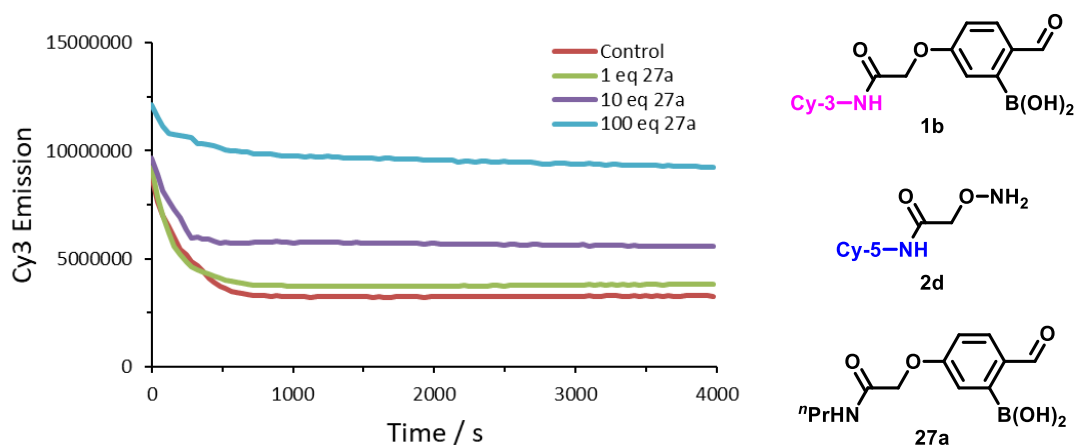


Figure 19: Emission at 580 nm after excitation at 480 nm for Cy3 oBA **1b** with Cy5 hydroxylamine **2d** with varying concentrations (1-100 equiv.) of propyl oBA **27a** trapping agents.

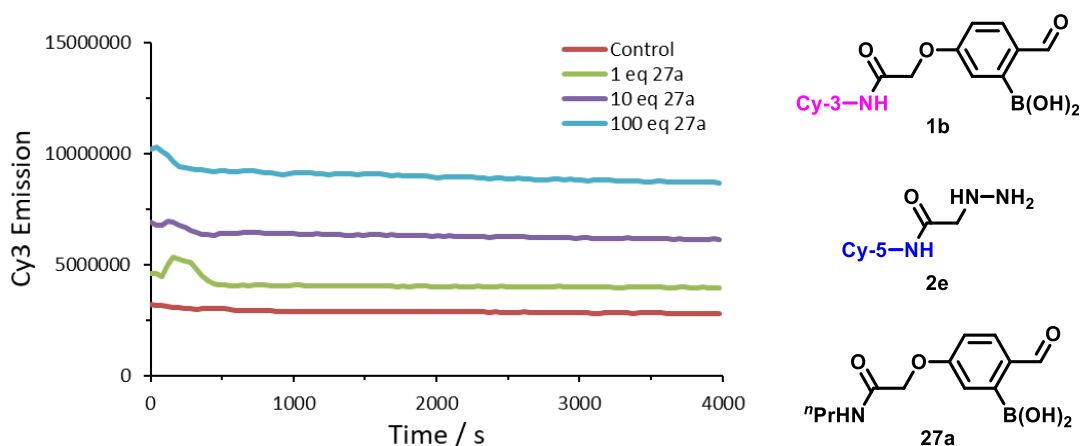


Figure 20: Emission at 580 nm after excitation at 480 nm for Cy3 oBA **1b** with Cy5 hydrazine **2e** with varying concentrations (1-100 equiv.) of propyl oBA **27a** trapping agents.

Using Fig. 17-20, these preliminary results from the plate reader showed a suppressed reduction in Cy3 emission intensity by using **27a** to trap 50% of the Cy5 amine-based nucleophile. As the concentration of propyl oBA **27a** increased (up to 100 equiv.), the Cy3

emission also increased. This suggests that more of **27a** is binding the Cy5 amine derivative as would be expected. It should be noted that, as described above, we would expect to see a 50% increase in Cy3 emission by addition of one equivalent of propyl oBA with relatively smaller increases upon increasing the number of competitor equivalents. Through the steady trend of an increase in Cy3 emission with increasing concentration of **27a**, this preliminary data warranted moving forward with fluorimeter studies to investigate this data further.

2.3. Fluorimeter Isomer Studies

Following on from the preliminary results on the plate reader to probe isomer effects on oBID formation, further and more accurate studies were performed on the fluorimeter. Cy3-oBA (**1b**) was reacted with a Cy5 1,2-diamino, 1,2-aminothiol, hydroxylamine and hydrazine derivatives (**2b-e**) in the presence of 10 equivalents of competing oBA/oBK isomers (**27a-d**), exciting at 480 nm and monitoring the emission between 520-700 nm as previously discussed. We had initially hypothesised that if we mixed a 1:1:1 ratio of **1b**, with one isomer of **27a-d** and one amine-based nucleophile **2b-e**, we would see a change in Cy3 emission intensity correlating to the isomer trapping agents. For example, if we mixed **1b**, **27b** and **2d** together in a 1:1:1 ratio at 2.5 μM , we could expect to see a decrease in Cy3 emission intensity if **1b** binds to **2d** as a result of FRET. However, if the oBA of **27b** binds preferentially to the hydroxylamine of **2d**, we would expect to see a decrease in Cy3 emission quenching by **27b** trapping the hydroxylamine nucleophile.

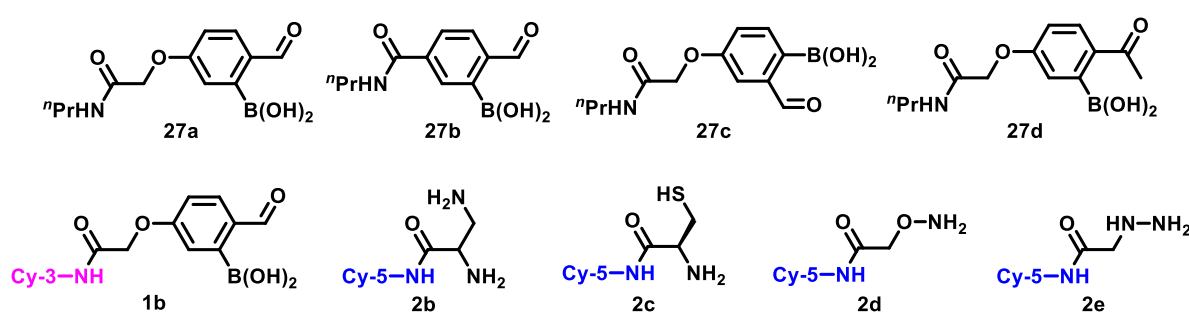


Figure 21: Cy3 oBA **1b** and Cy5-amine **2b-e** derivative used in combination with isomers **27a-d** to measure electronic effects on rates.

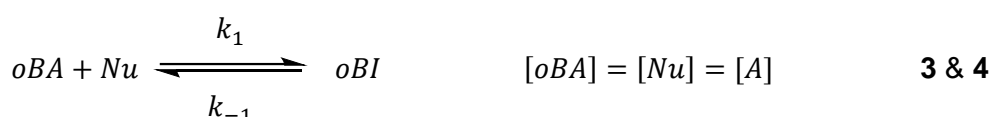
However, the results using a fluorimeter were not suitable and did not give any conclusive results, similar to fluorimeter results in Section 1.3, whereby reversibility was tested but could not control stoichiometric mixtures. FRET analysis was therefore deemed to be poorly suited to test a three-component system and was unable to provide qualitative data of this reaction mixture. There are many possible reasons for these inconclusive results,

ranging from changes in intensity with the addition of competing trapping agents **27a-d**, through to challenges calculating exact stoichiometries. Therefore, NMR studies were used instead to analyse the electronic and steric effects of **27a-d**.

2.4. NMR Competition Studies

NMR characterisation techniques have been well documented in the literature as the main analysis technique for *ortho*-boronimine bond formation.^{1,4-6,10-15} In Chapter 3, we highlighted the distinct advantages of using FRET over alternative techniques such as UV-vis and NMR as a highly sensitive method to monitor the rapid reactivity of *o*BAs. However, NMR can prove advantageous over FRET as it allows exact concentrations to be used directly rather than indirectly calculated. When using the plate reader and the fluorimeter for isomer studies, whereby 3 reactants are put together, it is difficult to decipher which species are contributing to the signal. NMR is more beneficial to analyse complex mixtures. NMR inherently requires higher concentration of reactants than fluorescence studies (~10 mM vs. ~100 nM). The position of equilibrium changes dramatically when working with higher concentrations, and therefore must be accounted for. Using literature dissociation constant values,⁹ as well as our own, we estimate the percentage conversion we would expect for each nucleophile under NMR conditions.

$$R = k[A]^n[B]^m \qquad R = [oBA]^n[Nu]^m \qquad \mathbf{1 \& 2}$$



$$K_d = \frac{k_1}{k_{-1}} \qquad K_d = \frac{[oBA][Nu]}{[oBI]} \qquad \mathbf{5 \& 6}$$

$$K_d = \frac{[A]^2}{[AB]} \quad \text{where } [AB] = c - [A] \quad K_d = \frac{[A]^2}{c-[A]} \qquad \mathbf{7 \& 8}$$

$$cK_d - K_d[A] = [A]^2 \qquad [A]^2 + K_d[A] - cK_d = 0 \qquad \mathbf{9 \& 10}$$

Using the quadratic formula: $x = \frac{b \pm \sqrt{b^2 - 4ac}}{2a} \qquad \mathbf{11}$

Using these derived equations (equation 1-10), and the quadratic equation (equation 11), as well as dissociation constants calculated previously, we can estimate which amine

nucleophile would undergo partial conversion at a specific concentration, and would be best suited to NMR studies. It was estimated that the 1,2-diamino **3b** or the 1,2-aminothiol **3c** were expected to achieve 50-95% conversion between the concentrations of 5-20 mM, which were the concentrations of the NMR sample reaction mixtures. As the 1,2-diamino group **3b** forms an IzB species which rapidly interchanges, its use would ensure that equilibrium would be reached with the most thermodynamically stable IzB product. Due to the simplicity of preparation of the 1,2-diamino **3b** reactive handle, this nucleophile was therefore chosen for NMR studies, which negates the need to use TCEP to break up disulfide bridges otherwise observed in the 1,2-aminothiol **3c** nucleophile. The reversibility of these reactive handles, together with partial conversion would then allow us to calculate the most stable thermodynamic product between the different *o*BA/BK isomers **27a-d** (Fig. 22).

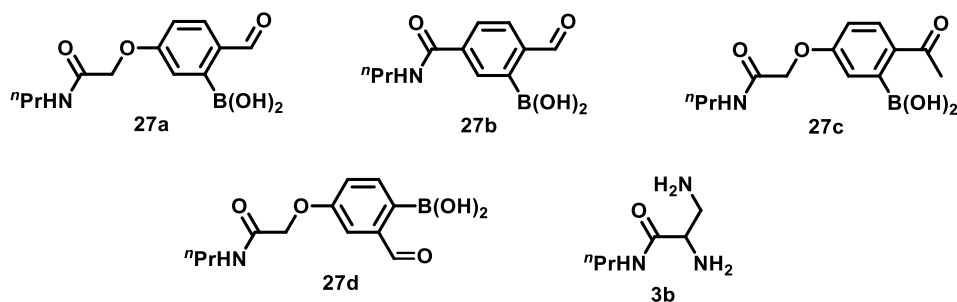


Figure 22: NMR experiments conducted with all of the *o*BA/BK isomers **27a-d** to be tested with 1,2-diamino **3b** small molecule to analyse the most stable thermodynamic product.

The NMR studies could be tracked, by simply monitoring the integration ratio of the aldehyde proton (~10 ppm), which was converted into one of two (or both) downfield shifted IzB imine peaks (~5-6 ppm) upon IzB formation **63** or **64** (Fig. 23). NMR studies tested each isomer (**27b-d**) against the *para*-phenoxy *o*BA **27a**. For each isomer, 5 experiments were run. An NMR of **27a** alone, **27a** with **3b** (2:1 equiv.), the isomer alone, the isomer with **3b** (2:1 equiv.), and finally both *o*BA's together with the propyl 1,2-diamine **3b** moiety (2:2:1 equiv.). 2 equivalents of propyl *o*BA **27a** and the competing isomer (**27b-d**) were used, whilst 1 equivalent of 1,2-diamino **3b** was used. This ensured that although the diamine **3b** would show only partial conversion of each IzB, the IzB complexes would be dynamic and rapidly interchange to form the most thermodynamically stable IzB product (Fig. 23). Starting with isomer **27b**, the stacked NMR data is shown in Fig. 24.

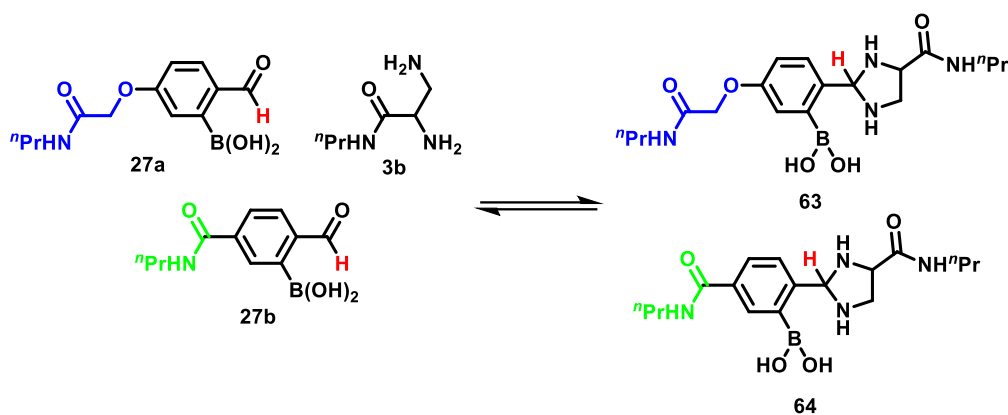


Figure 23: Reaction of **27a** with 1,2-diamino small molecule **3b** to see an aldehyde/acetal peak shift into an imine peak **63**, with a corresponding competing reaction with the electron withdrawing boronoaldehyde isomer **27b**.

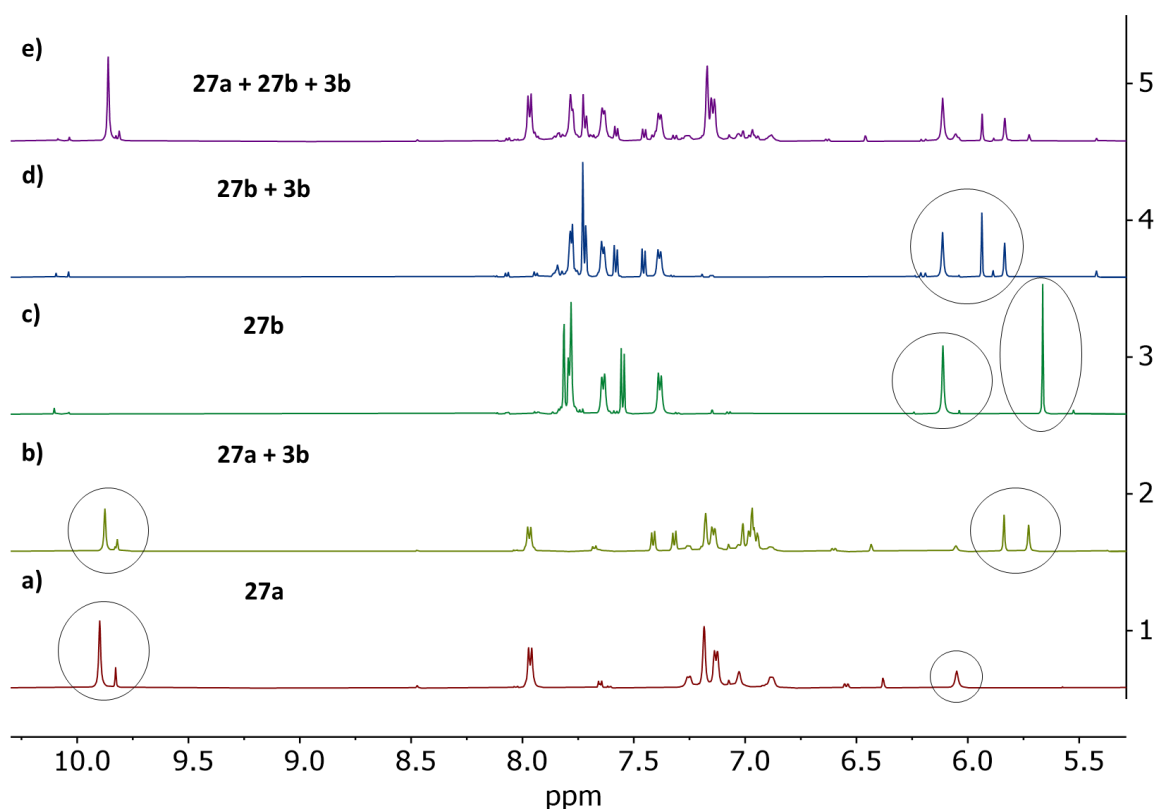


Figure 24: NMR experiments to monitor the aldehyde/acetal and imine shift between isomers **27a** and **27b** to determine the most thermodynamically stable *ortho*-iminoboronate.

During the formation of IzB **63** and **64** for both isomers, there was a distinct shift in peaks between the aldehyde and imine peaks. As seen in Fig. 24, there are two parent peaks for **27a** (Fig. 24a) 9.85 ppm, 0.7 intensity and 6.10 ppm, 0.3 intensity corresponding to the aldehyde and a hydrate peak in PBS. In the presence of a propyl diamino nucleophile **3b**, two new peaks formed (Fig. 24b) 5.83 ppm and 5.72 ppm with approx. equal intensity of 0.23 corresponding to the two possible isomers of IzB formation **63**. These two additional

peaks are from the imine proton of the 5-membered ring of IzB, which can form different isomers between the CHNH₂ structure and the CH₂NH₂ amines.¹⁰ Conversely, the electron withdrawing isomer **27b**, had two distinct peaks (Fig. 24c) 6.11 ppm, 0.56 intensity and 5.66 ppm, 0.43 intensity corresponding to hydrate formation in the PBS solvent. Similarly, with the addition of the 1,2-diamino nucleophile, these hydrate peaks shifted into two new peaks (Fig. 24d) 5.93 ppm, 0.28 intensity and 5.83 ppm, 0.23 intensity corresponding to IzB formation **64** with this isomer. Once the two isomers were mixed together with the 1,2-diamino **3b** nucleophile, the intensity of these peaks could then be compared with the standards and the ratios used to calculate K_d for the isomers. Where K_{d1} and K_{d2} are dissociation constants for each isomer, [A] and [B] are the concentration of reactants, and [AB] is the concentration of the product.

$$K_{d1} = \frac{[A][B]}{[AB]} \quad K_{d2} = \frac{[B][C]}{[BC]} \quad [B] = \frac{K_{d2}[BC]}{[C]} \quad \mathbf{12, 13 \& 14}$$

$$K_{d1} = \frac{[A]}{[AB]} \times \frac{K_{d2}[BC]}{[C]} \quad K_{D2} = \frac{K_{d1}[AB][C]}{[A][BC]} \quad \mathbf{15 \& 16}$$

$$K_{d2} = \frac{0.000043 \times 3 \times 14.38}{26.55 \times 6.99} \quad K_{d2} = 8.48 \times 10^{-6} M^{-1} \quad \mathbf{17 \& 18}$$

The peak intensities in NMR are relative to the respective IzB products formed for **63** and **64**, and therefore the concentration of [AB] and [BC] are relative to one another. With these intensities, we could then deduce [AB] and [BC]. Where [A] and [C] is the concentration of remaining starting material (equivalent to $-[AB]$), and the dissociation constant (K_{d1}) of **27a** is 4.3 μ M, as calculated in Chapter 3. We could therefore calculate the rate dissociation constant for **27b** to be 0.9 μ M, using equations 12-18. Hence, by having an electron withdrawing group *para*- to the aldehyde, this seems to increase the electrophilicity of the aldehyde, and subsequently forms an IzB which is >4x more stable than the original isomer **27a**.

With respect to isomer **27c**, where the electron donating oxygen is now *meta*- to the aldehyde (Fig. 25), we saw a similar increase in stability over the original isomer **27a**. In the instance of isomer **27c**, there were two predominant peaks (Fig. 26c) 6.04 ppm, 0.66 intensity and 5.60 ppm 0.19 intensity, corresponding to the hydrate peaks with PBS and a third smaller peak (9.99 ppm, 0.10 intensity) corresponding to trace aldehyde.

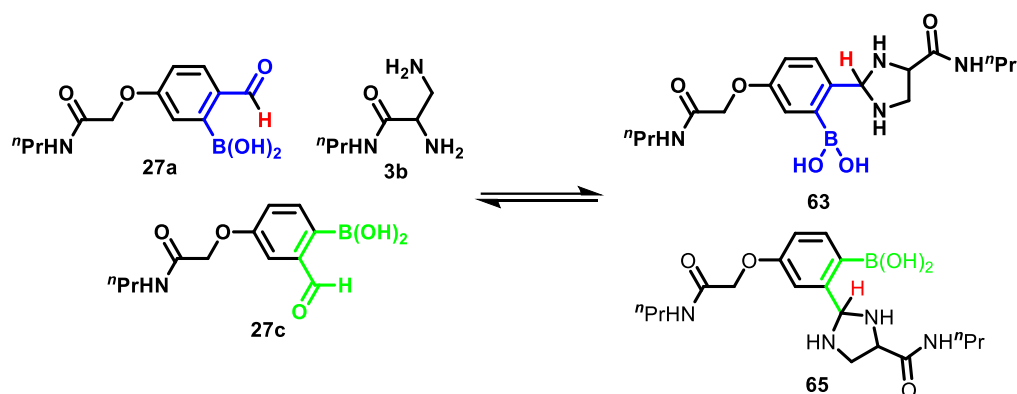


Figure 25: Reaction of **27a** with 1,2-diamino small molecule **3b** to see an aldehyde peak shift into an imine peak **63**, with a corresponding competing reaction with the boronoaldehyde isomer **27c**.

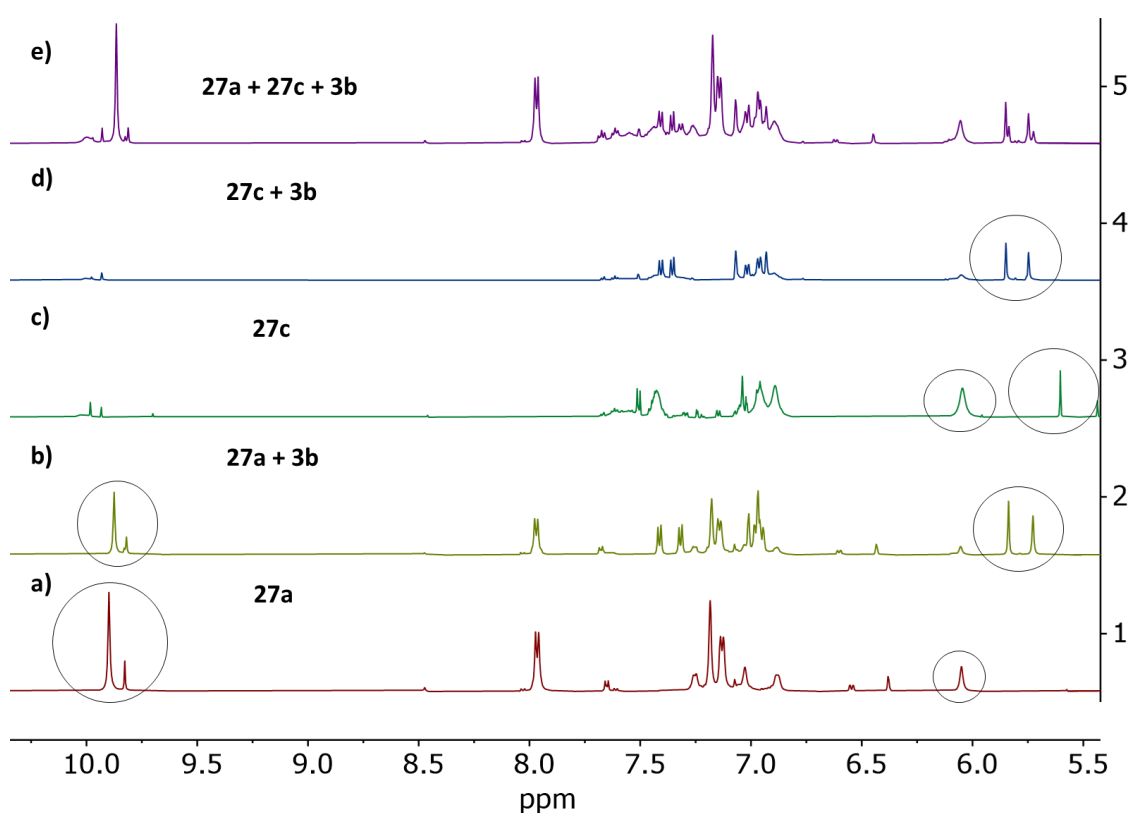


Figure 26: NMR experiments to monitor the aldehyde and imine shift between isomers **27a** and **27c** to determine the most thermodynamically stable *ortho*-iminoboronate.

When isomer **27c** was combined with the 1,2-diamino **3b** nucleophile, there was a clear shift into two new peaks (Fig. 26d) 5.85 ppm, 0.30 intensity and 5.75 ppm 0.27 intensity corresponding to IzB formation **65**. Once again, when the two isomers were mixed together with the 1,2-diamino **3b** nucleophile, the intensity of these peaks could then be compared with the standards, to calculate product ratios, and therefore which IzB forms the most thermodynamically stable product. Using the equations 12-18, we could deduce a K_d of 1.2 μM , which is almost 4 times more stable than the standard isomer **27a**. This result fits

well with our hypothesis, which suggested that as the electron donating oxygen sits *meta*- to the aldehyde, the electron density cannot conjugate through the aromatic ring and onto the aldehyde. However, in this configuration, the electron donating phenolic oxygen sits *para*- to the Lewis acidic boronic acid. Despite the reduction in Lewis acidity, the *meta*-phenoxy oBA isomer **27c** formed a more thermodynamically stable IzB than standard isomer **27a**.

In the instance of *ortho*-boronoketone **27d** (Fig. 27), we did not see any IzB **66** formation with *ortho*-boronoketone **27d** over the standard oBA isomer **27a**, and therefore we are unable to comment on the thermodynamic stability of the IzB complex **66**.

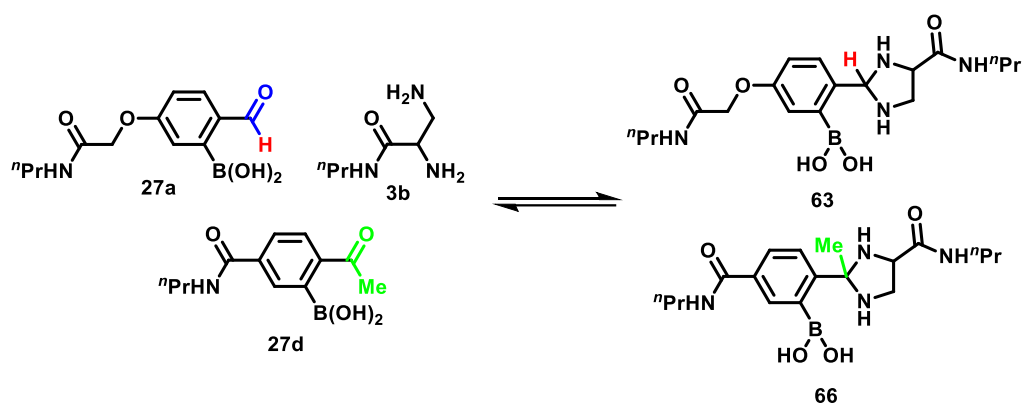


Figure 27: Reaction of **27a** with 1,2-diamino small molecule **3b** to see an aldehyde peak shift into an imine peak **63**, with a corresponding competing reaction with the *ortho*-boronoketone isomer **27d**.

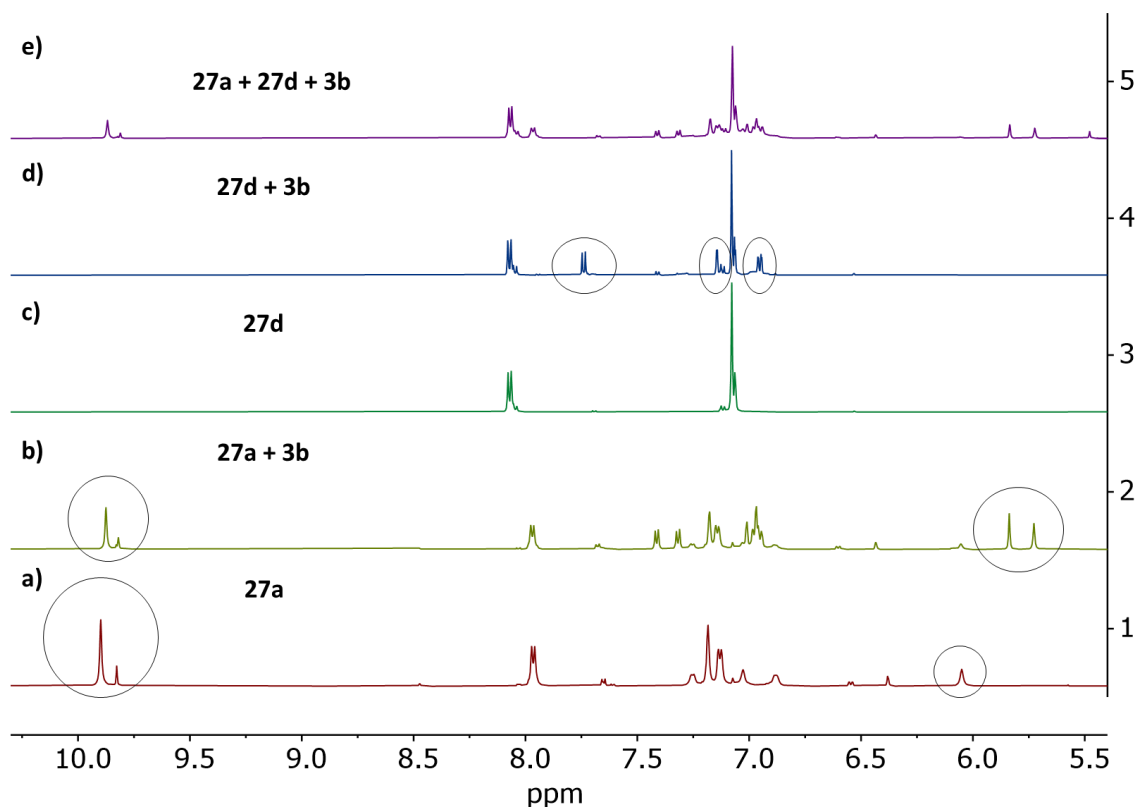


Figure 28: NMR experiments to monitor the aldehyde and imine shift between isomers **27a** and **27d** to determine the most thermodynamically stable *ortho*-iminoboronate.

The *ortho*-boronoketone did not have the same aldehyde proton shown in the previous examples. Therefore, we relied on the subsequent IzB structure **66** to shift the aromatic protons of the oBK (Fig. 28). When the oBK NMR was measured, there were two clear aromatic peaks (Fig. 28c) 8.07 ppm, 1.00 intensity and 7.08, 1.99 intensity corresponding to the aromatic protons. In the presence of the 1,2-diamino nucleophile, we saw a shift into 3 new peaks (Fig. 28d) 7.74 ppm, 7.14 ppm and 6.95 ppm, all at a 0.29 intensity corresponding to IzB **66** formation. It should be noted that the peak at 7.74 ppm had a distinct shift which did not overlap with any other peaks, and therefore was used as the reference point. As seen by Fig. 28e, there was no significant formation of the *ortho*-boronoketone IzB **66** structure upon addition of **3b** (small peak at 7.67 ppm, 0.04 intensity does not correspond). Therefore, isomer **27a** formed a far more stable IzB, and a dissociation constant for **27d** cannot be deduced. This could be due to the more sterically hindered ketone structure.

2.5. NMR Kinetic Isomer Studies

Due to the highly dynamic and reversible nature of IzB formation ($k_1 \sim 1000 \text{ M}^{-1} \text{ s}^{-1}$; $K_d \sim 5 \text{ } \mu\text{M}$) the experiments described above gave an important insight into the most thermodynamically stable oBID formed. However, in order to probe the kinetics of the system, we looked towards forming a rapid, and more stable linkage, which could be achieved using the hydrazine **3e**. When forming the hydrazone/DAB oBID linkage, we have found that the initial reaction is amongst the fastest bioconjugation reactions in the literature with a $k_1 \sim 2 \times 10^5 \text{ M}^{-1} \text{ s}^{-1}$, followed by a slower cyclisation to a 6-membered DAB structure **70** (Fig. 29), which is highly stable ($K_d = 15 \text{ } \mu\text{M}$), as determined by previous LC-MS studies (Section 1.6.2.), with very slow reversibility. Therefore, using hydrazine **3e** in combination with isomers **27a-d**, the fastest forming kinetic DAB isomer will initially form.

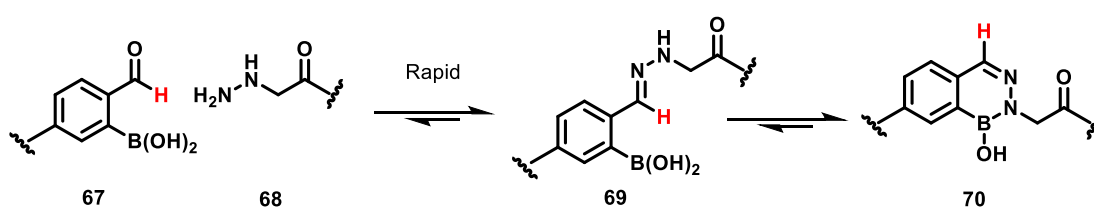


Figure 29: Nucleophilic attack of the hydrazine moiety **68** to form a hydrazone **69**, followed by a stable DAB formation **70**.

Therefore, propyl hydrazine **3e**, was used to test the reactivity of the isomeric oBA/BK pairs using NMR studies. These NMR studies could be tracked, by simply monitoring the integration ratio of the starting oBA aldehyde proton ($\sim 10 \text{ ppm}$), which were converted into a downfield shifted DAB peak ($\sim 8.9 \text{ ppm}$) upon DAB cyclisation. NMR studies tested each isomer (**27b-d**) against the original oBA **27a** to compare and contrast the kinetics of the systems. Therefore, for each isomer, 5 experiments were run. An NMR of **27a** alone, **27a** with **3e**, the isomer (**27b-d**) alone, the isomer with propyl hydrazine **3e**, and finally both oBAs together with the propyl hydrazine **3e** moiety (Fig. 30). Starting with isomer **27b**, the stacked NMR data is shown in Fig. 31. Propyl oBA **27a**, and the competing isomer (**27b-d**) were used each at 1 equivalent, whilst 0.5 equivalents of hydrazine **3e** was used, to ensure that full consumption of the hydrazine was achieved. The propyl hydrazine **3e** was added to a pre-mixed mixture of both isomers to enable a fair test for the reaction.

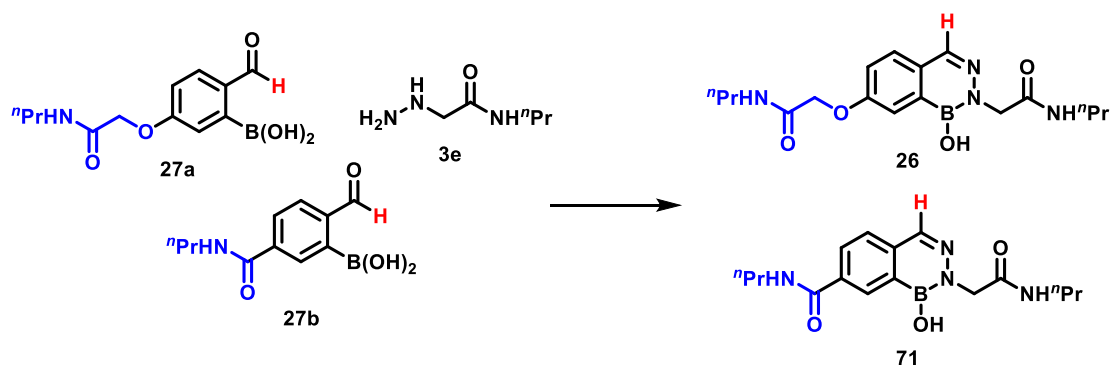


Figure 30: Reaction of **27a** with hydrazine small molecule **3e** to see an aldehyde peak shift into a DAB peak, with a corresponding competing reaction with the *ortho*-boronoketone isomer **27b**.

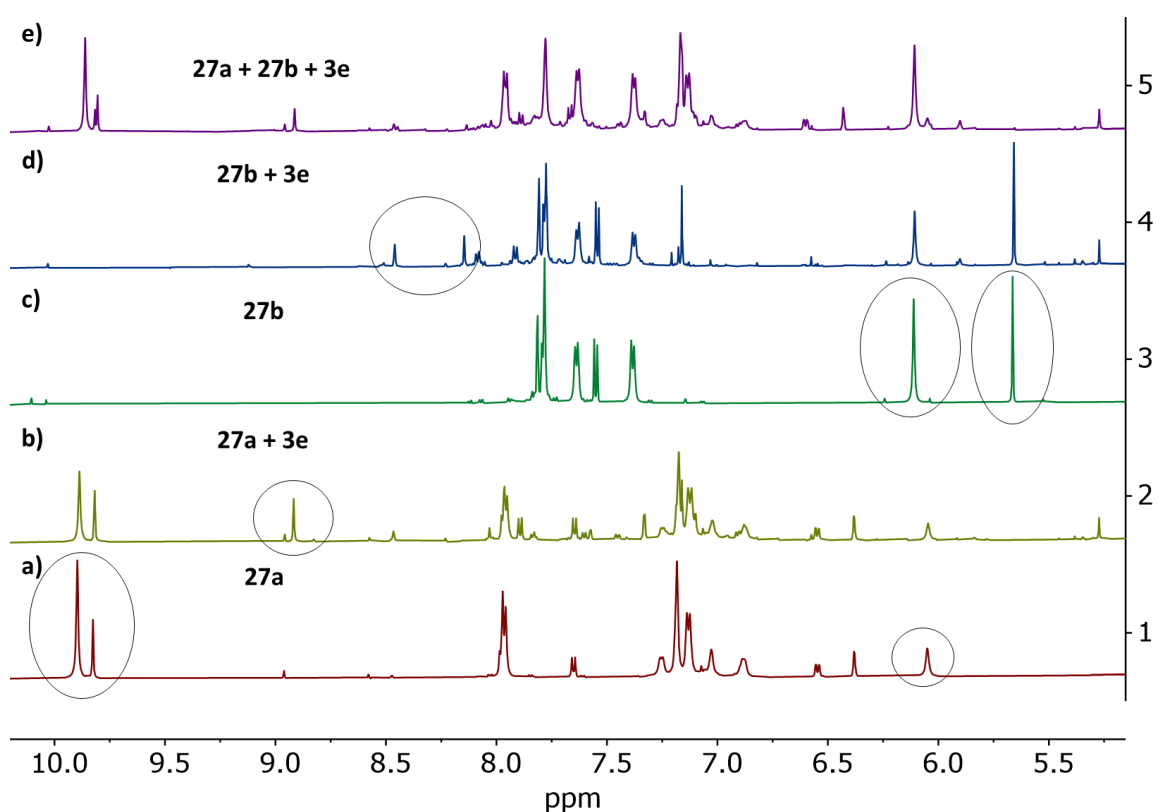


Figure 31: NMR experiments to monitor the aldehyde and DAB peak shift between isomers **27a** and **27b** to determine the most thermodynamically stable iminoboronate.

During the DAB formation for both isomers, there was a distinct shift in peaks between the aldehyde and DAB peaks. As seen in Fig. 31, there are two parent peaks for **27a** (Fig. 31a) 9.85 ppm, 0.7 intensity and 6.10 ppm, 0.3 intensity corresponding to the aldehyde and a subsequent hydrate peak formation in PBS. In the presence of a propyl hydrazine nucleophile **3e**, a new Cyclised DAB **26** peak (Fig. 31b) at 8.9 ppm, 0.31 intensity is formed. Conversely, the *para*-carboxy isomer **27b**, has two distinct peaks (Fig. 31c) (6.11 ppm, 0.56 intensity and 5.66 ppm, 0.43 intensity) corresponding to hydrate formation in the PBS solvent. Similarly, with the addition of the hydrazine nucleophile **3e**, these hydrate

peaks shifted into two new peaks (Fig. 31d) 8.46 ppm, 0.16 intensity and 8.14 ppm, 0.16 intensity) corresponding to DAB **71** formation with this isomer. Once the two isomers were mixed together with the hydrazine **3e** nucleophile, the integration of these peaks could be calculated to determine product ratios and therefore which DAB is kinetically favoured. In the instance with isomer **27b**, equal amounts of **26** and **71** were formed (Fig. 31e). This same result was found for *meta*-phenoxy *o*BA isomer **27c** and even for boronoketone **27d**. This result was particularly surprising for the *ortho*-boronoketone **27d**, as in the previous study using the 1,2-diamio molecule, there was virtually no *o*BID corresponding to the ketone product formed for the thermodynamic study. These studies therefore suggested that all of the isomers showed very similar rates of reaction. Considering the FRET conjugation studies, which were complete in a matter of seconds at 2.5 μ M concentration, it can be rationalised that the kinetic DAB formation is too rapid to be monitored using NMR, and therefore differences in product ratios would be minimal. It is noteworthy that this study highlights the benefits of our FRET approach, as without using this highly sensitive platform at the low μ M scale, we could not have monitored conversion for these rapid reactions as a function of time. In order to gain an insight into the kinetics of these various different isomers, a potential study could be performed using the hydroxylamine **3d** small molecule. The hydroxylamine **3d** reacts much slower than the hydrazine **3e** moiety, and therefore could give more valuable results, and so forms part of the future works of this project.

3 Additional Studies

3.1 DAB-Hydrazone pH Study

The Gillingham and Bane group have extensively studied the reactivity between FPBA and hydrazines.^{2,14,15} These groups have shown that reaction with FPBA and hydrazine leads to the formation of a hydrazone intermediate, which is then followed by a second intramolecular cyclisation reaction, via a dehydration step to form a highly stabilised 6-membered DAB aromatic ring at neutral pH. Due to the rapid kinetics of this step ($k_1 > 10^4 \text{ M}^{-1} \text{ s}^{-1}$ reported), studies by the Gillingham and Bane groups have had insufficient kinetic resolution into the initial hydrazone intermediate formation.^{2,14,16} Our FRET system that we developed in this work allowed us to work at concentrations as low as 750 nM, which have yielded $k_1 = 169030 \pm 6962 \text{ M}^{-1} \text{ s}^{-1}$, further supporting the previous reports that this reaction is amongst the fastest bioconjugation reactions reported. As these FRET studies reach equilibrium within in a matter of seconds, it is unlikely that the formation of DAB plays a significant role in our system, which reports on conjugation rather than the structure of the intermediates formed. This direct read out of conjugation further highlights the benefits of our platform, which analyses different combinations of intermediates and products *in situ*, independent of specific individual species which could potentially undergo exchange, but still contribute to overall conjugation. In a similar study to ours, Gu *et. al.* reacted carbohydrazides with 2-FPBA to form DAB linkages with a high pH dependency for this cyclisation reaction, and thus stability on the subsequent oBID linkage.¹⁴ Gu found that between pH 7-9, a highly stabilised cyclic DAB product was present, whereas at pH 4-6, a standard hydrazone was formed (Fig. 32). Although this system was different to ours, as we use a hydrazine in this work rather than a hydrazide, we wanted to probe the hydrazone-DAB equilibrium across a pH range.

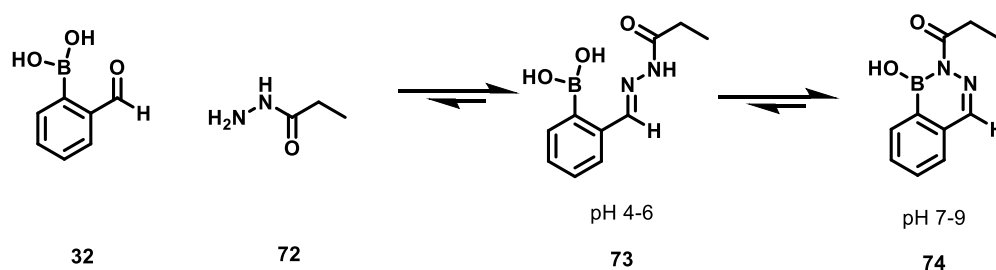


Figure 32: pH-dependent cyclisation reaction explored by Gu,¹⁴ showing hydrazone **73** at pH 4-6 and DAB **74** between pH 7-9.

Our data in Chapter 3 indicated that the reaction of the oBA with hydrazine proceeded with $k_1 = 22000-170000 \text{ M}^{-1} \text{ s}^{-1}$ between the range of pH 6-8. The remarkable stability of these conjugates formed is noteworthy, with $K_d = 10-300 \text{ pM}$, with very slow hydrolysis. Given

that our dissociation constant stays in the same order of magnitude of stability at pH = 6 ($K_d = 300$ pM), to pH 7 and 8 ($K_d = 10$ -200 pM), we wanted to investigate the structure formed across a pH range as reported by Gu *et al.* To track this, we used NMR studies which allowed us to monitor the shift in peak from the aldehyde proton (~9.8 ppm), which was converted into a downfield shifted DAB proton (~8.7 ppm, red) upon DAB **26** formation (Fig. 33) in line with literature for similar DABs.^{2,15} In this cyclisation reaction, we also saw the formation of a peak (~5.2 ppm, blue) corresponding to the CH₂-group shifted upfield via cyclisation from ~4.3 ppm, as it was experiencing a de-shielding effect. To conduct these studies, isomer **27a** was reacted with propyl hydrazine **3e** from pH 4-7.4 to see the difference of the integrated proton peak. Control NMR experiments were also run with only oBA **27a** and propyl hydrazine **3e**, across the pH changes, to serve as our controls. 0.9 equivalents of propyl hydrazine **3e** were used to ensure that most of the oBA **27a** had reacted.

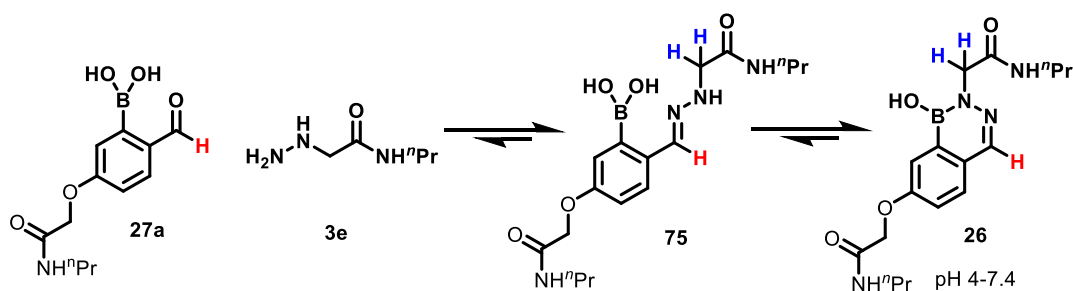


Figure 33: Reaction of **27a** and **3e** to form oBID linkage in cyclised DAB **26** formation between pH 4-7.4

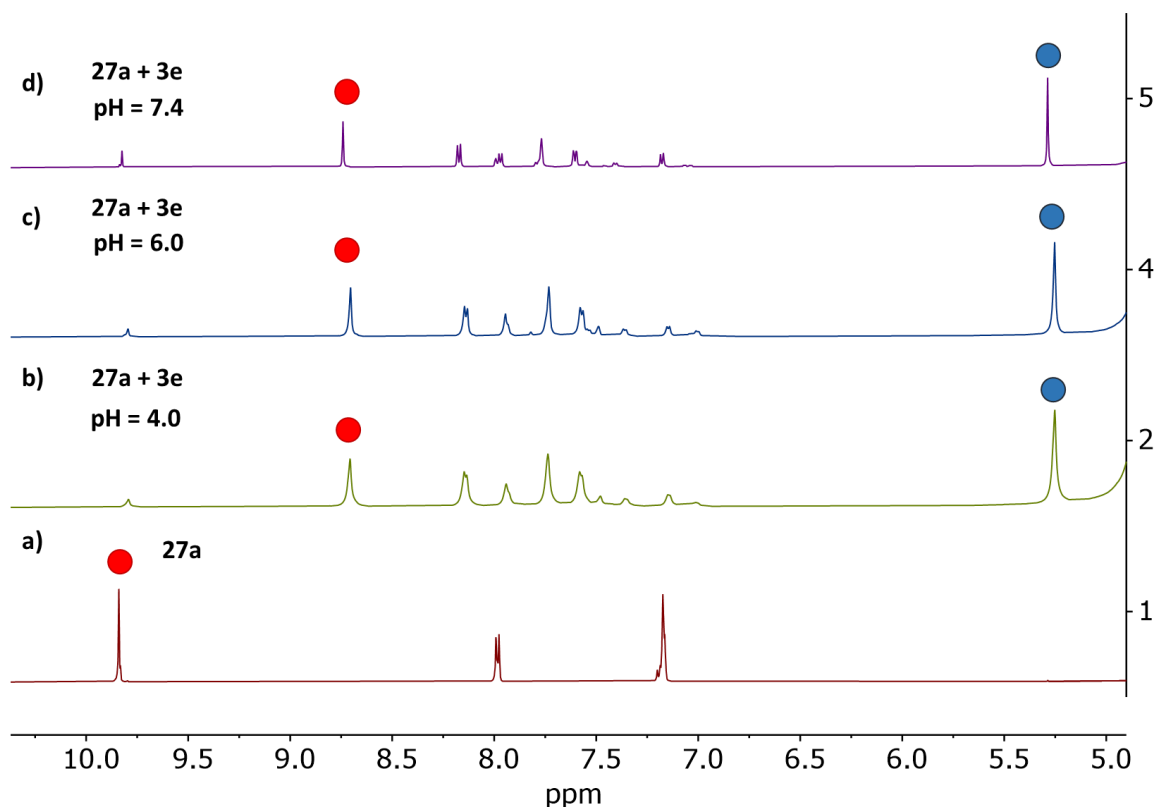


Figure 34: NMR experiment of DAB formation **26** between pH 4-7.4 **a)** oBA **27a** at pH = 7.5 showing aldehyde peak (red circle); **b)** oBA **27a** with 0.9 equiv. **3e** at pH = 4.0 to see DAB peak (red circle) for DAB formation; **c)** oBA **27a** with 0.9 equiv. **3b** at pH = 6.0 to see DAB peak (red circle) for DAB formation; **d)** oBA **27a** with 0.9 equiv. **3b** at pH = 7.5 to see DAB peak (red circle) for DAB formation.

Our NMR results showed that 6-membered ring DAB cyclisation occurs across all pHs, with no hydrazone being observed (Fig. 34), even as low as pH = 4, as indicated by a clear DAB peak at at ~8.7 ppm (Fig. 34b, red circle) across the pH range. This is in contrast to hydrazones explored by Gu *et. al.* who claimed that the open chain hydrazone oBID is dominant over the cyclic DAB **26** structure. These differences could have been due to the difference in reactivity between hydrazines and hydrazides which effect the stability of the subsequent DAB rings at acidic pH.

3.2. Glucose and Fructose Binding Study

Following on from our FRET studies in Chapter 3 which investigated whether glucose and fructose affected oBID formation, we wanted to study whether either sugar could bind to oximes or DABs once formed. Glucose and fructose covalently bind to boronic acids and there are many applications in chemical biology exploit these interactions.¹⁷⁻²¹ Monitoring

these interactions and understanding how these linkages work in the presence of these sugars is therefore very important when considering the applications of oBID formations to applications in chemical biology. To measure the binding constant of glucose and fructose, oxime **78** and DAB **26** linkages were pre-formed in an NMR tube, followed by the addition of 100 mM sugar (Fig. 35).

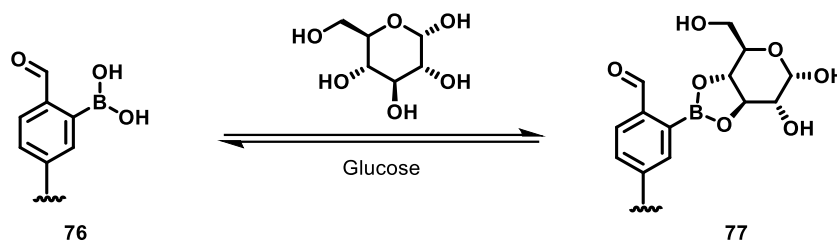


Figure 35: Glucose reversibly binding to a boronic acid of the oBA moiety **76**, to form **77**.

With this NMR study, we tracked the shift in peak from the aldehyde proton (~10 ppm), which was converted into a downfield shifted imine proton (~8-9 ppm) upon oxime/DAB formation which was used in Section 2.4. for NMR experiments. Upon addition of the 100 mM fructose and glucose, we expected to see a further slight shift in the imine peak if the fructose and glucose bound. From these differences in integration ratios, we proposed to calculate the binding constant of the respective sugars to the oBIDs. To conduct these studies, isomer **27a** was reacted with propyl hydroxylamine **3d** and propyl hydrazine **3e** in deuterated 100 mM PBS solution to see the difference of the integrated aldehyde/imine proton peak. Control NMR experiments were also run independently with oBA **27a**, propyl hydroxylamine **3d** and propyl hydrazine **3e**, in the presence of 100 mM glucose (Fig. 36 and 37) or fructose (Fig. 38 and 39). 0.9 equivalents of propyl hydroxylamine **3d** and hydrazine **3e** were used to ensure that most of the oBA **27a** had reacted.

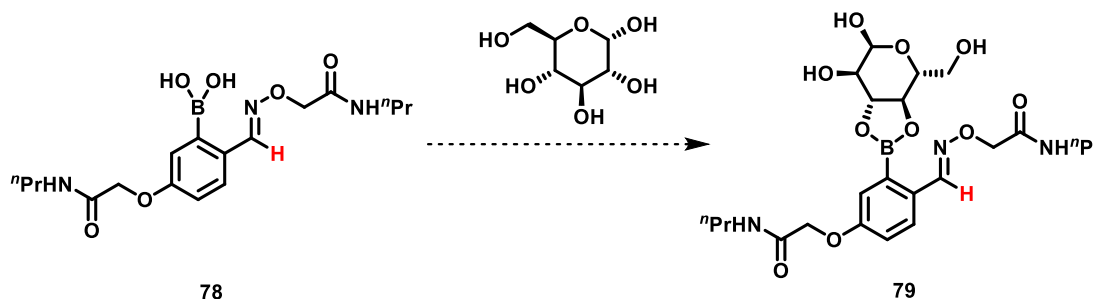


Figure 36: Proposed binding of glucose and fructose to boronic acid of **78** to form oxime **79**.

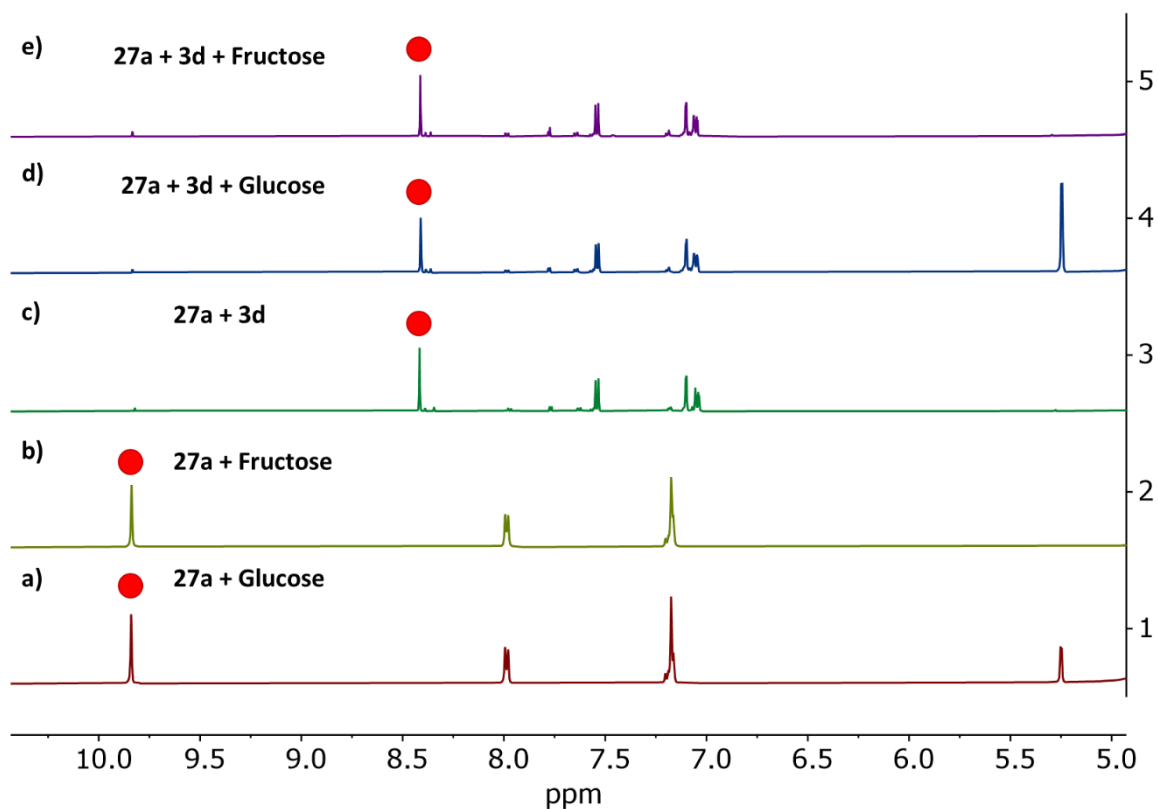


Figure 37: NMR studies of oBA **27a** in combination with propyl-hydroxylamine **3d** to form oxime oBID. Studies are performed in the presence of 100 mM glucose and 100 mM fructose to measure binding affinity.

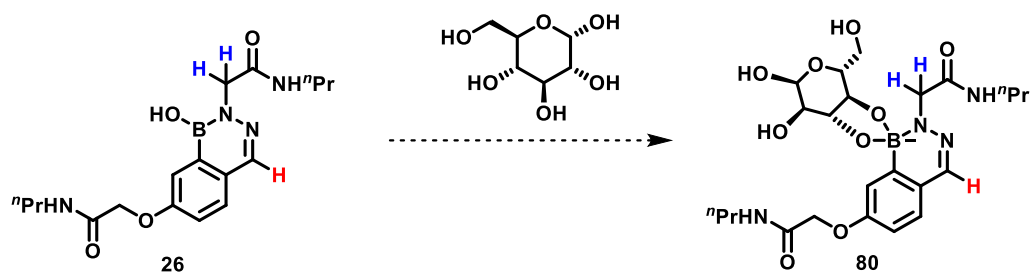


Figure 38: Proposed binding of glucose and fructose with pre-formed DAB **80** oBID conjugate.

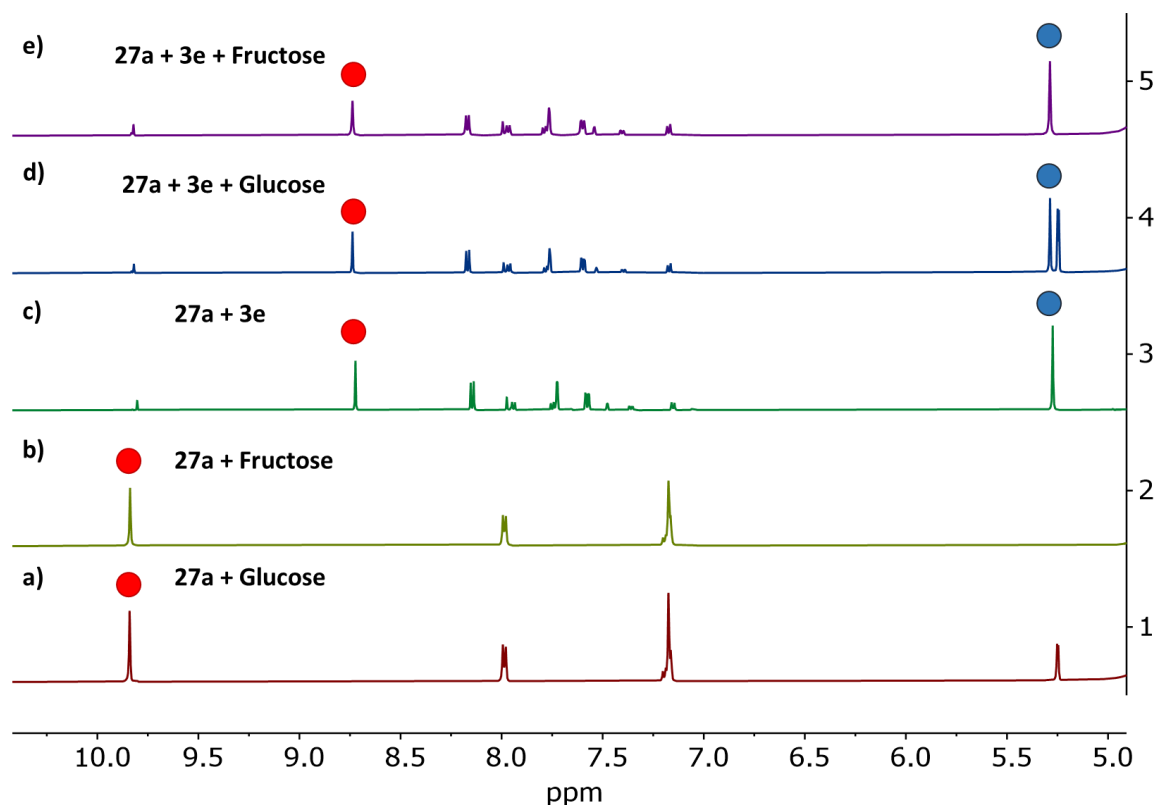


Figure 39: NMR studies of oBA **27a** in combination with propyl-hydroxylamine **3e** to form DAB **26** oBID. Studies are performed in the presence of 100 mM glucose and 100 mM fructose to measure binding affinity.

It was found that the isomer **27a** in the presence of glucose and fructose exhibits a similar aldehyde shift as it does in PBS solution (Fig. 37a/b and 40a/b). Therefore, either glucose is not binding to the boronic acid moiety in the oBA at the concentration used in these experiments, or if the glucose and fructose are binding to the boronic acid in the *ortho*-boronoaldehyde, there is no significant shift in ppm for the aldehyde. By addition of the propyl hydroxylamine **3d**, there was a clear shift in proton, with the aldehyde peak (Fig. 37a/b, red circle) at 9.8 ppm, shifted downfield due to DAB formation (Fig. 37c, red circle) at 8.4 ppm. When the oxime structure **78** was placed in glucose and fructose, there was no significant shift in the oxime peak (Fig. 37d and 37e), which indicates that glucose and fructose were again not binding. This result might be slightly surprising, as the boronic acid in the oxime structure **78**, appears to be electronically available, but the large steric repulsion by addition of the sugar could make this interaction unfavourable. By addition of propyl hydrazine **3e** to isomer **27a**, there was also a clear shift in protons, with the aldehyde peak (Fig. 39a/b, red circle) at 9.8 ppm, being shifted into a DAB peak (Fig. 39c, red circle) at 8.7 ppm. As a result of DAB cyclisation, the CH₂ group (blue circle) in the subsequent oBID is shifted further upfield from shielding effects. When the DAB structure **26**, was placed in glucose and fructose, there was no clear shift in ppm for the DAB peak (Fig. 39d/e). This result indicates that the sugars do not bind to the boronic acid, of the 6-

membered ring DAB structure either. This result is unsurprising, as the DAB formation is highly stabilised, by donation of the electrons from the nitrogen in the hydrazine into the boronic acid moiety. In order to form an interaction with the glucose or fructose, a negative charge would reside on the boronic acid, which may form a less stabilised structure. These results further validate previous FRET studies performed on the fluorimeter, where glucose and fructose caused little interference in the formation of the oxime and DAB conjugates. Due to this stability in the presence of these small molecule competitors, it may further their applications for *in vitro* studies which are stable in the presence of competing nutrients.

4. Conclusion

In conclusion, all of the oBID linkages that we formed in this work across pH 4-8 were dynamic, with dissociation constants spanning from 4.5 μM – 15 pM. This range in dissociation constants means that we could form linkages that are highly dynamic, and can dissociate in a matter of seconds, and we could also form linkages which are very stable, which could take weeks to dissociate. These linkages can be tuned to suit a specific function in chemical biology or tissue engineering. In the first instance, the plate reader and fluorimeter were used to identify a dissociative mechanism of oBID cleavage, with general trends for high reversibility ($k_{-1} \sim 10^{-2}$ - 10^{-3}) for the primary iminoboronate, IzB and TzB groups. For oxime and hydrazine linkages which were less dynamic ($k_{-1} \sim 10^{-5}$ - 10^{-6}), LC-MS studies were performed over the course of a week. This allowed us to calculate dissociation constants in the nM-pM range, which is to the best of our knowledge, the lowest reported dissociation value for an oBID in the literature.

Alternative isomers of *ortho*-boronoaldehydes were also explored, including a *para*-carboxy oBA **27b**, *meta*-phenoxy oBA **27c** and an *ortho*-boronoketone **27d**. These isomers were shown to have an effect on the electronics of the system, both at the aldehyde and boronic acid. The phenolic position of the electron donating oxygen atom had a significant effect on the electrophilicity of the aldehyde, rendering it less susceptible for nucleophilic attack when *para*- to the aldehyde. There seemed to be less of an electronic effect when the phenolic oxygen was *para*- to the boronic acid, despite suggestions that the boron centre would be less Lewis acidic for B–N interactions, as the *meta*-phenoxy oBA **27c** isomer was significantly more stable than the *para*-BA **27a**. The *para*-carboxy oBA **27b** with the electron withdrawing group *para*- to the aldehyde formed the most stable oBID linkages.

Additional studies were performed to show that a DAB aromatic structure was the most thermodynamically favoured structure across pH 4-8, confirmed by ^1H NMR studies. Finally, a glucose and fructose binding study was performed to see if monosaccharides could react with the boronic acid moiety once the oBIDs had been formed. ^1H NMR confirmed that the oxime and DAB oBID conjugates were stable in the presence of with 100 mM glucose and fructose, and therefore these sugars did not bind to the oBIDs significantly under these experimental conditions.

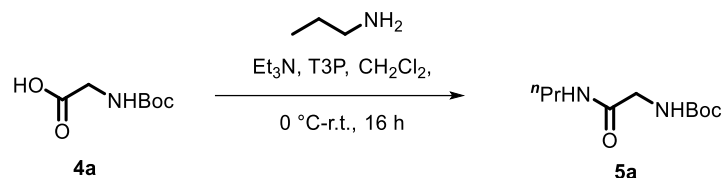
5. Future Works

In this work we summarise a novel FRET-based reporter assay which probes the rapid reaction rates of oBIDs in reversible covalent linkages. The ability to monitor the bioconjugation of oBIDs at low concentration with a high level of sensitivity provides a direct measurement conjugation irrespective of geometry and structural exchange, which reports on the cumulative formation of all species. Using this FRET reporter assay, we were able to calculate the kinetics of the reaction (k_1 , k_{-1} and K_d) for the most studied oBA-nucleophile pairs used previously in the literature, which allowed us to identify optimal pH ranges, additives, and reaction conditions. Our results also suggest that further tuning and optimisation of oBID chemistry is possible through even small changes to stereo-electronic configurations.

These results provide the foundation for the future works of this cutting-edge chemistry, to develop new functional methods relevant to bioconjugation and biomaterial chemistry. Further exploration and optimisation of the underlying chemistry presented in this work can be directly applied to growing up mesenchymal stem cells into high specialised cells. This work is currently underway in our lab, which uses this dynamic chemistry to attach and detach various proteins within a growth media, to stem cells within hydrogels. The hydrogels provide this system with a water-rich 3-dimensional scaffold upon which stem cells can grow and mature. This chemistry could therefore revolutionise the medicinal industry to repair or replaced damaged or diseased tissues. A much more robust example for this dynamic chemistry, is in the functionalisation of electrode surfaces. The attachment and detachment of different functional groups could help functionalise the electrode surface to help in electrochemistry applications. The optimised synthesis of Cy3 and Cy5 dyes can find uses in biological applications, to act as a fluorescent probe in the field of chemical biology. The application of the novel FRET-based reporter assay could be translated into similar chemistry, which requires very low concentrations of material in order to monitor the rapid reaction rates of a chemical reaction. Hence, this work can find uses in a range of future works, such as in chemistry, chemical biology and tissue engineering.

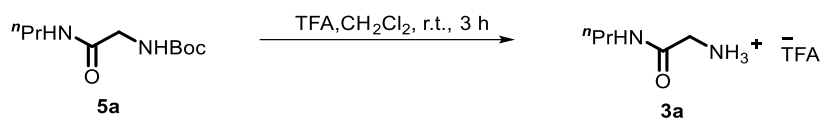
6. Experimental

6.1. Synthesis of Nucleophiles for NMR, LC-MS studies and FRET Controls



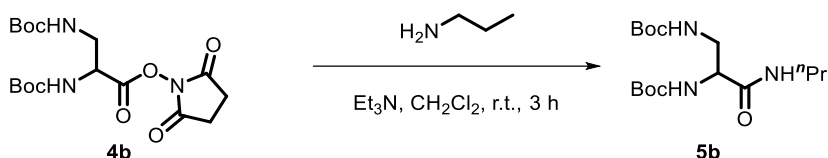
To a solution of Boc-Gly-OH (150 mg, 0.85 mmol), propylamine (178 μ L, 2.14 mmol) and triethylamine (593 μ L, 4.29 mmol) in dichloromethane (5 mL), was added propylphosphonic anhydride solution (50% w/w in EtOAc, 681 μ L, 2.14 mmol) at 0 °C and the mixture stirred at r.t. for 16 h. The reaction was then concentrated under reduced pressure. The residue was purified via flash column chromatography on silica gel eluting with EtOAc:Petrol (2:8). Fractions containing the product were concentrated under reduced pressure to provide a colourless oil (132 mg, 0.71 mmol, 49%).

R_f: 0.32 (2:8, EtOAc:Petrol); **¹H NMR** (400 MHz, CDCl₃) δ = 6.22 (s, 1H, NHCO), 5.21 (s, 1H, NHBoc), 3.75 (s, 2H, CH₂CO), 3.21 (t, J = 7.2 Hz, 2H, CH₂NH), 1.54-1.46 (m, 2H, CH₂CH₃), 1.43 (s, 9H, Boc), 0.90 (t, J = 7.2, 3H, CH₃); **¹³C NMR** (101 MHz, CDCl₃) δ = 169.5 (CON), 156.0 (COBoc), 80.4 (CH₂O), 44.6 (C(CH₃)₃), 41.2 (CH₂N), 28.4 (Boc), 22.8 (CH₂CH₃), 11.4 (CH₃); **HRMS**: m/z (ESI⁺) calc. for C₁₀H₂₀N₂O₃ [M+Na]⁺: 239.1366; Obs.: 239.1367; **ν_{\max}** : (FT-ATR)/cm⁻¹: 3312, 2968, 2933, 2876, 1656, 1512, 1365, 1248, 1164, 1049, 940, 864, 735, 551, 462.



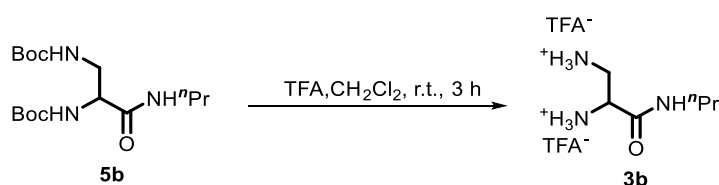
Trifluoroacetic acid (1 mL) was added dropwise to a stirred solution of **5a** (90 mg, 0.42 mmol) in dichloromethane (5 mL) and the solution was stirred at r.t. for 3 h. The reaction mixture was concentrated under reduced pressure and azeotroped with dichloromethane (4 \times 30 mL) to obtain a colourless oil. (48 mg, 0.42 mmol, quantitative yield).

R_f: 0.32 (2:8, EtOAc:Petrol); **¹H NMR** (400 MHz, CD₃OD) δ = 8.29 (m, 1H, NH), 3.68 (s, 2H, CH₂CO), 3.16 (t, J = 7.3 Hz, 2H, CH₂NH), 1.51 (dt, $J_1 = J_2 = 7.3$ Hz, 2H, CH₂CH₃), 0.89 (t, J = 7.3 Hz, 3H, CH₃); **¹³C NMR** (101 MHz, CD₃OD) δ = 165.8 (CON), 41.0 (CH₂O), 40.2 (CH₂N), 22.8 (CH₂CH₃), 10.29 (CH₃); **HRMS**: m/z (ESI⁺) calc. for C₅H₁₂N₂O [M+H]⁺: 117.1022; Obs.: 117.1022; **ν_{\max}** : (FT-ATR)/cm⁻¹: 3305, 2926, 1663, 1576, 1436, 1275, 1130, 840, 916, 798, 723, 518.



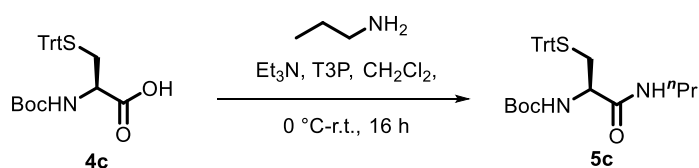
A mixture of **4b** (154 mg, 0.38 mmol), propylamine (96 μ L, 1.15 μ mol), and triethylamine (266 μ L, 1.92 mmol) in dichloromethane (5 mL) was stirred at r.t. for 3 h. The reaction was then concentrated under reduced pressure. The residue was purified via flash column chromatography on silica gel, eluting with EtOAc:Petrol (2:8). Fractions containing the product were concentrated under reduced pressure to provide a colourless oil (35 mg, 0.10 mmol, 27%).

R_f: 0.38 (3:7, EtOAc:Petrol); **¹H NMR** (400 MHz, CDCl₃) δ = 6.72 (s, 1H, NHPr), 5.84 (s, 1H, BocNHCH), 5.26 (s, 1H, BocNHCH₂), 4.16 (dt, $J_1 = J_2 = 6.1$ Hz, 1H, CHNH₂Boc), 3.49-3.40 (m, 2H, CH₂NHBoc), 3.22-3.15 (m, 2H, CH₂CH₂CH₃), 1.49 (q, $J = 7.5$ Hz, 2H, CH₂CH₃), 1.43-1.39 (m, 18H, 2 \times Boc), 0.88 (s, 3H, CH₃); **¹³C NMR** (101 MHz, CDCl₃) δ = 170.6 (CONH), 157.2 (COBoc), 156.3 (COBoc), 80.3 (C(CH₃)₃), 80.0 (C(CH₃)₃), 55.7 (CHNH₂Boc), 42.5 (CH₂NHBoc), 41.2 (CH₂CH₂CH₃), 28.4 (Boc), 28.4 (Boc), 22.8 (CH₂CH₃), 11.4 (CH₃); **HRMS**: m/z (ESI⁺) calc. for C₁₆H₃₂N₃O₅ [M+H]⁺: 346.2336; Obs.: 346.2335; **ν_{\max}** : (FT-ATR)/cm⁻¹: 3330, 2975, 2933, 2876, 1690, 1654, 1518, 1365, 1249, 1163, 1078, 868, 780, 644.



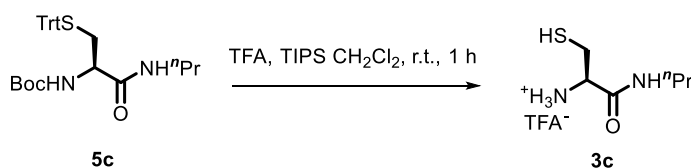
Trifluoroacetic acid (1 mL) was added dropwise to a stirred solution of **5b** (30 mg, 87 μ mol) in dichloromethane (5 mL) and the solution was stirred at r.t. for 3 h. The reaction mixture was concentrated under reduced pressure and azeotroped with dichloromethane (4 \times 30 mL) to obtain a colourless oil. (13 mg, 87 μ mol, quantitative yield).

R_f: 0.24 (3:7, EtOAc:Petrol); **¹H NMR** (400 MHz, CD₃OD) δ = 4.21 (t, $J = 7.2$ Hz, 1H, CHCO), 3.47-3.26 (m, 3H, CH₂NH, CONHCH₂), 3.12 (dt, $J = 13.7, 7.2$ Hz, 1H, ONHCH₂), 1.55 (tq, $J_1 = J_2 = 7.4$ Hz, 2H, CH₂CH₃), 0.93 (t, $J = 7.4$ Hz, 3H, CH₃); **¹³C NMR** (101 MHz, CD₃OD) δ = 165.3 (CON), 50.8 (CHNH₃⁺), 41.5 (CONHCH₂), 39.7 (CH₂NH₃⁺), 21.9 (CH₂CH₃), 10.3 (CH₃); **HRMS**: m/z (ESI⁺) calc. for C₆H₁₅N₃O [M+H]⁺: 146.1288; Obs.: 146.1288; **ν_{\max}** : (FT-ATR)/cm⁻¹: 3287, 2968, 2938, 2879, 1649, 1553, 1462, 1200, 1136, 837, 800, 722.



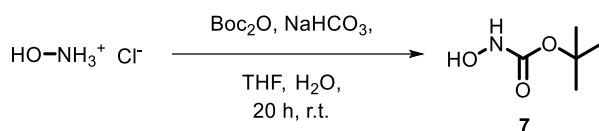
To a solution of Boc-Cys(Trt)-OH (200 mg, 0.431 mmol), propylamine (54 μ L, 0.647 mmol), and triethylamine (300 μ L, 2.16 mmol) in dichloromethane (5 mL), was added propylphosphonic anhydride solution (50% w/w in EtOAc, 343 μ L, 1.08 mmol) at 0 °C and the mixture stirred at r.t. for 16 h. The reaction was then concentrated under reduced pressure. The residue was purified via flash column chromatography on silica gel eluting with EtOAc:Petrol (2:8). Fractions containing the product were concentrated under reduced pressure to provide a colourless oil (205 mg, 0.43 mmol, 99%).

R_f: 0.29 (2:8, EtOAc:Petrol, UV active); **¹H NMR** (400 MHz, CDCl₃) δ = 7.44-7.38 (m, 6H, PhH₂), 7.31-7.25 (m, 6H, PhH₃), 7.23-7.18 (m, 3H, PhH₄), 5.94 (s, 1H, NH_{Boc}), 4.80-4.64 (m, 1H, NHPr), 3.80 (d, J = 6.4 Hz, 1H, CH_{NHBoc}), 3.16-3.09 (m, 2H, CH₂NH), 2.74-2.66 (m, 1H, CH₂STrt), 2.53-2.45 (m, 1H, CH₂STrt), 1.50-1.42 (m, 2H, CH₂CH₃), 1.40 (s, 9H, Boc), 0.86 (t, J = 7.4 Hz, 3H, CH₃); **¹³C NMR** (101 MHz, CDCl₃) δ = 170.4 (C_{CON}), 144.5 (C_{OBoc}), 129.7 (PhC₂), 128.2 (PhC₃), 127.0 (PhC₄), 82.3 (CH_{NHBoc}), 67.3 (CH₂STrt), 41.3 (CH₂NH), 28.4 (Boc), 22.8 (CH₂CH₃), 11.4 (CH₃); **HRMS**: m/z (ESI⁺) calc. for C₃₀H₃₆N₂O₃S [M+Na]⁺: 527.2335; Obs.: 527.2335; **v_{max}**: (FT-ATR)/cm⁻¹: 3300, 3058, 2967, 2931, 2875, 1655, 1526, 1489, 1366, 1248, 1165, 1047, 865, 739, 698, 621, 505.



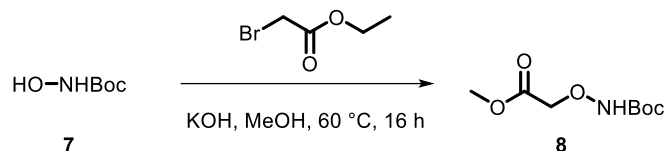
Trifluoroacetic acid (1 mL) was added dropwise to a stirred solution of **5c** (195 mg, 0.41 mmol) and triisopropylsilane (439 μ L, 2.04 mmol) in dichloromethane (5 mL), and the mixture stirred at r.t. for 16 h. The reaction was then concentrated under reduced pressure to ~5 mL, and the remaining solution added dropwise to diethyl ether (200 mL). The resultant precipitate was collected by filtration, washed with diethyl ether (30 mL), and dried in air. The solid was then dissolved in methanol (10 mL) and concentrated under reduced pressure to afford a colourless oil. (67 mg, 0.41 mmol, quantitative yield).

R_f: 0.18 (2:8, EtOAc:Petrol, UV active); **¹H NMR** (400 MHz, CD₃OD) δ = 3.98-3.90 (m, 1H, CH_{NH₃⁺}), 3.29-3.15 (m, 2H, CH₂NH), 3.04-2.87 (m, 2H, CH₂STrt), 1.59-1.48 (m, 2H, CH₂CH₃), 0.92 (t, J = 7.4 Hz, 3H, CH₃); **¹³C NMR** (101 MHz, CD₃OD) δ = 166.9 (C_{CON}), 54.8 (CH_{NH₃⁺}), 41.2 (CH₂NH), 25.0 (CH₂SH), 22.1 (CH₂CH₃), 10.4 (CH₃); **HRMS**: m/z (ESI⁺) calc. for C₆H₁₄N₂OS [M+Na]⁺: 185.0719; Obs.: 185.0720; **v_{max}**: (FT-ATR)/cm⁻¹: 3286, 3090, 2966, 1655, 1571, 1265, 1181, 1133, 838, 798, 722, 517.



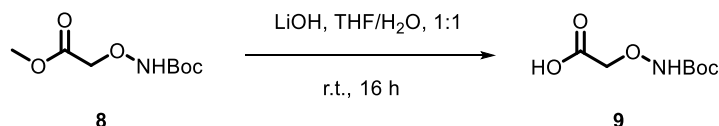
A solution of sodium hydrogen carbonate (2.44 g, 29.0 mmol) in water (30 mL) was added dropwise to a mixture of hydroxylamine hydrochloride (1.00 g, 14.5 mmol) and di-*tert*-butyl dicarbonate (3.16 g, 14.5 mmol) in tetrahydrofuran (20 mL), and the reaction stirred at r.t. for 20 h. Water (150 mL) was then added, and the aqueous was extracted with ethyl acetate (2 × 150 mL). The combined organics were washed with water (30 mL) and brine (2 × 30 mL), dried with MgSO₄, filtered, and concentrated to afford a colourless oil (1.71 g, 12.9 mmol, 89%). Data were consistent with those previously reported.^{22,23}

R_f: 0.30 (1:9, EtOAc:Petrol); **¹H NMR** (400 MHz, CDCl₃) δ = 7.02 (s, 1H, NH), 1.46 (s, 9H, Boc); **¹³C NMR** (101 MHz, CDCl₃) δ = 158.8 (C=O), 82.3 (CMe₃), 28.3 (Boc); **HRMS**: m/z (ESI⁺) calc. for C₅H₁₀NO₃ [M+Na]⁺: 156.0633; Obs.: 156.0633.



A mixture of ethyl bromoacetate (1.40 mL, 12.6 mmol), **7** (1.68 g, 12.6 mmol), and potassium hydroxide (0.71 g, 12.6 mmol) in methanol (15 mL) was stirred at 60 °C for 16 h. The reaction mixture was then concentrated under reduced pressure. Water (30 mL) was added to the residue and the aqueous was extracted with dichloromethane (4 × 30 mL). The combined organics were washed with brine (50 mL), dried with MgSO₄, filtered, and concentrated under reduced pressure. The residue was purified via flash column chromatography on silica gel, eluting with EtOAc:petrol (2:8). Pure fractions were concentrated under reduced pressure to provide a yellow solid (1.36 g, 6.63 mmol, 53%). Data were consistent with those previously reported.²⁴

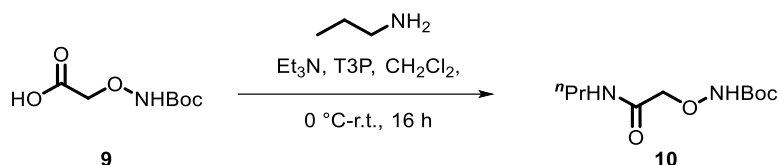
R_f: 0.33 (2:8, EtOAc:Petrol); **¹H NMR** (400 MHz, CDCl₃) δ = 7.75 (s, 1H, NH), 4.43 (s, 2H, CH₂O), 3.77 (s, 3H, OCH₃), 1.48 (s, 9H, Boc); **¹³C NMR** (101 MHz, CDCl₃) δ = 170.2 (CO), 156.3 (COONH), 82.3 (CMe₃), 72.6 (CONH), 52.2 (CH₃O), 28.2 (Boc); **HRMS**: m/z (ESI⁺) calc. for C₈H₁₄NO₅ [M+Na]⁺: 228.0842; Obs.: 228.0841; **v_{max}**: (FT-ATR)/cm⁻¹: 3305, 2979, 1737, 1439, 1368, 1216, 1165, 1117, 995, 848, 776, 713, 589; **m.p.**: 55-57 °C.



Lithium hydroxide (0.40 g, 16.6 mmol) was added to a solution of **8** (1.36 g, 6.63 mmol) in a mixture of tetrahydrofuran (5 mL) and water (5 mL), and the reaction was stirred at r.t. for 16 h. The tetrahydrofuran was then removed under reduced pressure and hydrochloric

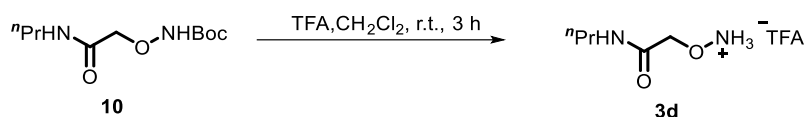
acid (1 M, 30 mL) was added. The aqueous was extracted with ethyl acetate (3 × 50 mL) and the combined organics dried with MgSO₄, filtered, and concentrated under reduced pressure to afford a cream-white solid (972 mg, 5.09 mmol, 77%).

R_f: 0.22 (1:1, EtOAc:Petrol); **¹H NMR** (400 MHz, CDCl₃) δ = 11.02 (s, 1H, OH), 8.21 (s, 1H, NH), 4.46 (s, 2H, CH₂O), 1.47 (s, 9H, Boc); **HRMS**: m/z (ESI⁺) calc. for C₇H₁₁NO₅ [M+H]⁺: 190.0721; Obs.: 190.0716; **v_{max}**: (FT-ATR)/cm⁻¹: 3266, 2981, 2936, 1721, 1479, 1395, 1370, 1251, 1163, 1122, 1054, 979, 847, 777, 675; **m.p.**: 102-105 °C.



To a solution of **9** (115 mg, 0.60 mmol), propylamine (125 μL, 1.51 mmol) and triethylamine (416 μL, 3.01 mmol) in dichloromethane (5 mL), was added propylphosphonic anhydride solution (50% w/w in EtOAc, 479 μL, 1.51 mmol) at 0 °C and the mixture was warmed to r.t. and stirred for 16 h. The reaction was then concentrated under reduced pressure. The residue was purified via flash column chromatography on silica gel eluting with EtOAc:Petrol (2:8). Fractions containing the product were concentrated under reduced pressure to provide a colourless oil (65 mg, 0.28 mmol, 46%).

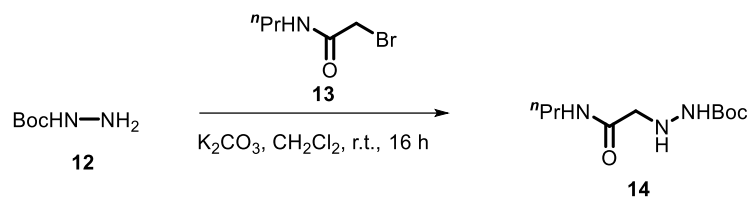
R_f: 0.36 (2:8, EtOAc:Petrol); **¹H NMR** (400 MHz, CDCl₃) δ = 8.15 (s, 1H, NH), 4.24 (s, 2H, CH₂O), 3.20 (t, *J* = 7.3 Hz, 2H, CH₂NH), 1.51 (dt, *J* = 7.3 Hz, 2H, CH₂CH₃), 1.42 (s, 9H, Boc), 0.88 (t, *J* = 7.3 Hz, 3H, CH₃); **¹³C NMR** (101 MHz, CDCl₃) δ = 169.1 (CONH), 158.0 (COBoc), 82.8 (C(CH₃)₃), 76.1 (CH₂CO), 40.9 (CH₂NH), 28.2 (Boc), 22.6 (CH₂CH₃), 11.5 (CH₃); **HRMS**: m/z (ESI⁺) calc. for C₁₀H₂₀N₂O₄ [M+Na]⁺: 255.1315; Obs.: 255.1311; **v_{max}**: (FT-ATR)/cm⁻¹: 3285, 2969, 2934, 2877, 1724, 1650, 1552, 1459, 1368, 1252, 1162, 1110, 776, 586.



Trifluoroacetic acid (1 mL) was added dropwise to a stirred solution of **10** (60 mg, 0.26 mmol) in dichloromethane (5 mL) and the solution was stirred at r.t. for 3 h. The reaction mixture was concentrated under reduced pressure and azeotroped with dichloromethane (4 × 30 mL) to obtain a colourless oil. (34 mg, 0.26 mmol, quantitative yield).

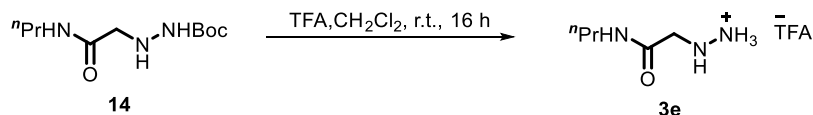
R_f: 0.27 (2:8, EtOAc:Petrol); **¹H NMR** (400 MHz, CD₃OD) δ = 4.20 (s, 2H, CH₂CO), 2.92 (t, *J* = 7.4 Hz, 2H, CH₂NH), 1.26 (dt, *J*₁ = *J*₂ = 7.4 Hz, 2H, CH₂CH₃), 0.64 (t, *J* = 7.4 Hz, 3H, CH₃); **¹³C NMR** (101 MHz, CD₃OD) δ = 168.5 (CONH), 71.4 (CH₂CO), 40.6 (CH₂NH), 22.2 (CH₂CH₃), 10.3 (CH₃); **HRMS**: m/z (ESI⁺) calc. for C₅H₁₂N₂O₂ [M+H]⁺: 133.0972; Obs.:

133.0967; ν_{max} : (FT-ATR)/ cm^{-1} : 3288, 3089, 2966, 2877, 1654, 1544, 1460, 1201, 1084, 833, 580.



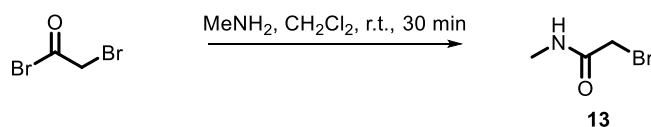
A mixture of **12** (371 mg, 2.81 mmol), **13** (603 mg, 3.37 mmol), and potassium carbonate (776 mg, 5.62 mmol) in dimethylformamide (5 mL) was stirred at 80 °C for 30 min. The mixture was then cooled to r.t. and diluted with water (50 mL). The aqueous was extracted with ethyl acetate (3 × 50 mL), and the combined organics washed with brine (2 × 30 mL), dried with MgSO_4 , filtered, and concentrated under reduced pressure. The residue was purified via flash column chromatography on silica gel eluting with EtOAc:Petrol (2:8). Fractions containing the product were concentrated under reduced pressure to provide a colourless oil (532 mg, 2.30 mmol, 82%).

R_f: 0.36 (2:8, EtOAc:Petrol); **¹H NMR** (400 MHz, CDCl_3) δ = 7.56 (s, 1H, NHP_r), 6.40 (s, 1H, NH_{Boc}), 4.19 (s, 1H, NH_{NHBoc}), 3.46 (s, 2H, CH_2CO), 3.20 (t, J = 7.4 Hz, 2H, CH_2NH), 1.55-1.49 (m, 2H, CH_2CH_3), 1.41 (s, 9H, Boc), 0.90 (t, J = 7.4 Hz, 3H, CH_3); **¹³C NMR** (101 MHz, CDCl_3) δ = 170.1 (CON), 156.8 (COBoc), 81.0 ($\text{C}(\text{CH}_3)_3$), 55.5 (CH_2O), 41.0 (CH_2NH), 28.3 (Boc), 22.8 (CH_2CH_3), 11.5 (CH_3); **HRMS**: m/z (ESI⁺) calc. for $\text{C}_{10}\text{H}_{21}\text{N}_3\text{O}_3$ [$\text{M}+\text{Na}$]⁺: 254.1475; Obs.: 254.1469; ν_{max} : (FT-ATR)/ cm^{-1} : 3298, 2969, 2934, 2877, 1714, 1650, 1545, 1460, 1367, 1282, 1250, 1159, 1046. 1022, 849, 754, 593.



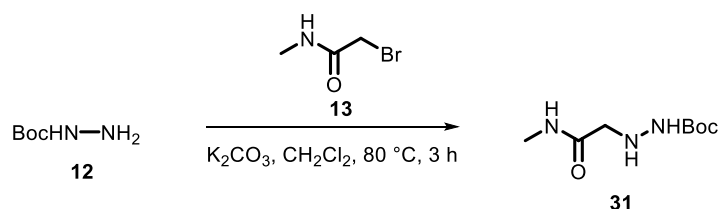
Trifluoroacetic acid (1 mL) was added dropwise to a stirred solution of **14** (70 mg, 0.142 mmol) in dichloromethane (5 mL), and the solution was stirred at r.t. for 16 h. The reaction mixture was then concentrated under reduced pressure and azeotroped with dichloromethane (4 × 30 mL) to obtain a colourless oil (40 mg, 0.142 mmol, quantitative yield).

R_f: 0.24 (2:8, EtOAc:Petrol); **¹H NMR** (400 MHz, CD_3OD) δ = 3.62 (s, 2H, $\text{CH}_2\text{NHNH}_3^+$), 3.16 (t, J = 7.3 Hz, 2H, CH_2NHCO), 1.58-1.48 (m, 2H, CH_2CH_3), 0.91 (t, J = 7.3 Hz, 3H, CH_3); **¹³C NMR** (101 MHz, CDCl_3) δ = 168.8 (CON), 50.4 ($\text{CH}_2\text{ONHNH}_3^+$), 40.8 (CH_2NH), 22.2 (CH_2CH_3), 10.3 (CH_3); **HRMS**: m/z (ESI⁺) calc. for $\text{C}_5\text{H}_{13}\text{N}_3\text{O}$ [$\text{M}+\text{Na}$]⁺: 132.1131; Obs.: 132.1130; ν_{max} : (FT-ATR)/ cm^{-1} : 3300, 2965, 2934, 2876, 1651, 1543, 1460, 1201, 1146, 721.



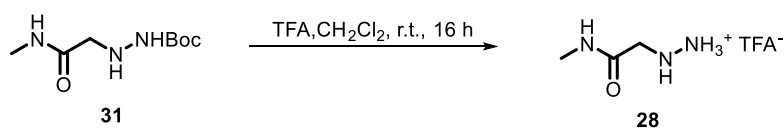
Methylamine (1.00 mL, 22.6 mmol) was added to a solution of bromoacetyl bromide (1.00 mL, 11.3 mmol) in dichloromethane (30 mL) and stirred at r.t. for 30 min. The mixture was then diluted with water (70 mL) and the aqueous was extracted with ethyl acetate (3 × 70 mL). The combined organics were washed with brine (2 × 100 mL), dried with MgSO₄, filtered, and concentrated under reduced pressure to provide a colourless oil (1.56 g, 1.03 mmol, 91%).

R_f: 0.29 (2:8, EtOAc:Petrol); **¹H NMR** (400 MHz, CDCl₃) δ = 3.80 (s, 2H, CH₂), 3.73 (s, 3H, CH₃); **¹³C NMR** (101 MHz, CDCl₃) δ = 167.8 (CON), 53.2 (CH₂), 25.7 (CH₃); **HRMS**: m/z (ESI⁺) calc. for C₃H₆NO [M+Na]⁺: 193.9525; Obs.: 193.9525; **v_{max}**: (FT-ATR)/cm⁻¹: 2956, 1736, 1437, 1280, 1165, 1113, 1006, 884, 708, 670, 549.



A mixture of **12** (500 mg, 3.79 mmol), **13** (732 mg, 4.55 mmol), and potassium carbonate (1.05 g, 7.58 mmol) in dimethylformamide (10 mL) was stirred at 80 °C for 3 h. The mixture was then cooled to r.t. and diluted with water (70 mL). The aqueous was extracted with ethyl acetate (3 × 50 mL), and the combined organics washed with brine (2 × 50 mL), dried with MgSO₄, filtered, and concentrated under reduced pressure. The residue was purified via flash column chromatography on silica gel, eluting with EtOAc:Petrol (2:8). Fractions containing the product were concentrated under reduced pressure to provide a colourless oil (50 mg, 0.25 mmol, 6%).

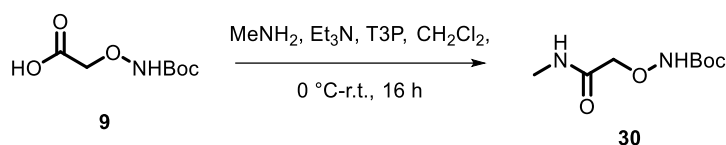
R_f: 0.26 (2:8, EtOAc:Petrol); **¹H NMR** (400 MHz, CDCl₃, data provided for major rotamer) δ = 6.53 (s, 1H, NHMe), 3.78-3.68 (m, 3H, CH₃), 3.60 (s, 2H, CH₂), 1.40 (s, 9H, Boc); **¹³C NMR** (101 MHz, CDCl₃, data provided for major rotamer) δ = 171.9 (CON), 162.9 (COBoc), 81.0 (C(CH₃)₃), 53.0 (CH₂), 52.2 (CH₃), 28.6 (C(CH₃)₃); **HRMS**: Product was not observed via HRMS; **v_{max}**: (FT-ATR)/cm⁻¹: 3320, 2978, 1714, 1438, 1367, 1209, 1149, 1049, 1017, 779.



Trifluoroacetic acid (1 mL) was added dropwise to a stirred solution of **31** (43 mg, 0.21 mmol) in dichloromethane (5 mL) and the solution was stirred at r.t. for 16 h. The reaction

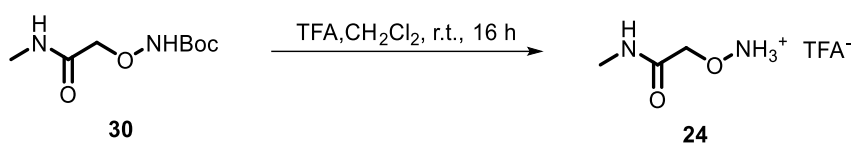
mixture was then concentrated under reduced pressure and azeotroped with dichloromethane (4 × 30 mL) to obtain a colourless oil (22 mg, 0.21 mmol, quantitative yield).

R_f: 0.18 (2:8, EtOAc:Petrol); **¹H NMR** (400 MHz, CD₃OD) δ = 3.82-3.76 (m, 2H, CH₂), 3.78-3.70 (m, 3H, CH₃); **¹³C NMR** (101 MHz, CD₃OD) δ = 171.8 (CON), 52.9 (CH₂), 50.6 (CH₃); **HRMS**: Product was not observed via HRMS; **v_{max}**: (FT-ATR)/cm⁻¹: 2959, 1730, 1438, 1205, 1154, 1047, 1005, 907, 761.



To a solution of **9** (300 mg, 1.57 mmol), methylamine (140 μL, 3.14 mmol), and triethylamine (1.09 mL, 7.85 mmol) in dichloromethane (5 mL), was added propylphosphonic anhydride solution (50% w/w in EtOAc, 1.25 mL, 3.93 mmol) at 0 °C, and the mixture was then stirred at r.t. for 16 h. The reaction was concentrated under reduced pressure and the residue was purified via flash column chromatography on silica gel eluting with EtOAc:Petrol (2:8). Fractions containing the product were concentrated under reduced pressure to provide a white solid (145 mg, 0.71 mmol, 45%).

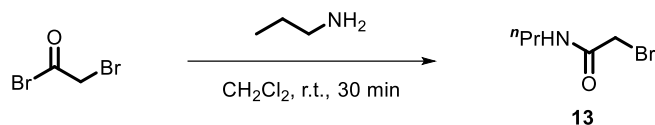
R_f: 0.31 (2:8, EtOAc:Petrol); **¹H NMR** (400 MHz, CDCl₃) δ = 8.03 (s, 1H, NH₂Boc), 7.60 (s, 1H, NHMe), 4.33 (s, 2H, CH₂), 2.86 (s, 3H, CH₃), 1.48 (s, 9H, Boc); **¹³C NMR** (101 MHz, CDCl₃) δ = 169.4 (CONH), 157.9 (COBoc), 83.4 (C(CH₃)₃), 76.6 (CH₂CO), 28.2 (C(CH₃)₃), 25.8 (CH₃); **HRMS**: m/z (ESI⁺) calc. for C₈H₁₆N₂O₄ [M+Na]⁺: 227.1002; Obs.: 227.1008; **v_{max}**: (FT-ATR)/cm⁻¹: 3287, 2979, 2939, 1723, 1658, 1559, 1480, 1369, 1280, 1253, 1163, 1112, 977, 583.



Trifluoroacetic acid (1 mL) was added dropwise to a stirred solution of **30** (60 mg, 0.26 mmol) in dichloromethane (5 mL) and stirred at r.t. for 3 h. The reaction mixture was concentrated under reduced pressure and azeotroped with dichloromethane (4 × 30 mL) to obtain a colourless oil. (34 mg, 0.26 mmol, quantitative yield).

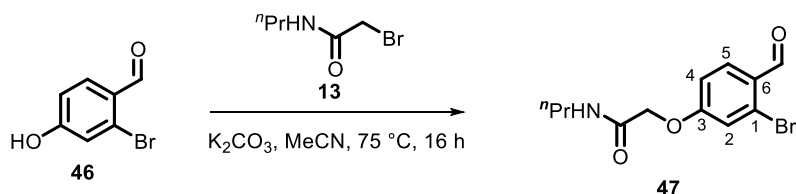
R_f: 0.22 (2:8, EtOAc:Petrol); **¹H NMR** (400 MHz, CD₃OD) δ = 4.50 (s, 2H, CH₂), 2.80 (s, 3H, CH₃); **¹³C NMR** (101 MHz, CD₃OD) δ = 170.1 (CON), 72.7 (CH₂), 25.9 (CH₃); **HRMS**: m/z (ESI⁺) calc. for C₃H₈N₂O₂ [M+H]⁺: 105.0659; Obs.: 105.0652; **v_{max}**: (FT-ATR)/cm⁻¹: 3313, 2924, 1654, 1553, 1414, 1199, 1135, 1085, 834, 800, 722, 577.

6.2. Synthesis of oBA Substrates for NMR and LC-MS Studies



Propylamine (3.78 mL, 45.4 mmol) was added to a solution of bromoacetyl bromide (2.00 mL, 22.6 mmol) in dichloromethane (40 mL) and stirred at r.t. for 30 min. The mixture was then diluted with water (150 mL) and the aqueous extracted with dichloromethane (3 × 70 mL). The combined organics were washed with brine (2 × 200 mL), dried with MgSO₄, filtered, and concentrated under reduced pressure to provide a colourless oil (3.40 g, 19.0 mmol, 84%).

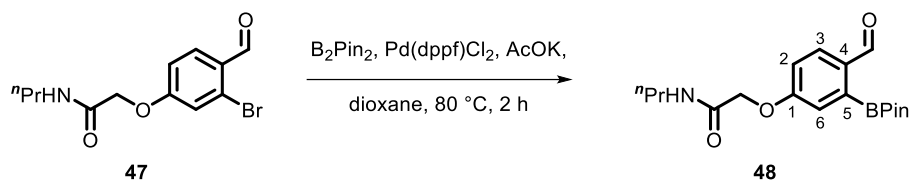
R_f: 0.32 (2:8, EtOAc:Petrol); **¹H NMR** (400 MHz, CDCl₃) δ = 6.67 (s, 1H, NH), 3.88 (s, 2H, CH₂Br), 3.28-3.15 (m, 2H, CH₂N), 2.00-1.91 (m, 2H, CH₂CH₃), 0.92 (t, *J* = 7.4 Hz, 3H, CH₃); **¹³C NMR** (101 MHz, CDCl₃) δ = 165.8 (CON), 42.0 (CH₂NH), 29.4 (CH₂Br), 22.6 (CH₂CH₃), 11.3 (CH₃); **HRMS**: *m/z* (ESI⁺) calc. for C₅H₁₀⁷⁹BrNO [M+H]⁺: 181.0019; Obs.: 181.0020; **v_{max}**: (FT-ATR)/cm⁻¹: 3265, 3073, 2965, 2934, 2876, 1738, 1650, 1550, 1460, 1437, 1313, 1211, 1150, 953, 651, 550.



A mixture of 2-bromo-4-hydroxybenzaldehyde (1.56 g, 8.57 mmol), **13** (1.72 g, 8.57 mmol) and potassium carbonate (2.01 g, 14.6 mmol) in acetonitrile (30 mL) was stirred at 75 °C for 16 h. The mixture was then cooled to r.t. and diluted with water (150 mL). The aqueous was extracted with ethyl acetate (3 × 70 mL), and the combined organics washed with brine (2 × 200 mL), dried with MgSO₄, filtered, and concentrated under reduced pressure to provide an orange oil (2.50 g, 8.32 mmol, 97%). Data were consistent with those previously reported.

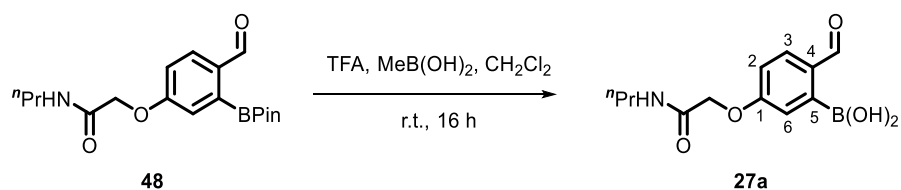
R_f: 0.30 (2:8, EtOAc:Petrol, UV active); **¹H NMR** (400 MHz, CDCl₃); δ = 10.20 (s, 1H, PhCOH), 7.89 (d, *J* = 8.7 Hz, 1H, PhH₅), 7.17 (d, *J* = 2.5 Hz, 1H, PhH₂), 6.96 (dt, *J* = 8.7, 2.5 Hz, 1H, PhH₄), 6.49 (s, 1H, NH), 4.54 (s, 2H, CH₂O), 3.30 (t, *J* = 7.4 Hz, 2H, CH₂N), 1.60-1.52 (m, 2H, CH₂CH₃), 0.91 (t, *J* = 7.4 Hz, 3H, CH₃); **¹³C NMR** (101 MHz, CDCl₃) δ = 190.5 (PhCOH), 166.6 (CON), 161.8 (PhC₃), 131.8 (PhC₅), 128.8 (PhC₆), 128.3 (PhC₁), 119.6 (PhC₂), 114.5 (PhC₄), 67.6 (CH₂O), 41.0 (CH₂N), 22.9 (CH₂CH₃), 11.4 (CH₃); **HRMS**: *m/z* (ESI⁺) calc. for C₁₂H₁₄NO₃ [M+Na]⁺: 324.0028; Obs.: 324.0028; **v_{max}**:

(FT-ATR)/cm⁻¹: 3319, 2974, 2934, 2876, 1679, 1590, 1540, 1412, 1336, 1215, 1142, 965, 852, 831, 675, 578.



47 (300 mg, 1.00 mmol), bis(pinacolato)diboron (660 mg, 2.60 mmol), 1,1'-[bis(diphenylphosphino)ferrocene]dichloropalladium(II) (146 mg, 0.20 mmol), and potassium acetate (530 mg, 5.40 mmol) were placed under a nitrogen atmosphere, and anhydrous dioxane (20 mL) was added. The reaction was degassed under a constant flow of nitrogen for 10 min, and then stirred at 80 °C for 16 h. After cooling to r.t., the reaction was concentrated under reduced pressure. The residue was purified via flash column chromatography on silica gel, eluting with EtOAc:Petrol (2:8). Fractions containing the product were concentrated under reduced pressure to yield a colourless oil (34 mg, 95 μmol, 9%).

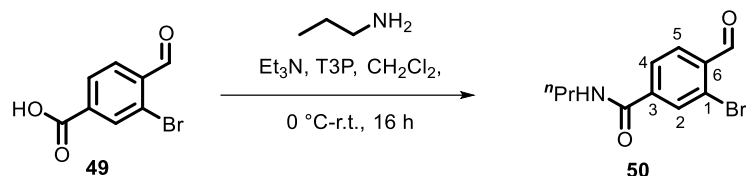
R_f: 0.25 (2:8, EtOAc:Petrol, UV active); **¹H NMR** (400 MHz, CDCl₃) δ = 10.29 (s, 1H, PhCOH), 7.86 (d, *J* = 8.6 Hz, 1H, PhH₃), 7.00 (dd, *J* = 8.6, 2.8 Hz, 1H, PhH₂), 6.80 (t, *J* = 2.8 Hz, 1H, PhH₆), 6.51 (s, 1H, NH), 4.51 (s, 2H, CH₂O), 3.22 (dt, *J*₁ = *J*₂ = 6.6 Hz, 2H, CH₂N), 1.51-1.45 (m, 2H, CH₂CH₃), 1.30 (s, 12H, Pin), 0.84-0.79 (m, 3H, CH₃); **¹³C NMR** (101 MHz, CDCl₃) δ = 193.0 (C=O), 167.8 (C=O), 160.7 (PhC₁), 135.6 (PhC₄), 130.7 (PhC₅), 122.3 (PhC₂), 121.0 (PhC₃), 116.6 (PhH₆), 84.6 (C(CH₃)₂), 82.8 (C(CH₃)₂), 67.1 (CH₂O), 40.9 (CH₂N), 24.8 (Pin), 22.7 (CH₂CH₃), 11.3 (CH₃); **HRMS**: *m/z* (ESI⁺) calc. for C₁₈H₂₆BNO₅ [M+Na]⁺: 370.1796; Obs.: 370.1802; **v_{max}**: (FT-ATR)/cm⁻¹: 3315, 2966, 2933, 2875, 1657, 1542, 1422, 1336, 1213, 1141, 1060, 964, 812, 675, 578.



Trifluoroacetic acid (2 mL) was added to a solution of **48** (34 mg, 95 μmol) and methylboronic acid (57 mg, 0.95 mmol) in dichloromethane (10 mL), and the mixture stirred at r.t for 16 h. The reaction was concentrated under reduced pressure and the residue azeotroped with dichloromethane (3 × 20 mL), then hydrochloric acid (0.1 M, 2 × 10 mL), to give a brown oil (25 mg, 95 μmol, quantitative yield).

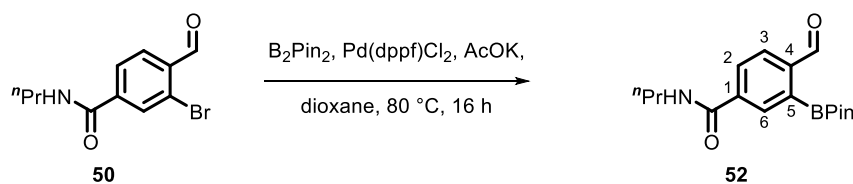
R_f: 0.18 (3:7, EtOAc:Petrol, UV active); **¹H NMR** (400 MHz, 100 mM deuterated PBS + 10% DMSO-*d*₆) δ = 9.84 (s, 1H, -CHO), 7.97-8.01 (m, 1H, PhH₃), 7.21-7.14 (m, 2H, PhH₆ and PhH₂), 4.75 (s, 2H, CH₂O), 3.25 (t, *J* = 6.9 Hz, 2H, CH₂N), 1.54 (tt, *J*₁ = *J*₂ = 6.9 Hz, 2H, CH₂CH₃), 0.88 (t, *J* = 6.9 Hz, 3H, CH₃); **¹³C NMR** (101 MHz, 100 mM deuterated PBS

+ 10% DMSO- d_6) δ = 195.2 ($\underline{\text{C}}\text{HO}$), 170.3 ($\underline{\text{C}}\text{ON}$), 161.9 ($\text{Ph}\underline{\text{C}}\text{1}$), 136.1 ($\text{Ph}\underline{\text{C}}\text{4}$), 132.4 ($\text{Ph}\underline{\text{C}}\text{5}$), 118.2 ($\text{Ph}\underline{\text{C}}\text{2}$), 115.3 ($\text{Ph}\underline{\text{C}}\text{3}$), 114.56 ($\text{Ph}\underline{\text{H}}\text{6}$), 66.6 ($\underline{\text{C}}\text{H}_2\text{O}$), 40.9 ($\underline{\text{C}}\text{H}_2\text{N}$), 21.9 ($\underline{\text{C}}\text{H}_2\text{CH}_3$), 10.6 ($\underline{\text{C}}\text{H}_3$); **HRMS**: m/z (ESI⁺) calc. for $\text{C}_{12}\text{H}_{16}\text{BrNO}_5$ [M-H]⁺: 288.1014; Obs.: 288.1018; ν_{max} : (FT-ATR)/ cm^{-1} : 3329, 3010, 2996, 2980, 1690, 1592, 1555, 1456, 1320, 1286, 1130, 911, 750, 512.



To a solution of 3-bromo-4-formylbenzoic acid (1.00 g, 4.37 mmol), propylamine (430 μL , 5.24 mmol) and triethylamine (2.79 mL, 21.8 mmol) in dichloromethane (5 mL), was added propylphosphonic anhydride solution (50% w/w in EtOAc, 3.47 mL, 10.9 mmol) at 0 °C and the mixture was warmed to r.t. and stirred for 16 h. The reaction was then concentrated under reduced pressure. The residue was purified via flash column chromatography on silica gel eluting with EtOAc:Petrol (1:9). Fractions containing the product were concentrated under reduced pressure to provide a colourless oil (547 mg, 2.03 mmol, 46%).

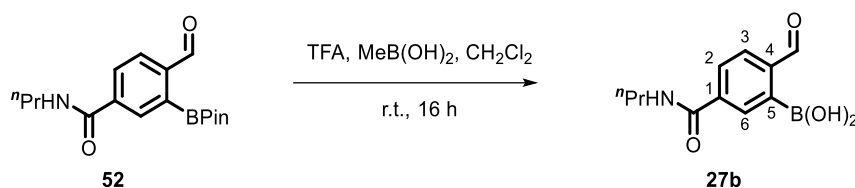
R_f: 0.28 (1:9, EtOAc:Petrol, UV active); **¹H NMR** (400 MHz, CDCl_3) δ = 10.36 (s, 1H, $\underline{\text{C}}\text{HO}$), 8.04 (d, J = 1.6 Hz, 1H, $\text{Ph}\underline{\text{H}}\text{2}$), 7.93 (d, J = 8.0 Hz, 1H, $\text{Ph}\underline{\text{H}}\text{5}$), 7.74 (dd, J = 8.0, 1.6 Hz, 1H, $\text{Ph}\underline{\text{H}}\text{4}$), 6.25 (s, 1H, $\underline{\text{NH}}$), 3.44-3.38 (m, 2H, $\underline{\text{C}}\text{H}_2\text{N}$), 1.67-1.61 (m, 2H, $\underline{\text{C}}\text{H}_2\text{CH}_3$), 0.98 (t, J = 7.4 Hz, 3H, $\underline{\text{C}}\text{H}_3$); **¹³C NMR** (101 MHz, CDCl_3) δ = 191.3 ($\underline{\text{C}}\text{HO}$), 165.2 ($\underline{\text{C}}\text{ON}$), 141.0 ($\text{Ph}\underline{\text{C}}\text{4}$), 135.2 ($\text{Ph}\underline{\text{C}}\text{3}$), 132.8 ($\text{Ph}\underline{\text{C}}\text{2}$), 130.1 ($\text{Ph}\underline{\text{C}}\text{1}$), 127.2 ($\text{Ph}\underline{\text{C}}\text{4}$), 126.1 ($\text{Ph}\underline{\text{C}}\text{5}$), 42.2 ($\underline{\text{C}}\text{H}_2\text{N}$), 22.9 ($\underline{\text{C}}\text{H}_2\text{CH}_3$), 11.5 ($\underline{\text{C}}\text{H}_3$); **HRMS**: m/z (ESI⁺) calc. for $\text{C}_{11}\text{H}_{12}^{79}\text{BrNO}_2$ [M+H]⁺: 270.1260; Obs.: 270.0124; ν_{max} : (FT-ATR)/ cm^{-1} : 3313, 3075, 2965, 2934, 2875, 1698, 1642, 1545, 1467, 1441, 1313, 1288, 1202, 1039, 891, 846, 758, 653.



50 (265 mg, 0.981 mmol), bis(pinacolato)diboron (648 mg, 2.55 mmol), 1,1'-[bis(diphenylphosphino)ferrocene]dichloropalladium(II) (144 mg, 0.19 mmol) and potassium acetate (520 mg, 5.30 mmol) were placed under a nitrogen atmosphere, and anhydrous dioxane (15 mL) was added. Nitrogen was bubbled through the reaction mixture for 10 min, which was then stirred at 80 °C for 16 h. After cooling to r.t., the reaction was concentrated under reduced pressure. The residue was purified via flash column chromatography on silica gel, eluting with EtOAc:Petrol (2:8). Fractions containing the

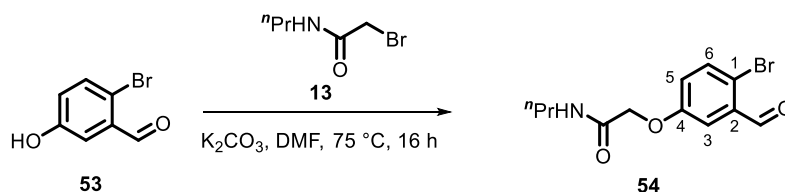
product were concentrated under reduced pressure to yield a colourless oil (206 mg, 0.619 mmol, 24%).

R_f: 0.37 (2:8, EtOAc:Petrol, UV active); **¹H NMR** (400 MHz, CDCl₃) δ = 10.52 (s, 1H, CHO), 8.15 (d, *J* = 1.4 Hz, 1H, PhH₆), 7.94-7.88 (m, 2H, PhH₂, PhH₃), 6.70 (t, *J* = 5.9 Hz, 1H, NH), 3.38-3.31 (m, 2H, CH₂N), 1.58 (dt, *J*₁ = *J*₂ = 7.5 Hz, 2H, CH₂CH₃), 1.32 (s, 12H, Pin), 0.91 (t, *J* = 7.5 Hz, 3H, CH₃); **¹³C NMR** (101 MHz, CDCl₃) δ = 194.2 (CHO), 166.8 (CON), 143.1 (PhC₄), 138.6 (PhC₁), 134.0 (PhC₆), 133.9 (PhC₅), 129.7 (PhC₂), 128.0 (PhC₃), 83.2 (C(CH₃)₂), 83.0 (C(CH₃)₂), 42.0 (CH₂N), 24.6 (Pin), 22.9 (CH₂CH₃), 11.5 (CH₃); **HRMS**: *m/z* (ESI⁺) calc. for C₁₁H₁₃BNO₄ [M-Pin]⁻: 234.0943; Obs.: 234.0948; **v_{max}**: (FT-ATR)/cm⁻¹: 3358, 2977, 1643, 1535, 1452, 1371, 1341, 1141, 982, 851, 673, 578,.



Trifluoroacetic acid (1.0 mL) was added to a solution of **52** (70 mg, 0.22 mmol) and methylboronic acid (132 mg, 2.21 mmol) in dichloromethane (5 mL), and the mixture stirred at r.t for 16 h. The reaction was azeotroped with dichloromethane (3 × 20 mL), and hydrochloric acid (0.1 M, 2 × 10 mL) was added, and concentrated under reduced pressure to give a yellow oil (52 mg, 0.22 mmol, quantitative yield).

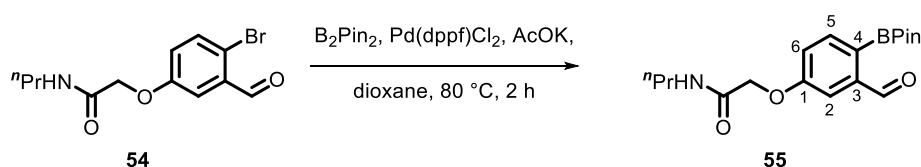
R_f: 0.29 (2:8, EtOAc:Petrol, UV active); **¹H NMR** (400 MHz, CD₃OD, for acetal) δ = 7.76-7.66 (m, 2H, PhH₆, PhH₂), 7.37 (d, *J* = 8.0 Hz, 1H, PhH₃), 5.45 (s, 1H, CH(OMe)₂), 3.27-3.19 (m, 2H, CH₂N), 1.53 (dt, *J* = 7.4 Hz, 2H, CH₂CH₃), 0.86 (t, *J* = 7.4 Hz, 3H, CH₃); **¹³C NMR** (101 MHz, CD₃OD, for acetal) δ = 168.8 (CON), 144.3 (PhC₄), 133.7 (PhC₁), 133.0 (PhC₆), 128.6 (PhC₅), 126.9 (PhC₂), 125.6 (PhC₃), 102.3 (CH(OMe)₂), 84.1 (C(CH₃)₂), 41.5 (CH₂N), 23.7 (Pin), 22.4 (CH₂CH₃), 10.5 (CH₃); **HRMS**: *m/z* (ESI⁺) calc. for C₁₁H₁₃BNO₄ [M-H]⁺: 234.0943; Obs.: 234.0945; **v_{max}**: (FT-ATR)/cm⁻¹: 3314, 2967, 2932, 1693, 1639, 1540, 1343, 1316, 1206, 1141, 1066, 964, 851, 813, 760.



A mixture of 2-bromo-4-hydroxybenzaldehyde (800 mg, 4.00 mmol), bromoacetate **13** (864 mg, 4.80 mmol) and potassium carbonate (1.10 g, 8.00 mmol) in dimethylformamide (30 mL) was stirred at 75 °C for 16 h. The mixture was then cooled to r.t. and diluted with water (150 mL). The aqueous mixture was extracted with ethyl acetate (3 × 70 mL), and the combined organics washed with brine (2 × 200 mL), dried with MgSO₄, filtered and

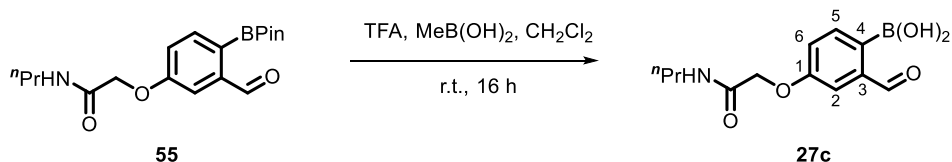
concentrated under reduced pressure. The residue was purified via flash column chromatography on silica gel eluting with EtOAc:Petrol (2:8). Fractions containing the product were concentrated under reduced pressure to provide a white solid (700 mg, 2.34 mmol, 59%).

R_f: 0.32 (2:8, EtOAc:Petrol, UV active); **¹H NMR** (400 MHz, CDCl₃) δ = 10.29 (s, 1H, CHO), 7.59 (d, *J* = 8.6 Hz, 1H, PhH₆), 7.45 (d, *J* = 1.6 Hz, 1H, PhH₃), 7.07 (dd, *J* = 8.6, 1.6 Hz, 1H, PhH₅), 6.50 (s, 1H, NH), 4.50 (s, 2H, CH₂O), 3.36-3.27 (m, 2H, CH₂N), 1.59-1.53 (m, 2H, CH₂CH₃), 0.94 (t, *J* = 7.6 Hz, 3H, CH₃); **¹³C NMR** (101 MHz, CDCl₃) δ = 191.4 (CHO), 167.1 (CON), 156.9 (PhC₄), 135.1 (PhC₆), 134.4 (PhC₁), 122.4 (PhC₅), 119.2 (PhC₂), 114.9 (PhC₃), 67.7 (CH₂O), 40.9 (CH₂N), 22.9 (CH₂CH₃), 11.4 (CH₃); **HRMS**: *m/z* (ESI⁺) calc. for C₁₂H₁₄⁷⁹BrNO₃ [M+H]⁺: 300.0231; Obs.: 300.0231; **v_{max}**: (FT-ATR)/cm⁻¹: 3350, 3075, 2963, 2870, 1667, 1540, 1285, 1227, 1068, 959, 824, 695, 597.



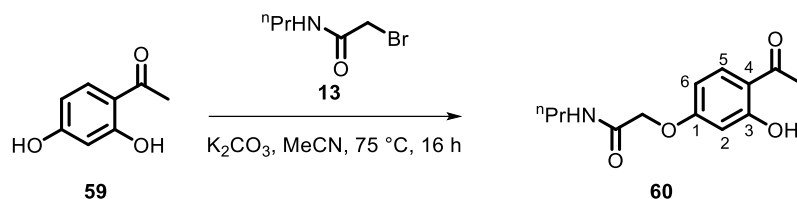
54 (200 mg, 0.66 mmol), bis(pinacolato)diboron (205 mg, 0.80 mmol), 1,1'-[bis(diphenylphosphino)ferrocene]dichloropalladium(II) (24 mg, 0.03 mmol) and potassium acetate (194 mg, 2.00 mmol) were placed under a nitrogen atmosphere, and anhydrous dioxane (5 mL) was added. Nitrogen was bubbled through the reaction mixture for 10 min, which was then stirred at 80 °C for 2 h. After cooling to r.t., the reaction was concentrated under reduced pressure. The residue was then dissolved in ethyl acetate (100 mL), and washed with water (2 × 70 mL) and brine (2 × 70 mL), and dried with MgSO₄, filtered and concentrated under reduced pressure. The residue was purified via flash column chromatography on silica gel, eluting with EtOAc:Petrol (2:8). Fractions containing the product were concentrated under reduced pressure to yield a colourless oil (190 mg, 0.55 mmol, 83%).

R_f: 0.34 (2:8, EtOAc:Petrol, UV active); **¹H NMR** (400 MHz, CDCl₃) δ = 10.64 (s, 1H, CHO), 7.90 (d, *J* = 8.4 Hz, 1H, PhH₅), 7.51 (d, *J* = 2.2 Hz, 1H, PhH₂), 7.13 (dd, *J* = 8.4, 2.2 Hz, 1H, PhH₆), 6.55 (s, 1H, NH), 4.54 (s, 2H, CH₂O), 3.30 (t, *J* = 7.4 Hz, 2H, CH₂N), 1.62-1.51 (m, 2H, CH₂CH₃), 1.36 (s, 12H, Pin), 0.92 (t, *J* = 7.6 Hz, 3H, CH₃); **¹³C NMR** (101 MHz, CDCl₃) δ = 194.4 (CHO), 167.4 (CON), 159.5 (PhC₁), 143.8 (PhC₄), 138.5 (PhC₅), 119.3 (PhC₆), 119.2 (PhC₃), 112.4 (PhC₂), 84.5 (C(CH₃)₂), 67.3 (CH₂O), 40.9 (CH₂N), 25.0 (Pin), 22.9 (CH₂CH₃), 11.4 (CH₃); **HRMS**: *m/z* (ESI⁺) calc. for C₁₈H₂₆BNO₅ [M+H]⁺: 348.1977; Obs.: 348.1981; **v_{max}**: (FT-ATR)/cm⁻¹: 3323, 2975, 1685, 1663, 1596, 1538, 1378, 1344, 1269, 1243, 1112, 1042, 962, 857, 652, 579.



Trifluoroacetic acid (2.0 mL) was added to a solution of **55** (132 mg, 0.42 mmol) and methylboronic acid (216 mg, 3.60 mmol) in dichloromethane (10 mL), and the mixture stirred at r.t for 16 h. The reaction was azeotroped with dichloromethane (3 × 20 mL), and hydrochloric acid (0.1 M, 2 × 10 mL) was added, and concentrated under reduced pressure to give a colourless oil (98 mg, 0.42 mmol, quantitative yield).

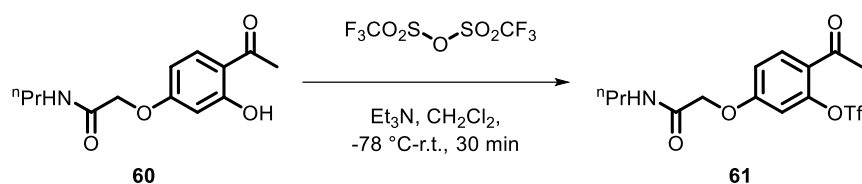
R_f: 0.21 (2:8, EtOAc:Petrol, UV active); **¹H NMR** (400 MHz, 100 mM deuterated PBS + 10% DMSO-*d*₆) δ = 9.97 (s, 1H, -CHO), 7.69-7.59 (m, 1H, PhH₆), 7.54 (d, *J* = 2.4 Hz, 1H, PhH₂), 7.32 (d, *J* = 8.3 Hz, 1H, PhH₅), 4.70 (s, 2H, CH₂O), 3.24 (t, *J* = 6.9 Hz, 2H, CH₂N), 1.57-1.47 (m, 2H, CH₂CH₃), 0.85 (t, *J* = 7.1 Hz, 3H, CH₃); **¹³C NMR** (101 MHz, CD₃OD, for acetal) δ = 169.6 (C=O), 158.1 (PhC₁), 143.5 (PhC₄), 131.8 (PhC₅), 114.2 (PhC₆), 111.9 (PhC₃), 102.3 (PhC₂), 66.9 (CH₂O), 40.6 (CH₂N), 22.4 (CH₂CH₃), 10.4 (CH₃); **HRMS**: *m/z* (ESI⁺) calc. for C₁₂H₁₆BNO₅ [M+Na]⁺: 288.1014; Obs.: 288.1016; **v_{max}**: (FT-ATR)/cm⁻¹: 3395, 2968, 2938, 2875, 1661, 1548, 1426, 1348, 1274, 1230, 1148, 807.



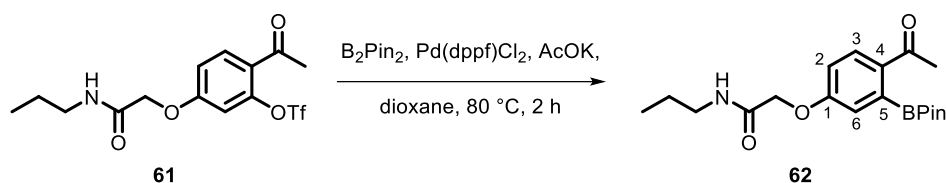
A mixture of 2,4-dihydroxybenzaldehyde (2.00 g, 13.2 mmol), propyl bromoacetate **13** (2.35 g, 13.2 mmol) and potassium carbonate (3.09 g, 22.4 mmol) in acetonitrile (40 mL) was stirred for 16 h at 75 °C. The mixture was then cooled to r.t. and diluted with water (150 mL). The aqueous mixture was extracted with ethyl acetate (3 × 70 mL), and the combined organics washed with brine (2 × 200 mL), dried with MgSO₄, filtered and concentrated under reduced pressure. The residue was purified via flash column chromatography on silica gel eluting with EtOAc:Petrol (2:8). Fractions containing the product were concentrated under reduced pressure to provide a colourless oil (935 mg, 3.73 mmol, 28%). Data were consistent with those previously reported.

R_f: 0.32 (2:8, EtOAc:Petrol, UV active); **¹H NMR** (400 MHz, CDCl₃) δ = 7.67 (d, *J* = 8.7 Hz, 1H, PhH₅), 6.48-6.42 (m, 2H, PhH₂, PhH₆), 4.50 (s, 2H, CH₂O), 3.30 (q, *J* = 7.3 Hz, 2H, CH₂N), 2.56 (s, 3H, CH₃), 1.56 (dt, *J*₁ = *J*₂ = 7.3 Hz, 2H, CH₂CH₃), 0.92 (t, *J* = 7.4 Hz, 3H, CH₃); **¹³C NMR** (101 MHz, CDCl₃) δ = 202.9 (CH₃C=O), 167.1 (PhC₁), 165.1 (PhC₄), 163.3 (C=O), 132.9 (PhC₅), 115.1 (PhC₃), 107.0 (PhC₂), 102.7 (PhH₆), 67.3 (CH₂O), 40.9 (CH₂N), 26.4 (CH₃), 22.9 (CH₂CH₃), 11.4 (CH₃); **HRMS**: *m/z* (ESI⁺) calc. for C₁₃H₁₈NO₄

[M+Na]⁺: 252.1230; Obs.: 252.1231; ν_{max} : (FT-ATR)/cm⁻¹: 3378, 2965, 2934, 1637, 1543, 1371, 1331, 1272, 1154, 1179, 1044, 806, 572.

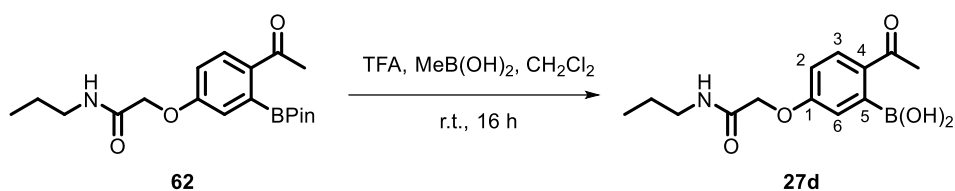


Triethylamine (2.44 mL, 17.6 mmol) was added dropwise to a solution of **60** (885 mg, 3.53 mmol) in anhydrous dichloromethane (20 mL) at -78 °C, which was stirred for 5 min. Triflic anhydride (2.38 mL, 14.2 mmol) was added dropwise to the solution which was stirred at -78 °C, for 15 min. The mixture was then allowed to warm to r.t., and was left for a further 30 min. The mixture was then diluted with water (150 mL). The reaction was quenched by addition of saturated sodium hydrogen carbonate (50 mL), and the mixture extracted with dichloromethane (3 × 70 mL), and the combined organics washed with brine (2 × 100 mL), dried with MgSO₄, filtered and concentrated under reduced pressure. The product was used immediately without further purification.



61 (464 mg, 1.52 mmol), bis(pinacolato)diboron (1.00 g, 3.94 mmol), 1,1'-[bis(diphenylphosphino)ferrocene]dichloropalladium(II) (222 mg, 0.36 mmol) and potassium acetate (802 mg, 8.19 mmol) were placed under a nitrogen atmosphere, and anhydrous dioxane (20 mL) was added. Nitrogen was bubbled through the reaction mixture for 10 min, which was then stirred at 80 °C for 2 h. After cooling to r.t., the reaction was concentrated under reduced pressure. The residue was purified via flash column chromatography on silica gel, eluting with EtOAc:Petrol (2:8). Fractions containing the product were concentrated under reduced pressure to yield a colourless oil (206 mg, 0.594 mmol, 39%).

R_f: 0.37 (2:8, EtOAc:Petrol, UV active); **¹H NMR** (400 MHz, CDCl₃) δ = 7.70 (d, J = 8.4 Hz, 1H, PhH₃), 6.91 (d, J = 2.6 Hz, 1H, PhH₆), 6.79 (dd, J = 8.4, 2.6 Hz, 1H, PhH₂), 6.58 (t, J = 6.0 Hz, 1H, NH), 4.42 (s, 2H, CH₂O), 3.19 (q, J = 6.7 Hz, 2H, CH₂N), 2.44 (s, 3H, CH₃), 1.47 (dt, $J_1 = J_2 = 7.4, 6.7$ Hz, 2H, CH₂CH₃), 1.34 (s, 12H, Pin), 0.82 (t, J = 7.4 Hz, 3H, CH₃); **¹³C NMR** (101 MHz, CDCl₃) δ = 198.4 (C=OCH₃), 167.4 (CON), 160.6 (PhC₁), 134.8 (PhC₄), 131.0 (PhC₅), 118.6 (PhC₂), 114.5 (PhC₃), 113.9 (PhH₆), 83.9 (C(CH₃)₂), 67.3 (CH₂O), 40.9 (CH₂N), 25.1 (CH₃CO), 25.0 (Pin), 22.9 (CH₂CH₃), 11.4 (CH₂CH₃); **HRMS**: m/z (ESI⁺) calc. for C₁₉H₂₈BNO₅ [M+Na]⁺: 383.1953; Obs.: 384.1949; ν_{max} : (FT-ATR)/cm⁻¹: 3320, 2972, 1663, 1564, 1420, 1333, 1259, 1143, 1059, 965, 853, 686, 635, 590.



Trifluoroacetic acid (1.0 mL) was added to a solution of **62** (140 mg, 0.388 mmol) and methylboronic acid (233 mg, 3.88 mmol) in dichloromethane (5 mL), and the mixture stirred at r.t for 16 h. The reaction was azeotroped with dichloromethane (3 × 20 mL), and hydrochloric acid (0.1 M, 2 × 10 mL) was added, and concentrated under reduced pressure to give a colourless oil (93 mg, 0.33 mmol, 86%).

R_f: 0.22 (3:7, EtOAc:Petrol, UV active); **¹H NMR** (400 MHz, CD₃OD) δ = 8.02 (d, *J* = 8.7 Hz, 1H, PhH₃), 7.06 (dt, *J* = 8.7, 2.6 Hz, 1H, PhH₂), 7.01 (d, *J* = 2.6 Hz, 1H, PhH₆), 4.61 (s, 2H, CH₂O), 3.23 (t, *J* = 7.3 Hz, 2H, CH₂N), 2.57 (s, 3H, CH₃), 1.56 (dt, *J*₁ = *J*₂ = 7.3 Hz, 2H, CH₂CH₃), 0.90 (t, *J* = 7.3 Hz, 3H, CH₃); **¹³C NMR** (101 MHz, CD₃OD) δ = 197.8 (CH₃C=O), 169.1 (PhC₁), 162.1 (CON), 133.6 (PhC₅), 131.4 (PhC₄), 130.6 (PhC₃), 116.7 (PhC₂), 114.0 (PhC₆), 66.8 (CH₂O), 40.7 (CH₂N), 26.4 (CH₃), 24.0 (CH₂CH₃), 22.3 (Pin), 10.4 (CH₃); **HRMS**: *m/z* (ESI⁺) calc. for C₁₃H₁₈BNO₅ [M-H]⁺: 279.1285; Obs.: 279.1284; **ν_{max}**: (FT-ATR)/cm⁻¹: 3312, 2966, 2934, 1658, 1542, 1416, 1217, 1055, 823, 732, 568.

6.3. Initial Screening of Cy3 Quenching

General procedure: A solution of Cy5-nucleophile (50 μL, 5 μM) in PBS buffer was added to a solution Cy3-*o*BA **1b** (50 μL, 5 μM) in PBS buffer in a 96-well plate, to give final Cy3 and Cy5 concentrations of 2.5 μM under second order conditions. Single-point fluorescence emission intensities (λ_{excitation} = 480 nm; λ_{emission} = 580 nm) in the Cy3 channel were then recorded every 1 min for a period of 25 min. After this time, a solution of non-labelled nucleophilic trapping agents **3a-e** (10 μL, 125 μM) in PBS buffer was added to a solution, to give a final concentration of **3a-e** of 25 μM (10 equivalents). Single-point fluorescence emission intensities (λ_{excitation} = 480 nm; λ_{emission} = 580 nm) in the Cy3 channel were then recorded every 1 min for a period of 60 h.

Negative control: Run as for the general procedure, using Cy3-*o*BA **1b** (50 μL, 5 μM) with Cy5-NHAc (50 μL, 5 μM) and **3a-e** (10 μL, 125 μM) in PBS buffer.

Positive control: The emission of a solution of Cy3-Cy5 covalent control (100 μL, 2.5 μM) with **3a-e** (10 μL, 125 μM) was recorded over time as described above.

Data processing: Emission at 580 nm was plotted as a function of time, relative to the negative (100%) and positive (0%) controls.

Controls to validate quenching via FRET: Run as for the general procedure, using PrNH-capped nucleophiles **3a-e** (50 μ L, 100 μ M) in place of the Cy5-nucleophile.

6.4. LC-MS Reversibility Studies

General procedure: Stock solutions of **27a** (3 μ L, 38 mM, 114 nmol) and propyl amide nucleophile **3d** or **3e** (6 μ L, 38 mM, 228 nmol) in methanol were added sequentially to the relevant buffer (300 μ L, final oBA concentration 370 μ M) and shaken for 30 min. At this point, a stock solution of the analogous methyl amide nucleophile **24** or **28** (30 μ L, 38 mM, 1140 nmol) was added and the mixture incubated at room temperature. Aliquots were analysed via LC-MS analysis every 24 h for 1 week.

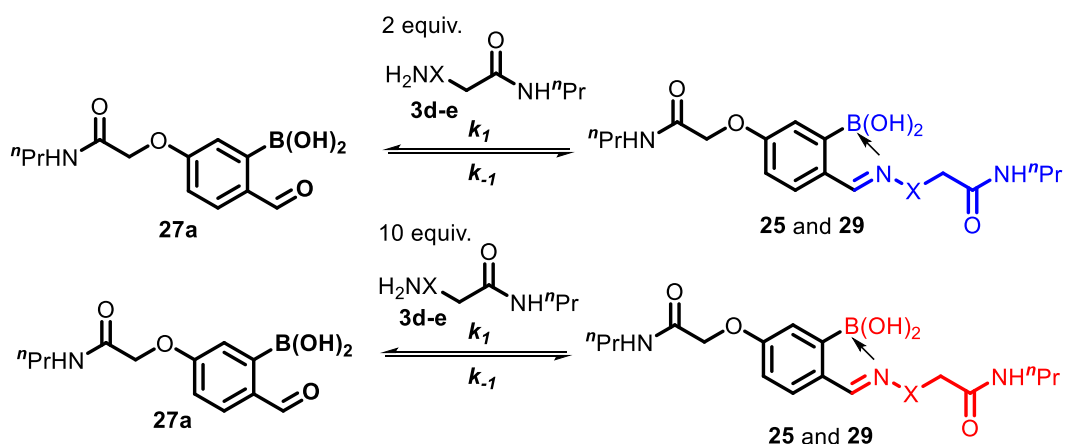
Negative control: Run as described above, but methanol (30 μ L) was added in place of the methyl amide nucleophile.

Positive control: Run as described above, but methanol (6 μ L) was added in place of the propyl amide nucleophile.

Data analysis: The absorbance at 280 nm at time $t = x$ (A_x) was integrated for peaks relating to propyl-oBID (elution time: 2.90 min) products. A plot of $\ln(\text{Integration})$ was used to determine the integration at $t = 0$ (intercept of linear regression). Data from the positive controls was used to calculate the expected integration at 100% exchange (B). Conversions were then calculated from:

$$\text{Conversion} = \frac{A_0 - A_x}{A_0 - B} \times 100$$

Data fitting: Data were fit to a two-reaction reversible kinetic model using Copasi 4.34.251, based on the following reactions:



k_1 calculated from the FRET studies were used to estimate k_{-1} , using the evolutionary programming method built into the software, with 200 generations and a population size

of 20, and with the assumption that rates of reactions were the same for propyl- and methyl-amide nucleophiles. Parameters were restricted within the confines of k_1 10^{-10} - 10^{-1} s⁻¹.

6.5. NMR Studies of pH Dependent DAB-Hydrazone Exchange

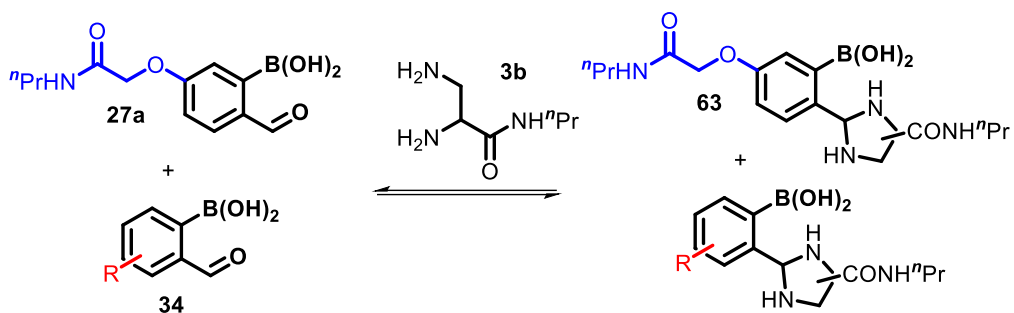
Solutions of oBA **27a** (2 mg, 7.5 μ mol) in DMSO-*d*₆ (25 μ L) and propyl-amide hydrazine **3e** (1.7 mg, 7.5 μ mol) in DMSO-*d*₆ were added sequentially to deuterated buffers (0.5 mL, 100 mM; pH 4 – acetate buffer, pH 5, 6, 7.4, 8 – phosphate buffer; prepared by evaporating standard buffer and then redissolving the residue in D₂O three times) and incubated for 30 min. The sample was then analysed by NMR and the ratio of DAB to hydrazone determined. In all cases, only signals from the cyclic DAB were observed, indicated by a singlet at $\delta \sim 8.6$, as previously reported by Gu *et al.*¹⁴

6.6. NMR Studies of Sugar Binding

Solutions of oBA **25** (2 mg, 7.5 μ mol) in DMSO-*d*₆ (25 μ L) and either propyl-amide hydrazine **77** or hydroxylamine **83** (7.5 μ mol) in DMSO-*d*₆ were added sequentially to deuterated PBS (0.5 mL, 100 mM; prepared by evaporating standard buffer and then redissolving the residue in D₂O three times) and incubated for 30 min. Glucose or fructose (7.5 μ mol) was then added and the samples incubated for a further 30 min. After this time the samples were analysed by NMR and shifts in the oxime/DAB peaks used to determine the extent of sugar binding. In all cases, no shift in signal was observed indicating no sugar binding was taking place under these conditions.

13. NMR studies of analogue reaction equilibria

General procedure: oBA **27a** (2 mg, 7.5 μ mol) and another oBA analogue **27b-d** (7.5 μ mol), were dissolved in a mixture of deuterated PBS (0.5 mL, 100 mM; prepared by evaporating standard PBS and then redissolving the residue in D₂O three times) and DMSO-*d*₆ (50 μ L). A solution of 1,2-diamine **3b** (1.1 mg, 7.5 μ mol) in deuterated PBS (0.5 mL) was then added and the mixture incubated for 2 hrs, prior to NMR analysis.



Data analysis: Peaks relating to oBID formation for both **27a** and the oBA analogue **27b-d** competitor were identified via prior control reactions in which each oBA was incubated with **3b** alone. Integration of peaks that fell within unique regions of the spectra relating to oBID formation were used to determine the ratio of products formed. This ratio was then used to calculate K_d for each analogue, as follows:

$$K_d(\mathbf{27a}) = \frac{[\mathbf{A}][\mathbf{B}]}{[\mathbf{C}]} \quad K_d(\mathbf{X}) = \frac{[\mathbf{D}][\mathbf{B}]}{[\mathbf{E}]}$$

Assuming $K_d(\mathbf{27a}) = K_d(\mathbf{1b})$, which is known from our FRET studies, these equations can be rearranged to:

$$[\mathbf{B}] = \frac{[\mathbf{C}]K_d(\mathbf{1b})}{[\mathbf{A}]} \quad K_d(\mathbf{X}) = \frac{[\mathbf{D}][\mathbf{C}]}{[\mathbf{E}][\mathbf{A}]} K_d(\mathbf{1b})$$

7. References

- 1 P. Schmidt, C. Stress and D. Gillingham, *Chem. Sci.*, 2015, **6**, 3329–3333.
- 2 C. J. Stress, P. J. Schmidt and D. G. Gillingham, 2016, **14**, 5529–5533.
- 3 J. P. M. António, R. Russo, C. P. Carvalho, P. M. S. D. Cal and P. M. P. Gois, *Chem. Soc. Rev.*, 2019, **48**, 3513–3536.
- 4 P. M. S. D. Cal, J. B. Vicente, E. Pires, A. V. Coelho, L. F. Veiros, C. Cordeiro and P. M. P. Gois, *J. Am. Chem. Soc.*, 2012, **134**, 10299–10305.
- 5 A. Bandyopadhyay and J. Gao, *Chem. Eur. J.*, 2015, **21**, 14748–14752.
- 6 A. Bandyopadhyay and J. Gao, *J. Am. Chem. Soc.*, 2016, **138**, 2098–2101.
- 7 P. M. S. D. Cal, R. F. M. Frade, C. Cordeiro and P. M. P. Gois, *Chem. Eur. J.*, 2015, **21**, 8182–8187.
- 8 H. Faustino, M. J. S. A. Silva, L. F. Veiros, G. J. L. Bernardes and P. M. P. Gois, *Chem. Sci.*, 2016, **7**, 5052–5058.
- 9 S. Cambray and J. Gao, *Acc. Chem. Res.*, 2018, **51**, 2198–2206.
- 10 K. Li, C. Weidman and J. Gao, *Org. Lett.*, 2018, **20**, 20–23.
- 11 A. Bandyopadhyay, S. Cambray and J. Gao, *J. Am. Chem. Soc.*, 2017, **139**, 871–878.
- 12 A. Bandyopadhyay, K. A. McCarthy, M. A. Kelly and J. Gao, *Nat. Commun.*, 2015, **6**, 6561.
- 13 A. Bandyopadhyay, S. Cambray and J. Gao, *Chem. Sci.*, 2016, **7**, 4589–4593.
- 14 H. Gu, T. I. Chio, Z. Lei, R. J. Staples, J. S. Hirschi and S. Bane, *Org. Biomol. Chem.*, 2017, **15**, 7543–7548.
- 15 H. Gu, S. Ghosh, R. J. Staples and S. L. Bane, *Bioconj. Chem.*, 2019, **30**, 10, 2604–2613
- 16 O. Dilek, Z. Lei, K. Mukherjee and S. Bane, *Chem. Comm.*, 2015, **51**, 16992–16995.
- 17 K. Sugita, Y. Suzuki, Y. Tsuchido, S. Fujiwara, T. Hashimoto and T. Hayashita, *RSC Adv.*, 2022, **12**, 20259–20263.
- 18 D. B. Cordes, S. Gamsey and B. Singaram, *Angew. Chem. Int. Ed.*, 2006, **45**, 3829–3832.
- 19 K. Unger and A. M. Coclite, *Biomacromolecules*, 2022, **23**, 4289–4295.
- 20 J. Ren, H. Hu, S. Wang, Y. He, Y. Ji, Y. Chen, K. Wang, H. Zhang, Y. Zhao and F. Dai, *ACS Appl. Mater. Interfaces*, 2022, **14**, 23182–23193.
- 21 H. Fang, G. Kaur and B. Wang, *J. Fluoresc.*, 2004, **14**, 481–489.
- 22 R. K. Varshnaya and P. Banerjee, *Euro. J. Org. Chem.*, 2016, **2016**, 4059–4066.
- 23 L. Bollans, J. Bacsá, J. A. Iggo, G. A. Morris and A. V. Stachulski, *Organic and Biomolecular Chemistry*, 2009, **7**, 4531–4538.
- 24 A. Weickgenannt, J. Mohr and M. Oestreich, *Tetrahedron*, 2012, **68**, 3468–3479.